

UNIVERZITA PALACKÉHO V OLOMOUCI

PŘÍRODOVĚDECKÁ FAKULTA

KATEDRA ANALYTICKÉ CHEMIE

**Využití analytické chemie pro studium hmotného
kulturního dědictví**

HABILITAČNÍ PRÁCE

2024

RNDr. Lukáš Kučera, Ph.D.

UNIVERZITA PALACKÉHO V OLOMOUCI

PŘÍRODOVĚDECKÁ FAKULTA

KATEDRA ANALYTICKÉ CHEMIE

**Využití analytické chemie pro studium hmotného
kulturního dědictví**

HABILITAČNÍ PRÁCE

RNDr. Lukáš Kučera, Ph.D.

Olomouc 2024

Prohlašuji, že jsem habilitační práci vypracoval samostatně a uvedl jsem všechny použité podklady a literaturu.

V Olomouci dne. 04. 03. 2024



Na tomto místě chci poděkovat všem, kteří mě podporovali či stále podporují v mém badatelském a pedagogickém snažení. V první řadě děkuji svému učiteli a kolegovi panu docentu Petru Bednářovi, který mi předal cenné rady a naučil mě správné organizaci vědecké práce, které je občas „zavalující“. Dále děkuji kolegům, kteří vytvářejí příjemné tvůrčí a přátelské prostředí, kteří mi pomáhají lidsky i profesionálně a jsou mi inspirací i vzorem. Poděkování patří také mým studentům, kteří se svou pilnou a poctivou prací na nejrůznějších tématech posouvají výzkumy rychlým krokem kupředu. Velké poděkování také patří mé rodině a ženě Pavle za toleranci, lásku a pochopení.

Obsah

Abstrakt.....	6
Seznam použitých zkratk 7	7
1. Úvod.....	9
2. Interdisciplinární přístup.....	10
3. Multimodální přístup.....	19
4. Destruktivní vs. nedestruktivní přístup.....	28
6. Literatura.....	41

Abstrakt

Aplikace přírodovědných analýz pro studium hmotného kulturního dědictví má velmi dlouhou tradici a v posledních několika desetiletích je toto propojení nedílnou součástí archeologie. V této práci je převážně diskutováno zapojení analytické chemie pro studium vzorků hmotného kulturního dědictví. Práce je dělena na tři samostatné kapitoly, jako je Interdisciplinární přístup, Multidisciplinární přístup a Destruktivní vs. nedestruktivní přístup. Ač jsou kapitoly diskutovány samostatně, tak jsou navzájem velmi úzce propojeny a analýza hmotného kulturního dědictví je tedy významně závislá na vzájemné komunikaci, na jejímž základě dojde k využití nejvhodnější analytické techniky od nedestruktivních postupů k těm invazivním a destruktivním.

Seznam použitých zkratek

AFM	mikroskopie atomárních sil
AL	akcentovaná linie
ASAP-MS	hmotnostní spektrometrií s přímou sondou
ASAP-IM-MS	ASAP-MS v kombinaci s iontovou mobilitou
CO	Cribra orbitalia
DM	digitální mikroskopie
dtm	odchylka od teoretické hmotnosti
EDJ	rozhraní mezi zubní sklovinou a dentinem
FIA/ESI-MS	průtoková injekční analýza s hmotností spektrometrií s ionizací elektrosprejem
FTIR	infračervená spektroskopie s Fourierovou transformací
GC/MS	plynová chromatografie s hmotnostní detekcí
ICP-MS	hmotnostní spektrometrie s indukčně vázaným plasmatem
LDI-MS	hmotnostní spektrometrie s laserovou desorpcí/ionizací
LM	mikroskopie ve viditelném světle
MALDI-MS	hmotnostní spektrometrie s laserovou/desorpcí ionizací za přítomnosti matrice
MRM	monitorování vícenásobných reakcí
PB	pruská modř
PCA	analýza hlavních komponent
py-GC/MS	GC/MS s pyrolýzní jednotkou
Q-TOF	hmotnostní analyzátor ve spojení kvadrupól-měření doby letu
RGB	barevné zobrazení, R červená, G zelená, B modrá
RM	Ramanova mikroskopie
RT	retenční čas
SEM/EDS	skenovací elektronová mikroskopie s energiově-disperzní rentgenovou spektroskopií

SIM	monitoringu vybraných iontů
TAG	triacylglycerol
XPS	rentgenová fotoelektronová spektroskopie
XRF	rentgenová fluorescenční spektroskopie
μ -XRPD	rentgenová prášková mikrodifrakcí

1. Úvod

Analytická chemie v analýze hmotného kulturního dědictví má velmi dlouhou tradici. Zejména stanovení chemického složení kovových archeologických artefaktů bylo využíváno již více než před dvě stě lety, a to především pro účely klasifikace materiálu. Jako jeden z příkladů může být uvedena kvantitativní analýza římských mincí Martinem Heinrichem Klaprothem v Berlíně v 1799 (pozn. tento chemik je známý spíše jako objevitelem prvku uran). Materiálová chemická analýza například také pomohla dánskému archeologovi Christian Jurgensen Thomsenovi ve dvacátých letech 19. století formálně zavést třístupňový systém pravěké archeologie - dobu kamennou, dobu bronzovou a dobu železnou.

V roce 1958 se poprvé objevil termín „vědecky podložená archeologie“ (z angl. science-based archaeology) nebo archeometrie. Termín archeometrie je v posledních několika desetiletích hojně využíván a většinou archeologů označován za nepostradatelnou a nedílnou součást archeologie. V přírodovědných analýzách pojem "archeometrie" označuje převážně vývoj a použití přírodovědných metod s cílem přispět k rozvoji archeologie a pochopení socio-ekonomických vztahů lidské populace v minulosti.

Tato práce je věnována využití analytické chemie při analýze hmotného kulturního dědictví. Práce vychází ze souboru dvanácti publikací [I-XII] uvedených v příloze, které vznikly v laboratořích na Katedře analytické chemie, Přírodovědecké fakulty Univerzity Palackého v Olomouci. Jejím cílem je poukázat na tři základní přístupy aplikované při analýze unikátních vzorků. Dvě práce IX a XII vznikly v rámci spolupráce se studenty středních škol při přípravě práce SOČ. Obě studentky takto dokázaly kromě práce SOČ také napsat plnohodnotný vědecký článek a příslušných publikacích jsou uvedeny jako prvoautorky.

2. Interdisciplinární přístup

Archeometrické projekty se zaměřují na relevantní archeologické otázky, k nimž se snaží přispět získáním nových poznatků. Problémem může být v položení archeologické otázky v takové formě, aby na ní bylo možné odpovědět přírodními vědami. Nicméně, následně je nutné získaná přírodovědná data převést zpět do takové podoby, aby je bylo možné interpretovat humanitními obory. Intenzivní a neustálá výměna informací mezi přírodovědnými a humanitními obory je tedy zásadní pro pokládání správných otázek a interpretaci získaných dat¹.

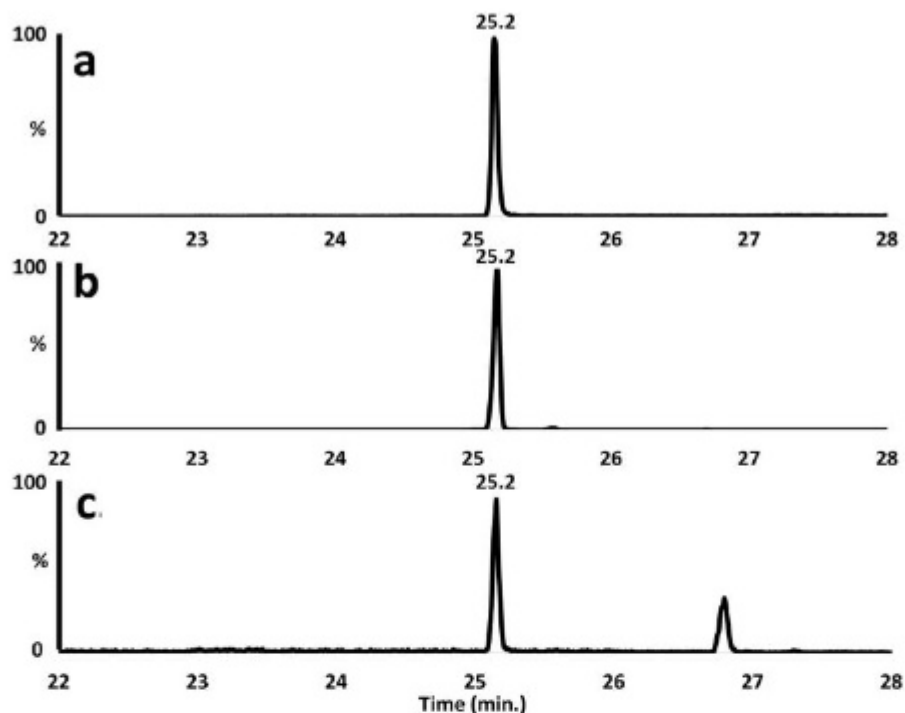
Práce I-IV popisují využití interdisciplinárního přístupu pro získání relevantních dat, díky kterým bylo možné detailně interpretovat archeologický kontext a přinést zásadní informace pro současnou archeologii.

V publikované práci I bylo cílem výzkumu chemická analýza výplně archeologické nádoby (záchranný výzkum v blízkosti obce Držovice; okres Prostějov) datované do období eneolitu. Vzorky výplně nádoby (tj. hlína z hrdla a horní části výduti) byly extrahovány postupně čtyřmi různými rozpouštědly, tj. voda, 0.05% hydroxid amonný v methanolu, 1% kyselina mravenčí v methanolu (obě v/v) a aceton. Všechny extrakty byly analyzovány pomocí technik plynové chromatografie s hmotnostní detekcí (GC/MS) a hmotnostní spektrometrií s přímou sondou (ASAP-MS). Ve srovnání s GC/MS (standardní technika pro detekci středně polárních a nepolárních látek z archeologických vzorků), technice ASAP-MS nepředchází chromatografická separace, ale díky kombinaci s tandemovou s vysoko-rozlišující hmotnostní spektrometrií je možné měření přesné hmoty (m/z). To nám následně umožňuje dopočítat prvkové složení látek, které má klíčový význam pro spolehlivou identifikaci analytu (mimo srovnání s autentickým standardem).

Pomocí GC/MS byl v chromatogramu vzorku hlíny detekován intenzivní signál m/z 440 (retenční čas 25,2 min.). Tato sloučenina byla identifikována jako rostlinný triterpenoid miliacin, který je popisován jako biomarker prosa setého (*Panicum miliaceum*). Je nutno zmínit, že tento signál nebyl nalezen ani v první a ani v druhé vrstvě půdy odebrané z nádoby (tj. horní vrstvy). Tato skutečnost vylučuje křížovou kontaminaci vzorků půdy. Na tomto místě je tedy nutné zmínit, že měření vhodných referenčních vzorků je tedy zásadní pro analýzu archeologických vzorků. Identifikace

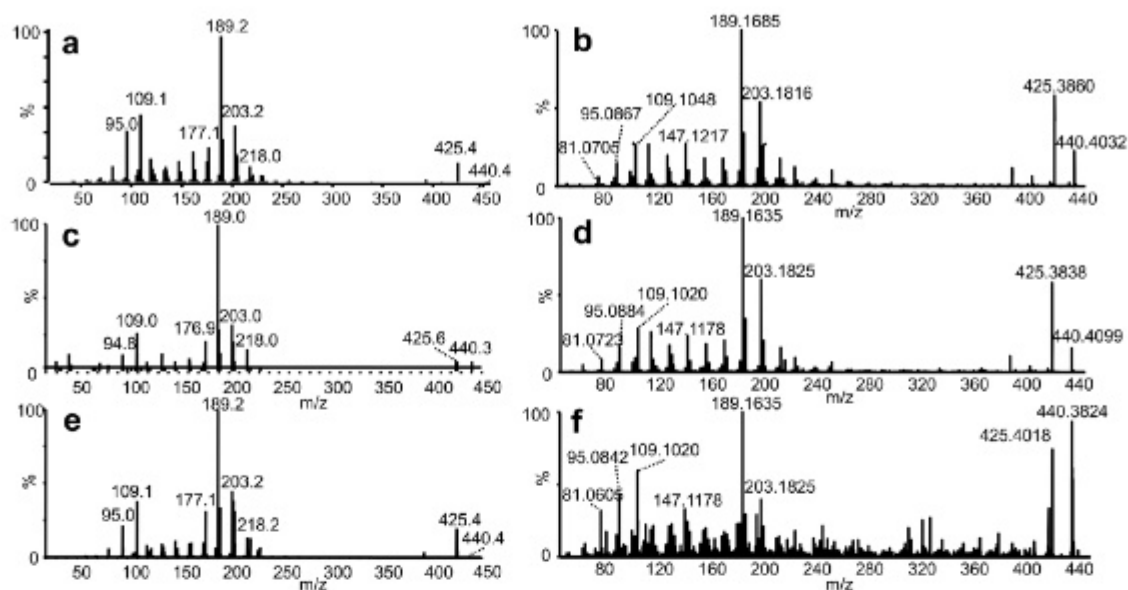
¹ Herrman, B., Wagner, G.A. Natural Science in Archaeology, Springer, Berlin 2009, DOI: 10.1007/978-3-540-87438-6

této sloučeniny byla založena na hodnotě m/z , porovnání s autentickým standardem, extraktem z prosa setého (hodnota m/z a retenční čas) a údajů z literatury (Obr. 1).



Obr. 1: Chromatogram standardu miliacinu (a), miliacin v prosu (b), neznámá sloučenina z výplně keramické nádoby (c).

Jednoznačné určení přítomnosti prosa není založeno pouze na přítomnosti miliacinu, ale také dalších pentacyklických triterpenů. Monitorování vícenásobných reakcí (MRM), tj. $440 \rightarrow 189$ detekovalo další dva píky (RT 27,3 a 30,0 min) ve vzorku, jejichž obsah byl výrazně nižší ve srovnání s miliacinem. Nicméně při monitoringu vybraných iontů (SIM) m/z 189 a 218 byla potvrzena přítomnost těchto fragmentů v látkách s RT 27,3 a 30,0, čímž byla potvrzena struktura pentacyklických triterpenů. MS/MS spektra miliacinu identifikováno ve vzorku dále potvrzuje identitu miliacinu (Obr. 2a,c,e).



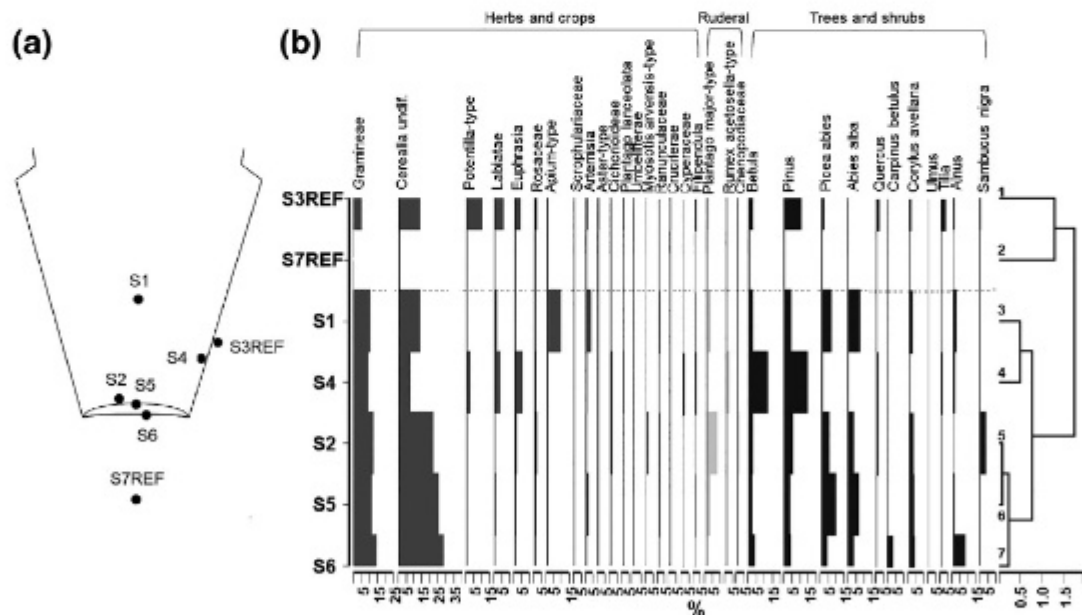
Obr. 2: Fragmentační spektra standardu miliacinu (a - GC/MS, b - ASAP-MS), miliacinu v prosu (c - GC/MS, d - ASAP-MS) a látky detekované ve výplni keramické nádoby (e - GC/MS, f - ASAP-MS)

V popisovaném článku byla také jako první využita technika ASAP-MS pro analýzu archeologického materiálu. Získané výsledky potvrzují přítomnost miliacinu ve vzorku (Obr. 2b,d,f). Technika ASAP-MS v použitém uspořádání (tj. v kombinaci s Q-TOF hmotnostním analyzátozem) poskytla informaci o přesné hmotnosti miliacinu v archeologickém vzorku, která silně podporuje identifikaci (byla naměřena m/z 440,3824 odpovídající s relativně malou odchylkou od jeho teoretické hmotnosti, dtm, 0,0194 Da, $C_{31}H_{52}O$). Nejdůležitější fragmenty detekované ve spektru jsou hodnoty m/z 203,1825 ($C_{15}H_{23}^+$, dtm 0,0025 Da), 189,1635 ($C_{14}H_{21}^+$, dtm - 0,0008 Da) a 109,1020 ($C_8H_{13}^+$, dtm - 0,0003 Da), které lze vysvětlit jako štěpení uhlovodíkového skeletu triterpenoidů (2,4a,7,7-tetramethyl-1-methylene-1,2,3,4,4a,5,6,7-oktahydronaftalen-yl, 2,7,7-trimethyl-1-methylene-1,2,3,4,4a,5,6,7-oktahydronaftalen-ylum a protonovaný 5,5-dimethyl-cyklohexa-1,3-dien). ASAP-MS má velký potenciál při analýze archeologického materiálu díky vysoké citlivosti a možnosti měření přesné hmoty (v konfiguraci s vysokorozlišujícím hmotnostním spektrometrem), ovšem bez možnosti rozlišení polohových izomerů.

Získaná data byla následně vyhodnocena odborníky z oblasti archeobotaniky (kolegové z Laboratoře archeobotaniky a paleoekologie, Jihočeská univerzita). Dosavadní výzkumy poukazují, že používání prosa v Čechách a na Moravě mezi neolitem a střední dobou bronzovou jsou řídké a náhodné. Na druhou stranu, využívání

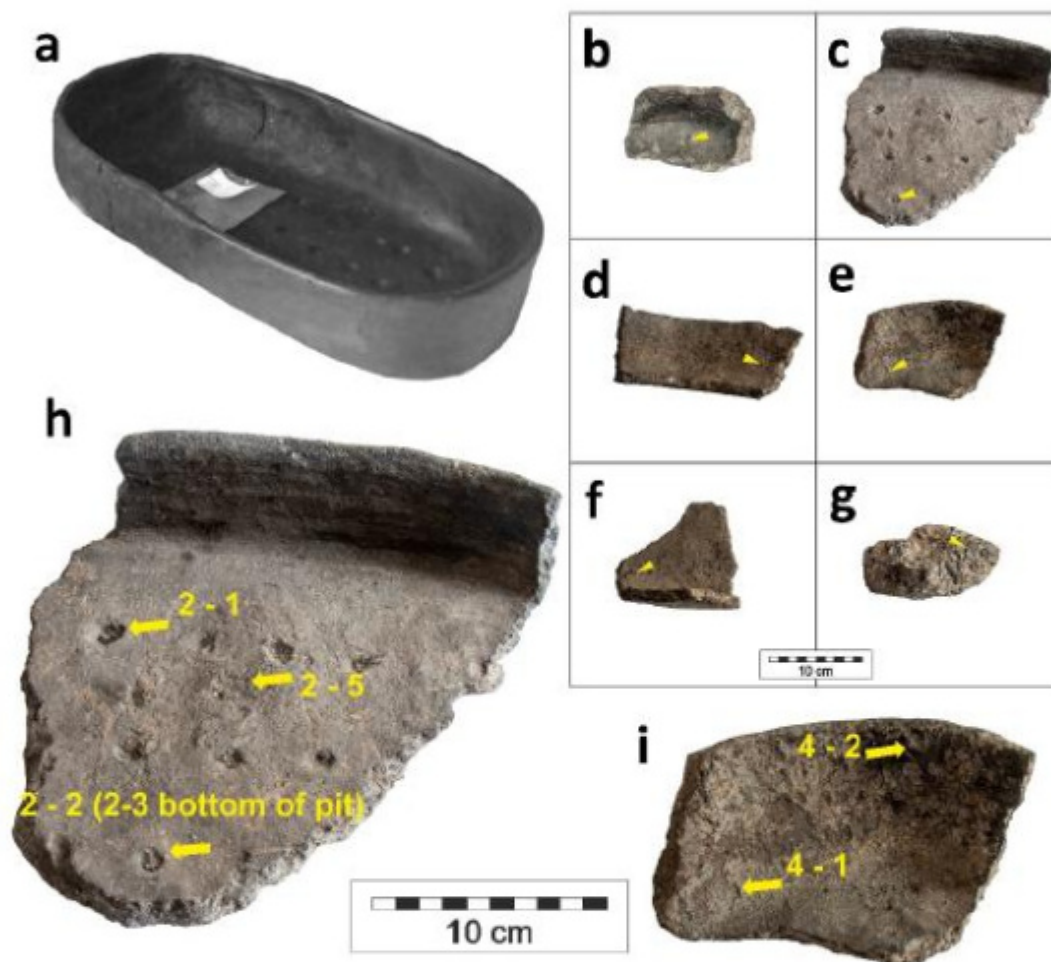
prosa se stalo běžnou praxí v průběhu střední doby bronzové (první objevy botanických zbytků prosa). Detekce biomarkerů prosa v pohřebním kontextu kultury se šňůrovou keramikou (Eneolit) je velmi důležitá a mimořádná. Je možné ji hodnotit jako první přímý důkaz využívání prosa ve střední Evropě.

Publikace II také popisuje detekci miliacinu pomocí GC/MS v archeologické nádobě a musíme říci, tento výsledek by bez dalších přírodních věd neposkytl důkaz nejstaršího bylino-prosného piva ve Střední Evropě. Nejvýznamnější je palynologická analýza popisující přítomnost spektra bylin a stromů (Obr. 3). Některé rody mají charakteristické vlastnosti (aroma, chuť, lékařské využití) a jsou známé jako přísada pro přípravu bylinných piv. Dále archeobotanická analýza škrobových zrn pomocí optické mikroskopie v polarizovaném světle poukazuje na tepelné a kvasné procesy v minulosti. Kombinace výsledků z přírodovědných analýz tedy poskytla informaci o bylino-prosné směsi, která byla vystavena „mokrému“ teplu (vaření) a kvasným procesům. Přenesení tohoto výsledku do archeologie a kulturní antropologie poukázalo na jistou podobnost s izolovanými africkými kmeny, kde se do současnosti vyrábí prosné pivo dle historických postupů. To následně vedlo k závěru, že nádoba obsahovala nápoj.



Obr. 3: Odběrová místa pro palynologickou analýzu (a; S1 – výplně ve střední části, S2 – dno, S3REF – vnější povrch, S4 – vnitřní povrch, S5 – horní bronzový kryt dvojitého dna; S6 – spodní bronzový kryt dvojitého dna, S7REF – písek z okolí), pylový diagram (b)

Interdisciplinární přístup je nejlépe patrný na publikaci III, která je zaměřena analýzu archaeobotanických a organických reziduí ze 7000 let starých keramických pekáčů (Obr. 4).

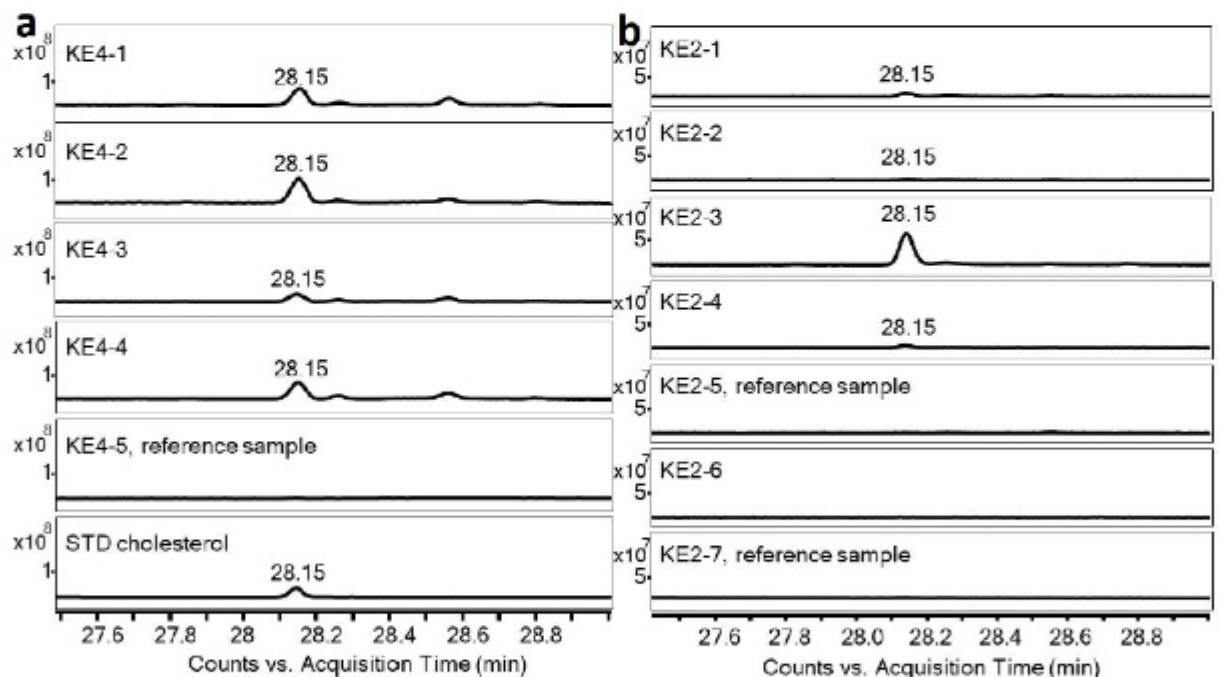


Obr. 3: Rekonstruovaný keramický pekáč KE7 (a), odebrané vzorky KE1 (b), KE2 (c), KE3 (d), KE4 (e), KE5 (f), KE6 (g), detail KE2 (h) a KE4(i).

GC/MS analýza organických reziduí odebraných z povrchu keramických pekáčů KE1-KE7 prokázala přítomnost živočišné složky bohaté na tuky na základě signálu cholesterolu (Tab 1). Identifikace cholesterolu byla potvrzena na základě srovnání s autentickým standardem cholesterolu, retenčním časem a fragmentačním spektrem (Obr. 4). Nejvýznamnějším vzorkem z keramických pekáčů byl vzorek KE4, kde byly nalezeny silné vrstvy připálené hmoty. Obsah cholesterolu v těchto vzorcích se pohyboval v rozmezí 0,44 – 0,66 mg.g⁻¹ (v referenčním vzorku z horního okraje pekáče byla koncentrace cholesterolu pod 0,01 mg.g⁻¹). Tento významný rozdíl v koncentraci cholesterolu ve vzorcích KE4 vylučuje křížovou kontaminaci z okolí. Vzorky z KE4

byly také analyzovány pomocí imunologických testů pro detekci denaturovaných proteinů. Tyto testy nejsou standardně vyráběny pro archeologickou praxi, ale v případě dodržení přesných postupů výrobce, je možné využít testy pro detekci alergenů. Vzorek KE4-2 (s vysokou koncentrací cholesterolu), poskytl pozitivní reakci na vepřové proteiny. Pozitivní reakce však byla zjištěna také u referenčního vzorku KE4-5. Na základě těchto výsledků byly provedeny testy kontaminace na vepřové bílkoviny, kde testy poukázaly na rozdíly ve vepřových proteinech u vzorku KE4-2 a KE4-5. Proteiny ve vzorku KE4-2 byly denaturovány při vysokých teplotách, zatímco u vzorku KE4-5 se vyskytovaly pouze nativní vepřové proteiny (pravděpodobně z vepřové kejdy).

Vedle cholesterolu byly ve vzorcích detekovány pomocí GC/MS také látky poukazující na přítomnost rozloženého dřeva/pryskyřic, tj. 18-norabietan (RT 16,65 min.) a reten (RT 18,64 min.). Tyto látky byly detekovány také v referenčním vzorku, avšak intenzita signálu byla 2-32krát nižší.

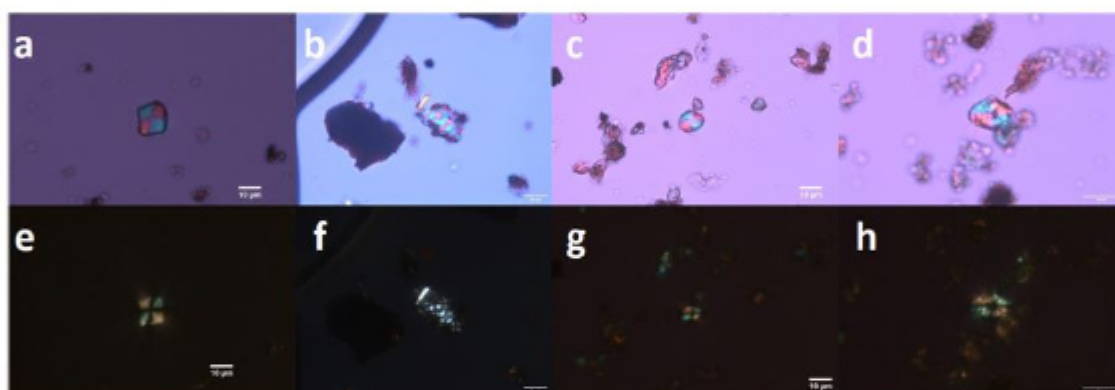


Obr. 4: GC chromatogram standardu cholesterolu a látky ve vzorcích odebraných z keramických pánví KE4 (a) a KE2 (b)

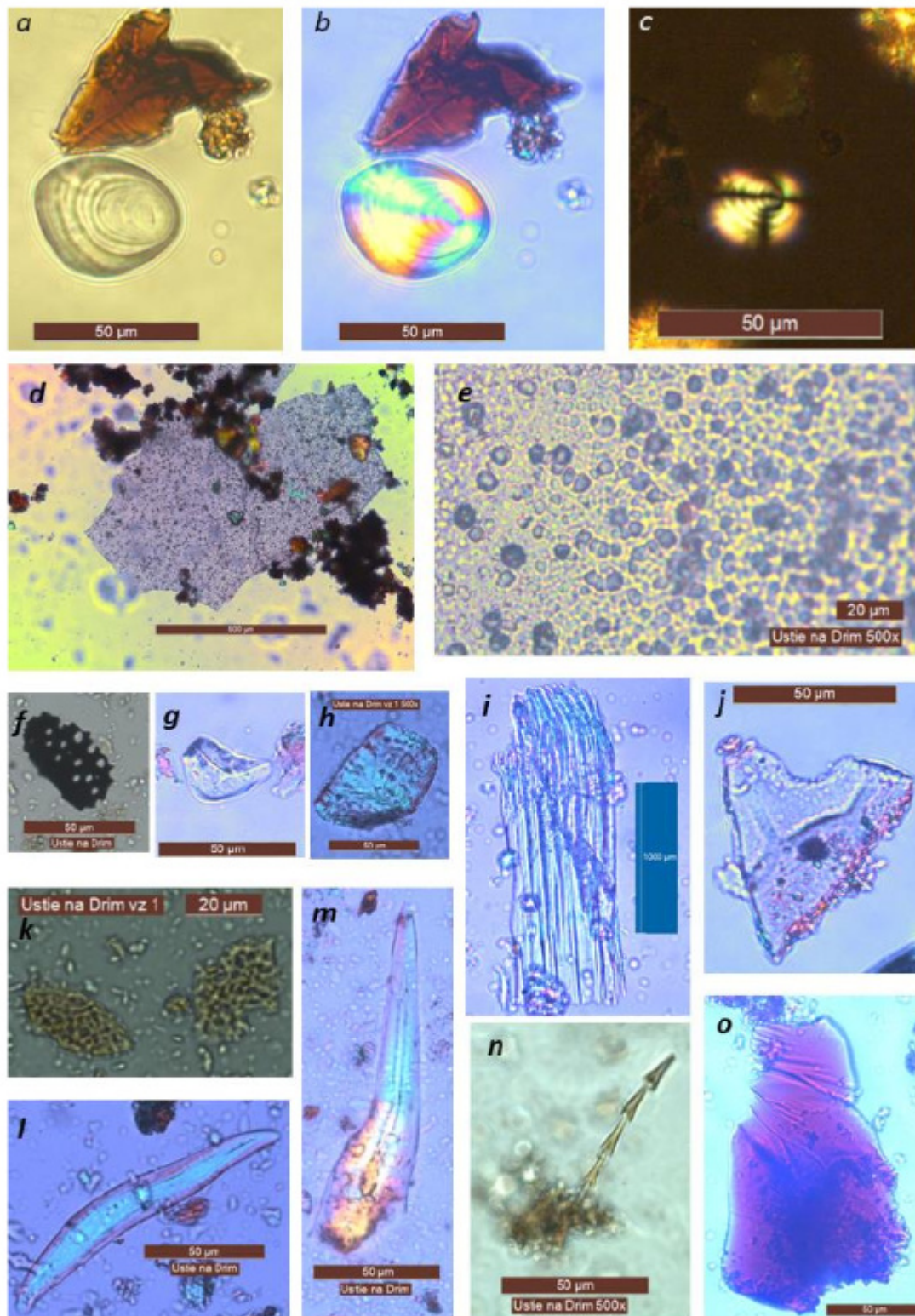
Tab. 1. Seznam analyzovaných vzorků se zaměřením na koncentraci cholesterolu, identifikaci škrobových zrn, fytolitu a mikrozbytků. SP: vzorek byl odebrán k mikroskopickému vyhodnocení; pozitivní: byl nalezen mikroobjekt; negativní: nebyl nalezen mikroobjekt).

Artefact	Sample	Concentration of Cholesterol (mg/g)	Phytoliths and Non-Pollen Objects	Starch	Position of Sample in Ceramic Pan
KE1	1	0.05	-	-	pit (residue)
KE1	2	0.08	-	-	pit (ceramic under KE1-1)
KE1	3	0.00	-	-	edge, the reference sample
KE1	SP1	-	positive	positive	pit
KE1	SP2	-	-	positive	edge
KE2	1	0.03	-	-	pit (residue)
KE2	2	0.01	-	-	pit (ceramic under KE2-1)
KE2	3	0.92	-	-	pit (residue)
KE2	4	0.04	-	-	pit (ceramic under KE2-3)
KE2	5	0.00	-	-	bottom, the reference sample
KE2	6	0.00	-	-	inner surface (organic temper)
KE2	7	0.01	-	-	surface (the reference sample)
KE2	SP3	-	-	negative	pit
KE2	SP4	-	-	-	pit
KE2	SP5	-	-	positive	edge
KE3	1	0.02	-	-	inner surface (close bottom part, baked mass)
KE3	2	0.13	-	-	inner surface (under edge, baked mass)
KE3	3	0.01	-	-	inner surface (ceramic under KE3-1)
KE3	4	0.34	-	-	inner surface (ceramic under KE3-2)
KE3	5	0.04	-	-	edge (the reference sample)
KE3	SP6	-	positive	positive	pit
KE3	SP7	-	-	negative	pit
KE4	1	0.44	-	-	inner edge (close bottom part, baked layer)
KE4	2	0.66	-	-	inner edge (close upper part, baked layer)
KE4	3	0.19	-	-	inner edge (ceramic under KE4-1)
KE4	4	0.46	-	-	inner edge (ceramic under KE4-2)
KE4	5	0.01	-	-	edge (the reference sample)
KE4	SP8	-	positive	positive	pit
KE4	SP9	-	-	positive	pit
KE5	1	0.09	-	-	inner edge (close bottom part, thin layer)
KE5	2	0.24	-	-	inner edge (close to KE5-1)
KE5	3	0.02	-	-	inner edge (ceramic under KE5-1)
KE5	4	0.16	-	-	inner edge (ceramic under KE5-2)
KE5	5	0.01	-	-	edge (the reference sample)
KE6	1	0.00	-	-	wall (close upper part, baked mass)
KE6	2	0.02	-	-	wall (close to KE6-1)
KE6	3	0.00	-	-	edge (the reference sample)
KE7	1	0.17	-	-	organic residue (taken before conservation)

Archaeobotanické analýzy prokázaly přítomnost různých druhů rostlin na základě přítomnosti škrobových zrn (Obr. 5) a fytolitů (Obr. 6). Přítomnost čeledi Lipnicovitých není jednoznačným ukazatelem využívání obilovin. Nicméně, ve vzorcích byly nalezeny chloupky larvy kožojedovitého brouka (*Trogoderma sp.*, Obr. 6n), který je hlavním škůdcem skladovaných produktů. Entomologická analýza přiřadila chloupek larvě *Trogoderma granarium* (Rušník obilní), která je hlavním škůdcem v obilí, luštěninách a výrobcích z nich. Kombinace pokročilé chemické analýzy s mikroskopickým hodnocením přineslo nové důkazy o životě pravěkých lidí. Nalezené keramické pánve tedy byly pravděpodobně použity pro přípravu pokrmů obsahujících maso z běžných hospodářských zvířat v kombinaci s obilovinami a planě rostoucími rostlinami.



Obr. 5: Škrobová zrna Běru z keramického pekáče KE2-SP5 (a,e); škrobová zrna Orobince nalezená v KE4-SP9 (b, f); škrobová zrna Lipnicovitých z KE2-SP5 (c,g); škrobová zrna Dubu v KE2-SP5 (d,h) (snímky pořízeny ve viditelném světle (a–d); snímky v polarizovaném světle (e–h)).



Obr. 6: Mikrozbýtky ve vzorcích SP1 (h,i,k), SP6 (f,l-o) a SP8 (a-e,g,j). (a-c) pravděpodobně škrobové zrna z vyšších rostlin, Liliovitě; (d,e) struktura složená z malých sféroidních fytolitů; (f) fragment dřevěného uhlí; (g-k) fytolity; (l-o) jiné organické zbytky (pravděpodobně živočišné); (n) fragment chlupu larev kožojedovitého brouka. Zvětšení 500x (kromě d,i).

3. Multimodální přístup

V mnoha případech je chemická analýza pouze jednou technikou nedostačující a získaná data je možná brát jako jeden z dílků „skládačky“. Z tohoto důvodu je vhodné správně kombinovat moderní instrumentální metody pro dosažení co nejdetailnějšího popsání, ve většině případů unikátního, vzorku. Publikace IV je zaměřena na rozbor surové barevné hmoty, která byla v 19. století používána pro přípravu fajánsů (Obr. 7). Je nutné zmínit, že v této době si každý toufar² hlídal své míchání barevných směsí a jejich dílna připomínala alchymistickou laboratoř.



Obr. 7: Surové hmoty fajánsů z 19. století nalezených v keramické nádobě (Prostějov)

V prvním kroku byla provedena geochemická analýza vzorků barevných směsí pomocí elektronové mikroskopie (Tab. 2). V případě bílého prášku byl nalezen výrazný obsah olova v rozmezí od 6 % do 18 %. S největší pravděpodobností se olovo vyskytuje ve formě oxidu z důvodu nízké koncentrace síry ve vzorku. Pozoruhodné je, že vysoké množství olova v různých formách bylo potvrzeno také LDI-MS v obou ionizačních módech, kde dominují signály klastrů s různým elementárním složením. Růžově zbarvený, jemnozrnný, prášek obsahoval oxidy SiO_2 , Al_2O_3 , CaO , PbO a K_2O (dále (hydr)oxidy P_2O_5 , FeO , TiO_2 , MgO a Na_2O v množství <1 hmot. %). Modrý prášek obsahuje hojné krystaly barytu (analýza EDX), který je běžnou přísadou při výrobě fajánsů. Tento minerál plnil funkci jako tavidlo, zvýšení lesku glazury a snížení množství bublin při tavení. Zbývající hmota obsahuje také SiO_2 , Al_2O_3 , PbO a FeO a v menších nebo stopových množstvích také CaO , P_2O_5 , MgO , SrO nebo Na_2O .

Kromě SEM-EDX byla provedena ICP-MS analýza pro získání přesné koncentrace prvků ve studovaných práscích a za účelem odhalení původu barvy (Tab. 3.). Jedním z nejběžnějších červených pigmentů používaných v glazurách/fajánsech bývá hematit

² Řemeslník (hrnčíř) vyrábějící fajánsové nádoby

α -Fe₂O₃ (resp. maghemit γ -Fe₂O₃), který způsobuje červené až hnědé odstíny v závislosti na podmínkách během vypalování. ICP-MS analýza poukázala, že barvivo v růžovém prášku je způsobeno sloučeninou železa, které se zde nachází v koncentraci 0,50 mg.g⁻¹, pravděpodobně ve formě hematitu. V historii se v minulosti také využívala měď ve formě měďnatých nebo měděných nanočástic jako červené barvivo ve sklářství, ale množství Cu použité v takových případech bylo asi 100x větší než v červeném prášku z Prostějova (0,26 mg.g⁻¹).

Tab. 2: EDX výsledky tří vzorků fajansů (wt%)

No. of Analysis	Sample	Na	Mg	Al	Si	P	S	K	Ca	Ti	Fe	Sr	Ba	Pb	Sum
1	#1	0.98	0.17	8.52	65.21	0.05	0.22	2.42	0.22	ND	0.94	ND	0.27	11.76	90.76
2	#1	0.85	0.27	6.40	66.54	0.05	0.15	1.87	0.27	ND	1.30	ND	ND	18.13	95.82
3	#1	0.36	0.28	0.62	101.83	0.42	0.43	0.11	0.05	ND	0.05	ND	ND	0.13	104.26
4	#1	1.37	0.69	9.21	75.92	0.54	0.65	2.16	0.33	1.45	1.70	ND	ND	6.59	100.62
1 (bulk)	#2	0.26	0.60	20.95	38.58	1.39	1.31	1.69	4.21	0.69	0.60	ND	ND	1.97	72.24
1 (bulk)	#3	0	0	4.23	9.17	0	8.51	0.04	0.83	ND	1.33	0.19	20.34	9.22	53.84
3 (bulk)	#3	0.03	0.32	21.92	33.99	2.67	1.11	1.08	4.22		7.85	0.67	0.27	8.21	82.34
2 (baryte)	#3						17.81		0		0	0	52.60	0	70.40
4 (baryte)	#3	0	0	0			27.83	0	0		0	0	56.26	0	84.09

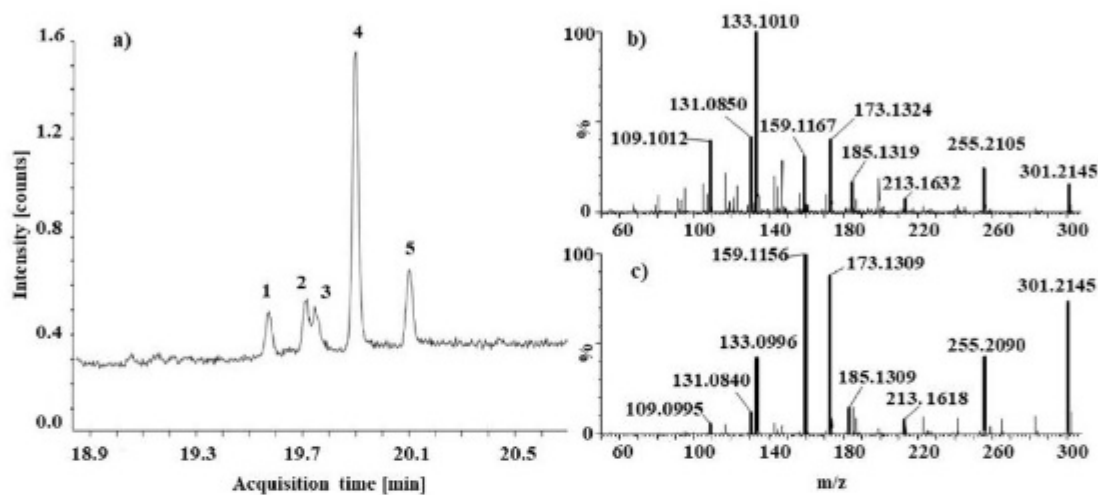
Tab. 3: ICP-MS výsledky v mg.g⁻¹

Sample	P	S	Ca	Na	Mg	Al	Si	K	Ti	V	Mn	Fe	Cu	Zn	Ga	Sr	Sn	Sb	Ba	Hg	Pb
1	0.3	0.6	<LOD	34.6	0.8	32	317	5.2	0.86	0.02	0.02	2.0	0.08	0.01	0.02	0.02	0.44	0.01	0.3	<LOD	6
2	3.2	3.3	4.4	1.1	1.3	51	223	4.0	0.07	0.03	0.01	0.5	0.26	0.02	0.22	0.15	0.02	0.05	4.3	0.01	35
3	0.6	14.0	14.0	1.2	0.6	11	101	0.9	0.04	0.03	0.03	4.0	0.13	0.10	4.84	3.32	0.17	0.10	86.0	0.43	232

U vzorku byla také provedena analýza za účelem potvrzení/vyvrácení přítomnosti organického pojiva. GC/MS s pyrolýzní jednotkou (py-GC/MS) prokázala přítomnost kyseliny abietové a pimarové ve vzorku růžové směsi. Tyto látky jsou v přírodě významně zastoupeny v pryskyřici produkované jehličnany, např. borovice, modřín či smrk.

Pro detailní analýzu organických látek se zaměřením jak na polární, tak i nepolární látky, byla aplikovaná metoda ASAP-MS v kombinaci s iontovou mobilitou (ASAP-IM-MS). Tato metoda potvrdila přítomnost pryskyřice. Sloučenina s m/z 301,2145 (C₂₀H₂₉O₂⁺) odpovídá struktuře protonované kyseliny dehydroabietové s odchylkou od teoretické hmotnosti (dtm) -2,3 mDa. Fragmentační spektra kyseliny dehydroabietové v růžovém prášku a autentického standardu kyseliny dehydroabietové jsou uvedena na obrázku 8b,c. Kromě signálů náležejících k pryskyřici byly ve vzorku detekovány signály s hodnotou m/z 463,4858, 491,5186 a 519,5491 odpovídají látkám C₃₂H₆₃O₁⁺, C₃₄H₆₇O₁⁺, C₃₆H₇₁O₁⁺. Tyto signály byly předběžně identifikovány jako degradované složky včelího vosku na základě srovnání s hmotnostním spektrem standardu. Důkazem

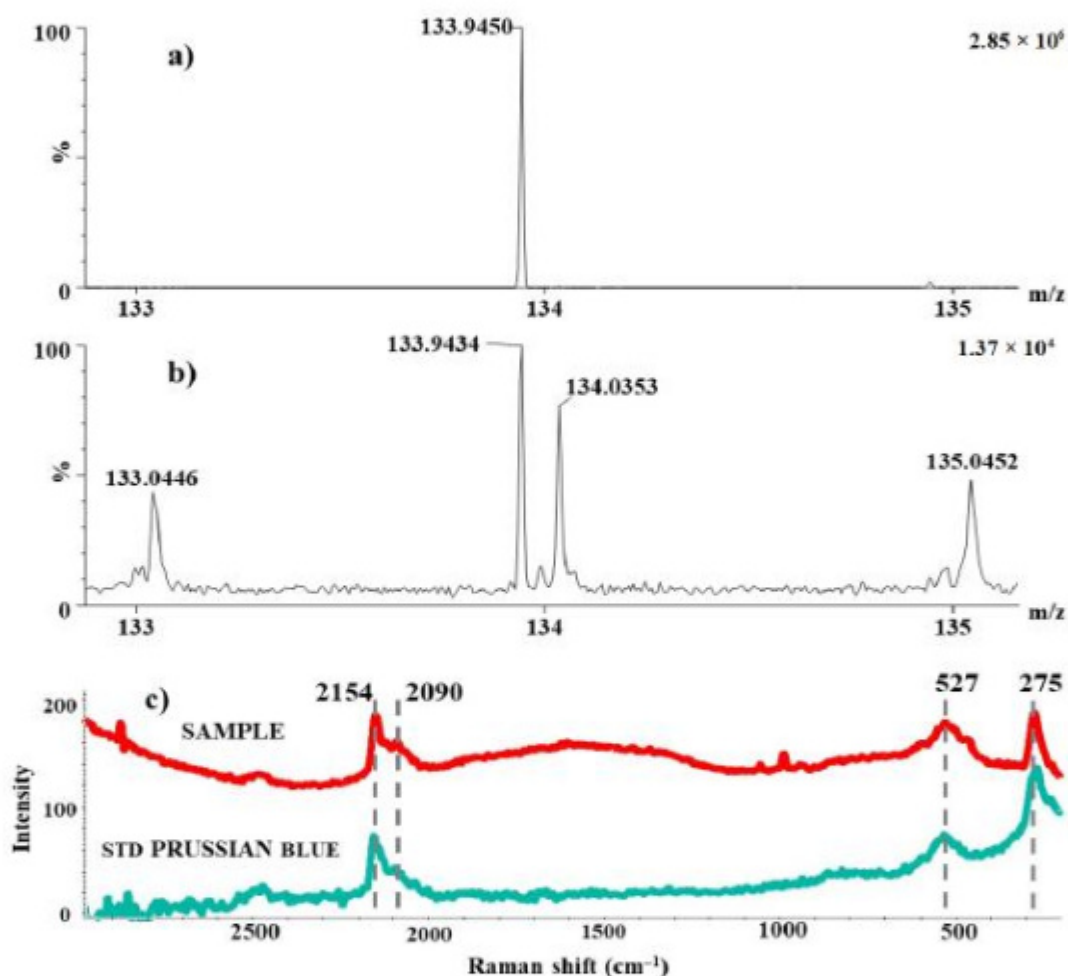
přítomnosti včelího vosku byla molekula $C_{42}H_{83}O_2^+$ (619,6393 Da) s dtm $-0,8$ mDa indetifikována jako ester kyseliny palmitové, který je typickou složkou včelího vosku. Kromě toho byly detekovány také diacylglyceroly s m/z 607,5640 ($C_{39}H_{75}O_4^+$; dtm $-2,5$ mDa; distearoylglycerol, SS), 579,5327 ($C_{37}H_{71}O_4^+$; dtm $-2,5$ mDa; palmitoyl-stearoyl glycerol; PS) a 551,4991 ($C_{35}H_{67}O_4^+$; dmt $-4,8$ dtm; dipalmitoylglycerol, PP). Tyto sloučeniny se běžně nacházejí v materiálech bohatých na tuky. Růžový prášek byl tedy pravděpodobně připravován podobným způsobem jako pigmenty pro tradiční olejomalby.



Obr. 8: Pyrogram růžového prášku (1: kyselina pimarová, 2: kyselina isopimarová, 3: neznámá sloučenina, 4: kyselina dehydroabietová a 5: kyselina abietová) (a); ASAP-IM-MS fragmentační spektra sloučeniny m/z 301.2152 v růžovém prášku (kolizní energie 20 V) (b) a ve standardu kyseliny dehydroabietové (kolizní energie 20 V) (c).

Při analýze modrého prášku se vycházelo z předpokladu, že modré barvy při výrobě glazury se běžně dosahuje přidávkem Cr, Co nebo Cu. Nicméně, ve vzorku prášku nebyl detekován žádný z výše uvedených prvků. Na základě výsledků ICP-MS obsahovala většina modrého prášku zvýšené množství železa (přibližně $4 \text{ mg} \cdot \text{g}^{-1}$), které by mohlo být zdrojem modrého zbarvení jako hexakynoželezitanový pigment $\text{Fe}_4[\text{Fe}(\text{CN})_6]_3$, běžně známý jako pruská modř (PB). Přítomnost PB byla následně identifikována a prokázána pomocí průtokové injekční analýzy s kombinací s hmotnostní spektrometrií s ionizací elektrosprejem (FIA/ESI-MS) a Ramanovy spektroskopie. Spektrum FIA/ESI-MS standardu PB obsahovalo nejintenzivnější signál $[\text{Fe}(\text{CN})_3]^-$ při m/z 133,9443 Da (Obr. 9a). Stejný signál byl detekován také ve vzorku modrého prášku, tj. m/z 133,9434, dtm $-0,8$ mDa (Obr. 4b). Tyto výsledky byly následně

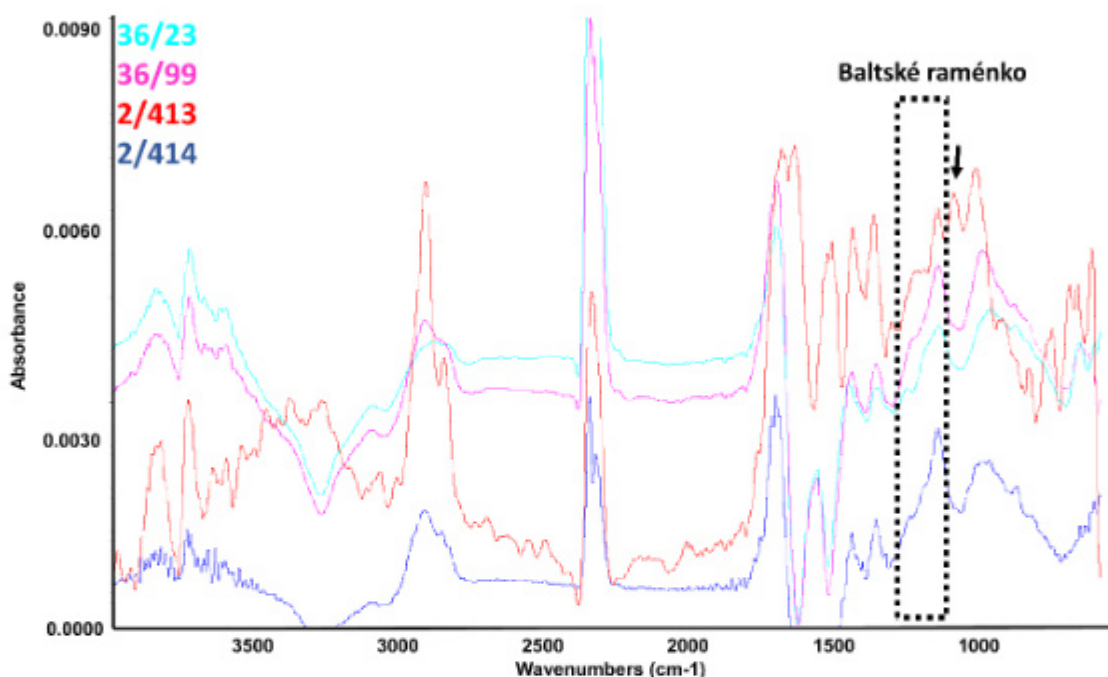
podpořeny Ramanovými spektry referenčního materiálu a vzorku (Obr. 9c). V Ramanových spektrech byly nalezeny čtyři významné pásy, tj. 2154, 2090, 527 a 275 cm^{-1} . Vibrace při 2154 cm^{-1} a 2090 cm^{-1} odpovídá $\nu(\text{C}\equiv\text{N})$ vibraci. Zbývající dva pásy při 527 a 275 cm^{-1} odkazují na vibrace vazby Fe–C a deformační vibrace vazby Fe–CN–Fe. Pomocí SEM-EDX a ICP-MS bylo ve vzorku stanoven vyšší obsah síry, který pravděpodobně poukazuje na tradiční přípravu PB, tj. použití zeleného vitriolu ($\text{FeSO}_4 \cdot 7\text{H}_2\text{O}$) a sušená hovězí krev jako zdroj kyano a/nebo ferrokyanidových skupin.



Obr. 9: MS spektrum PB standardu (a) a připraveného extraktu ze vzorku modrého prášku (b), spektrum modrého prášku a PB standardu měřeno pomocí Ramanovy spektroskopie (c).

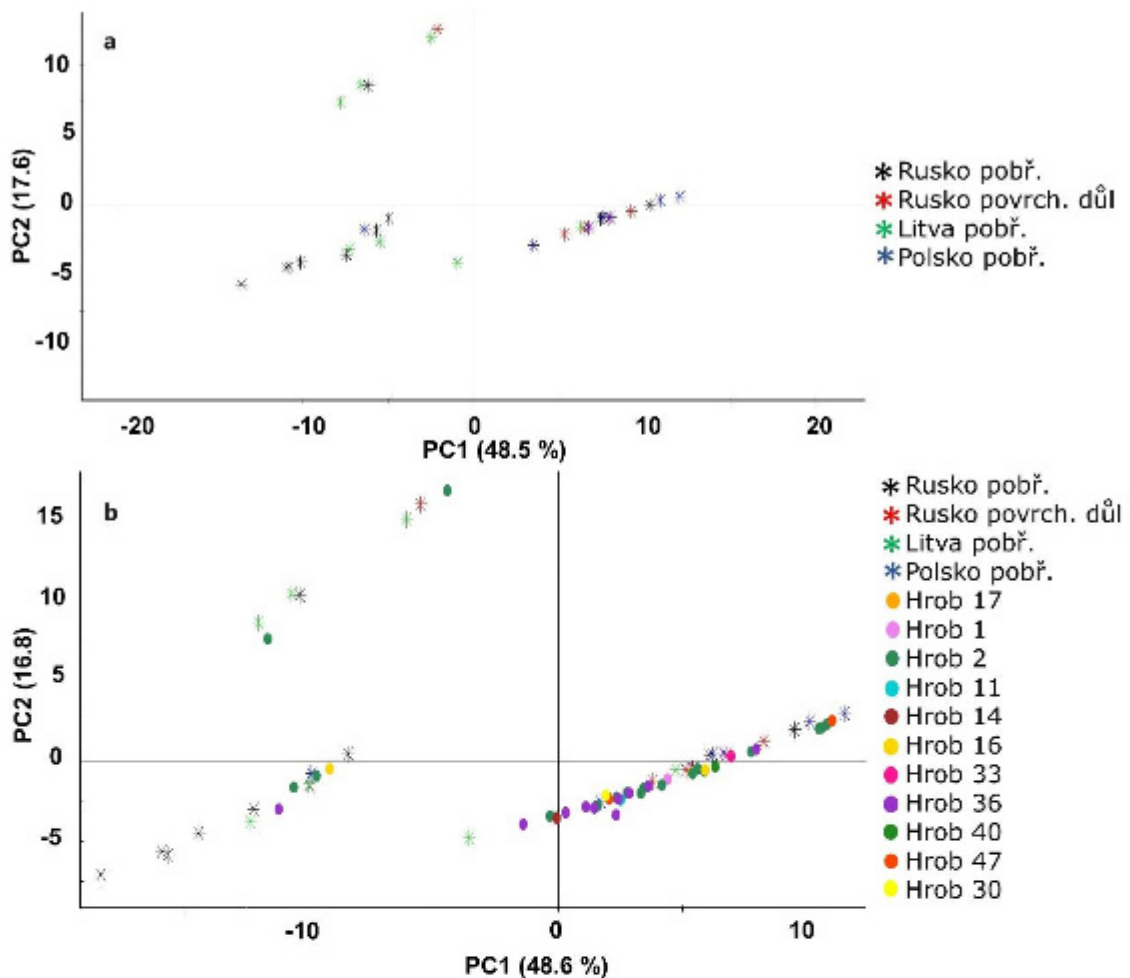
V publikacích V a VI je zdůrazněna nutnost aplikování série různých analytických technik pro stanovení původu jantarových artefaktů. Jantar, jak je známo, je fosilizovaná pryskyřice a její ložiska lze v podstatě nalézt po celém světě. Vznik jantaru je ovlivněn mnoha faktory (druh rostliny, stáří, geografickým podnebím atd) a z tohoto

důvodu se jednotlivé vzorky mohou lišit svými chemickými a fyzikálními vlastnostmi. V současné době se k analýze jantarových artefaktů využívá velká řada analytických technik, kde nejrozšířenější je infračervená spektroskopie s Fourierovou transformací (FTIR), u které je sledován pás s vrcholem při 1160 cm^{-1} a raménkem od 1175 do 1250 cm^{-1} (signál je označován jako tzv. „Baltské raménko“) (Obr. 10)



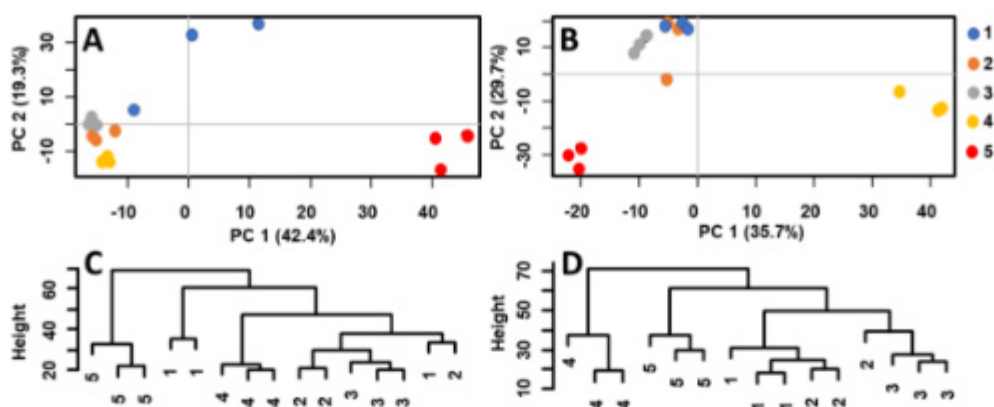
Obr. 10: Infračervená spektra jantaru z archeologického výzkumu v Mikulovicích u Pardubic

Pro podrobnější charakteristiku jantaru byla na našem pracovišti jako první aplikována LDI-MS v kombinaci s vícerozměrnou analýzou (analýza hlavních komponent, PCA). Předběžná data z LDI-MS analýzy surových jantaru z pobřeží Ruska (Donskoe), Litvy (Palanga) a Polska (Gdaňsk) a povrchového Ruského dolu (Jantarny) poukázaly na chemickou podobnost vzorků z pobřeží Polska a ruského povrchového dolu (Obr. 11a). Do připraveného statistického modelu byla následně zahrnuta data z LDI-MS analýzy vzorků jantaru z lokality Mikulovice u Pardubic. V PCA modelu je patrná segregace dat ve směru první komponenty. Většina studovaných vzorků se nachází v klastru odpovídající lokalitám polského pobřeží a/nebo ruského povrchového dolu (Obr. 11b).



Obr. 11: PCA score plot vzorků surových jantarů z lokalit v blízkosti Baltského moře (a) a archeologické vzorky z lokality Mikulovice (b).

Statistická analýza, jako hlavní nástroj pro nalezení významných rozdílů v datech, byla aplikována také v publikaci VII. Extrakty ze dvou výplní nádob byly analyzovány pomocí hmotnostní spektrometrie s laserovou/desorpcí ionizací za přítomnosti matrice (MALDI-MS) a naměřená data byla následně vyhodnocena pomocí statistických metod jako je PCA, klastrová analýza a ortogonální projekce do latentních struktur – diskriminační analýza (OPLS-DA) (lokalita a postup extrakce je stejný jako v publikaci I). Z obrázku 12 je patrné, že vzorky hlíny ze dna (tj. vrstvy 4 a 5) se výrazně liší od vzorků hlíny z horní části nádoby. Tento výsledek nám ukazuje výraznou změnu chemického složení horních a spodních částí výplně nádob. Ke studiu podobnosti konkrétních vrstev bylo použito hierarchické shlukování. Obrázek 12C,D ukazuje dendrogramy vztahů mezi měřenými vzorky z keramických nádob č. 4 a 5.



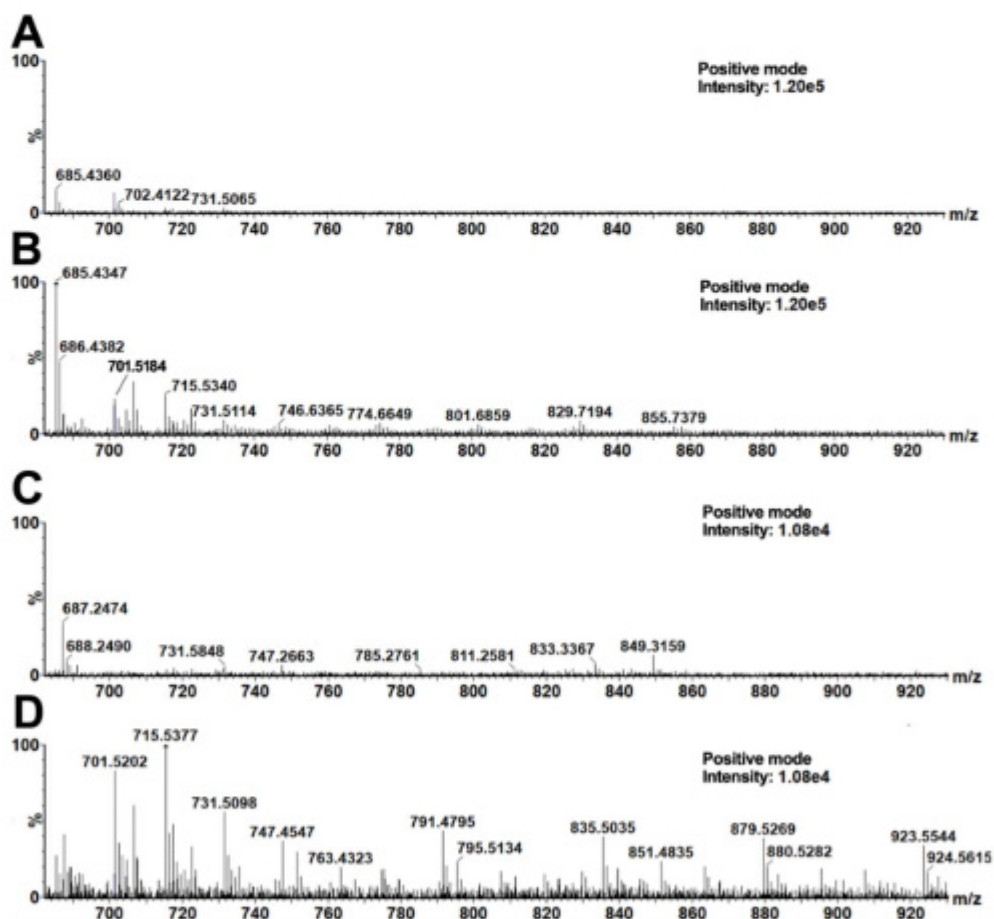
Obr. 12: PCA analýze MALDI-MS dat z acetonových extraktů hlíny a dendrogramy pro nádobu č. 4 (A,C) a nádobu č. 5 (B,D).

Pro nalezení významných markerů ve spodních vrstvách výplně nádob byla použita OPLS-DA. Markery s nejvyšší variabilitou a současně spolehlivostí byly odebrány z nízkorizikové oblasti vhodného S-grafu. Pro naše účely byl region s nízkým rizikem definován jako rámeček s následujícími souřadnicemi: $p[1] = 30\text{--}100\%$ a $p[2] = 75\text{--}100\%$ od nejvyšší hodnoty na ose x a y. Tab. 4 zobrazuje významné markery spodních půdních vrstev z keramických nádob č. 4 a č. 5. Rozdíly mezi dvěma sousedními signály příslušných markerů odpovídaly homologním přírůstkům skupiny CH_2 (tj. $\Delta m/z(1) = 687,4951\text{--}673,4808 = 14,0143$; $\Delta m/z(2) = 14,0163$; $\Delta m/z(3) = 14,01$) a kyslík $\Delta m/z(4) = 15,9721$). Tyto byly identifikovány jako draselné adukty triacylglycerolů (TAG). Výsledky byly srovnávány s literaturou³ a profil detekovaných TAG odpovídá mléčným tukům.

³ Picariello, G.; Sacchi, R.; Addeo, F. (2007) One-step characterization of triacylglycerols from animal fat by MALDI-TOF MS. *Eur. J. Lipid Sci. Technol* 109, 511–524.

Tab. 4: Seznam nejvýznamnějších markerů detekovaných ve spodních vrstvách keramických nádob (CN – počet uhlíků v molekule; DB – počet dvojitých vazeb).

	<i>m/z</i>	CN/DB	Theoretical Formula	dtm (mDa)
Ceramic vessel no. 4	673.4879	36:2	C ₃₉ H ₇₀ O ₆ K	-7.0
	687.5005	37:2	C ₄₀ H ₇₂ O ₆ K	-3.9
	701.5178	38:2	C ₄₁ H ₇₄ O ₆ K	-5.6
	715.5337	39:2	C ₄₂ H ₇₆ O ₆ K	-5.8
	731.5103	39:2	C ₄₂ H ₇₆ O ₇ K	12.5
Ceramic vessel no. 5	673.4808	36:2	C ₃₉ H ₇₀ O ₆ K	0.1
	687.4951	37:2	C ₄₀ H ₇₂ O ₆ K	1.5
	701.5114	38:2	C ₄₁ H ₇₄ O ₆ K	0.8
	715.5286	39:2	C ₄₂ H ₇₆ O ₆ K	-0.7
	731.5007	39:2	C ₄₂ H ₇₆ O ₇ K	22.1



Obr. 13: MALDI-MS spektra acetonových extraktů půdních vzorků z keramické nádoby č. 4 (A,B) a č. 5 (C,D). Spektra A,C jsou referenční extrakty z horních vrstev nádob a spektra B,D ze dna nádob.

Výsledky z MALDI-MS dokázaly celý výzkum nasměřovat konkrétním směrem, a z toho důvodu bylo nutné provést cílené imunochemické testy na nativní β -laktoglobulin (Tab. 5). Data potvrdila přítomnost zbytků hovězí mléčné bílkoviny ve spodní vrstvě půdy nádoby č. 5 (u vzorku půdy ze dna nádoby č. 4 nebyla pozitivní reakce na β -laktoglobulin). Přítomnost mléčných výrobků byla také testována ELISA kitem na kasein. Pozitivní reakce byla pozorována v obou studovaných nádobách. Tyto údaje potvrdily přítomnost mléčných výrobků v obou keramických nádobách. Využití mléčných výrobků ve starověké stravě již prokázalo mnoho autorů, ale v tomto konkrétním příkladu se jedná o první aplikaci hmotnostní spektrometrie s laserovou desorpčí/ionizací za spoluúčasti matrice pro analýzu zbytků mléčného tuku v pravěkých keramických nádobách. Tyto výsledky představují první přímý doklad o využití mléčných výrobků v období eneolitu v kultuře Moravské šňůrové keramiky. Naše data týkající se využití mléka v období raného neolitu–eneolitu ve východní střední Evropě (střední Podunají) významně rozšiřují dřívější důkazy o používání mléčných výrobků v západní střední Evropě (Německo, Švýcarsko)

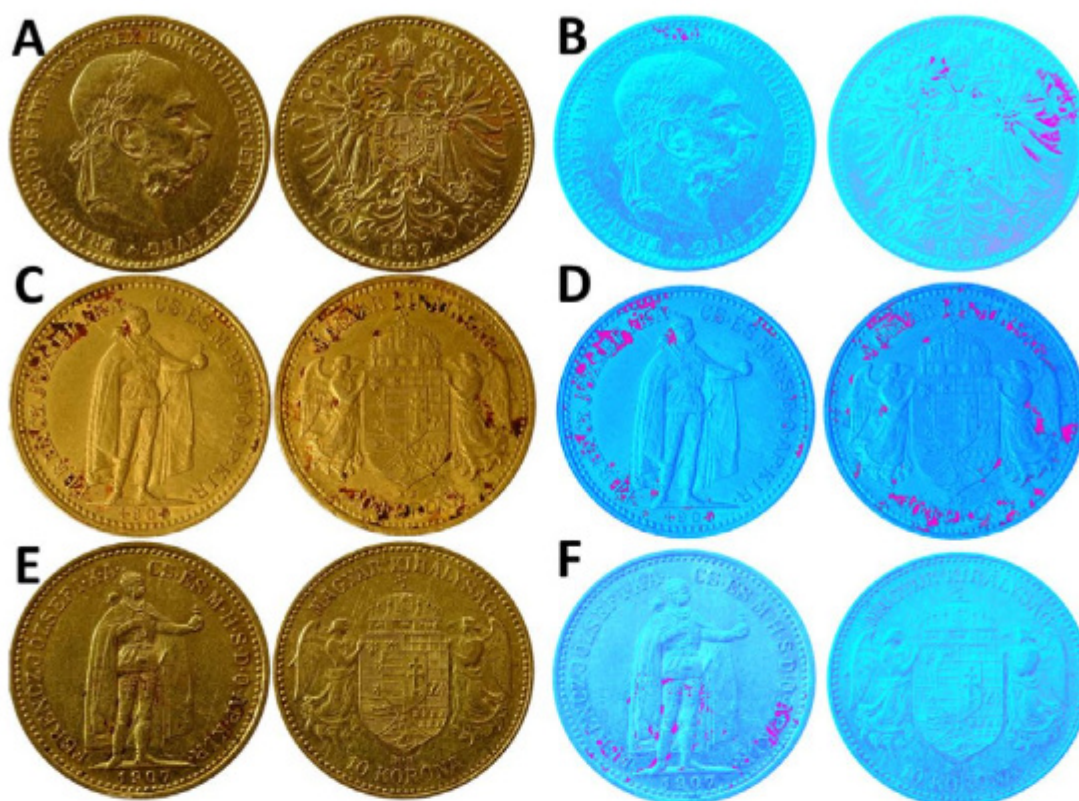
Tab. 5: Výsledky imunochemických testů vzorků hlíny ze dna nádob.

	Casein (ppm)	Evaluation	Cattle β LG (ppm)	Evaluation
Negative control	0.02	0	1.32	0
Positive control	0.2 *	+	0.021 **	+
Ceramic vessel no.4	0.36	+	1.81	0
Ceramic vessel no.5	0.52	+	0.044	+

4. Destruktivní vs. nedestruktivní přístup

Spolupráce mezi filozofickými (archeologie, historie umění apod.) a přírodními vědami nabývá se vzrůstajícími technickými možnostmi stále většího významu. S vývojem instrumentálních technik a současným zvyšováním citlivosti těchto přístrojů jsou požadavky na množství vzorku stále menší. Nicméně, před započítím odběru vzorků je velmi důležité provést průzkum pomocí neinvazivních a nedestruktivních metod. Tento přístup je preferován, neboť většina vzorků hmotného kulturního dědictví podléhá určitému typu ochrany a odběry nejsou žádoucí. Navíc je možné takto zachovat strukturu a vlastnosti vzorku, což je důležité pro další studium nebo aplikace. Příkladem nedestruktivního přístupu jsou publikace VIII a IX.

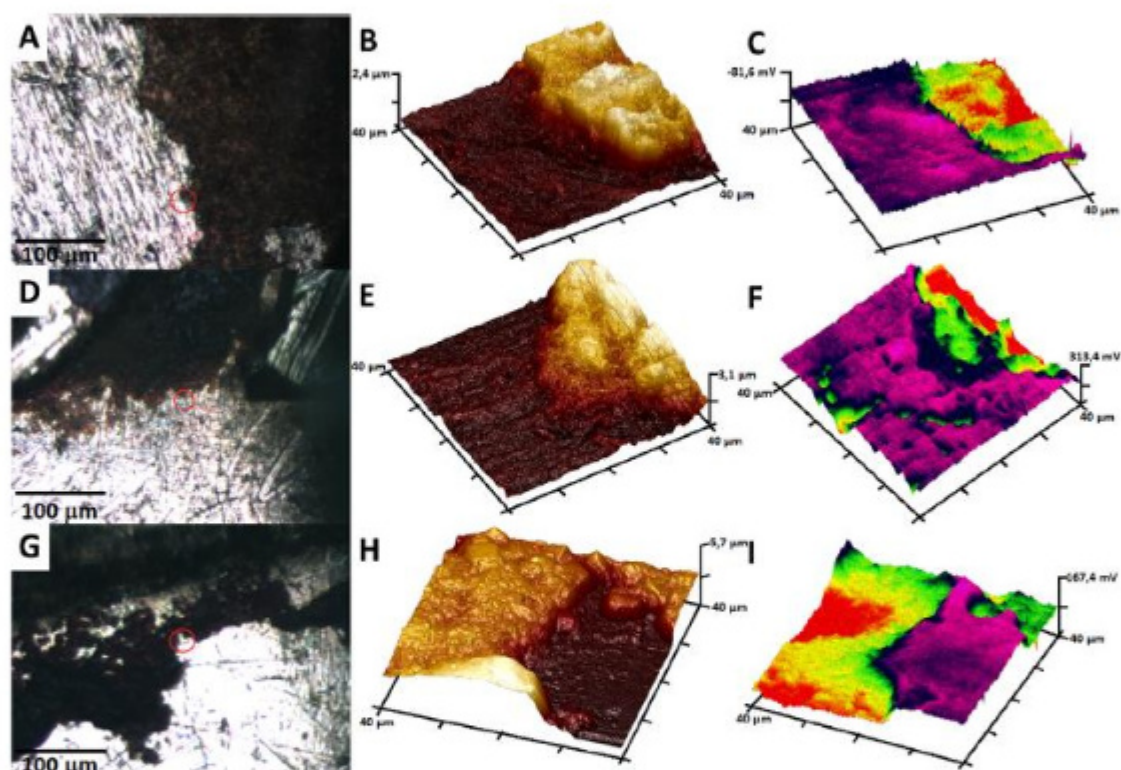
Publikaci VIII by sice bylo možné zařadit do kapitoly Multimodální přístup z důvodu využití velkého množství analytických technik, ale hlavní cílem byla nedestruktivní analýza "zkorodovaných" zlatých mincí (Obr. 14) pomocí energiově-disperzní rentgenové fluorescenční spektroskopie (XRF), mikroskopie ve viditelném světle (LM) a digitální mikroskopie (DM), skenovací elektronové mikroskopie kombinované s energiově-disperzní rentgenovou spektroskopií (SEM/EDS), rentgenovou fotoelektronovou spektroskopií (XPS), Ramanovou mikroskopií, rentgenovou práškovou mikrodifrakcí (μ -XRPD), mikroskopií atomárních sil (AFM) a Mössbauerovou spektroskopií s za účelem určení původ červených („korozních“) skvrn.



Obr. 14: Tři Rakousko-uherské 10 Korony 1897 (mincovna Vídeň, A,B), a 10 Korona 1905 (C, D) a 1907 (E, F) (mincovna Kremnice). Obrázky B, D, F jsou zobrazeny ve falešných barvách pro zvýraznění „korozních“ vrstev.

Mince v této studii byly ve větším měřítku pokryty červenými skvrnami. Pomocí digitální mikroskopie bylo možné přibližně stanovit tloušťku povrchové vrstvy, která se pohybovala okolo 14 μm . Pro detailní určení morfologie a elektrochemického potenciálu v oblastech zasažených "korozí" byla použita technika AFM. Zaznamenané topografické snímky ukazují rovný povrch zlaté mince a poté výrazně vyvýšené zkorodované části (Obr. 15). Výškový rozdíl činí přibližně 1,7, 2,2 a 4,6 μm u zlatých mincí. Tyto hodnoty jsou zhruba 12-33krát nižší než výška stanovená z digitální mikroskopické analýzy. Tento rozdíl v určení výškového profilu může být způsoben měřením relativně menší plochy a okraje skvrny technikou AFM ve srovnání s DM. Naopak měření tloušťky v DM může být silně ovlivněno odrazem (tj. DM nemůže přesně zaostřit). Současně získaná mapa elektrochemických potenciálů z povrchu vzorku (Obr. 15 C,F,I) ukazuje rozdíl mezi zkorodovanou částí (červená) a zbytkem skenované oblasti (fialová), která je na základě vyššího potenciálu tvořena ušlechtlejšími kovy.

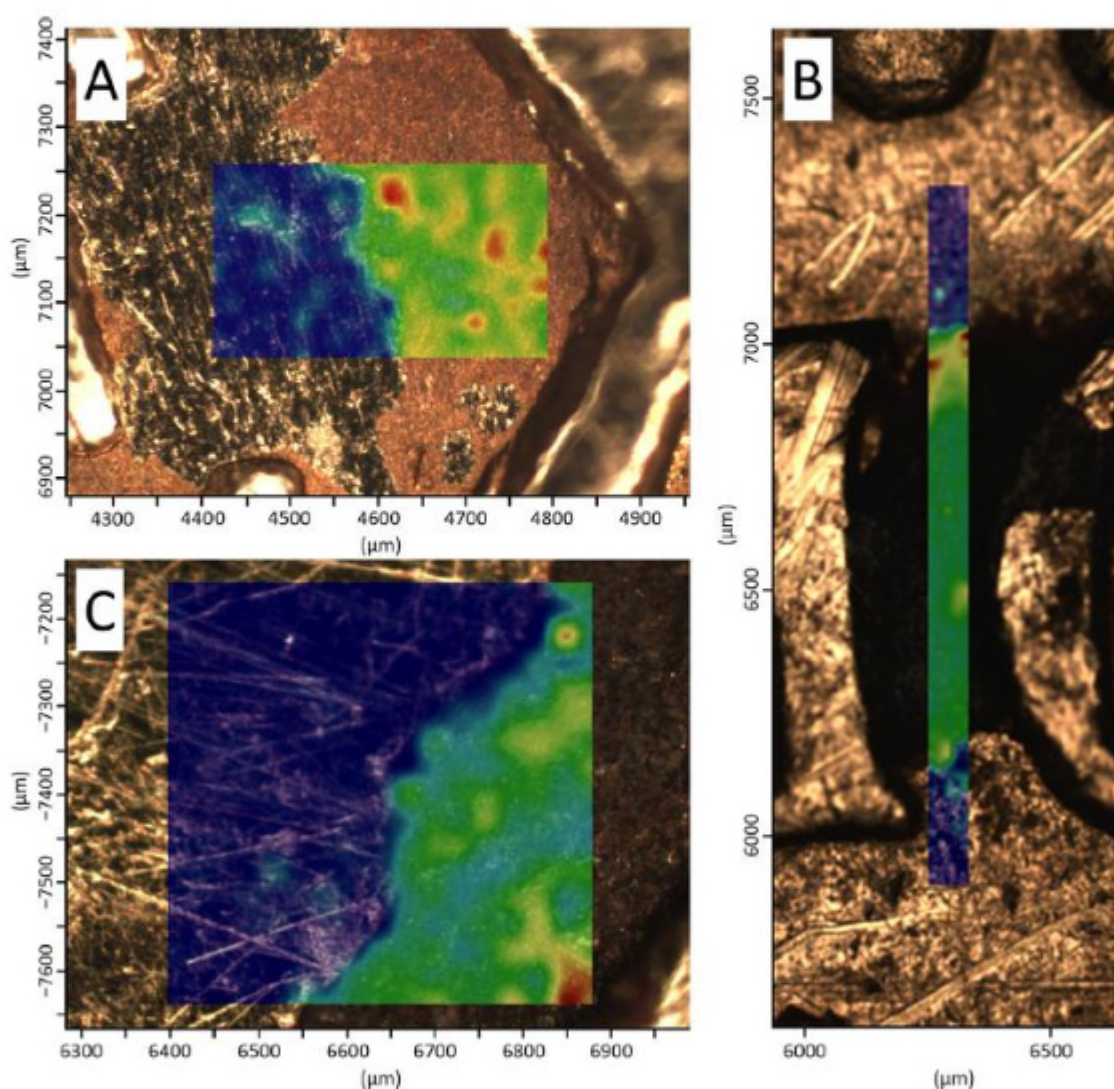
Stanovení chemického složení červených skvrn bylo v prvním kroku provedeno pomocí XRF s Mo aperturou. Přístroj XRF Spectro Xepos neumožňuje přesnou lokalizaci rentgenového paprsku na vzorku a měření velké plochy může být nepraktické. Z tohoto důvodu byla pro přesné vymezení zájmové oblasti vytvořena Mo apertura (do Mo plíšku byl vyříznut otvor o velikosti $3,1 \times 3,3$ mm, tj. $10,5$ mm²), která byla umístěna přímo na povrch mince. Měření ukazuje vyšší obsah železa ve všech třech vzorcích zlatých mincí. K podobným závěrům bylo dosaženo pomocí Mössbauerovy spektroskopie, tedy že korozní vrstva je tvořena železem.



Obr. 15: Vybraná oblast na povrchu mincí z let 1897, 1905 a 1907 (A, D, G), 3D topografický obraz získaný pomocí AFM v režimu „Tapping Mode“ a 3D potenciálová mapa mince z roku 1897 (B, C), 1905 (E, F) a 1907 (H, I)

Pro určení oxidačního stavu železa byla použita technika XPS, kdy bylo prokázáno, že v korozní vrstvě převažuje oxidační stav Fe^{3+} , nicméně oxidační stav Fe^{2+} byl detekován také, i když ve výrazně nižší intenzitě. Tím, že korozní vrstva je tvořena krystalickou strukturou železa, bylo možné využít Ramanovu mikroskopii pro přesnější určení složení Fe vrstvy, kdy předpokládáme přítomnost goethitu nebo hematitu. Goethit lze v Ramanově spektru snadno identifikovat díky pásu při 385 cm⁻¹. Nicméně,

někdy jsou pásy goethitu překryty pásem hematitu při 412 cm^{-1} (vibrace Fe-O), tím může dojít k posunu maxima pro pás 385 cm^{-1} . V analyzovaných vzorcích byl detekován nejvýznamnější pás při 394 cm^{-1} . Tento signál náleží Fe-O/-OH. Zajímavý poznatek byl, že zvyšováním energie laseru z 10 na 20 mW docházelo k přeměně goethitu na hematit, což bylo možné pozorovat změnou poměru signálů $394/293\text{ cm}^{-1}$. Výsledky z Ramanovy mikroskopie ukazují konzistentní distribuci goethitu v červených skvrnách při 394 cm^{-1} (Obr. 16 A-C). Pro jednoznačné potvrzení fázového složení korozního produktu železa bylo použito μ -XRPD, kde spektra jednoznačně potvrzují přítomnost oxy-hydroxidu železa v červených skvrnách.



Obr. 16. Ramanova mikroskopie povrchu Rakousko-Uherské 10 Korony 1897 (A), 1905 (B) a 1907 (C) a distribuce pásu při 394 cm^{-1} . (Nejnižší intenzita signálu je zobrazena modrou barvou a nejvyšší červenou barvou).

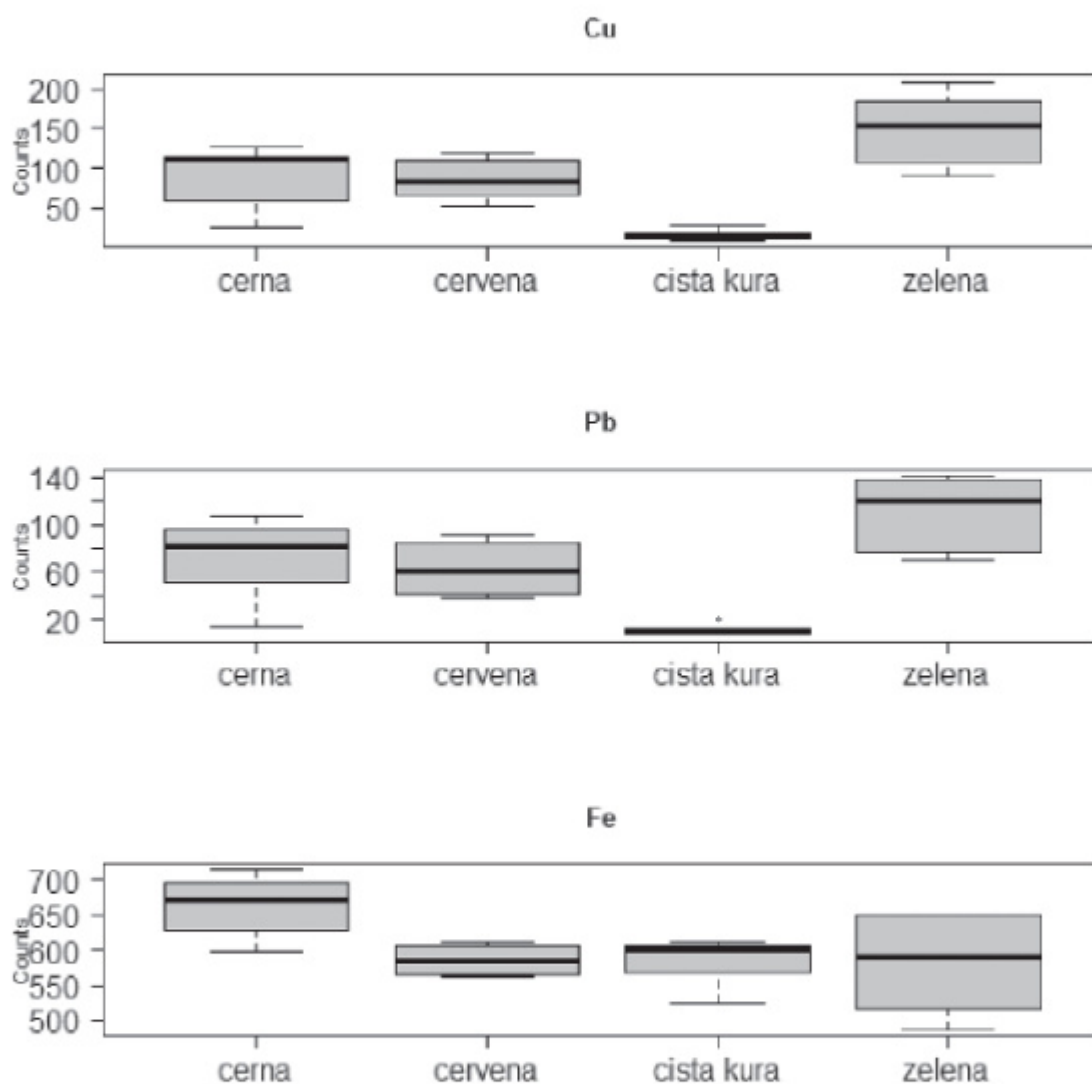
Ramanova mikroskopie a XRF byly také hlavními technikami v publikaci IX. Během archeologického výzkumu v kostele sv. Marka v Litovli v roce 1999 byla nalezena březová kůra s kresleným ornamentem s rostlinným motivem (Obr. 17). Na kůře je vyobrazen zelený list, stonky s červeně zbarveným poupětem a vše je zvýrazněno tmavou linkou. Jelikož se jedná o unikátní nález bylo vyžadováno použití pouze nedestruktivních a neinvazivních metod.



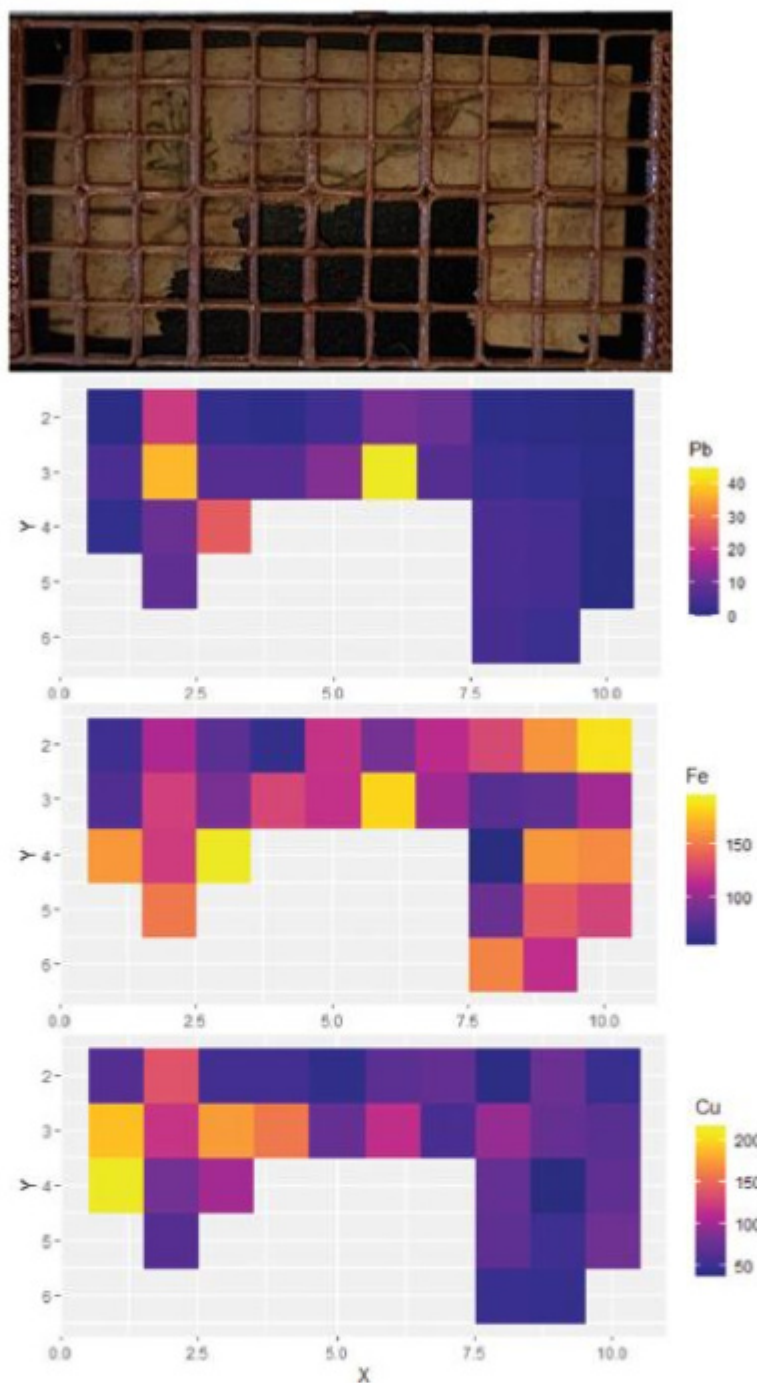
Obr. 17: Fotografie vzorku březové kůry

V prvním kroku byly vybrané barevné oblasti měřeny pomocí ručního XRF a naměřené intenzity jednotlivých prvků byly zobrazeny v podobě krabicových grafů (každá oblast byla měřena 6krát; Obr. 18). Zajímavý je zvýšený obsah železa v černé oblasti, který může poukazovat na použití železito-duběnkového inkoustu. V zelené oblasti byl pozorován zvýšený obsah mědi, což pravděpodobně souvisí s nejběžnějším pigmentem v minulosti malachitu. V těchto oblastech byla také pozorován zvýšený obsah olova. Pro zjištění distribuce jednotlivých prvků na povrchu březové kůry bylo provedeno měření pomocí vytvořené mřížky (Obr. 19). Vyšší obsah mědi se vyskytuje v oblasti lístků a zelené části květu. Ve stejné oblasti je patrný také vyšší obsah olova. Můžeme předpokládat, že byl připraven světlejší pigment smícháním malachitu a olovnaté běloby. Distribuce železa je bohužel velmi heterogenní a není tedy možné jednoznačně určit vyšší obsah železa v konkrétních částech kresby. Pro přesnější určení pigmentů byla použita Ramanova mikroskopie a získaná data byla srovnávána s autentickými standardy. Červený pigment obsahoval charakteristické pásy pro hematit a můžeme tedy konstatovat, že se jedná o červenou hlínu. Spektrum zeleného

pigmentu se v základních signálech shodovalo se standardem malachitu. Získaná data jsou tedy ve shodě s XRF výsledky. Tato publikace byla původně zpracována jako Středoškolská odborná činnost. Studentka projevila zájem práci rozvíjet dál dokázala již na střední škole vytvořit vědecko-výzkumný článek. Publikace navíc ukazuje potenciál využití kombinace nedestruktivního měření pomocí ručního přístroje XRF a statistického zpracování dat v programu R pro zobrazení rozdílů v ploše.



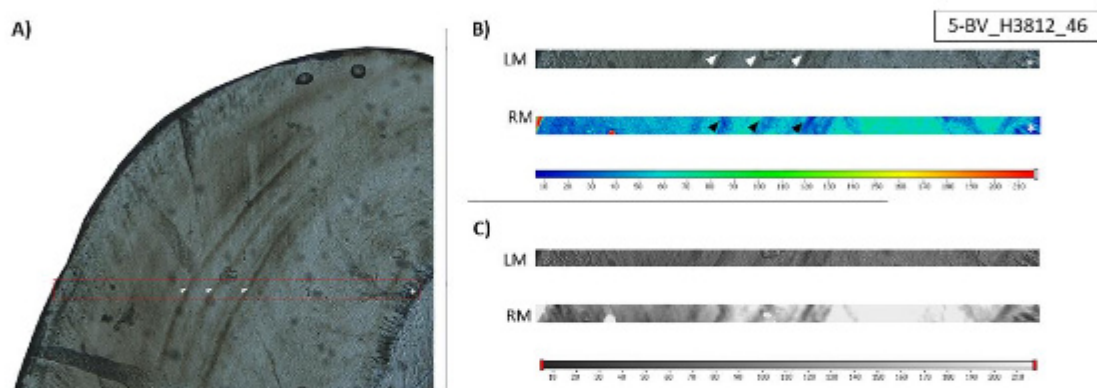
Obr. 18: Krabicové grafy intenzit Cu, Pb a Fe na vzorku březové kůry



Obr. 19: XRF zobrazování distribuce prvků na vzorku březové kůry

Dalším možným přístupem je invazivní zásah do materiálu, ale odebraný vzorek je měřen nedestruktivně, čímž je uchován pro případná měření v budoucnu. Tento postup byl aplikován v publikacích X a XI.

Během života člověka může dojít k narušení metabolických procesů, což následně ovlivní mineralizaci zubní skloviny, v níž dojde ke vzniku zvýrazněných linií (akcentované linie). Tyto zvýrazněné linie ve sklovině souvisejí se stresovými událostmi, které daný jedinec absolvoval v různých ontogenetických fázích. Akcentované linie je možné pozorovat ve výbrusu zubu pomocí optické mikroskopie v procházejícím světle (tmavší než okolí), ale jejich vzhled je však proměnlivý i v rámci jednoho zubu. Cílem této studie bylo sledovat distribuci fosfátů v lidské sklovině pomocí Ramanovy mikroskopie (RM) a porovnat naměřená data se záznamy z optické mikroskopie.



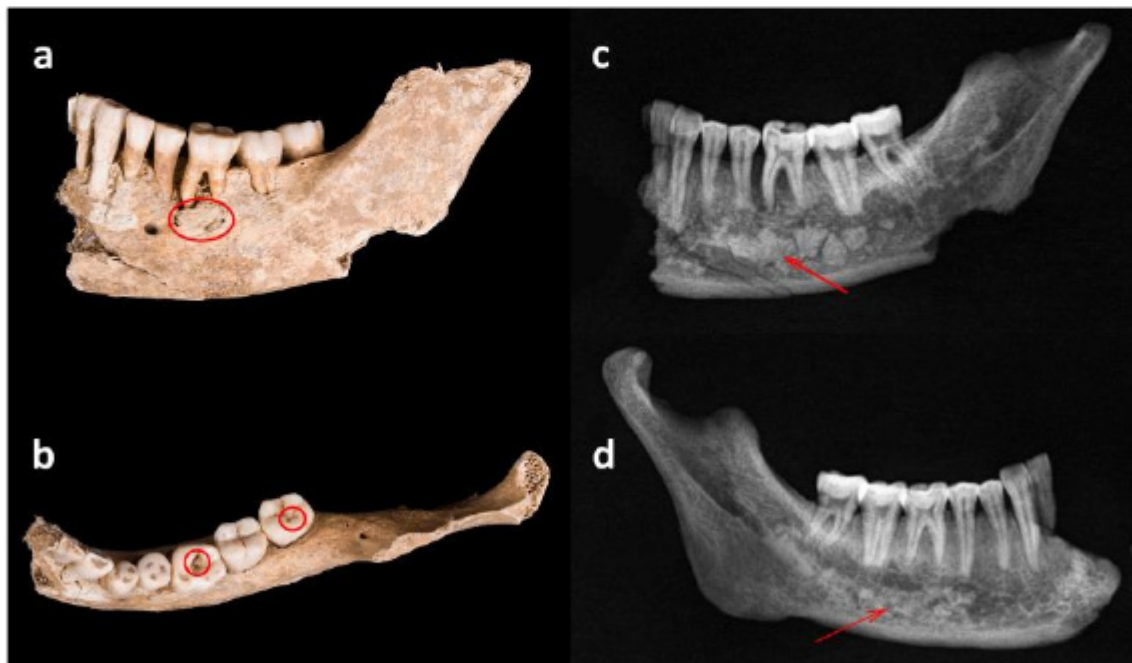
Obr. 20: Mikrofotografie pravého 1. moláru (A; zvětšení 50×). Červený tečkovaný obdélník vymezuje oblast analýzy pomocí RM. Šipky ukazují na AL ve sklovině, hvězdička na rozhraní sklovina-dentin (EDJ). Detail řezu z části A (B, zvětšení 100×). Řezy z části B převedené do stupňů šedi. (C; LM = záznam z transmisního světelného mikroskopu, RM = záznam z Ramanova mikroskopu, AL = akcentovaná linie).

Kombinovaná data z LM a RM jsou na většině vzorků v dobré shodě a poukazují na fakt, že místa stresových linií jsou hypomineralizována (nízký obsah fosfátů; signál při 960 cm^{-1}). Nicméně může nastat situace, kdy RGB zobrazení je ve shodě se záznamem LM (pokles signálu v jedné poloze AL a v poloze přechodu sklovina-dentin, EDJ), ale záznam RM ve stupních šedi se od LM ve stupních šedi liší. Jedna z možných variant vysvětlení je, že režim zobrazování ve stupních šedi vnesl více "šumu" do výsledků LM a tím bylo následně ovlivněno statistické vyhodnocení. Další komplikací pro správné vyhodnocení připraveného nábrusu je dodržení stejné tloušťky výbrusu napříč zubem. Kvalita záznamu světelné mikroskopie silně závisí na kvalitě tenkého řezu. Pokud je výbrus relativně tlustý (v důsledku nedůslednosti při přípravě), může být

výsledný záznam z mikroskopie v procházejícím světle posunutý/rozmažený, a proto se nemusí dobře shodovat s Ramanovým mikroskopem. Publikace X poukázala na nové možnosti studia zubní skloviny pomocí nedestruktivní Ramanovy mikroskopie v případech, kdy připravený nábrus nesplňuje požadavky pro světelnou mikroskopii.

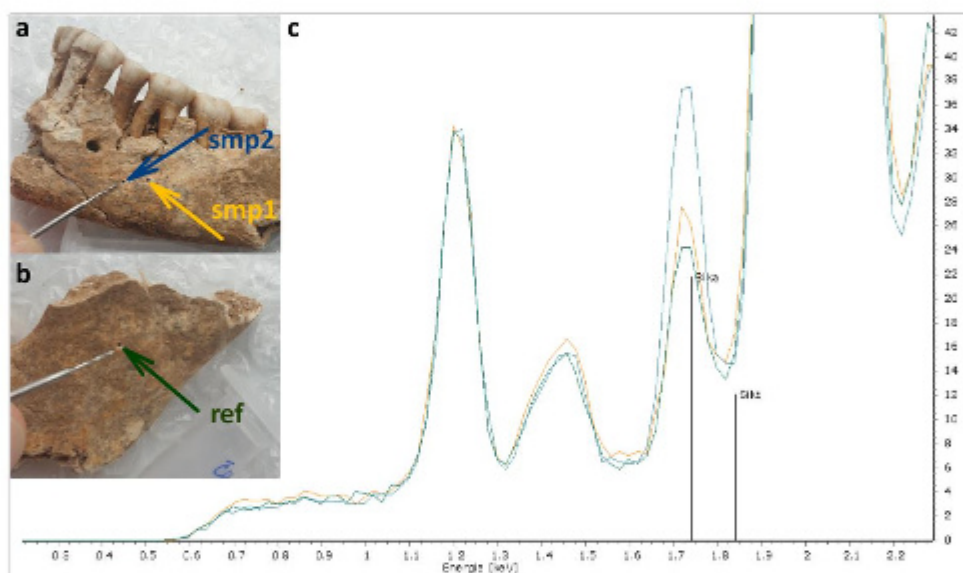
Obecně lze ovšem říct, že při práci s naměřenými daty z kosterních pozůstatků je nutné počítat tafonomickými faktory, které mohou ovlivnit mikrostrukturu skloviny (bakteriální degradace a rozklad skloviny) a metodické faktory (např. bublinky v pryskyřici) mohou vnést "šum", který může vážně zvýšit složitost výsledků a ztížit jejich vyhodnocení. V některých případech je nutné také počítat na možnou kontaminaci vzorků okolním prostředím, což může mít za následek nesprávnou interpretaci.

Kosterním pozůstatkům je věnována také publikace XI, kde jsou popisovány makroskopicky viditelné patologické změny na dolní čelisti. Rentgenové snímky kostní tkáně poukazují na četná, do značné míry splývající, zastínění husté hmoty (Obr. 21) a místy jsou přítomny granulární a fibrilární struktury.



Obr. 21. Levá dolní čelist v bočním (a) a horním (b) pohledu s vyznačenými kazovými defekty na prvním a třetím zubu; rentgenové snímky levé (c) a pravé dolní čelisti (d) s místy s vyšší hustotou (šipky).

Na základě předcházejících výsledků byla vyslovena hypotéza, že oblasti s vyšší hustotou mohou být způsobeny aluviálními sedimenty. Za tímto účelem byly vzorky z dolní čelisti analyzovány pomocí rentgenové fluorescenční spektrometrie (XRF) se zaměřením na vyhodnocení obsahu křemíku, vápníku, a fosforu. Vzhledem k tomu, že křemík se v horninách a půdě vyskytuje hlavně ve formě oxidu křemičitého, zvýšený obsah křemíku by mohl poukazovat na mechanický průnik materiálu do vnitřních struktur kosti (voda+písek). Obr. 22 zobrazuje intenzitu $K\alpha$ linie křemíků v odebraných vzorcích. Výsledky tedy potvrdily hypotézu a průniku sedimentu do vnitřních pórů kostní tkáně. Publikace XI ilustruje užitečnost mezioborové spolupráce během paleopatologického hodnocení a důležitost rozlišování „skutečných“ patologií od posmrtných změn.



Obr. 22: Odběrová místa pro XRF měření (a, b); Srovnání intenzit křemíků ve vzorcích (barvy odběrových míst odpovídají barvám linií spektra; c).

XRF analýza pro analýzu kosterního materiálu je velmi užitečná díky své jednoduchosti. Nicméně, stále je zde otázka, zdali tato semikvantitativní analýza je vhodná k tomuto účelu. Studium patologie Cribra orbitalia (Obr. 23) byla věnována publikace XII, kde byl testován jak destruktivní (ICP-MS), tak i nedestruktivní (XRF) přístup pro měření kosterního materiálu. Během záchranného archeologického výzkumu v centru města Olomouc (Morava, Česká republika) bylo nalezeno několik hrobů. Tyto hroby byly součástí zaniklého hřbitova, který se nacházel na území v dnešní době neexistujícího kostela Petra a Pavla.

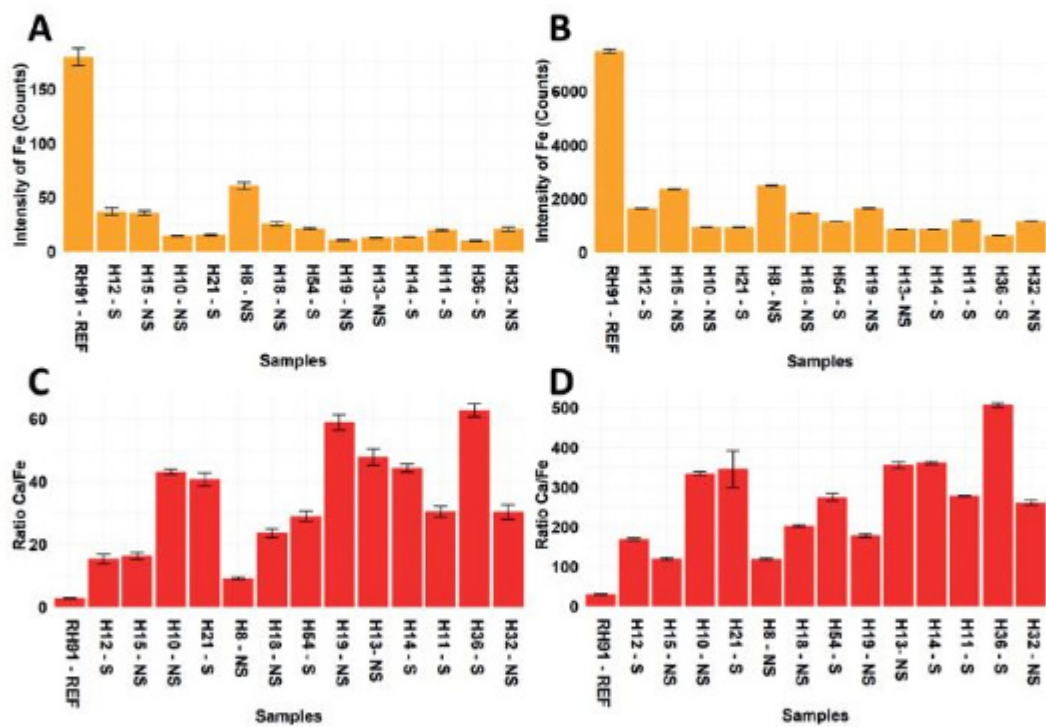


Obr. 23: Ukázka poškození kostní tkáně (Cribra orbitalia)

Výzkum byl zaměřen na analýzu 13 vzorků dětských lebek postižených chronickým onemocněním známým jako "cribra orbitalia" (CO, Tab. 6). Hlavními technikami pro analýzu vzorků byla nedestruktivní rentgenová fluorescenční analýza (XRF) a destruktivní hmotnostní spektrometrie s indukčně vázaným plasmatem (ICP-MS). Obr. 24 ukazuje vysokou intenzitu železa v referenčním vzorku a velmi nízkou intenzitu ve vzorcích kostí postižených CO. Můžeme tedy předpokládat, že u těchto jedinců s CO by snížená hladina železa v kostech mohla být příčinou vzniku anémie. Pokud se však zaměříme na poměr Ca/Fe (Obr. 23CD), můžeme vidět závislost obsahu železa na věku. Tento poměr se postupně zvyšuje s věkem dítěte, ale nekoreluje se stupněm poškození kostní tkáně. Výsledky tedy poukazují, že běžně uváděný závěr o korelaci mezi anemií a mírou poškození CO není správný. Snížený obsah železa u jedinců s CO je tedy pravděpodobně pouze doprovodný jev. V rámci této studie je důležité si také všimnout dobré shody mezi nedestruktivním měřením pomocí XRF a destruktivním měřením ICP-MS. V případě vzorků, u kterých není umožněn odběr vzorků kostní tkáně je možné využít XRF.

Tab. 6: Seznam studovaných vzorků s uvedením věku, míry poškození a zjištěných patologií

Grave #	Age	Location of CO	CO grading	Observed disease
RH91	2 years (\pm 8 months)	-	0	-
H12	2 years (\pm 8 months)	left orbit	3	anemia, rickets
H15	2 years (\pm 8 months)	right orbit	1	-
H10	2–4 years	left orbit	1	-
H21	2–4 years	both orbits	4	rickets
H8	2–4 years	right orbit	2	-
H18	4 years (\pm 12 months)	both orbits	2	-
H54	4–6 years	left orbit	3	rickets
H19	6 years (\pm 24 months)	right orbit	1	-
H13	6–9 years	both orbits	1	anemia
H14	9–12 years	right orbit	3	-
H11	10 years (\pm 30 months)	right orbit	3	anemia
H36	10 years (\pm 30 months)	right orbit	3	anemia
H32	12–15 years	right orbit	1	-



Obr. 24: Intenzity Fe ve studovaných vzorcích měřené metodami XRF (A) a ICP-MS (B) a poměr signálu Ca/Fe z XRF dat (C) a ICP-MS dat (D) (REF - referenční vzorek, S - významná pórovitost CO, NS – bez významné pórovitosti CO).

5. Závěr

Výsledky uvedeny v této habilitační práci prezentují nutné zapojení analytické chemie do studia vzorků hmotného kulturního dědictví. Práce byla dělena na tři samostatné kapitoly:

1) Interdisciplinární přístup, kde byla demonstrována nezbytnost úzké spolupráce mezi přírodovědnými obory, ale také s obory z jiných, nepřírodovědných, oblastí. Každý z nás je odborníkem na specifickou oblast, a tudíž nemusíme být schopni dokonale zasadit výsledky do konkrétních historických souvislostí.

2) druhá kapitola, Multidisciplinární přístup, poukázala na nutnost kombinovat analytické techniky. V případě hmotného kulturního dědictví se ve většině případů jedná o necílenou analýzu, kde sice existuje předpoklad, jaké látky mohly zůstat zachovány ve vzorku, a kompletní náhled na vzorek pomocí různých technik (detekce různých skupin látek) je nezbytný. V případě malého množství vzorku je volba vhodné techniky pouze na chemikovi, ale měla by jí předcházet odborná diskuse se zadavatelem. Je zde tedy úzká provazba mezi obory (Interdisciplinární přístup).

3) poslední kapitola, Destruktivní VS nedestruktivní přístup, popisuje možnosti nedestruktivního měření, která je zásadní pro vzácné vzorky hmotného kulturního dědictví. Nedestruktivní přístup je také důležitý pro uchování vzorků pro případné budoucí měření technikami, které dokážou získat nová data.

Závěrem lze tedy říci, že všechny tři kapitoly jsou navzájem úzce propojeny a analýza hmotného kulturního dědictví je tedy významně závislá na vzájemné komunikaci a spolupráci, na základě které dojde k využití nejvhodnější analytické techniky. V prvním kroku se aplikují nedestruktivní postupy a teprve až poté invazivní a destruktivní postupy.

6. Literatura

- I. Kučera, L., Peška, J., Fojtík, P., Barták, P., Kučerová, P., Pavelka, J., Komárková, V., Beneš, J., Polcerová, L., Králík, M., & Bednář, P. (2019). First direct evidence of broomcorn millet (*Panicum miliaceum*) in Central Europe. *Archaeol. Anthropol. Sci.* 11, 4221–4227. DOI:10.1007/s12520-019-00798-4
- II. Jilek, J., Golec, M., Bednar, P., Chytráček, M., Vich, D., Zavoral, T., Mirova, Z., Petr, L., Kovarnik, J., Milo, P., Kucera, L., 2021, The oldest millet herbal beer in the Europe? The ninth century BCE bronze luxury bucket from Kladina, Czech Republic, *Archaeometry*. DOI: 10.1111/arcm.12711
- III. Beneš, J., Todoroska, V., Budilová, K., Kovárník, J., Pavelka, J., Atanasoska, N., Bumerl, J., Florenzano, A., Majerovičová, T., Vondrovský, V., Ptáková, M., Bednář, P., Richtera, L., Kučera, L., 2021. What about Dinner? Chemical and Microresidue Analysis Reveals the Function of Late Neolithic Ceramic Pans, *Molecules* 26, 3391. DOI: 10.3390/molecules26113391
- IV. Jagošová, K.; Moník, M.; Kapusta, J.; Pechancová, R.; Nádvorníková, J.; Fojtík, P.; Kurka, O.; Závodná, T.; Bednář, P.; Richtera, L.; Kučera, L., 2022, Secret Recipe Revealed: Chemical Evaluation of Raw Colouring Mixtures from Early 19th Century Moravia. *Molecules* 27, 5205. DOI: 10.3390/molecules27165205
- V. Bliujiene A., Kučera L.: Some remarks on amber usage tradition and amber provenance in the interfluvium of Nemunas and Daugava rivers in the migration period, in: Niezabitowska-Wisniewska B. a kol. *Studia Barbarica*, UMCS, Lublin 2018, ISBN 978-83-7825-044-9
- VI. Kučera L., Bednář, P., Chemická analýza vzorků jantaru, in: Enreé, M., Langová, M. (Eds) *Mikulovice – Pohřebiště starší doby bronzové na Jantarové stezce*, Archeologický ústav AVČR, Praha 2020, ISBN 978-80-7581-025-0
- VII. Kučera, L., Peška, J., Fojtík, P., Barták, P., Sokolovská, D., Pavelka, J., Komárková, V., Beneš, J., Polcerová, L., Králík, M., & Bednář, P. (2018). Determination of Milk Products in Ceramic Vessels of Corded Ware Culture from a Late Eneolithic Burial. *Molecules*, 23(12), 3247. DOI:10.3390/molecules23123247
- VIII. Kučera, L., Rozsypal, J., Bednář, P., Březina, M., Kalina, L., Bezdička, P., Mašláň, M., Richtera, L., 2021. “Gold corrosion”: An alternative source of red stains on gold coins, *Materialia* 15, 101025. DOI:10.1016/j.mtla.2021.101025

- IX. Schönwälderová N; Šlězár P; Kučera L. 2022, Analýza zbytků barev z fragmentu kresby na březové kůře z Litovle, *Studia archaeologica Brunensia* 27 (1), 143-152.
- X. Vacková, S., Králík, M., Marečková, K., Ráčková, L., Quade, L., Sedláčková, L., Fojtík, P., Kučera, L. (2021) Human “barcode”: Link between phosphate intensity changes in human enamel and light microscopy record of accentuated lines, *Microchemical Journal* 168, 106370. DOI: 10.1016/j.microc.2021.106370
- XI. Fojtová, M; Krístek, J; Kucera, L. 2023, A pathological lesion or a postmortem artefact? An interdisciplinary approach to deal with an interesting early medieval case, *Int. J. Paleopath* 43, 93-98. DOI:10.1016/j.ijpp.2023.10.003
- XII. Lundova, M; Sin, L; Dehnerova, H; Pechancova, R; Kurka, O; Bednar, P; Kucera, L, 2022, Evaluation of chemical composition of cribra orbitalia from post-medieval children graves (Olomouc, Czech Republic), *Preahistorische Zeitschrift*, 2022-2045. DOI: 10.1515/pz-2022-2045

7. Přílohy – autorovy publikace použité v habilitační práci



First direct evidence of broomcorn millet (*Panicum miliaceum*) in Central Europe

Lukáš Kučera¹ · Jaroslav Peška² · Pavel Fojtik³ · Petr Barták¹ · Pavla Kučerová¹ · Jaroslav Pavelka⁴ · Veronika Komárková⁵ · Jaromír Beneš⁵ · Lenka Polcerová⁶ · Miroslav Králík⁶ · Petr Bednář¹

Received: 11 July 2017 / Accepted: 24 January 2019 / Published online: 14 February 2019
© Springer-Verlag GmbH Germany, part of Springer Nature 2019

Abstract

Chemical analysis of archaeological objects is an important part of current investigations. In the presented study, a soil from an archaeological vessel from rescue excavation close to the village Držovice (Central Moravia Region, Czech Republic; findings dated to Eneolithic period) was analyzed using gas chromatography/mass spectrometry and firstly in archaeological science by atmospheric pressure solids analysis probe with atmospheric pressure chemical ionization mass spectrometry. Miliacin, a chemical marker of a broomcorn millet, was unambiguously confirmed by both techniques. The obtained results can help to understand the diet habits of Corded Ware population and connection between Central Europe and Asia, where broomcorn millet has been domesticated. The identification of miliacin as a “chemical imprint” of millet from the end of Eneolithic period of Moravia is therefore extraordinarily important.

Keywords Archaeological pottery · Gas chromatography · Mass spectrometry · Atmospheric pressure solids analysis probe · Millet · Miliacin

Introduction

In modern archaeological research, a close multidisciplinary collaboration with other branches is necessary, especially with natural sciences (e.g., anthropology, archaeobotany, and chemistry). Mutual collaboration and harmonization of particular parts of research bring a series of unexpected and important findings in the context of prehistoric research nowadays. A number of analytical techniques have been already applied to the study of specific classes of compounds in archaeological

context, such as lipids (Evershed et al. 1990; Evershed et al.; 1999), waxes (Evershed et al. 1997; Heron et al. 1994), and terpenoids (Bossard et al. 2013; Eerkens 2002). Organic residues on ceramic vessels can be analyzed by spectroscopic methods, such as infrared (IR), Raman, and nuclear magnetic resonance (NMR) spectroscopy, which provide mainly fingerprint (mixed spectrum of all present organic compounds that absorb the applied radiation) of studied material (Lambert et al. 2000; Edwards et al. 2004). On the other hand, separation techniques (gas and liquid chromatography) are needed for

Electronic supplementary material The online version of this article (<https://doi.org/10.1007/s12520-019-00798-4>) contains supplementary material, which is available to authorized users.

✉ Petr Bednář
petr.bednar@upol.cz

¹ Regional Centre of Advanced Technologies and Materials, Department of Analytical Chemistry, Faculty of Science, Palacký University, 17. listopadu 12, 779 00 Olomouc, Czech Republic

² Archaeological Centre Olomouc, U Hradiska 42/6, 779 00 Olomouc, Czech Republic

³ Institute of Archaeological Heritage Brno, Kaloudova 1321/30, 614 00 Brno, Czech Republic

⁴ Centre of Biology, Geoscience and Environmental Education, University of West Bohemia, Sedláčkova 15, 306 14 Pilsen, Czech Republic

⁵ Laboratory of Archaeobotany and Palaeoecology, Faculty of Science, University of South Bohemia, Na Zlaté stoce 3, 370 05 České Budějovice, Czech Republic

⁶ Laboratory of Morphology and Forensic Anthropology (LaMorFA), Department of Anthropology, Faculty of Science, Masaryk University, Kotlářská 2, 611 37 Brno, Czech Republic

detailed identification of particular organic compounds present in food residues (e.g., cereals, milk, meat, fruit). Chromatography is routinely hyphenated with mass spectrometry nowadays (Pecci et al. 2013; Soberl et al. 2008; Buckley et al. 2013; McGovern et al. 2009).

The analysis of soil content of archaeological vessel from grave belonging to Moravian Corded Ware population (2600/2500–2300/2200 BC) using modern instrumental analytical techniques gas chromatography/mass spectrometry (GC/MS) and atmospheric pressure solids analysis probe with atmospheric pressure chemical ionization mass spectrometry (ASAP-MS) is discussed in this communication. To the best of our knowledge, this is the first evidence of the using of ASAP-MS in analysis of archaeological samples. A new method for sampling of soil from archaeological potteries allowing comparative chemical analysis was developed. The used analytical approaches allowed to prove the presence of miliacin that evidences the oldest utilization of millet in Central Europe.

Materials and methods

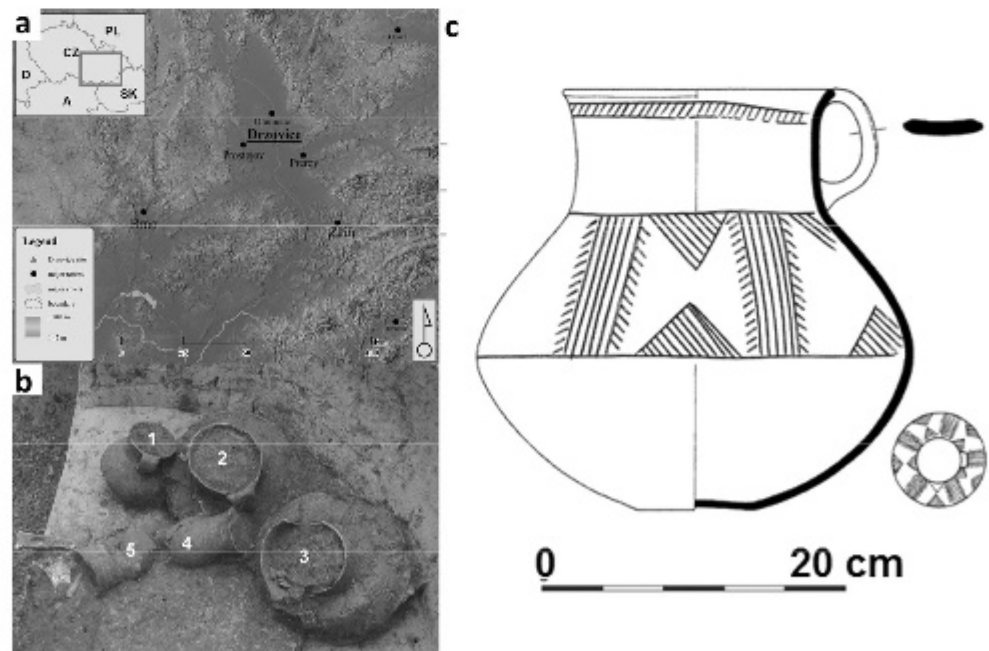
Archaeological description of the place of finding and sample preparation

During a rescue excavation (2014–2015) close to the village Držovice (Prostějov, Central Moravia, Czech Republic, Fig. 1a, b), the biritual burial ground with five graves at considerable distances from each other (range 17–48 m) was found. The burial ground belongs to the Moravian Corded Ware population (MCW; generally 2600/2500–2300/

2200 BC). The exact dating was performed by radiocarbon dating (Beta Analytic Radiocarbon Dating, Miami, USA) of a bone chisel found in the grave. A high-probability density range method, Intcal 13, was used. Calibration was calculated using database 2013 INTCAL. In accordance with measurement, the age of the bone material falls in the ranges 2707–2571 BC (probability, prob = 62.3%), 2863–2807 (prob = 22%), 2759–2717 (prob = 9.9%), and 2513–2503 (prob = 1.1%). Those data ensure the age of the bone chisel and consequently the grave to the twenty-seventh century BC (Encolith). The graves were laid at southwest gradient above terrace of Český potok (distance 100–200 m) at an altitude of 220–228 m.s.l. (Fojtík 2015) and were oriented in the axis N–S (NE–SW). The subject of further interest was the cremation grave (H4) disrupted by the excavation of the manhole (approximately 1/3). The ceramic jug of Dřevohostice type (ceramic vessel No. 2; volume 8.5 L, Fig. 1b) was analyzed by GS/MS and ASAP-MS. Besides, another three ceramic vessels were analyzed for miliacin content, i.e., ceramic jug (No. 1, 1.9 L) and two Corded Ware beakers (No. 4, 0.8 L and No. 5, 0.6 L, respectively).

The ceramic vessel was found cracked but compact. After picking the vessel up, the sherds were gently removed and the internal content of ceramic vessel (soil) was reinforced by plastic foil and transported to a laboratory. The soil material from ceramic vessel No. 2 (i.e., soil from neck and upper bulge) was analyzed. The soil from neck was divided horizontally into two equal parts (first and second layer). The soil from upper bulge was divided to a “surface” layer contiguous to inner ceramic surface and the layer farther from the surface (third and fourth layer; equal mass of each part was taken for extraction). Each part was consecutively extracted by four different solvents, i.e.,

Fig. 1 Place of rescue excavation (a), ceramic vessels in grave (b), and drawing of ceramic vessel No. 2 (c)



water, 0.05% ammonium hydroxide in methanol, 1% formic acid in methanol (both *v/v*), and acetone. All chemicals used for preparation of the extraction media were purchased from Penta Ltd. (Prague, Czech Republic). After that, individual extracts were filtered through a cellulose filter paper (black label, Schleicher & Schuell A.G., Feldmeilen, Switzerland) and concentrated to defined volume 1 mL using a fine stream of nitrogen. Aqueous extracts were freeze-dried and the residues were dissolved and reconstituted to defined volume with water to reach 100 times concentrated extract. The concentrated extracts were subjected to analysis by GC/MS and ASAP-MS techniques. Parameters of all methods are given below.

2.5 mg of modern broomcorn millet grains was pulverized in a mortar and then extracted by 10 mL of acetone (gradient grade, Penta Ltd.). Then, the sample was centrifuged for 6 min at 4400 RPM. 8.5 mL of supernatant was diluted to final volume 20 mL. The miliacin standard (PhytoLab GmbH & Co., Germany) was prepared at concentration 50 mg L⁻¹ in 1:1 acetone:CHCl₃ solution (*v/v*). The prepared samples were directly analyzed by GC/MS and ASAP-MS.

Gas chromatography/mass spectrometry

Gas chromatography/mass spectrometry (GC/MS) was used for determination of semi-polar and non-polar compounds in extracts. Agilent 7010 Triple Quadrupole GC/MS system with Mass Hunter software (Agilent Technologies, Palo Alto, USA) was used for analysis. The separation was performed on two (5%-phenyl)-methylpolysiloxane capillary columns HP-5 ms Ultra Inert connected in series (15 m × 0.25 mm × 0.25 μm, each) with constant flows at 1.0 and 1.2 mL min⁻¹, respectively. Nitrogen (Messer Group GmbH, Germany) was used as a collision gas with a flow rate at 1.5 mL min⁻¹ and helium (He 5.0, Siad, Italy) as a quench gas with a flow rate of 2.25 mL min⁻¹. The initial oven temperature was 70 °C for 5 min; the oven was heated up with the rate 15 °C min⁻¹ to the value of 300 °C, which was held for 10 min. An injection volume of extracts was 0.5 μL with splitless injection. The multiple reaction monitoring (MRM) screening method was used for detection of miliacin in prepared samples (MRM transition was 440 → 189). Besides, MS1 SIM scan type (*m/z* 189, 204, 218) was used for additional experiments for identification of miliacin and detection of pentacyclic triterpenes (PTMEs).

Atmospheric pressure solids analysis probe with atmospheric pressure chemical ionization mass spectrometry

Mass spectrometer Synapt G2-S (Waters, Milford, USA) equipped with atmospheric pressure solids analysis probe combined with atmospheric pressure chemical ionization (ASAP-MS) was used for untargeted analysis of individual extracts as well. The extract was deposited in a thin film on

a glass stick provided with the ASAP probe (the glass stick was immersed in the extract and the solvent was consequently left to evaporate). Then, the glass stick was fixed to ASAP probe and inserted to APCI ion source. The probe was then gradually heated and desorbed compounds were ionized in an electrical discharge. Method parameters were as follows: ASAP mode, positive; time of analysis, 3 min (0–1 min, probe temperature, PT, 100 °C, 1–2 min PT 250 °C, and 2–3 min PT 400 °C). Full MS scan was done in the range 50–1000 Da (trap collision energy, 4 eV; transfer collision energy, 2 eV). MS/MS scan was performed for confirmation. *m/z* of miliacin (*m/z* 440.4) was isolated, trap collision energy 20 eV and transfer collision energy 2 eV were used for fragmentation.

Results and discussion

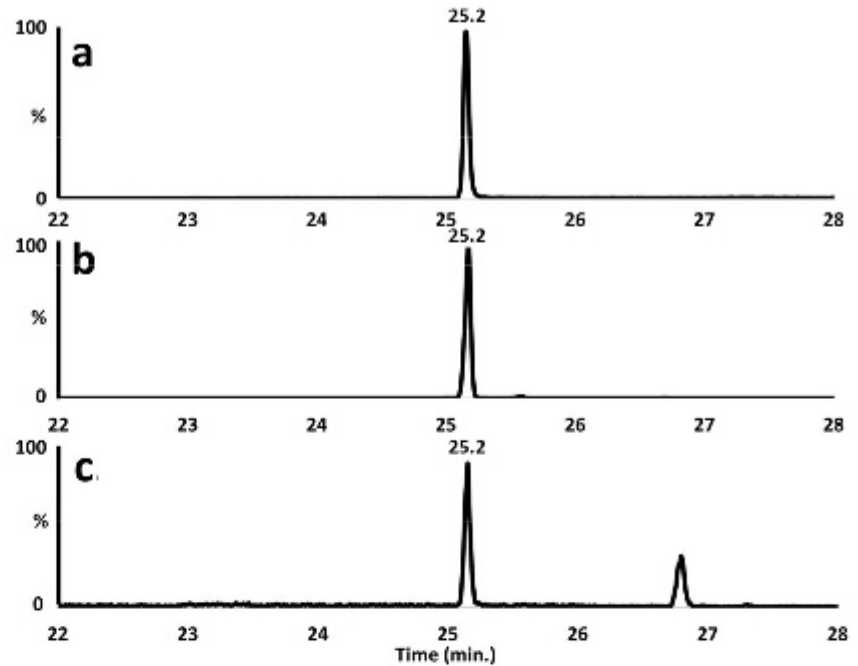
GC/MS and ASAP-MS analysis

All extracts were analyzed using GC/MS and ASAP-MS techniques suitable for analysis of semi-polar and non-polar volatile compounds. Compared with GC/MS (as standard technique nowadays), ASAP-MS technique is not preceded by a chromatographic separation of studied compounds but due to its commercial availability in combination with a tandem high-resolution mass spectrometer, its selectivity is enhanced by high mass resolution and the possibility of MS/MS spectra collection. The exact mass measurement capability provides information about elemental composition that is of key importance for reliable identification of analyte.

An intensive signal of ion at *m/z* 440 was found by GC/MS in the sample of soil taken from the upper bulge of vessel No. 2 (retention time 25.2 min.). This compound was ascribed to plant triterpenoid miliacin—a biomarker of broomcorn millet (*Panicum miliaceum*). This signal was found neither in the first and second soil layers taken from the neck of the vessel No. 2 nor in the soil taken from the other vessels found in the grave. This fact excludes the cross-contamination of soil samples from vessel No. 2. Identification of this compound in our vessel was based on *m/z* value, comparison of analytical parameters with analytical standard, broomcorn millet extract (*m/z* value and retention time), and data from the literature (Bossard et al. 2013). Retention times of miliacin standard, a compound from recent broomcorn millet extract and from soil extract of ceramic vessel, were identical (Fig. 2).

Motuzaitė-Matuzevičiūtė et al. (2013) discussed the potential of miliacin but also another pentacyclic triterpenes as biomarkers of broomcorn millets primarily due to their antifungal/antibacterial properties. Multiple reaction monitoring (MRM) screening (MRM transition was 440 → 189) done in our study revealed two more peaks in archaeological soil sample. The concentration of these compounds is lower than concentration of miliacin in the sample. In targeted SIM measurements (MS1

Fig. 2 Chromatogram of miliacin standard (b), compound from broomcorn millet extract (b), and unknown compound from the soil from third soil layer from ceramic vessel No. 2 (c)



SIM scan type) of miliacin (RT = 25.2 min), characteristic fragments at m/z 189, 204, and 218 were observed with sufficient intensity in the standard solution, recent broomcorn millet, and archaeological sample (soil taken in the upper bulge of vessel No. 2). The same pattern was observed during fragmentation of the other two compounds eluting at 27.3 and 30.0 min. Comparison of this pattern and retention order with former literature (Bossard et al. 2013; Motuzaitė-Matuzevičiūtė et al. 2016) suggests that those compounds belong to the PTME group (e.g., isosawamilletin or urs-12-en-3 β -ol ME). However, the signal intensities of those two compounds are much lower (50.3 and 12.6 times, respectively) compared to miliacin (the lower intensity is also in agreement with the former literature). The related chromatograms are given in Supplementary Material 1. The concentration of miliacin in the upper bulge soil sample (the fourth soil layer) of the studied ceramic vessel is approximately 0.24 $\mu\text{g/g}$ of soil.

The fragmentation spectrum (targeted MS/MS, ionization energy 70 eV, and collision energy 20 eV) of miliacin standard (a), compound from broomcorn millet (c), and compound with m/z 440 from the fourth soil layer ceramic vessel No. 2 (e) are very similar (Fig. 3). MS/MS spectra further confirm the identity of miliacin.

ASAP-MS data, obtained by different ionization modes (at atmospheric pressure conditions), well support the obtained results (see spectra b, d, and f in Fig. 3). ASAP-MS technique in the used arrangement (i.e., in combination with Q-TOF mass analyzer) provided information about the exact mass of miliacin in the archaeological sample that strongly supports the identification (m/z 440.3824 was measured corresponding with relatively small deviation from its theoretical mass, dtm,

0.0194 Da, $\text{C}_{31}\text{H}_{52}\text{O}$). The m/z values of fragments observed after collision-induced dissociation of the ion in the studied soil sample correspond with the fragments observed in spectrum of broomcorn millet extract as well as with those found in the literature (Bossard et al. 2013). The most important fragments are signals at m/z 203.1825 ($\text{C}_{15}\text{H}_{23}^+$, dtm 0.0025 Da), 189.1635 ($\text{C}_{14}\text{H}_{21}^+$, dtm -0.0008 Da), and 109.1020 ($\text{C}_8\text{H}_{13}^+$, dtm 0.0003 Da) that can be explained by scission of triterpenoid hydrocarbon skeleton (formation of 2,4a,7,7-tetramethyl-1-methylene-1,2,3,4,4a,5,6,7-octahydronaphthalene-ylum, 2,7,7-trimethyl-1-methylene-1,2,3,4,4a,5,6,7-octahydronaphthalene-ylum and protonated 5,5-dimethylcyclohexa-1,3-diene). Note that to the best of our knowledge, this is the first evidence of using the potential of ASAP-MS technology for analysis of archaeological samples. Apparently, the method has one weakness, which is a low resolution in relation to positional isomers. We therefore were not able to distinguish miliacin from the other minor PTMEs. This could be in principle done by utilization of ion mobility separation (collisional cross-section differences among particular positional isomers) during mass spectrometric measurement that is objective of our further research. Despite this, in any case, ASAP-MS proved to be efficient and fast technique for miliacin detection in archaeological samples. GC/MS and ASAP-MS are mutually validating methods for that purpose.

As discussed above, miliacin was unambiguously detected in an extract from soil filling of the ceramic vessel. Although no grains or visible grain residues were found in grave, a chemical imprint of millet formed by miliacin and other PTMEs persisted in the inner part of the ceramic jug. The

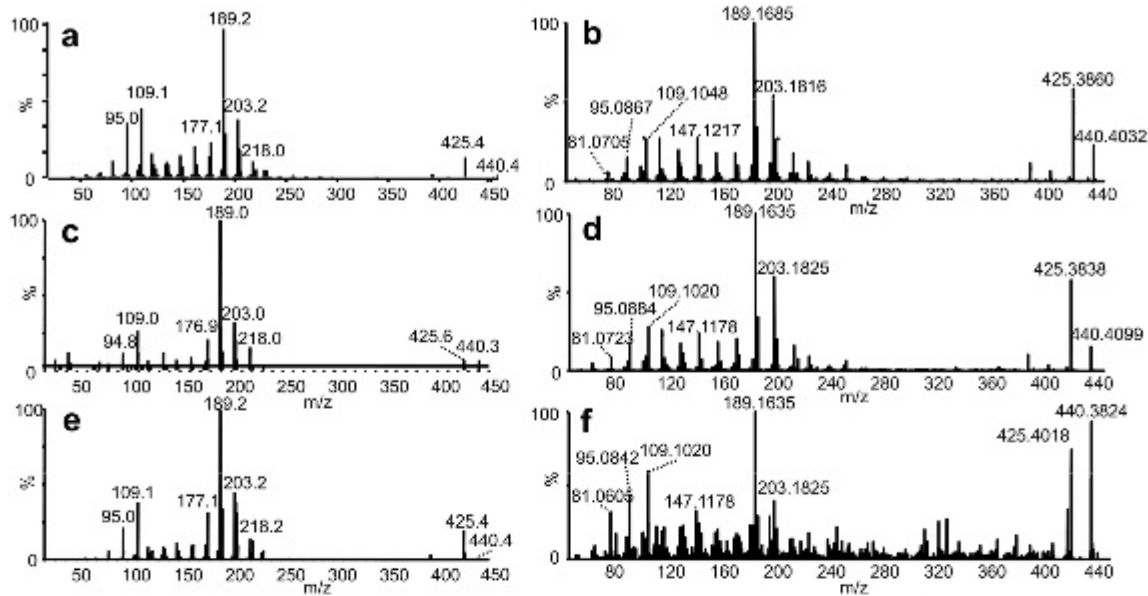


Fig. 3 Fragmentation spectra of miliacin standard (a GC/MS, b ASAP-MS), compound from broomcorn millet (c GC/MS, d ASAP-MS), and unknown compounds from ceramic vessel No. 2 (e GC/MS and f ASAP-MS)

biomarker was present only in the third and fourth soil layers (lower layers taken from bulge). As already mentioned, the marker was found neither in the other samples of soil in the upper part of this ceramic vessel nor in other ceramic vessels excavated in the studied grave (i.e., vessels No. 1, 4, 5). Note that no miliacin and other PTMEs residues were found by analysis of ceramic material of the jug. The absence of miliacin in the soil taken from neck of the ceramic vessel and ceramic matrix suggest that inner part of the content (i.e., the third and fourth layer) was effectively enough isolated from the surrounding environment that, as already indicated, excludes a chemical and/or botanical contamination (either that time or recent). Heron et al. (2016) reported that a small portion of miliacin is transferred from grains to the ceramic matrix during cooking (elevated temperature increase the penetration of analyte into the matrix structure). Based on archaeological expertise, the vessel discussed in our study was used for storage of the food present inside; thus, no cooking is expected. It can be assumed that transfer of miliacin to the ceramic at “cold” conditions is occurring to a very small extent and its content in ceramic would be very low and below the detection limit that is in conformity with data from chemical analysis.

***Panicum miliaceum* evidence in archaeological and archaeobotanical context**

Broomcorn millet (*Panicum miliaceum*) is a warm-season crop which stands up well to intense heat, poor soils, and severe droughts, completing its life cycle in a very short time (60–90 days) and succeeding in areas with short rainy seasons. Today, *P. miliaceum* is grown mainly in eastern and central

Asia, in India, and in southwest Asia (Zohary et al. 2013). Broomcorn millet was domesticated in Northern China around 8000 BP (Hu et al. 2008, Liu et al. 2009, Zhao 2011) and then species was quickly distributed westwards across Eurasia (Motuzaitė-Matuzevičiūtė et al. 2013). The last-mentioned authors made critical account and direct AMS 14C dating of broomcorn millet in an archaeological context of the Neolithic period in Europe. All finds formerly associated with the Neolithic period were assigned as much later. Broomcorn millet was probably in Central Europe cultivated as crops or alternatively existed as weeds since Linear Pottery Culture period, but scarce solitary finds of the grain indicate the second possibility (Hunt et al. 2008). Some authors interpreted rare or solitary finds as arable weeds and/or only inferred intentional cultivation where large quantities of grain are present (Kreuz et al. 2005). Species appeared in different Central and Eastern European settlements since the Neolithic, but always in small amounts, indicating that it was not an important crop (Litynska-Zajac and Wasylkowa 2005; Hajnalová 2012; Stika and Heiss 2013). This situation persisted until the Middle Bronze Age, when millet appeared in higher abundance and was quite ubiquitous (Calderoni et al. 1998; Moskal-del Hoyo et al. 2015). Real value of broomcorn millet seeds in prehistoric agriculture seems to be overestimated due to small size of seeds (Hejcman et al. 2016). On the other side, the existence of broomcorn millet “grain rich” assemblages indicates that cultivation of millet as staple starts from the Late Bronze Age in Europe (Stika and Heiss 2013; Hajnalová 2012). High abundance of millet is recorded for example in some sunken features in Březnice in South Bohemia, Czech Republic, where is millet recorded as one from key crops (Šálková 2010). In Poland, millet became

more frequent especially in the last stage of the Late Bronze Age (Tomczynska 2003).

The results of our analysis of extract of internal side of vessel No. 2 proved the usage of an ancient form of broomcorn millet in past. The miliacin (broomcorn millet chemical marker) was found in the upper bulge of the vessel and not in soil from ceramic vessel neck. Based on this data, we could consider that ceramic vessel was filled by broomcorn millet below the neck. The evidence of broomcorn millet in ceramic vessel is beneficial for the archaeobotanical research in Central Europe (especially in the Czech Republic). Dreslerová and Kočár (2013) analyzed representative datasets of archaeobotanical samples related to the using of millet in Bohemia and Moravia and suggest that evidence of millet between the Neolithic and the Middle Bronze Age is sparse and incidental. On the other hand, the usage of millet substantially increased during the Middle Bronze Age when the first “grain rich” assemblages occurred. Millet identification in the context of Corded Ware burial is very important and extraordinarily and it can be evaluated as the first such direct evidence in Central Europe. Connection between this find and new knowledge about Corded Ware population genetic studies (Haak et al. 2015, Kristiansen et al. 2017) indicates a strong link among Corded Ware groups and Eastern Asia through Pontic-Caspian Yamnaya populations.

Conclusion

Ceramic vessels from Corded Ware burial context were analyzed by gas chromatography/mass spectrometry. Analysis by this technique revealed broomcorn millet marker—miliacin in a big jug of Dřevohostice type (Central Moravia region, Czech Republic, dated to 27 century BC). The identity of miliacin was strongly supported by atmospheric pressure solids analysis probe combined with atmospheric pressure chemical ionization mass spectrometry that was applied in archaeological research for the first time. The combination of ASAP ionization with a high-resolution tandem mass analyzer (as commercially available nowadays) provided information about the exact mass of the studied compound and its fragments. The identification of presence of millet in Eneolithic context is very important and extraordinary. It can be considered as the first such direct evidence of broomcorn millet in Central Europe. The obtained results based on effective combination of analytical and archaeological data can help to understand the diet habits of Corded Ware Population and cultural connection between Central Europe and Asia, where ceramic vessels (even household ones) have significant meaning during burial ritual. Therefore, in this case, the millet could represent a part of diet and the equipment of the deceased on his “next journey” in the same time.

Funding information The authors gratefully acknowledge the support of the Czech Science Foundation [17-17346S], Ministry of Education, Youth and Sports of the Czech Republic by the project CZ.1.05/2.1.00/19.0377 and LO1305 and Palacký University Olomouc [project IGA PrF 2018 027] for the financial support.

Publisher's note Springer Nature remains neutral with regard to jurisdictional claims in published maps and institutional affiliations.

References

- Bossard N, Jacob J, Le Milbeau C, Sauze J, Terwilliger V, Poissonnier B, Vergès E (2013) Distribution of miliacin (olean-18-en-3 β -ol methyl ether) and related compounds in broomcorn millet (*Panicum miliaceum*) and other reputed sources: implications for the use of sedimentary miliacin as a tracer of millet. *Org Geochem* 63:48–55
- Buckley M, Melton ND, Montgomery J (2013) Proteomics analysis of ancient food vessel stitching reveals > 4000-year-old milk protein. *Rapid Commun Mass Spectrom* 27(4):531–538
- Calderoni G, Guglielmin M, Tellini C (1998) Radiocarbon dating and postglacial evolution, Upper Valtellina and Livignese area Sondrio, Central Italian Alps Permafrost Postglacial Process, 9: 275–284
- Dreslerová D, Kočár P (2013) Trends in cereal cultivation in the Czech Republic from the Neolithic to the migration period (5500 B.C.–A.D. 580). *Veg Hist Archaeobot* 22(3):257–268
- Edwards HGM, Sibley MG, Derham B, Heron CP (2004) Raman spectroscopy of archaeological samples from the Barber-Surgeon's medicine chest on the Mary Rose. *J Raman Spectrosc* 35(8–9):746–753
- Eerkens J (2002) The preservation and identification of pinon resins by GC-MS in pottery from the Western Great Basin. *Archaeometry* 44: 94–105
- Evershed RP, Dudd SN, Charters S, Mottram H, Stott AW, Raven A, van Bergen PF, Bland HA (1999) Lipids as carriers of anthropogenic signals from prehistory. *Philos Trans R Soc Lond Ser B Biol Sci* 354(1379):19–31
- Evershed RP, Heron C, Goad LJ (1990) Analysis of organic residues of archaeological origin by high-temperature gas-chromatography and gas-chromatography mass-spectrometry. *Analyst* 115(10):1339–1342
- Evershed RP, Mottram HR, Dudd SN, Charters S, Stott AW, Lawrence GJ, Gibson AM, Conner A, Blinkhorn PW, Reeves V (1997) New criteria for the identification of animal fats preserved in archaeological pottery. *Naturwissenschaften* 84:402–406
- Fojtik P (2015) Držovice na Moravě (okr. Prostějov): IS pro 25 RD v poloze “Pastviska” (parc. č. 702, 703/1). *Kultura se šňůrovou keramikou. Pohřebišťe. Záchraný výzkum. Přehled výzkumů* 56(1), /in print/
- Haak W, Lazaridis I, Patterson N, Rohland N, Mallick S, Llamas B, Brandt G, Nordenfelt S, Harney E, Stewardson K, Fu Q, Mittnik A, Bánffy E, Economou C, Francken M, Friederich S, Pena RG, Hallgren F, Khartanovich V, Khokhlov A, Kunst M, Kuznetsov P, Meller H, Mochalov O, Moiseyev V, Nicklisch N, Pichler SL, Risch R, Rojo Guerra MA, Roth C, Szécsényi-Nagy A, Wahl J, Meyer M, Krause J, Brown D, Anthony D, Cooper A, Alt KW, Reich D (2015) Massive migration from the steppe was a source for Indo-European languages in Europe. *Nature* 522(7555):207–211. <https://doi.org/10.1038/nature14317>
- Hajnalová M (2012) Archeobotanika doby bronzovej na Slovensku. Štúdie ku klíme, prírodnému prostrediu, poľnohospodárstvu a paleoekonomii, Nitra
- Hejzman M, Hlíšnikovský L, Hejzmanová P, Šálková T, Beneš J (2016) Kernel weights of triticum, hordeum, avena, secale and panicum species can be used for better estimation of importance of different

- cereal species in archaeobotanical assemblages. *IANS* 7(2):189–196. <https://doi.org/10.24916/iansa.2016.2.4>
- Heron C, Nemcek N, Bonfield KM, Dixon D, Ottaway BS (1994) The chemistry of Neolithic beeswax. *Naturwissenschaften* 81:266–269
- Heron C, Shoda S, Breu Barcons A, Czebreszuk J, Eley Y, Gorton M, Kirleis W, Kneisel J, Lucquin A, Müller J, Nishida Y, Son J, Craig OE (2016) First molecular and isotopic evidence of millet processing in prehistoric pottery vessels. *Sci Rep* 6(1):–9
- Hu Y, Wang S, Luan F, Wang C, Richards MP (2008) Stable isotope analysis of humans from Xiaojingshan site: implications for understanding the origin of millet agriculture in China. *Jour Archaeol Sc* 35(11):2960–2965. <https://doi.org/10.1016/j.jas.2008.06.002>
- Hunt HV, Linden MV, Liu X, Motuzaitė-Matuzevičiūtė G, Colledge S, Jones MK (2008) Millets across Eurasia: chronology and context of early records of the genera *Panicum* and *Setaria* from archaeological sites in the Old World. *Veg Hist Archaeobotany* 17:S5–S18. <https://doi.org/10.1007/s00334-008-0187-1>
- Kreuz A, Marinova E, Schäfer E, Wiethold J (2005) A comparison of early Neolithic crop and weed assemblages from the Linearbandkeramik and the Bulgarian Neolithic cultures: differences and similarities. *Veg Hist Archaeobot* 14:237–258
- Kristiansen K, Allentoft ME, Frei KM, Iversen R, Johannsen NN, Kroonen G, Pospieszny L, Price TD, Rasmussen S, Sjögren K, Sikora M, Willerslev E (2017) Re-theorising mobility and the formation of culture and language among the corded ware culture in Europe. *Antiquity* 2017 91(356):334–347
- Lambert JB, Shawl CE, Stearns JA (2000) Nuclear magnetic resonance in archaeology. *Chem Soc Rev* 29(3):175–182
- Lityńska-Zajac M, Wasylkowska K (2005) Przewodnik do Badań Archeobotanicznych. In: Poznań
- Liu X, Hunt HV, Jones MK (2009) River valleys and foothills: changing archaeological perceptions of North China's earliest farms. *Antiquity* 83(319):82–95. <https://doi.org/10.1017/S0003598X00098100>
- McGovern PE, Mirzoiian A, Hall GR (2009) Ancient Egyptian herbal wines. *P Natl Acad Sci USA* 106:7361–7366
- Moskal-Del Hoyo M, Lityńska-Zajac M, Korczyńska M, Cywa K, Kienlin TL, Cappenberg K (2015) Plants and environment: results of archaeobotanical research of the Bronze Age settlements in the Carpathian Foothills in Poland. *J Archaeol Sci* 53:426–444
- Motuzaitė-Matuzevičiūtė G, Staff RA, Hunt HV, Liu X, Jones MK (2013) The early chronology of broomcorn millet (*Panicum miliaceum*) in Europe. *Antiquity* 87:1073–1085. <https://doi.org/10.1017/S0003598X00049875>
- Motuzaitė-Matuzevičiūtė G, Jacob J, Telizhenko S, Jones MK (2016) Millicin in palaeosols from an Early Iron Age in Ukraine reveal in situ cultivation of broomcorn millet. *Archaeol Anthropol Sci* 8(1): 43–50
- Pecci A, Ontiveros MAC, Garnier N (2013) Identifying wine and oil production: analysis of residues from Roman and Late Antique plastered vats. *J Archaeol Sci* 40:4491–4498
- Šáľková T (2010) Analýza rastlinných makrozbytků z objektů sídlisté mladší doby bronzové v Břežnici. *Popolnicové polia a doba halštatská Bratislava*:308–316
- Stika HP, Heiss AG (2013) Plant cultivation in the Bronze Age. Chapter 19 in H. Fokkens & A. Harding (eds.), *The Oxford Handbook of the European Bronze Age*. Oxford University Press, Oxford, 348–369
- Soberl L, Gasparic AZ, Budja M, Evershed RP (2008) Early herding practices revealed through organic residue analysis of pottery from the early Neolithic rock shelter of Mala Triglavca, Slovenia. *Doc Praehist* 35:253–260
- Tomczynska Z (2003) Wyniki analizy gatunkowej wegla drzewnych ze stanowiska Paprotki Kolonia st. 1 (sezony 1991–2002). Typescript in archive of the Institute of History and Political Sciences, Białystok
- Zhao Z (2011) New archaeobotanic data for the study of the origins of agriculture in China. *Curr Anthropol* 52(Suppl. 4):S295–S306. <https://doi.org/10.1086/659308>
- Zohary D, Hopf M, Weiss E (2013) Domestication of plants in the Old World. Oxford University Press, pp 69–71

ORIGINAL ARTICLE

The oldest millet herbal beer in the Europe? The ninth century BCE bronze luxury bucket from Kladina, Czech Republic

Jan Jílek^{1,2}  | Martin Golec³  | Petr Bednář⁴  |
 Miloslav Chytráček⁵ | David Vích⁶  | Tomáš Zavoral² |
 Zuzana Mírová⁷  | Libor Petr⁸ | Jaromír Kovárník⁹ |
 Peter Milo¹  | Lukáš Kučera⁴ 

¹Department of Archaeology and Museology, Faculty of Arts, Masaryk University, Brno, Czech Republic

²East Bohemian Museum, Pardubice, Czech Republic

³Department of History, Faculty of Arts, Palacký University, Olomouc, Czech Republic

⁴Department of Analytical Chemistry, Faculty of Science, Palacký University, Olomouc, Czech Republic

⁵Institute of Archaeology of the Czech Academy of Sciences, Prague, Czech Republic

⁶Regional Museum in Vysoké Mýto, Vysoké Mýto, Czech Republic

⁷Department of Archeology, Faculty of Arts, Charles University, Prague, Czech Republic

⁸Department of Botany and Zoology, Faculty of Science, Masaryk University, Brno, Czech Republic

⁹Laboratory of Archaeobotany and Palaeoecology, Faculty of Science, University of South Bohemia, České Budějovice, Czech Republic

Correspondence

Lukáš Kučera, Department of Analytical chemistry, Faculty of Science, Palacký University, 17. listopadu 12, 77900, Olomouc, Czech Republic.
 Email: lukas.kucera@upol.cz

Funding information

Palacký University Olomouc, Grant/Award Number: FPVČ_UPOL 452101601/30; Czech Science Foundation, Grant/Award Number: 17-17346S

Abstract

In 2017, a luxury bronze bucket was discovered near Kladina village in the Czech Republic. The bucket is dated to the ninth century BCE, and it is a unique artefact, having no parallel in Europe. Stylistically, it is a “transition type” dated between the Late Bronze Age (11th–10th century BCE) and the Hallstatt Period (eighth–sixth century BCE). Detailed palynological analysis of verdigris and soil infill of the bucket identified a wide range of pollen grains belonging mainly to herbs, with bitter-sour properties, and cereals. Subsequent chemical analysis by gas chromatography/mass spectrometry of soil extracts revealed the presence of the compound miliacin that is a chemical marker of millet. Moreover, a starch analysis reveals the presence of enzymatically modified starch grains. These data, with the help of archaeological knowledge, indicate

that the original content may have been millet-based food/beverage with addition of herbs. We suggest that this luxury vessel, given the contents we have identified, was deposited, in the late spring/summer months of the year.

KEYWORDS

bronze bucket, gas chromatography, herbs, Late Bronze Age, mass spectrometry, miliacin, palynology

INTRODUCTION

The earliest known evidence of the deliberate preparation of beer (using various bases and herbs) is known from China (the Yangshao culture, 5,000–3,000 BCE), where beer was produced primarily from rice and broomcorn millet. Herbs were used as additives, for example, *Panax ginseng*, *Lingusticum wallichii*, *Zingiber* sp. (Aouizerat et al., 2019; Liu et al., 2019; McGovern et al., 2004). Other very early finds of beer came from the pre-ceramic neolithic period in Anatolia (Rodzińska-Nowak, 2018), Mesopotamia (approx. 3,500 BCE) and Egypt (3,500–3,400 BCE) (Nelson, 2005). Some ceramics from Scotland (approx. 3,000 BCE) contained organic residues, indicating the presence of cereal and honey, that point to beer and currently are considered as the oldest finds in Europe. Cereals, pollen, meadowsweet (*Filipendula ulmaria*) and henbane (*Hyoscyamus niger*) residues are also known from the Grooved Ware Period (3,000 BCE) from Scotland the same site. Meadowsweet has often been used as a natural preservative, especially in Scottish and Danish sites such as Kinloch (2000 BCE) or in a cremation burial in bronze ciste found at North Mains, Strathallan, and Ashgrove Farm, Methill (approx. 1,600–1,500 BCE) (Dickson, 1978; Dickson & Dickson 2000). Traces of lime, meadowsweet and white clover pollen, wheat grains, sweetgale, cowberry, and cranberry were discovered in a birch vessel of the famous girl from Egtved (Nelson, 2005). Note, that wine, barley beer and mead, from the years 740–700 BCE, were also found in the Midas mound, in Turkey. This richly equipped grave proves that beer was still an elite drink during this period (McGovern, 2017).

The presence of herbal beer in 560 BCE was proven in a tomb in Pombia, North-West Italy. This Etruscan “grog” contained bitter ingredients like *Artemisia* and *Humulus* (Whitehead, 2013). There is also evidence for the preparation of barley beer in the sixth century BCE in Hochdorf, southwest Germany. Statistical analysis of archaeobotanical samples from over 250 locations in central Neckar showed beer additives in the form of mugworts (*Artemisia vulgaris*) and carrot (*Daucus carota*) (Stika, 2011). An interesting find is a ritually placed bronze strainer, part of bronze hoard from Ikervár (northwest Hungary) dated to the sixth century BCE. The infill of the strainer provided a pollen spectrum, which, besides *Cerealia*, contained a number of herbs such as *Artemisia*, *Plantago lanceolata*, *Menta longifolia*, *Althea officinalis*, *Allium*, *Achillea*, and so on. Those results were used to determine the hoard deposition period and it pointed to late summer, which could be associated with the Greek ritual drink *kykeon* consumed at Eleusin (Nagy et al., 2012). Soroceanu (2005) assume that bronze luxury vessels from the transition period from the Late Bronze Age to the Early Iron Age in Central Europe could be part of a cult/ritual ceremony (Soroceanu, 2005).

During European prehistory, millet or millet beer played an important role that we cannot yet fully identify and interpret, due to the lack of sufficient data. Noteworthy clues are found in ancient texts, including the Bible. Celtic, Germanic, and Slavic mythology also feature remarkable references (Garine, 2001; Hell, 1991; Nelson, 2005; O'Brien, 2006;

Rodzińska-Nowak, 2018). The preparation of millet alcoholic beverages from cereals can be still found from the Balkan Peninsula to Central Asia. In Europe this beverage is found mainly in Romania and Bulgaria, where it is called boza. Note, that the production of millet beer is still known among cultures of Africa (Gariné, 2001) where a millet beer is involved in every aspect of daily life such as: sacrifices, rites of passage, dances, births, marriages, burials and funeral celebrations, welcoming a guest, sealing a contract, agricultural cooperatives, domestic construction projects (barn raising), discussions between village elders, or social gatherings at home and market. One of the oldest texts describing the use of beer is the Epic of Gilgamesh, in which the wild man Enkidu becomes a man by drinking beer, eating bread, and having sex, later he meets the goddess of fermentation Siduri who convinces him to enjoy earthly pleasures. Alcohol helps humans to connect with gods, via altered states of consciousness (especially when adding hallucinogenic or slightly poisonous substances such as *Hyoscammus niger* or *Artemisia absinthium*) and serves to worship deities (Long et al., 2000; Padosch et al., 2006).

The aim of this research is detailed characterization of soil content from the extraordinary 145 litre bronze Kladina bucket bearing the decoration of the solar barge (a key mythological motif of the Late Bronze Age), which is a missing link in the line of European bronze buckets at the end of Bronze Age (9th century BCE). It follows on from the oldest buckets, from 11th–10th century BCE (North-East Hungary) and leads up to the later ones, from eighth–sixth century BCE (Alpine region and North Italy). The techniques used were pollen analysis, gas chromatography combined with mass spectrometry and starch analysis. The combination of these techniques and archaeological knowledge of such vessels in the ninth century BCE brings new information the Central European mythology of the Celts and the Nordic mythology of the Germans.

MATERIALS AND METHODS

Archaeological context

The bronze bucket, with the motif of a solar barge, was discovered on 21 September, 2017 in a sand dune rising slightly above the surrounding terrain at Kladina cadastre (plot number 299/2), Pardubice District, on the site “Obecní les” (Figure 1a,c). The bronze bucket was accidentally found during digging in the sandy soil by Mr. Pavel Rybka. The site is located at 227 m above sea level. The focus of the second phase of field work was to find out whether it was a hoard, a settlement situation, or a grave. The result of the sondage (trench measuring 290 × 330 cm and a maximum depth of 132 cm, Figure 1b,d) showed that the bronze vessel is an isolated find and is a monodeposit, which was also confirmed by a geophysical survey (Ferex fluxgate magnetometer, Förster; grid: 0.25 × 0.50 m; area 30 × 35 m) carried out by Peter Milo with the aim of identifying possible archaeological objects in the vicinity of the finding. Analysis of the metal composition of the bronze bucket was performed by particle induced x-ray spectroscopy (PIXE). This technique proved the alloy to be bronze; 87.6% Cu, 9.9% Sn and 1.2% Pb (m/m; measured on polished surface) (Angyal et al., 2018). The vessel is now stored in the collections of the East Bohemian Museum in Pardubice, Acq. No. 412/2017.

The bronze bucket (height 69 cm, max. Width 60 cm, base diameter 29.5 cm; Figure 2) was already partially damaged, and cracks were observed close to the bottom part. When the bucket was lifted the base had separated from the body. The bucket rim is a separate part, which was mounted on the wall of the neck and then to the body. The body of the vessel is made of four bronze sheets, which are connected by rivets at the edges. The base was also separate. The shoulder of bucket is decorated with a moulded cordon and small studs (Figure 2a). The same decoration is also present on the four handles (Figure 2e). The handles divide the decorative area into four equal quarters in which identical decoration is repeated, and they are decorated

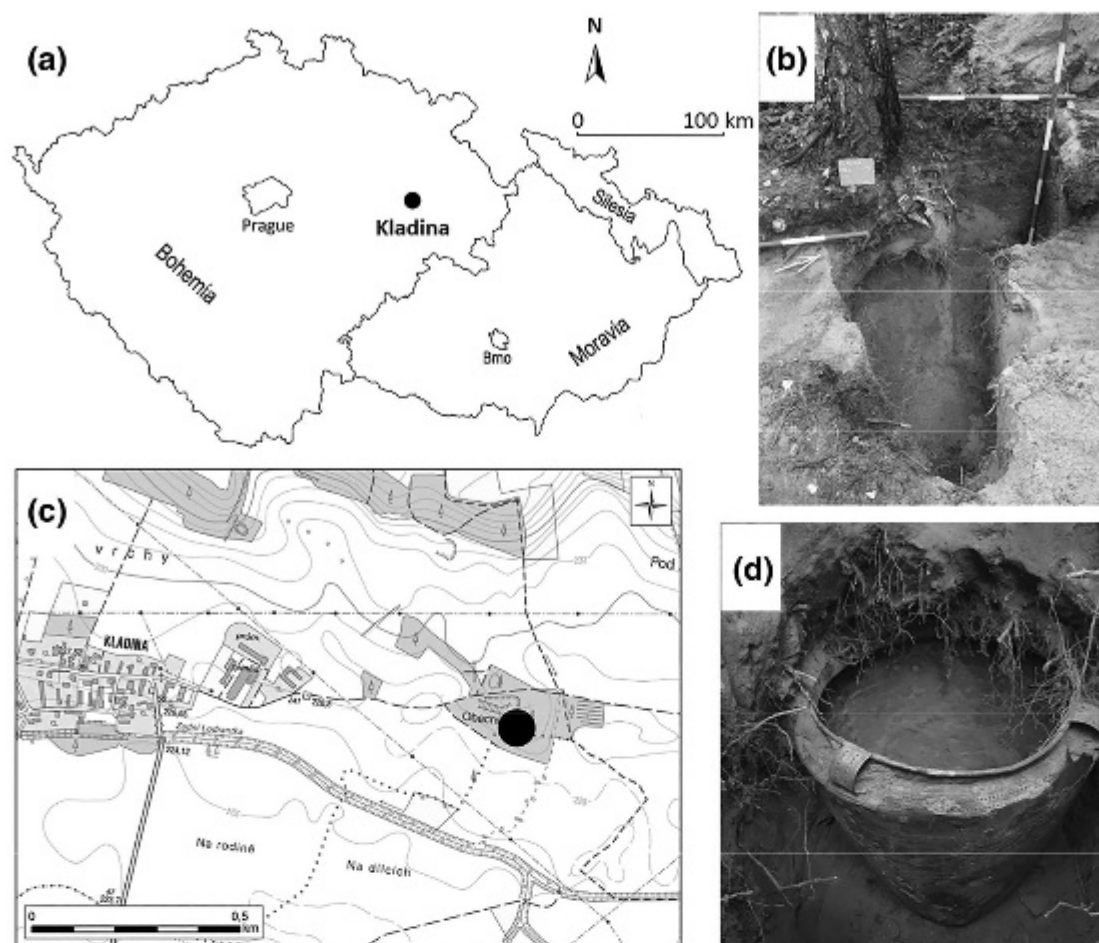


FIGURE 1 (a) Map of the Czech Republic showing the village of Kladina in north-East Bohemia (b) excavation pit after extraction of the bronze vessel (c) locality of the find, east of the village Kladina (d) bronze vessel in situ in the terrain

with two rings and swallow tail-shaped pendants (Figure 2e). In each quarter there is a central motif of the solar barge (Figure 2a) finely embossed from lines of tiny studs. The composition of the central décor consists of concentric discs with a central stud (sun motif). Above and to either side of the sun there are two mirror-image waterfowl (“Apollo’s Swans”), which are connected to the orbital line, also composed from tiny studs. Two isolated waterfowl are embossed in the opposite lower part of the solar disc. The motif of the solar barge thus consists of a central stud surrounded by four stylized waterfowl. Between the individual motifs of the solar barge are two further waterfowl, the upper is always connected to the orbital line, the lower is isolated. The base consists of two sheets and is connected by a central rivet (Figure 2c). The space between the outer and inner sheets was filled with a slightly burnt ceramic material (a substance close to the daub). Note that daub cannot be found in the surrounding area. The bottom plate is reinforced by a rosette with thirteen radial strips and is again connected by a central rivet (Figure 2d). The workmanship of the whole motif is very fine and sophisticated.

Pollen analysis

Overall, six samples were taken from the bronze vessel surface: S1 – filling of the central part of the vessel; S2 – bottom of the vessel; S3REF – the outer surface of the vessel; S4 – the inner surface of the vessel; S5 – upper sheet of the double bottom; and S6 – lower sheet of the double bottom. Surrounding soil was used as a next reference sample (S7REF). The analysis of samples

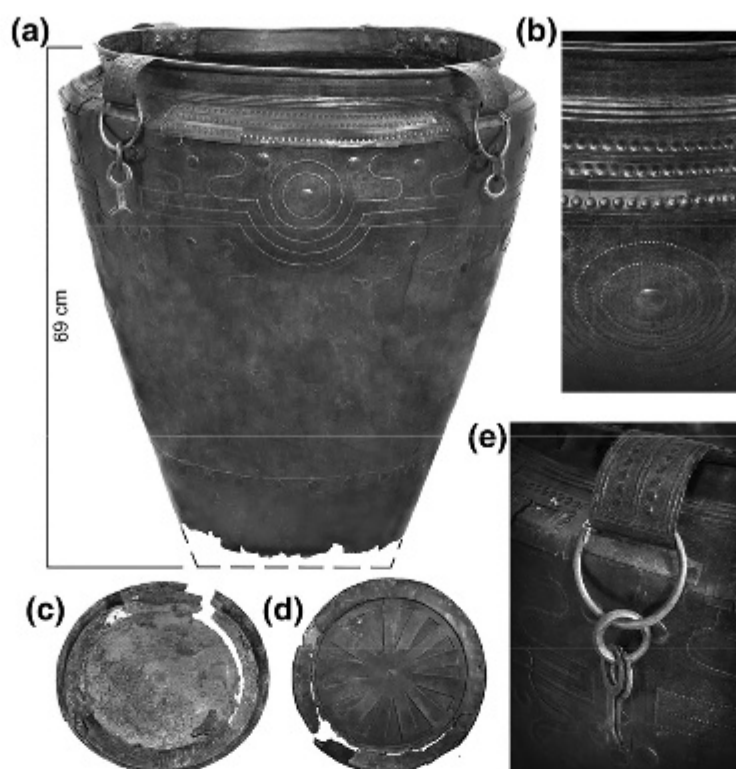


FIGURE 2 (a) The object studied – a bronze bucket of Kurd type, Kladina variant, with four handles with pendants and embossed decoration of the solar barge on the body, (b) detail of decoration technique, (c) upper part of the bottom, top view, (d) lower part of the bottom with rosette reinforcement, bottom view, (e) handle and pendant detail

can also help to determine the environment and vegetation cover around the site at the time of deposit. All samples consisted of a mixture of clay, fine sand, and verdigris. The volume of verdigris was limited by the need to preserve and protect the vessel; we have used only pieces which were already detached. Pollen samples were sieved on a mesh after KOH treatment; only the fine fraction was used for the next step. Approximately 0.5 cm^3 of material was used for pollen processing. Samples were processed by a standard method of acetolysis, including using hydrofluoric acid (Moore et al., 1991). Pollen atlases (Beug 2004; Moore et al., 1991) were used for pollen grain identification. Hard task is distinction between *cerealia* type and *Poaceae*. Briefly, the distinction between cereals and grasses is possible according to two features: (1) relative size of the pollen grain and (2) the size of annulus, which is about two times larger in *cerealia*. However, sometimes those features cannot be found in deformed pollen grains. Safranin was used for pollen grain staining. At least 300 grains were counted in each sample. Plant names follow the Database of Czech Flora and Vegetation (www.pladias.cz). The pollen diagram was made using the freeware environment for statistical computing, R-project, version 4.0.0 (R Core Team, 2020) including the package “rioja” (Juggins, 2020). For cluster analysis the package “vegan” was used (Oksanen et al., 2020).

Gas chromatography/mass spectrometry (GC/MS)

The soil infill of the bronze bucket was divided horizontally into three parts (first, second, and third layer, marked as SL1, SL2 and SL3, respectively). The third layer contained the soil from the double bottom of the bucket. Surrounding soil was used as a reference sample (SLREF). 200 mg of each sample were directly extracted by 1 mL acetone/chloroform solution (50:50, v/v) and consequently centrifuged at 14.000 RPM for 2 minutes (Kučera et al., 2019). Agilent

7,010 Triple Quadrupole GC/MS system with Mass Hunter software (Agilent Technologies, Palo Alto, USA) was used for analysis. The separation was performed on two (5%-Phenyl)-methylpolysiloxane capillary columns HP-5 ms Ultra Inert connected in series (15 m × 0.25 mm × 0.25 µm, each) with constant flow 1.0 and 1.2 mL min⁻¹, respectively. Nitrogen (Messer Group GmbH, Germany) was used as a collision gas with flow rate 1.5 mL min⁻¹ and helium (He 5.0. Siad, Italy) as a quench gas with flow rate 2.25 mL min⁻¹. Initial oven temperature was 70°C for 5 min, then the oven was heated up at a rate of 15°C min⁻¹ to the value of 300°C, which was held for 10 min. Injection volume was 0.5 µL with splitless injection. The multiple reaction monitoring (MRM) screening method was used for detection of miliacin in prepared samples (MRM transition was 440 → 189). The MRM is highly specific and sensitive technique for quantification of compound of interest. In complex matrix, as a soil, a coeluting compounds could be found. The application of MRM eliminate this nuisance (Kuzyk et al., 2009). Besides MS1, SIM scan type (m/z 189, 204, 218) was used for identification of miliacin and detection of other pentacyclic triterpenes (PTMEs). For identification and quantification of miliacin in a sample an authentic standard of miliacin (PhytoLab GmbH & Co., Germany; concentration 50 mg L⁻¹ in 1:1 acetone: CHCl₃ solution [v/v]) was used.

Morphological analysis of starch grains

Soil taken from the bottom of the bronze bucket was transferred into a test tube with ethanol solution. A drop of ethanol solution containing the microresidues was placed on a glass slide. The slide was sealed with transparent nail polish. Identification is conducted by direct observation and comparison with specimens of a reference collection (Coil et al., 2003; Li et al., 2013; Messner et al., 2008; Pagan-Jimenez et al., 2015; Therin et al., 1997; Yeung et al., 2015). The analysis of starch grains is based on microscopic observation of samples in polarized and non-polarized light. The structures found in the samples taken from the archaeological artifact (vessel) were recognized on the basis of the optical properties and the morphological features of the starch grains.

RESULTS

Typological, chronological and cultural aspects of the bronze vessel

The bronze bucket from Kladina is ranked in the Bohemian horizons of hoards of bronze objects Ha B2–B3 Hostomice and Lžovice-Slezské Předměstí. It falls culturally into the Silesian phase (Ib–II) of the Silesian-Platěnice culture of the Lusatian Urnfield culture (Jiráň, 2013). From a social point of view, we can attribute the bucket from Kladina to the elites. This bucket from Kladina, dated to the ninth century BCE is unique, and it has no parallel in all the known bronze buckets described in Supplement 1 (Figure 3; Supplement 1). We can classify it as a Kurd type bucket, Kladina variant (see Supplement 1). It is a “transition type” between the older stage of the Late Bronze Age (11th–10th century BCE) and the Hallstatt Period (8th–6th century BCE), and is the most luxurious object from the period Ha B1–B3 in the Czech Republic.

Pollen analysis

A detailed characterization of soil content from the Kladina bronze bucket was performed using pollen and starch morphological analysis, and gas chromatography combined with mass

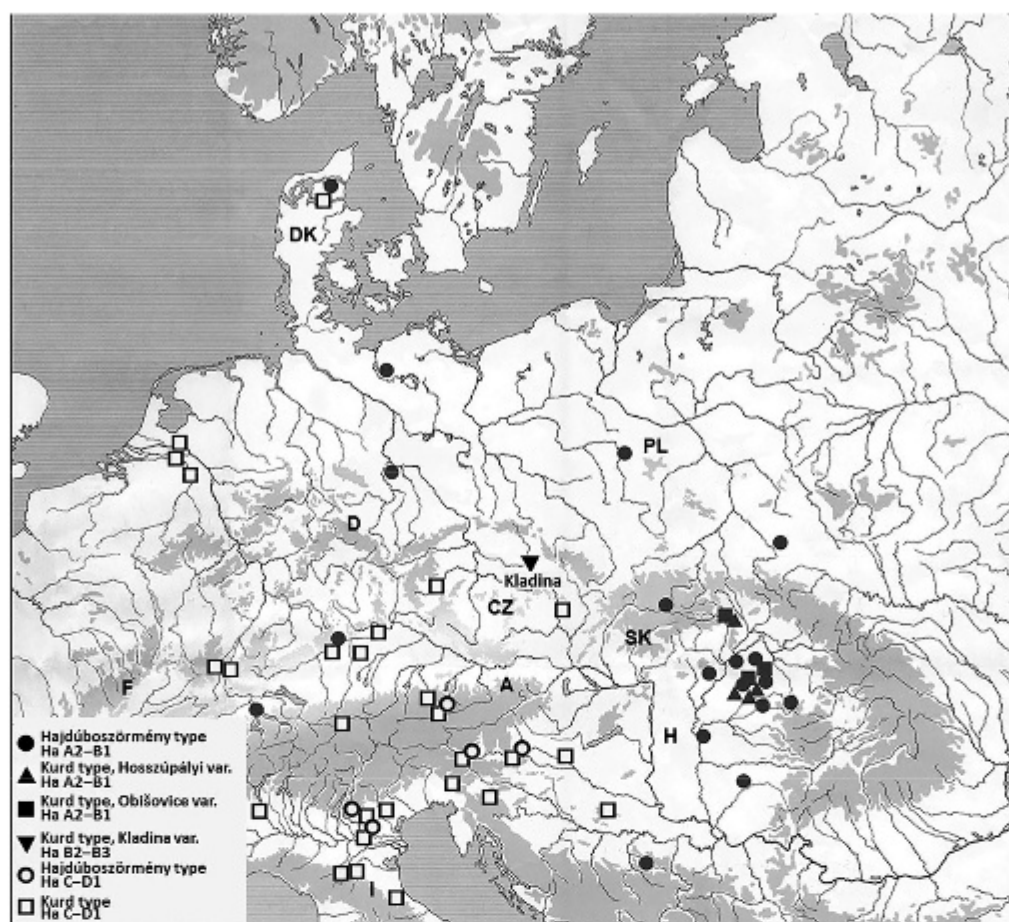


FIGURE 3 Map of the occurrence of bronze buckets of the Hajdúböszörmény (Ha A2–B1; black dot and Ha C–D1; white circle) and Kurd type in Europe, belonging to the three time periods – Ha A2–B1 (11th–10th century BCE; black triangle – Hosszúpályi variant; black square – Obišovice variant), Ha B2–B3 (9th century BCE, inverted black triangle – Kladina variant) and Ha C–D1 (8th–6th century BCE; white square) (Egg & Kramer, 2013; Szabó & Bálint, 2016)

spectrometry. The samples for pollen analysis were taken from six places on the bronze vessel and one from the area near the bucket (Figure 4a). All analysed samples of the bronze bucket contained pollen grains from trees and herbs (Figure 4b). All analysed samples had an arboreal to non-arboreal (AP/NAP) ratio of pollen grains of about 40%, a proxy for vegetation openness of vegetation. The prevailing pollen types were cereals and grasses. The Bronze Age Period is remarkable for the presence of silver fir (*Abies*) and hornbeam (*Carpinus*) in lowlands (Kozáková et al., 2011). Various spectra of arboreal pollen can reflect a vegetation mosaic or the seasonal period (e.g. the absence of hazel [*Corylus*], which flowers from February to March, whereas other trees flower during April and May). Birch pollen indicates woodland disturbances and early succession vegetation. Despite the present-day site being pine woodland, there is a low abundance of pine (*Pinus*). The absence of pollen grains in surrounding sand excludes postdeposition contamination of modern pollen grains. Interestingly, there is an abundance (higher in sample S4, i.e. 6%) of *Euphrasia/Rhinanthus*-type pollen grains (Figure 4b). Those plant hemiparasites occur in open habitats or open canopy woodland, but their abundance in the pollen assemblages is unusually high. Note that, *Euphrasia* was used in natural healing, and their abundance in the pollen spectrum may be the result of such practices. The abundance (37%) of cereal pollen on the bottom of vessel has its origin in the vessel contents. It should be noted that the large pollen grains (mainly coniferous and cereals) were often damaged and degraded and, therefore, detailed determination of those types by pollen analysis is sometimes impossible. Pollen samples contain an abundance of herbs, ruderal species, and indicators of

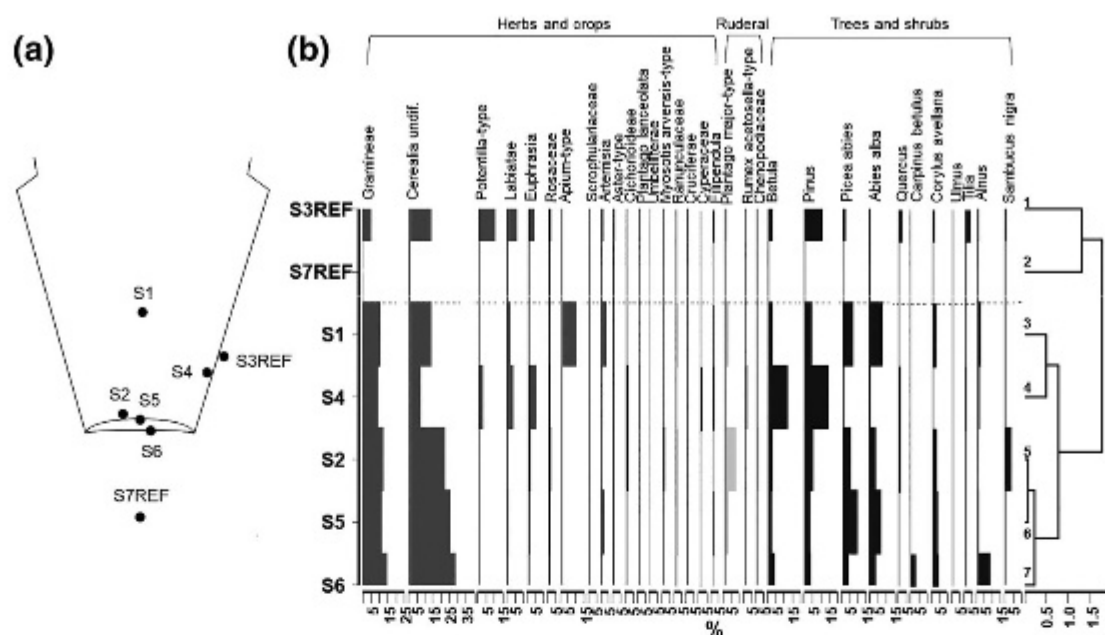


FIGURE 4 (a) Sampling places for palynological analysis from bronze bucket, (b) S1 – Filling of the central part of the vessel; S2 – Bottom of the vessel; S3REF – The outer surface of the vessel; S4 – The inner surface of the vessel; S5 – Upper sheet of the double bottom; S6 – Lower sheet of the double bottom; S7REF – Sand outside the vessel; relative pollen diagram of samples from inside and outside the bucket with content $\geq 1\%$

trampling such as *Plantago major*, *Plantago lanceolata* and *Rumex acetosella*. The presence of herbs, such as *Artemisia*, *Aster*-type, *Plantago lanceolata*, *Plantago major*, *Euphrasia*, Cichorioideae, Ranunculaceae, Rosaceae, *Filipendula*, and Cyperaceae (Figure 4b), may indicate deliberate addition to the contents due to their specific properties: healing, taste, aroma, possibly others (e.g. the ability to preserve) (Behre, 1999; Hintz, Matthews, & Di, 2015; Nelson, 2005). Raw data of pollen analysis are shown in Supplement 2 including pollen grains with content $< 1\%$. Microcharcoals were prevalent in all samples and, given their elongated shape with wavy edges and dark brown colour, can be considered as burned grasses. The sharp-edged black microcharcoal, typical of wood, had low frequency. Hierarchical clustering (HCA) was used to study the similarity of pollen samples. Figure 4b shows the dendrograms of the relationships among the samples (S1-S6) and reference samples (S3REF and S7REF). Generally, the soil samples from the Kladina bucket (S1, S2, S4, S5, and S6) were located in separated clades (i.e., leaves 3, 4, 5, 6 and 7) compared with the reference samples (i.e. leaves 1 and 2). HCA points out that all samples from the Kladina bucket differ significantly from the reference ones.

Gas chromatography/mass spectrometry

Even if the cereal seeds are no longer present in soil, their ‘chemical imprint’ still persists. For the exact determination of cereal origin, a GC/MS method was used (Kučera et al., 2019). In samples (Figure 5a) from the bottom (SL3) and middle (SL2; Figure 5a) parts of the internal soil content an intensive signal of ion at m/z 440 was found (retention time 25.3 min, mass spectrum and TIC chromatogram in Supplement 3A). This compound was ascribed to a plant triterpenoid miliacin–biomarker of broomcorn millet (*Panicum miliaceum*) (Bossard et al., 2013; Heron et al., 2016; Jacob et al., 2008). This signal was found neither in the first soil layer (SL1) taken from the internal part of the bronze bucket nor in the surrounding soil (SLREF). This fact excludes cross-contamination of soil samples from the bottom and middle parts of the bucket. Identification of this compound in our vessel was based on m/z value,

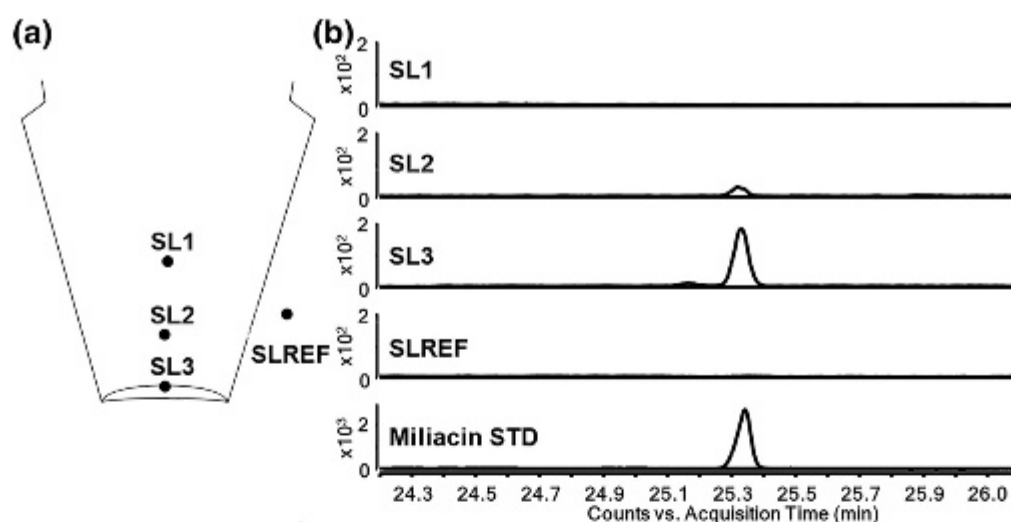


FIGURE 5 (a) Sampling places for GC/MS analysis, (b) chromatograms of MRM transition 440 → 189 of soil extracts and miliacin standard

comparison of analytical parameters with analytical standards, and data from literature (Bossard et al., 2013; Kučera et al., 2019). Retention times of the miliacin standard and the compound from the soil extract of the bronze bucket were identical (RT = 25.3 min; Figure 5b). The concentrations of miliacin in samples SL2 and SL3 of the studied bronze bucket are approximately 5 and 33 $\mu\text{g g}^{-1}$ of soil, respectively (single point quantification using miliacin standard at concentration level 50 mg L^{-1}). Motuzaite-Matuzeviciute et al. (2013) discussed the potential of not only miliacin but also other pentacyclic triterpenes as biomarkers of broomcorn millet, primarily due to their antifungal/antibacterial properties and therefore their ability to survive to the present day. Multiple reaction monitoring (MRM) screening (MRM transition was 440 → 189) done in our study revealed one more peak in an archaeological soil sample (RT = 26.9; Supplement 3B). Characteristic fragments at m/z 189, 204, 218 were observed within this peak in targeted SIM measurements (MS1 SIM scan type). Moreover, these characteristic fragments were observed during fragmentation of another three compounds eluting at 25.4, 26.9 and 29.7 min (Supplement 3B). Note, that concentration of those compounds in the samples is very low, which prevents identification of the parent mass. However, comparison of this pattern and retention order with former literature (Bossard et al., 2013; Heron et al., 2016; Jacob et al., 2008; Motuzaite-Matuzeviciute et al., 2016) suggests that those compounds belong to the PTMEs group (e.g. isosawamilletin or urs-12-en-3 β -ol ME).

Morphological analysis of starch grains

The results mentioned above point to the presence of millet and herbs in the Kladina bucket. Moreover, a morphological analysis of starch grains was performed. Three starch granules with damaged structure and weak light exposure in polarized light were found in the sample from the bottom of Kladina bucket (Figure 6). The first starch granule is oval/ovoid in shape, and its size is 28.6 μm by 18 μm . This grain has a weak optical expression with a slight hint of growth rings (Figure 6a,b). The second starch granule (size of the object is 39. μm by 30 μm) is round to slightly oval with a significant crack and surface erosion. Optical activity is very faintly visible (Figure 6c,d). The third structure is a small (4.5 μm) square or rather trapezoidal grain with intact exterior, but the inner part of the mass of the object is missing. The rest of the border in polarized light shows the characteristics markers for starch (Figure 6e,f). (Hayden et al., 2013; Ma et al., 2019; Wang et al., 2017; Wang et al., 2019). Deteriorated optical properties of starch

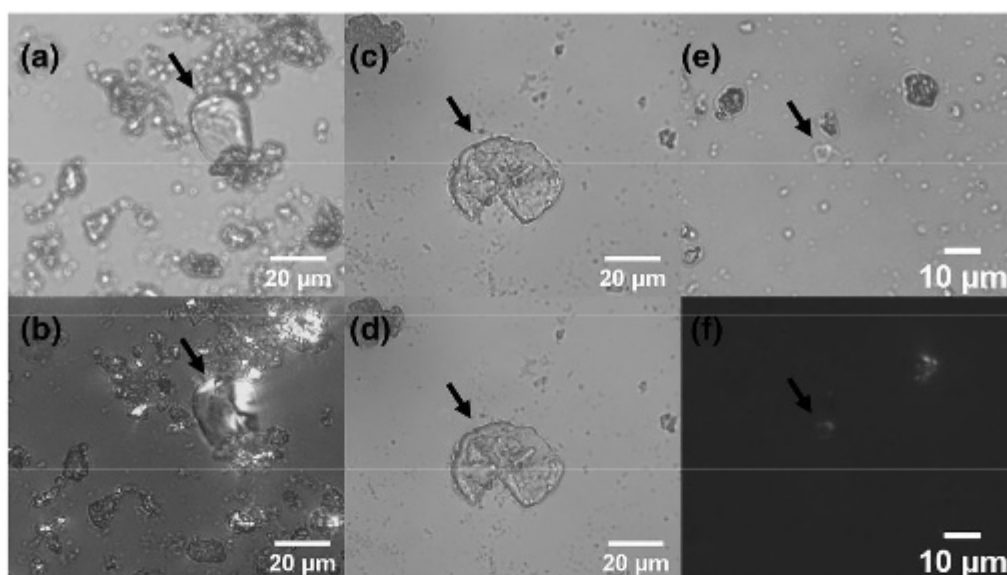


FIGURE 6 Starch grains found in soil samples taken from the bottom of Kladina bucket. (a – oval/ovoid object in transmitted light and b – In polarized light; c – Slightly oval object with a significant crack and surface erosion in transmitted light and d – In polarized light; e - small square or rather trapezoidal object without inner part of the mass in transmitted light and f – In polarized light)

grains indicate damage due to high temperature and enzymatic activity (Bemiller & Whistler 2009; Henry et al., 2009; Messner et al., 2008). Henry et al. (2009) studied the effect of boiling on different varieties starch grainules. Application of high temperature in the absence of water caused large damage to the starch granules (i.e. extreme swelling and cracking). However, heating in the presence of water caused the starch grains to lose their extinction crosses and to appear softer. Author pointed out that, the appearance of the extinction cross is often a tangible indicator of cooking damage, even when the starch grain appears relatively undamaged under normal light. This pattern was found for third starch granule (Figure 6f), which means that the contents of the vessel were boiled (in brewing industry called mashing). Wang et al. (2017) analyse different starch types to find a typical pattern for beer making in ancient times. The process starts with enzymatic attacks followed by a pattern of endocorrosion, creating pitting on the granule surface and then completely digesting the interior core of the granule (Humia et al., 2019; Wang et al., 2017). This feature, called ‘pizza crust’ or ‘donut’ shape is visible in our samples as well.

DISCUSSION

Possibility of the presence of millet-based food with addition of herbs

The unique discovery of the millet ‘chemical imprint’, starch grains and the spectrum of the stored herbs indicates that the bronze bucket contained millet grains/mash in combination with fresh/dried herbs or millet beverage (herbal beer). The presence of herbal beer can be suggested from the spectrum of herbs or trees (Figure 4b). For most of them, only higher scientific classifications were identified, such as genus or subfamily. Certain genera have characteristic properties (aromaticity, taste, medical use) and are known as an additive for the preparation of beers (Behre, 1999; Nelson, 2005). It is very conspicuous that only two tree species were represented in the bucket (with no proven presence in the surrounding soil)–*Quercus* sp. and *Sambucus nigra*. Leaves and bark of oak are characterized by a high content of lignans that makes its taste

significantly bitter, and they are used in the food industry as additives (Winstel & Marchal, 2018). Both trees were already used as additives for flavoring hop-free beers (Behre, 1999). The addition of flavorings and other additives is necessary to improve the taste, quality, and shelf life of beer (Behre, 1999). Nowadays, mainly hops are used, and that has been widespread since the 14th century AD. Until then, beers were produced with the addition of various herbs, the so-called gruit (Vilsteren, 1996). To achieve the right taste of beer, it is necessary to balance the basic flavors, bitter and sour (the sweet taste originates from the malt). Herbs with a high content of tannins, alkaloids, flavonoids, terpenes, or phenols are most often added to provide the bitter taste of beer (Drewnowski & Gomez-Carneros 2000). Herbs, mainly from the Lamiaceae family (e.g. *Thymus* sp., *Teucrium* sp., *Betonica officinalis*, *Salvia officinalis*, *Origanum vulgare*, *Mentha* sp., *Melissa officinalis*), are also added for acidity or specific smell and Apiaceae family plants (e.g. *Carum carvi*, *Meum athamanticum* and *Petroselinum crispum*) for their distinctive aroma and taste (Behre, 1999; Heath, 1981). Herbs with acid properties are desirable for preservative properties rather than taste, like *Artemisia*, *Potentilla*, Lamiaceae, *Plantago*, *Euphrasia*, *Ranunculaceae*, *Rosaceae*, and *Filipendula* (Hintz et al., 2015). Note that commonly used natural preservatives for beers are *Potentilla anserina*, *Achillea millefolium*, *Plantago lanceolata*, and *Filipendula ulmaria* (Behre, 1999). Many of the above mentioned plants are also used in medical and folk medicine applications, such as *Euphrasia*, *Plantago lanceolata*, *Filipendula ulmaria* (Najafian et al., 2018; Oreagba et al., 2011; Paduch et al., 2014). Pollen grains of the plants discussed were found in the bronze vessel from Kladina (Figure 4b). Note, that the pollen spectrum has the same species as ruderal habitats, or dry grassland of the Bronze Age Period, but the abundance of selected species (e. g. *Euphrasia*) does not correspond to natural habitats of the then cultural landscape (Pokorný, 2006, 2015). Based on the facts about taste, aromatic and preservative properties mentioned above the authors assume that the spectrum of herbs found is not random or 'natural' in origin (clogged by intrusion) but was deliberately used to prepare a bitter food/beverage with potentially 'healing' properties.

Due to the large dimension (volume of about 145 liters), authors assume that millet was in the bucket as a beverage/liquid mash (millet beer). Large dimensions of vessels could be the first archaeological indicators of the possible brewing of beer. In the 13th century beer was brewed in vessels of 100–150 liters (Vilsteren, 1996). Another indicator could be the expanding (conical) shape of the vessel, as seen in buckets used for brewing beer in ancient Egypt (O'Brien, 2006). It is also worth noting the rosette-reinforced double bottom (Figure 2c,d), which contained a partially burnt clay like daub. The authors believe that this is a technical matter. The reinforced bottom could serve to improve the thermodynamics of the bucket (less burning during cooking) and to better withstand pressures up to 150 kg. Thus, it is not excluded that the vessel served not only for storage but also as a "beer brewing pot" for a large volume of beer. Note, that it is, in the ninth century BCE, the largest metal vessel north of the Alps. It also seems important to place the vessel vertically with the bottom on the ground, as was also true for hoards of buckets from Remetea Mare, Siem Mariensminde (Soroceanu, 2005). In our case, we can combine information about the packing and the content of vessel. Considering that the bucket in Kladina was stored at the time of the millet harvest, and the beer was brewed from a new crop, signifying the "first fruit" ritual, it should have been late summer. Almost all the herbs would then be used as fresh.

CONCLUSION

Analysis of soil infill of bronze bucket from Kladina shows the deliberate placement of herbs, which were found in considerable (relative) amount, and their combination points to the original vessel content. GC/MS analysis of the soil extracts from Kladina bucket showed a chemical imprint of millet. The presence of millet was also confirmed by starch analysis, where

thermally and enzymatically modified starch grains were found. The results from analyses points to the presence of millet grains or millet 'extract'. The combination of millet and herbs with bitter taste and aromatic, preservative, and/or healing properties offers the most likely interpretation, the storage of millet-based food/beverages with addition of herbs. The authors also hypothesized that the content of the bronze bucket from Kladina could be the oldest European herbal beer. The depiction of the two groups of motifs of the solar barge and separate waterfowl on the vessel from Kladina, in conjunction with the food/beverage content, strongly suggests the deliberate ritual deposition of the vessel, in the presence of the elites that owned the vessel.

ACKNOWLEDGEMENT

The authors gratefully acknowledge the support of the Czech Science Foundation [17-17346S] and Palacký University Olomouc [FPVČ_UPOL 452101601/30] for financial support. Authors also would like to thank Luděk Vojtěchovský for photodocumentation of bronze bucket.

PEER REVIEW

The peer review history for this article is available at <https://publons.com/publon/10.1111/arcm.12711>.

ORCID

Jan Jilek  <https://orcid.org/0000-0003-1751-6030>

Martin Golec  <https://orcid.org/0000-0002-3811-8819>

Petr Bednář  <https://orcid.org/0000-0001-7070-6015>

David Vích  <https://orcid.org/0000-0003-2178-8194>

Zuzana Mírová  <https://orcid.org/0000-0002-7831-2093>

Peter Milo  <https://orcid.org/0000-0002-4625-0078>

Lukáš Kučera  <https://orcid.org/0000-0002-3773-6439>

REFERENCES

- Angyal, A., Ákos, C., Kertész, Z., Papp, E., Szikszai, Z., Szoboszlai, Z., & Török, Z. (2018). Research report of Atomki IBA laboratory on the IPERION-CH TNA project LTB-SIT-Kladina, Institute for Nuclear Research of Hungarian Academy of Sciences. Debrecen.
- Aouizerat, T., Gutman, I., Paz, Y., Maeir, A. M., Gadot, Y., Gelman, D., Szitenberg, A., Drori, E., Pinkus, A., Schoemann, M., Kaplan, R., Ben-Gedalya, T., Copenhagen-Glazer, S., Reich, E., Saragovi, A., Lipschits, O., Klutstein, M., & Hazan, R. (2019). Isolation and characterization of live yeast cells from ancient vessels as a tool in bio-archaeology. *MBio*, 10, e00388-19.
- Behre, K. E. (1999). The history of beer additives in Europe – A review. *Vegetation History and Archaeobotany*, 8, 35–48. <https://doi.org/10.1007/BF02042841>
- Bemiller, J. N., & Whistler, R. L. (2009). *Starch: Chemistry and technology* (3rd ed.). Amsterdam: Academic Press.
- Beug, H. J. (2004). *Leitfaden der Pollenbestimmung für Mitteleuropa und angrenzende Gebiete*. München: Dr. Friedrich Pfeil Verlag.
- Bossard, N., Jacob, J., Le Milbeau, C., Sauze, J., Terwilliger, V., Poissonnier, B., & Vergès, E. (2013). Distribution of miliacin (Olean-18-en-3 β -ol methyl ether) and related compounds in broomcorn millet (*Panicum miliaceum*) and other reputed sources: Implications for the use of sedimentary miliacin as a tracer of millet. *Organic Geochemistry*, 63, 48–55. <https://doi.org/10.1016/j.orggeochem.2013.07.012>
- Coil, J., Korstanje, M. A., Archer, S., & Hastorf, C. A. (2003). Laboratory goals and considerations for multiple microfossil extraction in archaeology. *Journal of Archaeological Science*, 30(8), 991–1008. [https://doi.org/10.1016/S0305-4403\(02\)00285-6](https://doi.org/10.1016/S0305-4403(02)00285-6)
- R Core Team. (2020). *R: A language and environment for statistical computing*, R Foundation for Statistical Computing, Vienna, Austria.
- Dickson, C., & Dickson, J. H. (2000). *Plants and people in ancient Scotland*. Stroud: Tempus.
- Dickson, J. H. (1978). Bronze Age Mead. *Antiquity*, 52, 108–113. <https://doi.org/10.1017/S0003598X00071921>
- Drewnowski, A., & Gomez-Carneros, C. (2000). Bitter taste, phytonutrients, and the consumer: A review. *American Journal of Clinical Nutrition*, 72(6), 1424–1435. <https://doi.org/10.1093/ajcn/72.6.1424>
- Egg, M., & Kramer, D. (2013). Die hallstattzeitlichen Fürstengräber von Kleinklein in der Steiermark: Der Kröllkogel. *Monographien des Römisch-Germanischen Zentralmuseums 110*. Mainz: Verlag des Römisch-Germanisches Zentralmuseum.

- Garine, E. (2001). An ethnographic account to the many roles of millet beer in the culture of the Duupa agriculturalists (Poli Mountains, Northern Cameroon). In I. Garine & V. Garine (Eds.), *Drinking. An anthropological approach* (pp. 191–204). Oxford: Berghahn Books. <https://doi.org/10.2307/j.ctt1x76dvt.22>
- Hayden, B., Canuel, N., & Shanse, J. (2013). What was brewing in the Natufian? An archaeological assessment of brewing technology in the Epipaleolithic. *Journal of Archaeological Method and Theory*, 20(1), 102–150. <https://doi.org/10.1007/s10816-011-9127-y>
- Heath, H. B. (1981). *Source book of flavors*. New York: Springer.
- Hell, B. (1991). La force de la bière. Approche d'une récurrence symbolique dans les systèmes de représentations de l'Europe nord-occidentale. In D. Fournier & S. D'Onofrio (Eds.), *Le Ferment Divin. Ethnologie de la France 12* (pp. 109–123). Paris: Éditions de la Maison des sciences de l'homme.
- Henry, A. G., Hudson, H. F., & Piperno, D. R. (2009). Changes in starch grain morphologies from cooking. *Journal of Archaeological Science*, 36, 915–922. <https://doi.org/10.1016/j.jas.2008.11.008>
- Heron, C., Shoda, S., Breu, B., A., Czebreszuk, J., Eley, Y., Gorton, M., Kirleis, W., Kneisel, J., Lucquin, A., Müller, J., Nishida, Y., Son, J.-H., & Craig, O. E. (2016). First molecular and isotopic evidence of millet processing in prehistoric pottery vessels. *Scientific Reports*, 6, 38767. <https://doi.org/10.1038/srep38767>
- Hintz, T., Matthews, K. K., & Di, R. (2015). The use of plant antimicrobial compounds for food preservation. *BioMed Research International*, 2015, 1–13. <https://doi.org/10.1155/2015/246264>
- Humia, B. V., Santos, K. S., Barbosa, A. M., Sawata, M., Mendonca, M. D., & Padilha, F. F. (2019). Beer molecules and its sensory and biological properties: A review. *Molecules*, 24(8), 1568.
- Jacob, J., Disnar, J. R., Arnaud, F., Chapron, E., Debret, M., Lallier-Vergès, E., Desmet, M., & Revel-Rolland, M. (2008). Millet cultivation history in the French Alps as evidenced by a sedimentary molecule. *Journal of Archaeological Science*, 35, 814–820. <https://doi.org/10.1016/j.jas.2007.06.006>
- Jiráň, L. (2013). *The prehistory of Bohemia 4. The Bronze Age*. Praha: Archeologický ústav AV ČR, Praha, v. v. i.
- Juggins, S. (2020). *rioja: Analysis of Quaternary Science Data*, R package version (0.9-26). (<https://cran.r-project.org/package=rioja>)
- Kozáková, R., Šamonil, P., Kuneš, P., Novák, J., Kočár, P., & Kočárová, R. (2011). Contrasting local and regional Holocene histories of *Abies alba* in the Czech Republic in relation to human impact: Evidence from forestry, pollen and anthracological data. *Holocene*, 21(3), 431–444. <https://doi.org/10.1177/0959683610385721>
- Kučera, L., Peška, J., Fojtík, P., Barták, P., Kučerová, P., Pavelka, J., Komárková, V., Beneš, J., Polcerová, L., Králík, M., & Bednář, P. (2019). First direct evidence of broomcorn millet (*Panicum miliaceum*) in Central Europe. *Archaeological and Anthropological Sciences*, 11, 4221–4227. <https://doi.org/10.1007/s12520-019-00798-4>
- Kuzyk, M. A., Smith, D., Yang, J., Cross, T. J., Jackson, A. M., Hardie, D. B., Anderson, N. L., & Borchers, C. H. (2009). Multiple reaction monitoring-based, multiplexed, absolute quantitation of 45 proteins in human plasma. *Molecular & Cellular Proteomics*, 8, 1860–1877. <https://doi.org/10.1074/mcp.M800540-MCP200>
- Li, M. Q., Yang, X. Y., Ge, Q. S., Ren, X. Y., & Wan, Z. W. (2013). Starch grains analysis of stone knives from Changning site, Qinghai Province, Northwest China. *Journal of Archaeological Science*, 40(4), 1667–1672. <https://doi.org/10.1016/j.jas.2012.11.018>
- Liu, L., Wanga, J., Levin, M. J., Sinnott-Armstrong, N., Zhaod, H., Zhaoe, Y., Shaof, J., Dif, N., & Zhangf, T. (2019). The origins of specialized pottery and diverse alcohol fermentation techniques in early Neolithic China. *PNAS*, 116(26), 12767–12774. <https://doi.org/10.1073/pnas.1902668116>
- Long, D., Tipping, R., Holden, T., Bunting, M., & Milburn, P. (2000). The use of henbane (*Hyoscyamus niger* L.) as a hallucinogen at Neolithic 'ritual' sites: A re-evaluation. *Antiquity*, 74(283), 49–53. <https://doi.org/10.1017/S0003598X00066138>
- Ma, Z. K., Perry, L., Li, Q., & Yang, X. Y. (2019). Morphological changes in starch grains after dehusking and grinding with stone tools. *Scientific Reports*, 9(1), 1–13.
- McGovern, P. E. (2017). *Ancient brews. Rediscovered and re-created*. New York: W. W. Norton & Company.
- McGovern, P. E., Zhang, J. H., Tang, J. G., Zhang, Z. Q., Hall, G. R., Moreau, R. A., Nunez, A., Butrym, E. D., Richards, M. P., Wang, C. S., Cheng, G. S., Zhao, Z. J., & Wang, C. S. (2004). Fermented beverages of pre- and proto-historic China. *PNAS*, 101, 17593–17598. <https://doi.org/10.1073/pnas.0407921102>
- Messner, T. C., Dickau, R., & Harbison, J. (2008). Starch grain analysis: Methodology and applications in the north-east. *Curr Northeast Paleoethnol*, 11, 111–127.
- Moore, P. D., Webb, J. A., & Collingson, M. E. (1991). *Pollen analysis*. Oxford: Blackwell Science.
- Motuzaitė-Matuzevičiūtė, G., Jacob, J., Telizhenko, S., & Jones, M. K. (2016). Miliacin in palaeosols from an early iron age in Ukraine reveal in situ cultivation of broomcorn millet. *Archaeological and Anthropological Sciences*, 8(1), 43–50. <https://doi.org/10.1007/s12520-013-0142-7>
- Motuzaitė-Matuzevičiūtė, G., Staff, R. A., Hunt, H. V., Liu, X., & Jones, M. K. (2013). The early chronology of broomcorn millet (*Panicum miliaceum*) in Europe. *Antiquity*, 87, 1073–1085. <https://doi.org/10.1017/S0003598X00049875>
- Nagy, M., Sümegi, P., Persaits, G., Gulyás, S., & Töröcsik, T. (2012). The Iron Age hoard found at Ikervár (Vas County, Hungary) in the Western Region of the Carpathian Basin. In S. Berecki (Ed.), *Iron age rites and*

- rituals in the Carpathian Basin*. Proceedings of the International Colloquium from Târgu Mureş, 7–9 October 2011. (pp. 31–64). Târgu Mureş: Editur Mega.
- Najafian, Y., Hamed, S. S., Farshchi, M. K., & Feyzabadi, Z. (2018). Plantago major in traditional Persian medicine and modern phytotherapy: A narrative review. *Electronic Physician*, 10(2), 6390–6399. <https://doi.org/10.19082/6390>
- Nelson, M. (2005). *The barbarian's beverage: A history of beer in ancient Europe*. New York: Routledge. <https://doi.org/10.4324/9780203309124>
- O'Brien, C. M. (2006). *Fermenting revolution: How to drink beer and save the world*. Gabriola Island: New Society Publishers.
- Oksanen, J., Blanchet, F. G., Friendly, M., Kindt, R., Legendre, P., McGinn, D., Minchin, P. R., O'Hara, R. B., Simpson, G. L., Solymos, P., Stevens, M. H. H., Szoecs, E., & Wagner, H. (2020). *Vegan: Community ecology package*. R Package Version 2.5–7. <https://CRAN.R-project.org/package=vegan>
- Oreagba, I. A., Oshikoya, K. A., & Amachree, M. (2011). Herbal medicine use among urban residents in Lagos, Nigeria. *BMC Complementary and Alternative Medicine*, 11, 117. <https://doi.org/10.1186/1472-6882-11-117>
- Padosch, S. A., Lachenmeier, D. W., & Kröner, L. U. (2006). Absinthism: A fictitious 19th century syndrome with present impact. *Substance Abuse Treatment, Prevention, and Policy*, 1, 14. <https://doi.org/10.1186/1747-597X-1-14>
- Paduch, R., Woźniak, A., Niedziela, P., & Rejdak, R. (2014). Assessment of eyebright (*euphrasia officinalis* L.) extract activity in relation to human corneal cells using in vitro tests. *Balkan Medical Journal*, 31(1), 29–36. <https://doi.org/10.5152/balkanmedj.2014.8377>
- Pagan-Jimenez, J. R., Rodriguez-Ramos, R., Reid, B. A., van den Bel, M., & Hofman, C. L. (2015). Early dispersals of maize and other food plants into the southern Caribbean and northeastern South America. *Quaternary Science Reviews*, 123, 231–246. <https://doi.org/10.1016/j.quascirev.2015.07.005>
- Pokorný, P. (2006). Insight into the environment of a pre-Roman iron age hillfort at Vladař, Czech Republic, using a multi-proxy approach. *Vegetation History and Archaeobotany*, 15, 419–433. <https://doi.org/10.1007/s00334-006-0064-8>
- Pokorný, P. (2015). Mid-Holocene bottleneck for central European dry grasslands: Did steppe survive the forest optimum in northern Bohemia, Czech Republic? *Holocene*, 25, 716–726. <https://doi.org/10.1177/0959683614566218>
- Rodzińska-Nowak, J. (2018). Napoje alkoholowe mieszkańców Barbaricum. In B. Niezabitowska-Wiśniewska (Ed.), *Studia Barbarica. Profesorowi Andrzejowi Kokowskiemu w 65 rocznicę urodzin* (pp. 580–588). Lublin: Tom II.
- Soroceanu, T. (2005). Zu den Fundumständen der europäischen Metallgefäße bis in das 8. Jh. v. Chr. Ein Beitrag zu deren religionsgeschichtlicher Deutung. In T. Soroceanu (Ed.), *Bronzefunde aus Rumänien II*. Biblioteca Muzeului Bistrița, Seria Historica 11. (pp. 387–428). Cluj-Napoca: Accent.
- Stika, H. P. (2011). Early iron age and late mediaeval malt finds from Germany—attempts at reconstruction of early Celtic brewing and the taste of Celtic beer. *Archaeological and Anthropological Sciences*, 3, 41–48. <https://doi.org/10.1007/s12520-010-0049-5>
- Szabó, G. V., & Bálint, M. (2016). Hajúböszörmény 2,0: An old hoard in a new perspective. *Hungarian Archaeology, E-Journal*, 2016, 1–7.
- Therin, M., Torrence, R., & Fullagar, R. (1997). Australian Museum starch reference collection. *Australian Archaeology*, 44, 52–53. <https://doi.org/10.1080/03122417.1997.11681589>
- Vilsteren, V. T. (1996). From herbs to hops: Outlines of the brewing process in medieval Europe. *Halve Maen—Magazine of the Dutch Colonial Period in America*, LXIX(3), 41–46.
- Wang, J., Liu, L., Georgescu, A., Le, V. V., Ota, M. H., Tang, S., & Vanderbilt, M. (2017). Identifying ancient beer brewing through starch analysis: A methodology. *Journal of Archaeological Science*, 15, 150–160.
- Wang, J. J., Zhao, X. Y., Wang, H., & Liu, L. (2019). Plant exploitation of the first farmers in Northwest China: Microbotanical evidence from Dadiwan. *Quaternary International*, 529, 3–9. <https://doi.org/10.1016/j.quaint.2018.10.019>
- Whitehead, J. (2013). The brewing of Etruscan beer. *Etruscan News*, 15, 14.
- Winstel, D., & Marchal, A. (2018). Lignans in spirits: Chemical diversity, quantification, and sensory impact of (±)-Lyoniresinol. *Molecules*, 24(1), 117. <https://doi.org/10.3390/molecules24010117>
- Yeung, E. C. T., Stasolla, C., Summer, M. J., & Huang, B. Q. (2015). *Plant microtechniques and protocols*. Cham, Switzerland: Springer International Publishing. <https://doi.org/10.1007/978-3-319-19944-3>







SUPPORTING INFORMATION

Additional supporting information may be found online in the Supporting Information section at the end of this article.

How to cite this article: Jílek, J., Golec, M., Bednář, P., Chytráček, M., Vích, D., Zavoral, T., Mírová, Z., Petr, L., Kovárník, J., Milo, P., & Kučera, L. (2022). The oldest millet herbal beer in the Europe? The ninth century BCE bronze luxury bucket from Kladina, Czech Republic. *Archaeometry*, 64(2), 454–467. <https://doi.org/10.1111/arcm.12711>

Article

What about Dinner? Chemical and Microresidue Analysis Reveals the Function of Late Neolithic Ceramic Pans

Jaromír Beneš ^{1,2} , Valentina Todoroska ³, Kristýna Budilová ¹, Jaromír Kovárník ¹, Jaroslav Pavelka ⁴, Nevenka Atanasoska ^{1,2}, Jiří Bumerl ^{1,2}, Assunta Florenzano ⁵ , Tereza Majerovičová ^{1,2}, Václav Vondrovský ⁶ , Michaela Ptáková ¹, Petr Bednář ⁷ , Lukáš Richtera ^{8,9}  and Lukáš Kučera ^{7,*} 

- ¹ Laboratory of Archaeobotany and Palaeoecology, Faculty of Science, University of South Bohemia, Na Zlaté stoce 3, 370 05 České Budějovice, Czech Republic; benes.jaromir@gmail.com (J.B.); krr.budilova@gmail.com (K.B.); jkovarnik@prf.jcu.cz (J.K.); nevenka_atanasoska@yahoo.com (N.A.); jbumca@gmail.com (J.B.); tmajerovicova@gmail.com (T.M.); mdivisova@seznam.cz (M.P.)
- ² Institute of Archaeology, Faculty of Philosophy, University of South Bohemia, Branišovská 31, 370 05 České Budějovice, Czech Republic
- ³ Kej 8 Noemvri br.24/6, 6330 Struga, North Macedonia; t.valentina23@gmail.com
- ⁴ Centre of Biology, Geosciences and Environmental Education, University of West Bohemia, Univerzitni 8, 30614 Plzen, Czech Republic; japetos@cbg.zcu.cz
- ⁵ Laboratory of Palynology and Paleobotany, Department of Life Sciences, University of Modena and Reggio Emilia, via G. Campi 287, 41125 Modena, Italy; assunta.florenzano@unimore.it
- ⁶ Institute of Archaeology of the Czech Academy of Sciences, 118 01 Prague, Czech Republic; vaclav.vondrovsky@gmail.com
- ⁷ Department of Analytical Chemistry, Faculty of Science, Palacký University, 17. Listopadu 12, 779 00 Olomouc, Czech Republic; petr.bednar@upol.cz
- ⁸ Department of Chemistry and Biochemistry, Mendel University in Brno, Zemědělská 1, 613 00 Brno, Czech Republic; richtera@mendelu.cz
- ⁹ Central European Institute of Technology, Brno University of Technology, Technická 123, 612 00 Brno, Czech Republic
- * Correspondence: lukas.kucera@upol.cz



Citation: Beneš, J.; Todoroska, V.; Budilová, K.; Kovárník, J.; Pavelka, J.; Atanasoska, N.; Bumerl, J.; Florenzano, A.; Majerovičová, T.; Vondrovský, V.; et al. What about Dinner? Chemical and Microresidue Analysis Reveals the Function of Late Neolithic Ceramic Pans. *Molecules* **2021**, *26*, 3391. <https://doi.org/10.3390/molecules26113391>

Academic Editor:
Przemysław Niedzielski

Received: 14 May 2021
Accepted: 2 June 2021
Published: 3 June 2021

Publisher's Note: MDPI stays neutral with regard to jurisdictional claims in published maps and institutional affiliations.



Copyright: © 2021 by the authors. Licensee MDPI, Basel, Switzerland. This article is an open access article distributed under the terms and conditions of the Creative Commons Attribution (CC BY) license (<https://creativecommons.org/licenses/by/4.0/>).

Abstract: The Late Neolithic palafitte site, Ustie na Drim, in the northern part of Lake Ohrid (North Macedonia), excavated in 1962, offered ceramic fragments of large, flat, elongated pans. These artifacts could be dated by relative chronology to roughly around 5200–5000 BC. According to their shape and technological traits, the ceramic pans were probably used for baking. The attached materials on the surface of studied pan fragments were sampled for consequent chemical and microscopical analyses (i.e., analyses of starch, phytoliths, and microscopic animal remains). An immunological method revealed the presence of pork proteins in samples. The presence of organic residues of animal origin was, moreover, confirmed by the detection of cholesterol using gas chromatography coupled to mass spectrometry. Analysis of detected microscopic botanical objects revealed starch grains of several plants (i.e., oak, cattail, and grasses). An interesting find was the hair of a beetle larva, which could be interpreted contextually as the khapra beetle, a pest of grain and flour. Based on our data, we suppose that the ceramic pans from Ustie na Drim were used for the preparation of meals containing meat from common livestock in combination with cereals and wild plants.

Keywords: archaeobotany; ceramic vessel; cholesterol; pests; phytoliths; starch; proteins; gas chromatography

1. Introduction

One of the major topics in the contemporary bioarchaeology of artifacts is the investigation of archaeological vessels using the latest instrumental methods of chemical research and the recent tools of archaeobotanical, genetic and microbiological investigation. An

analysis of the shape, quality of material, and volume of a found vessel enables an estimation of its use in the initial living context before being discarded and its existence during cultural deposition [1]. It is also possible to record the 'life of artifacts' from the time of their production and the beginning of their use to the moment of their exclusion. Today great attention is given to the residual content of vessels in Mediterranean regions due to chemical signals in residue content on the inner surface of vessels [2–6]. Analogically, ceramic vessels from the Iron Age in Central Europe have been subjected to chemical research that has revealed the presence of several compounds indicating food remains [7]. Besides ceramic vessels, special interest has been focused on analyzing the content of bronze vessels where organic residues could be 'trapped' in corrosion products [8,9]. The aim of the research on archaeological vessels is to identify their original function in society and contribute to an understanding of the subsistence principles as well as ritual customs of past human populations [2,10].

The Neolithic period in the Near East, Anatolia [11,12], and Europe [13] could be characterized by the movement of people and the diffusion of new modes of life. However, it should be noted that the development of populations in the Neolithic period was long and diverse [14]. Variability in their forms of settlement was also reflected in the development of ceramics: from a relatively simple ceramic type in the Early Neolithic to more complex variability in the Late Neolithic/Eneolithic. Current research on the functional traits of Neolithic pottery is targeted towards organic bulk remains on the inner surface of ceramics as well as chemical signals of organic penetration in the microporous matrix of ceramic vessels [15,16].

Detailed chemical analysis of soil content and/or organic residues in ceramic vessels and pans can provide information about their usage and former content. The analysis of lipid residues present therein is an important part of this research due to the chemical stability of nonpolar compounds in archaeological contexts (i.e., lipids, steroids, and terpenes) [17,18]. A frequently used technique for the characterization and identification of fat origins is the analysis of isotope ratios of individual fatty acids adsorbed in prehistoric, antiquity, and medieval ceramics using gas chromatography-combustion-isotope ratio mass spectrometry (GC-C-IRMS) [19,20]. However, 'conventional' gas chromatography combined with mass spectrometry (GC/MS) can provide similar information, and sometimes even more significant, when the use of the multiple-reaction monitoring method (MRM transition) is compared to GC-C-IRMS. The use of GC/MS together with MRM transition has been applied in the analysis of soil extracts from Neolithic ceramic vessels where a broomcorn millet marker miliacin has been found. The obtained results have improved our knowledge concerning the use of millet in the past and can be highlighted as the first direct evidence of usage of broomcorn millet in Central Europe [21]. Another technique for the analysis of original and intact lipid molecules, i.e., di- and tri-acylglycerols, is matrix-assisted laser desorption/ionization mass spectrometry [22,23]. As mentioned above, the stability of nonpolar compounds is much higher than the stability of polar compounds in an archaeological context due to the higher level of hydrolysis and water leaching of polar compounds [17,18]. For example, sterols, such as cholesterol in animals and β -sitosterol in plants, are reasonably resistant to post-burial degradation and can therefore be a marker of fat origin [9,24].

Until recently, only a few research teams have worked with the chemical signals and archaeobotanical micro-objects from the residual material of the inner walls of archaeological vessels [16,25–27]. The aim of this article was to combine advanced chemical analysis (gas chromatography/mass spectrometry and immunological analysis) with microscopic evidence of the microremains (starch grains, phytoliths, molds, yeast cells, and other microremains) to determine the function of ceramic pans from the Late Neolithic palafitte site of Ustie na Drim in the Lake Ohrid shore area in the town of Struga, North Macedonia.

2. Results and Discussion

The gas chromatography/mass spectrometry of organic residues attached on the surface of ceramic pans KE1–KE7 revealed a cholesterol signal (Table 1, Figure 1). The presence of cholesterol in all samples was confirmed by the authentic cholesterol standard, retention time, and fragmentation spectrum (Figure 2). The most significant sample was from ceramic pan KE4, where a high amount of a thin, baked mass was found. The concentrations of cholesterol in the sample taken from this thin, baked layer on the bottom of ceramic pan KE4-1 was $0.44 \text{ mg}\cdot\text{g}^{-1}$, while in the sample under the inner edge of vessel KE4-2, it was $0.66 \text{ mg}\cdot\text{g}^{-1}$; for the sample under the residue of sample KE4-1 (i.e., KE4-3) it was $0.19 \text{ mg}\cdot\text{g}^{-1}$, and in the sample of the mass under sample KE4-2 (i.e., KE4-4) it was $0.46 \text{ mg}\cdot\text{g}^{-1}$ (Figure 2a). The reference sample from the edge of vessel KE4 contained only traces of cholesterol (below $0.01 \text{ mg}\cdot\text{g}^{-1}$). This significant difference in the concentration of cholesterol in the KE4 samples excludes the cross-contamination of pan pits by surrounding material at the storage location. The samples from KE4 were also analyzed using immunological tests for the detection of denatured proteins. This methodology has been successfully tested many times [28,29] and was also used as a control for mass spectrometric data [23]. The sample KE4-2, with a high concentration of cholesterol, provided a positive reaction for porcine proteins. However, a positive reaction was also found in the reference sample KE4-5. Based on these results, contamination tests were performed for porcine proteins [29]. The contamination tests pointed to different origins for the porcine proteins in samples KE4-2 and KE4-5. The proteins in sample KE4-2 had been denatured by high temperatures compared with the ‘unchanged’ (undenatured) proteins in KE4-5. The results obtained by immunological analysis confirmed different chemical compositions of both examined layers. Moreover, a signal of 18-norabietane (RT 16.65 min.) and retene (18.64 min.) was found in samples KE4-2 and KE4-4, pointing to the presence of resin/decayed wood [30]. Note that these compounds were also found in other samples, and in the reference samples, the content of 18-norabietane and retene was 32 times and 8 times lower, respectively, than that of sample KE4-2. The total ion current (TIC) chromatogram of other compounds identified in sample KE2-4 is shown in Supplemental Figure S1 and Table S1.

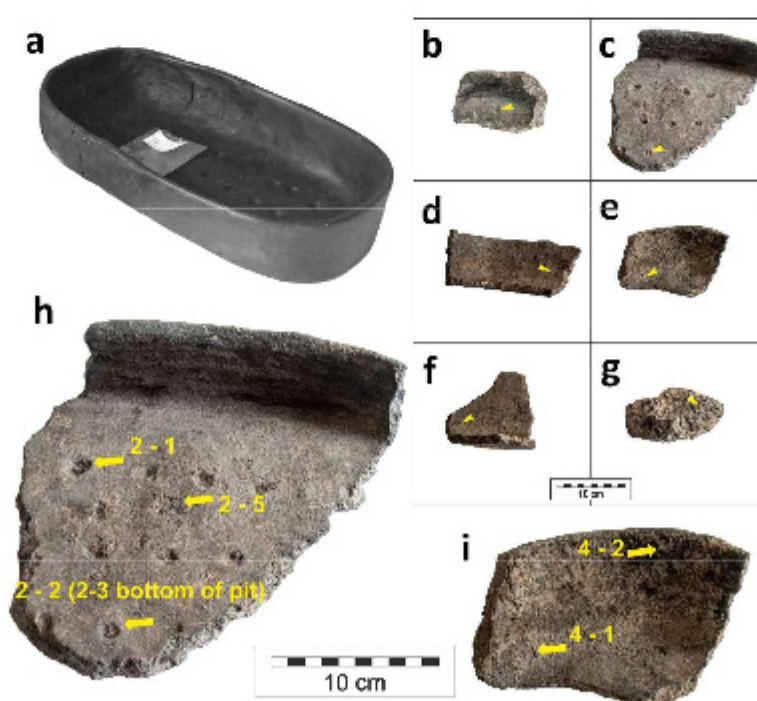


Figure 1. Reconstructed ceramic pan KE7 (a), sampled fragments KE1 (b), KE2 (c), KE3 (d), KE4 (e), KE5 (f), KE6 (g), and significant samples from KE2 and KE4 ((h,i), respectively).

Table 1. List of studied samples with the focus on the concentration of cholesterol, starch grains, phytolith, and non-pollen objects. SP: sample was taken for microscopical evaluation of microremains; positive: microobject was found in the prepared sample; negative: no microobject was found).

Artefact	Sample	Concentration of Cholesterol (mg/g)	Phytoliths and Non-Pollen Objects	Starch	Position of Sample in Ceramic Pan
KE1	1	0.05	-	-	pit (residue)
KE1	2	0.08	-	-	pit (ceramic under KE1-1)
KE1	3	0.00	-	-	edge, the reference sample
KE1	SP1	-	positive	positive	pit
KE1	SP2	-	-	positive	edge
KE2	1	0.03	-	-	pit (residue)
KE2	2	0.01	-	-	pit (ceramic under KE2-1)
KE2	3	0.92	-	-	pit (residue)
KE2	4	0.04	-	-	pit (ceramic under KE2-3)
KE2	5	0.00	-	-	bottom, the reference sample
KE2	6	0.00	-	-	inner surface (organic temper)
KE2	7	0.01	-	-	surface (the reference sample)
KE2	SP3	-	-	negative	pit
KE2	SP4	-	-	-	pit
KE2	SP5	-	-	positive	edge
KE3	1	0.02	-	-	inner surface (close bottom part, baked mass)
KE3	2	0.13	-	-	inner surface (under edge, baked mass)
KE3	3	0.01	-	-	inner surface (ceramic under KE3-1)
KE3	4	0.34	-	-	inner surface (ceramic under KE3-2)
KE3	5	0.04	-	-	edge (the reference sample)
KE3	SP6	-	positive	positive	pit
KE3	SP7	-	-	negative	pit
KE4	1	0.44	-	-	inner edge (close bottom part, baked layer)
KE4	2	0.66	-	-	inner edge (close upper part, baked layer)
KE4	3	0.19	-	-	inner edge (ceramic under KE4-1)
KE4	4	0.46	-	-	inner edge (ceramic under KE4-2)
KE4	5	0.01	-	-	edge (the reference sample)
KE4	SP8	-	positive	positive	pit
KE4	SP9	-	-	positive	pit
KE5	1	0.09	-	-	inner edge (close bottom part, thin layer)
KE5	2	0.24	-	-	inner edge (close to KE5-1)
KE5	3	0.02	-	-	inner edge (ceramic under KE5-1)
KE5	4	0.16	-	-	inner edge (ceramic under KE5-2)
KE5	5	0.01	-	-	edge (the reference sample)
KE6	1	0.00	-	-	wall (close upper part, baked mass)
KE6	2	0.02	-	-	wall (close to KE6-1)
KE6	3	0.00	-	-	edge (the reference sample)
KE6	1	0.17	-	-	organic residue (taken before conservation)

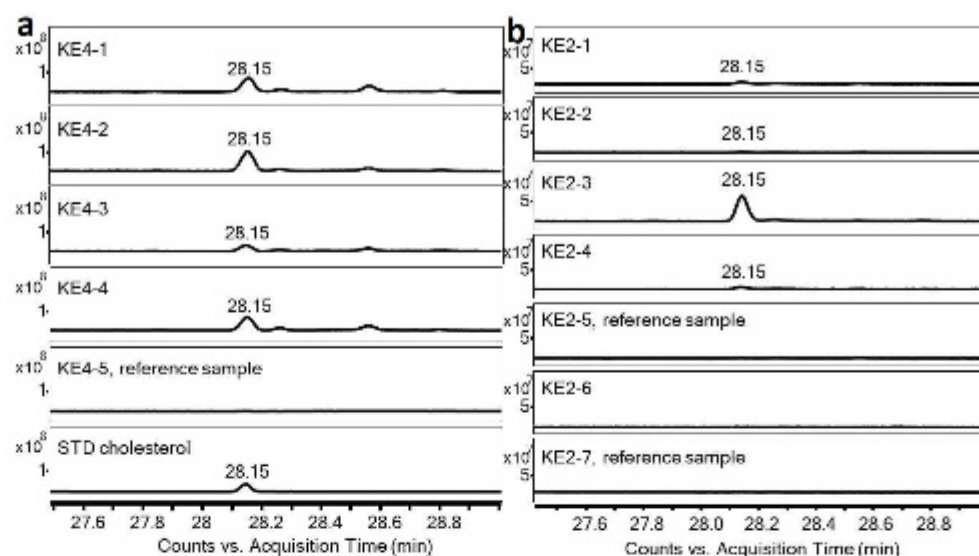


Figure 2. GC chromatogram of cholesterol in samples taken from ceramic pans KE4 (a) and KE2 (b).

The highest concentration of cholesterol was found in the pit of pan KE2 (Figure 1h, Figure 2b), i.e., $0.92 \text{ mg}\cdot\text{g}^{-1}$. Other samples taken from KE2 contained only a trace amount of cholesterol (i.e., the reference sample from the surface, KE2-7, $0.01 \text{ mg}\cdot\text{g}^{-1}$; sample of ceramic from the pit, KE2-2, $0.01 \text{ mg}\cdot\text{g}^{-1}$; sample of ceramic from the pit, KE2-4, $0.04 \text{ mg}\cdot\text{g}^{-1}$). Note that in the second reference sample (KE2-5, sample from the bottom of the pan) and in sample KE2-6, cholesterol was not detected. This significant difference in concentration of cholesterol in KE2 samples excludes the possibility of cross-contamination of ceramic pans' pits by the surrounding material at the storage location. In ceramic pan KE1, the highest concentration of cholesterol was found in a sample taken from a pit similar to ceramic pan KE2; however, in the reference sample KE1-3, cholesterol was not detected. Besides the samples from pits, the organic residues attached to the bottoms and edges of ceramic pans KE3–KE6 were also analyzed. The concentration of cholesterol in these samples was 3–66 times higher compared to the appropriate reference sample (Table 1). Finally, baked organic mass (Figure 3) associated with the reconstructed ceramic pan (KE7) was analyzed by GC/MS. Cholesterol was found at a concentration of $0.17 \text{ mg}\cdot\text{g}^{-1}$. Abietic acid was also detected, but due to the fact that a suitable reference sample was unavailable, we did not try to interpret this. In this organic mass, baked remains of fungi hyphae have been observed through the glassy mass (Figure 3c,d).

The samples from KE4-2 and KE7 were dated using the AMS radiocarbon method. Comparing both resulting dates, we can see that they are statistically inconsistent at the 5% significance level ($T = 7.9$, $T(5\%) = 3.8$, $df = 1$). Though the calibrated probability distributions partially intersect, the KE 7 sample was earlier than sample KE 4-2 (Table 2). Both dates significantly contradict the archaeological chronology of the site (ca. 5200–5000 BC), and we, therefore, considered them unreliable, particularly because the carbonized food residues adhering to pottery have been proved to be generally problematic material for radiocarbon dating. Due to their heterogeneous composition, it is difficult to remove all sources of exogenous carbon [31]. Analyses of replicate measurements have evinced that dating food residues can produce inaccuracies of between 15% and 30% in the results, and offsets between replicate measurements can reach more than 1000 radiocarbon years [32,33]. As both radiocarbon dates from the Ustie na Drim site had approximately the same deflection from the expected chronology, we should also consider that they may have been influenced by a reservoir/hard water effect from Lake Ohrid [34], for which the modern rate has been estimated at ca. 1500 radiocarbon years [35]. Despite the sampled food residues being of terrestrial origin (see above), it should be noted that even terrestrial animals from within a food web related to lacustrine environments (e.g., by grazing aquatic plants) can also suffer from a reservoir effect [36].

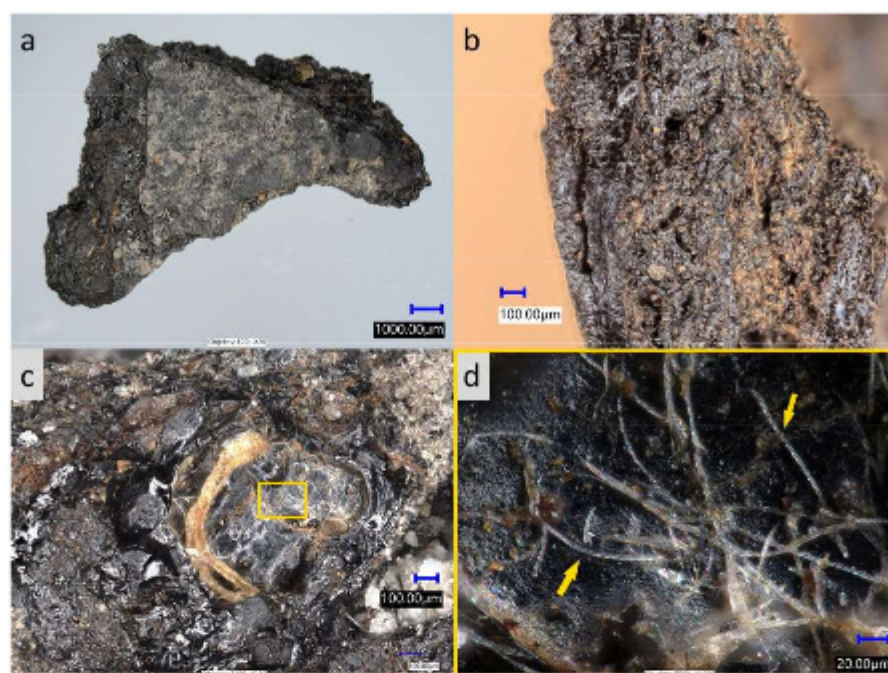


Figure 3. Ustie na Drim. Organic mass taken from ceramic pan KE7 before reconstruction. (a) profile of organic mass, (b) profile detail—the glassy edge burn-on, and (c,d) glassy mass with fungi hyphae baked inside.

Table 2. Radiocarbon dates from organic residuals. Calibrated in OxCal 4.4 software using IntCal20 calibration curve [37,38].

Sample	Lab. Code	BP Age	cal BC 68.4%	cal BC 95.4%
KE 4-2	UGAMS-49232	7370 ± 30	6341–6313 (13.2%)	6369–6297 (22.6%)
			6260–6216 (31.3%)	6269–8209 (35.6%)
			6142–6092 (23.7%)	6198–6085 (37.2%)
			6411–6366 (36.3%)	6422–6332 (53.3%)
KE 7	UGAMS-49233	7480 ± 25	6308–6265 (32.0%)	6319–6319 (42.1%)

Several types of microscopic organic particles were obtained along with several amorphous clusters of various different materials. The first type of obtained micro-residuals were phytoliths, starch grains, and faunal remains (Figures 4 and 5, Table 1). The most abundant (but still scarce, because generally, the amount of material gained for the microscopy was very low) were phytoliths named spheroid psilate aggregate (Figure 4d,e), which were observed in almost every sample. Some skeletons (aggregates) or single cells of a polyhedral shape were recorded (Figure 4g,j), as well as a particle reminding one of an elongate psilate skeleton (Figure 4i), but appearing blue in the cross-polarized light; hence its plant origin was not particularly certain. A few phytoliths could perhaps be attributed to silicified vessel elements. Polyhedral epidermal cells are the most common type of dicot phytoliths; they are formed in the leaves of many deciduous trees as well as produced by many of the studied herbaceous dicotyledons [39]. The spheroid psilate morphotype often arise as vesicular infillings of the epidermal and parenchyma cells of foliage and reproductive organs in a wide range of dicots, monocots, and some gymnosperms [40].

Note that none of the observed phytoliths could be attributed to cereal remains. The phytoliths which would undoubtedly point to the Poaceae family were not found at all.

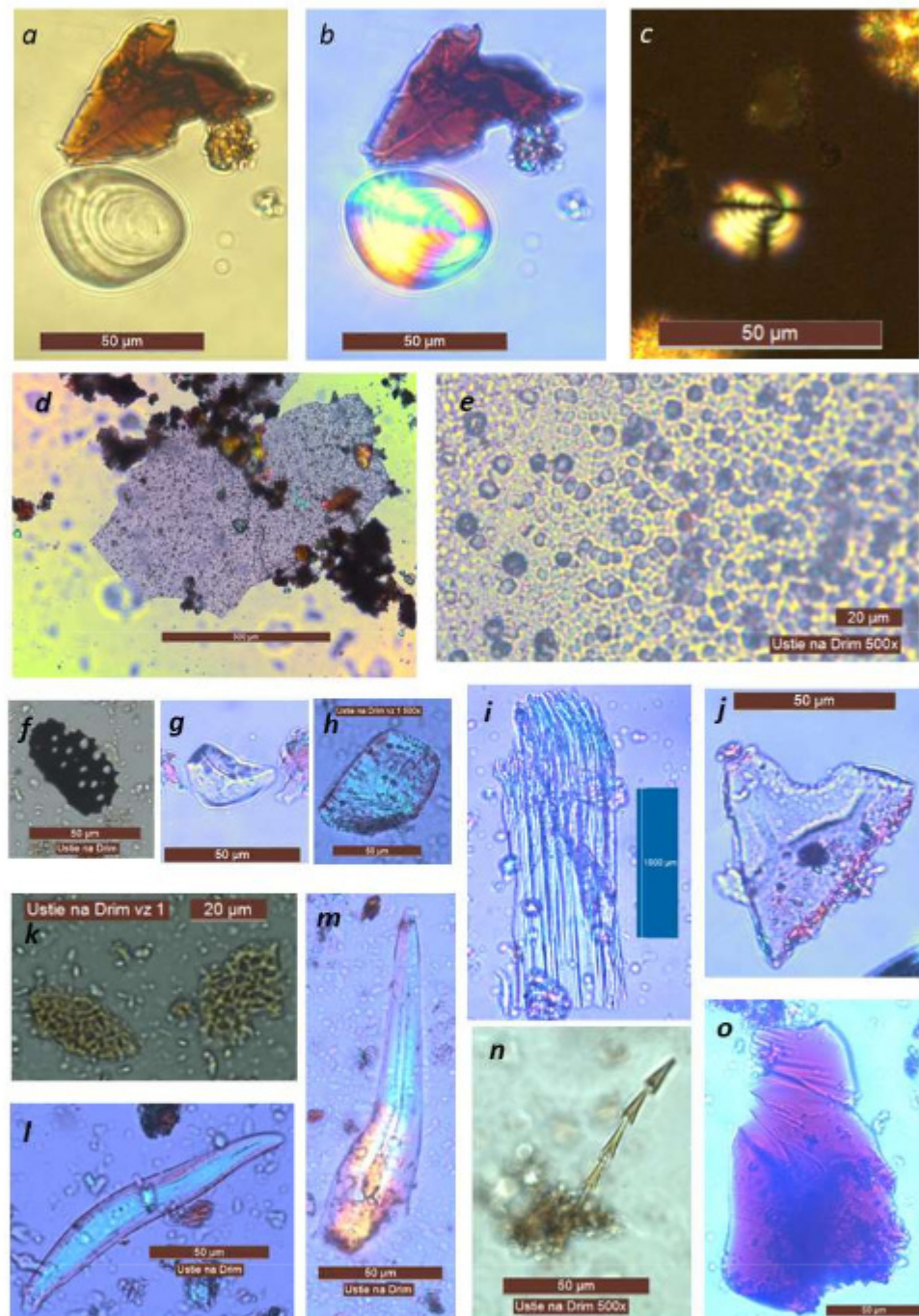


Figure 4. Microresidues in samples SP1 (h,i,k), SP6 (f,l-o) and SP8 (a-e,g,j). (a-c) starch grain, probably the underground storage organ of higher plants, cf. Liliaceae; (d,e) skeleton consisting of small spheroid psilate phytoliths; (f) wood charcoal fragment; (g-k) phytoliths; (l-o) other organic residues (probably faunal); (n) hair fragment of dermestid beetle larvae, cf. *Trogoderma* sp.). Magnification 500× (except (d,i)).

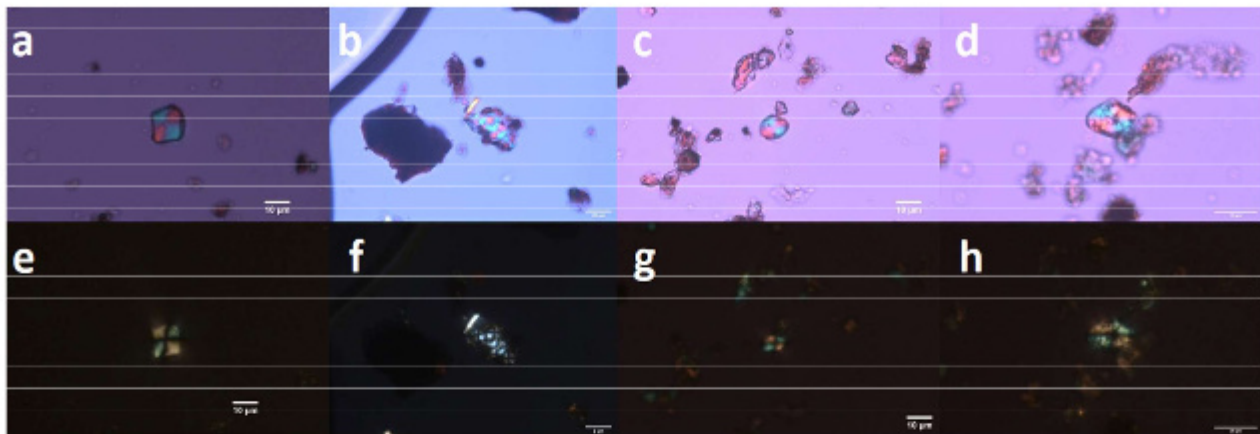


Figure 5. Starch grains of *cf. Setaria* from the ceramic pans KE2, sample SP5 (a,e); starch grains of *cf. Typha* found in KE4, SP9 (b,f); starch grains of *cf. Poaceae* from KE2, SP5 (c,g); starch grains of *cf. Quercus* in KE2, SP5 (d,h). Images were taken in visible light (a–d) and in cross-polarized light (e–h).

Starch as a natural substance is subject to destruction. Starch grains can be damaged mechanically (by breaking), chemically (by the action of acids), enzymatically (by amylase), or by heat (food preparation and cooking). Due to the effect of higher temperatures (above 50–70 °C) on starch grains, especially in humid environments, the gelatinization process can begin. Starch granules gain in volume and lose their typical properties. If the damage is extensive, the morphological identification method cannot be used [41]. Starch is also affected by enzymatic activity, especially amylase from the glycosidases group of enzymes. The source of amylase can be animals, plants, and microorganisms [42]. Despite a number of factors, which may damage or destroy the starch grains, it is possible to find starch grains undamaged or in a state which allows microscopic analysis. As the works of Henry et al. (2009) and Crowther (2012) showed, concerning cooked starchy foods, it is common to observe a variety of reactions to cooking where some granules will appear completely unaffected, while other starch will be partially or fully gelatinized [43–45]. An analysis of starch remains was conducted on nine samples. In sample KE1-SP1 one small, round starch granule and an undefined starch were found. In sample KE1-SP2 an oval starch grain, undefined (*cf. Poaceae*), was found. In samples KE2-SP3 and KE2-SP4, the finding was negative. In contrast, sample KE2-SP5 was rich in starch grains (Figure 5). In this sample following objects were found: an oval starch grain, undefined (*cf. Poaceae*); a small, round, undefined starch (*cf. Poaceae*); an oval starch grain, damaged and undefined; a round, damaged, and undefined starch; an elongated atypical starch (*cf. Quercus*) [46,47], and a square-shaped starch (*cf. Setaria*, [46,48]). In the KE3-SP6 sample, a round, undefined starch (*cf. Poaceae*) was found. Sample KE4-SP8 contained a trapezoid, starch shape with growth rings (*cf. Liliaceae*) [49]. The last sample, KE4-SP9, contained a round undefined starch (*cf. Poaceae*) and a cluster of starch grains (*cf. Typha*) [50]. A microscopic investigation was further conducted to reveal the remains of animal structures. The most interesting finding was a fragment of hair belonging to a larval segment of Coleoptera of the family Dermestidae, *cf. Trogoderma* sp. [51] (Figure 4n). This ‘hair’ was identified thanks to its peculiar microstructure; hastisetae (or hastate setae), located on the dorsolateral surface of the tergites of larvae and pupae, are generally quite small (estimated length between 150 and 900 µm) and inserted in setal sockets on the integument through a pedicel. Hastisetae microstructure consists of two main parts: the shaft and the apical head (Figure 4n). The shaft is made by repeated modules constituted by one cylindrical segment provided with one wreath of spines/scales posterolaterally oriented in the distal part. The head of the seta is a subconical anchor-like structure subdivided into five to seven longitudinal elements; the apex of the head is blunt. This arrow-shaped hair residue is already known from archaeological samples as sporadic non-pollen palynomorphs from the Early Bronze

Age to Medieval contexts in Georgia [52,53] and generally occurs in stored animal or plant products.

The identification of starch cf. Poaceae and cf. *Setaria* does not mean the detection of Cerealia on a microscopic level; however, in an archaeological context, their presence on cooking artifacts of this Late Neolithic site allows the possibility of interpreting these findings as to the presence and use of flour from both domesticated and wild plants. Interestingly, the larval hair of a dermestid beetle (cf. *Trogoderma* sp., a genus to which pests of stored plant and animal products belong) was found coincidentally with the above-mentioned types of starch. This combination led to the possible identification of the *Trogoderma granarium* species (khapra beetle) in the record. This insect is generally known as a grain pest; in its larval stage, it is a voracious feeder of stored grains and regularly occurs mainly in cereals, pulses, and their products [54]. The starch grains found from cf. *Typha* and cf. *Quercus* revealed the use of wild plant foods. Both plants are known to be used as food resources for Palaeolithic and Mesolithic hunter-gatherers [55–58]. Cattail (*Typha* sp.) represents an extraordinarily versatile plant with many uses, such as for roof thatching and making mats or baskets. Moreover, many of its parts, such as the rhizomes, young stems, flower spikes, or pollen of this plant, are edible and are widely known to be used for human consumption [59]. The occurrence of cattail starch in a pan can most likely be explained by its facility for being ground into a nutritive and tasty flour-like cereal flour [60]. Furthermore, acorns have always been an attractive food resource within various resource strategies, including that of agrarian societies. Acorns in prehistoric agricultural communities may have played a role as a food substitute or as a reserve for times of crop failure [61–63].

The combination of advanced chemical analysis with microscopic evaluation of the microremains brings new evidence about the life of prehistoric people. We propose that the studied ceramic pans were used for the preparation of meals containing meat from common livestock in combination with cereals and wild plants.

3. Materials and Methods

3.1. Archaeological Samples

The Ustie na Drim site is located to the immediate north of Lake Ohrid along the banks of the river Crn Drim in Struga (Figure 6). The site is situated in a north-south direction along the riverbed. It is registered in the archaeological map of the Republic of Macedonia as a palafitte settlement from prehistoric times [64]. The initiative for the research of this locality started during some work on regulating the riverbed in 1961, when stone, flint, and bone tools, as well as ceramic fragments, came to the surface. This was reason enough to start protective archaeological excavations. The excavation was conducted over a short period in 1962. Three trenches were opened (trench I with dimensions of 6 × 12 m, trench II with dimensions of 2 × 4 m, and trench III with dimensions of 2 × 2 m) with a total open area of 84 m² [65,66]. Researchers solved the problem of the inflowing river water by constructing a canal along the left bank of the river and smaller canals along the excavated area in the southern and western profile where the water accumulated. Such a remedy allowed digging to continue in relatively dry conditions. The strategy was to excavate in mechanical layers of 15 to 20 cm. In the third mechanical layer, the team came across a deposit of charred and non-charred wooden planks. The situation was interpreted as constructions that had never been destroyed by floods. In the next two mechanical layers, archaeological finds of stone artifacts, bone tools, and pottery were made, together with wooden piles belonging to a Late Neolithic settlement (Figure 6b,c).

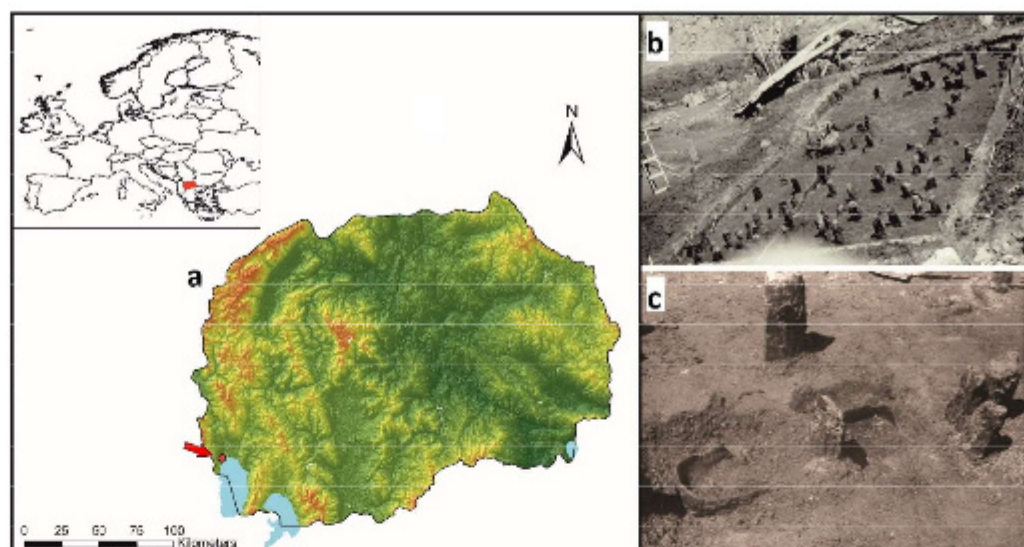


Figure 6. Location of Ohrid area and Ustie na Drim in the North Macedonia (a), with archive pictures from the excavation of the palafitte site in 1961 (b,c). The large archaeological trench with wooden poles (b), and the site with an in situ ceramic pan (c).

Among the ceramic material, the most common forms were the large, flat, elongated pans (тави), which are shallow oval vessels with pits in the flat bottom. Most of them belonged to a group of ‘rough pottery’ with a dark grey surface and were probably made for some special use [67]. Similar ceramic forms have been found on the Stranata site, named “српни/црепни”; these are round shallow vessels with a flat bottom, but here without any fingerprints. These vessels have large dimensions and usually a rough texture [68,69]. Outside of today’s borders of the Republic of North Macedonia, a similar ceramic form has been found on the site of Barç, in the Korçë region of Albania [70]. The mentioned sites correspond, according to the relative chronology based on pottery typology, with the second phase of the Late Neolithic in Pelagonia and with the relative chronological position of the Vinca-Tordos II phase or during the Vinca B2 phase in the Central Balkans and the Arapi and Otzaki phases of the Dimini [70–72]. This chronological horizon could be dated back to around 5200–5000 BC.

3.2. Residual Sample Extraction

The ceramic fragments from the archaeological research in 1962 were stored at the Struga Museum. As a coarse ceramic, there was still sediment on their surfaces. In 2019, ceramic fragments were sampled for their bioarchaeological residuals and chemistry by a research team from the University of South Bohemia. The list of analyzed samples from ceramic pans are listed in Table 1. It must be pointed out that the pits or depressions made by fingers into the vessel’s surface are technical elements, which were fabricated before the ceramic was fired in the kiln. This technological step with subsequent firing completely eliminates all organic compounds in the ceramic material along with any contamination. On the other hand, the pits were ‘traps’ for residual organic material in the process of baking food. A special case was the fragment of the organic mass from the already-reconstructed pan 7 (Figure 1a). This organic mass fragment was provided in a zip-lock bag separately.

Sampling was performed in two ways (Figure 1). First, the material was scraped from the finger pits with a scalpel directly to polypropylene 2 mL microcentrifuge tubes (series KE1-7, positions KE1-1, KE1-2, and KEx-y). The second series of sampling was processed by liquid extraction using distilled water (sub-series SP for KE1-4, see below). Samples were stored in a refrigerator and transported to the laboratories.

3.3. Sampling for Starch, Phytoliths, and Non-Pollen Objects

A micro-pipetting method was used to sample starch grains from the ceramic fragments. A small quantity of distilled water (approximately 100 μL) was placed directly onto the surface of the examined object or pores in the structure of the ceramic pans. Consequently, the water drop containing the extracted residues was collected with a pipette set to 20 μL . Samples were stored in microtubes with an ethanol solution. A drop of the sample was placed on a slide and covered with a coverslip. The corners of the coverslip were fixed with clear nail polish, and samples were left to dry. A drop of distilled water was added to the dried sample before microscopy. Identification was accomplished by direct observation (using a microscope Leica DM2500 P) and comparison with specimens from a reference collection [73–76]. The analysis of starch grains was based on the microscopic observation of samples in polarized and non-polarized light. The structures found in the samples taken from the archaeological artifacts (ceramic pans) were recognized on the basis of their optical properties and the morphological features of the starch grains.

Furthermore, an analysis of phytoliths and non-pollen objects was performed. Samples in microtubes, originally mounted in ethanol, were transferred to distilled water, left to sedimentation overnight, and after pipetting off the water, the pellet was dried in a laboratory drier at 50 $^{\circ}\text{C}$ (4 h). Then 1 mL of a heavy liquid (sodium polytungstate, SPT) calibrated at a density of 2.35 $\text{g}\cdot\text{m}^{-3}$ was added to every tube in order to separate phytoliths and other less dense organics from mineral particles. Samples were centrifuged at 800 rpm for 5 min. After that, the supernatant with its floating fraction was transported to new tubes. Subsequently, 2 mL of distilled water was added, and the samples were centrifuged three times (3 min/1500 rpm) to clean the SPT residue. Residues were mounted in distilled water and observed by a Leica DM2500P polarizing microscope (with attached camera). Whenever possible, phytoliths were named following the International Code for Phytolith Nomenclature ICPN 2.0 [38]. Organic matter from the reconstructed KE7 basin was observed using a Keyence VHX 7000 digital microscope (Figure 3). Part of sample KE7 (and KE4-2) was analyzed by radiocarbon dating at the University of Georgia, Center for Applied Isotope Studies using the CAIS 0.5 MeV accelerator mass spectrometer.

3.4. Gas Chromatography/Mass Spectrometry (GC/MS)

Gas Chromatography/Mass Spectrometry (GC/MS) was used for the determination of the semi-polar and nonpolar compounds in the acetone/chloroform extract sample [21]. Briefly, the solid material was taken from the inner part of ceramic pans, and 16–50 mg of the material was directly extracted using 1 mL acetone/chloroform solution (50:50, *v/v*). Note that from each ceramic pan, the weight of the sample for analysis was the same. After centrifugation (4400 RPM), the liquid part was transferred to a 1.5 mL glass vial, dried by a fine stream of nitrogen, and consequently derivatized using 20 μL *N,O*-bis(trimethylsilyl)trifluoroacetamide (Sigma-Aldrich, St. Louis, MO, USA) and 20 μL pyridine (HPLC grade, Sigma-Aldrich, St. Louis, MO, USA). The measurement was performed by an Agilent 7010 Triple Quadrupole GC/MS system with Mass Hunter software (Agilent Technologies, Palo Alto, CA, USA). The separation was performed on two (5% Phenyl)-methylpolysiloxane HP 5 ms Ultra Inert capillary columns connected in a series (15 m \times 0.25 mm \times 0.25 μm , each) with a constant flow of 1.0 and 1.2 $\text{mL}\cdot\text{min}^{-1}$, respectively. Nitrogen (N2 4.8. Messer Group GmbH, Germany) was used as a collision gas with a flow rate of 1.5 $\text{mL}\cdot\text{min}^{-1}$ and helium (He 5.0. Siad, Italy) as a quench gas with a flow rate of 2.25 $\text{mL}\cdot\text{min}^{-1}$. The initial oven temperature was 70 $^{\circ}\text{C}$ for 5 min; then, the oven was heated at a rate of 15 $^{\circ}\text{C}\cdot\text{min}^{-1}$ to the value of 320 $^{\circ}\text{C}$, which was held for 10 min. The injection volume of the extracts was 1 μL with splitless injection. The identification of the compounds was made using the NIST 14 library. Comparison and quantification were made using the authentic standard of cholesterol (Sigma-Aldrich, St. Louis, MO, USA).

3.5. Enzyme-Linked Immunosorbent Assay (ELISA)

For the determination of the animal species of organic residues (proteins), an ELISA was used [28,77]. BioKits for Speciation and Identification allowed for the distinguishing between beef, pork, poultry, and mutton proteins. This ELISA used microwell modules and thermostable species-specific muscle proteins. It is a non-competitive, sandwich-type assay (Neogen, Lansing, MI, USA) and was used according to the manufacturer's instructions with some changes, such as a lower volume of the sample as available in the archaeological material [28]. Additionally, aside from the instructions, samples were not boiled due to the fact that proteins in the archaeological objects could have been heat-treated in the past. In the case of the test for the presence of pork, the samples were boiled for the second replication and compared with the results from the previous (the first) replication; thus, possible contamination from the non-boiled proteins could be detected. Contamination by non-boiled proteins is usually caused by midgut mucosa that is present in animal feces [29].

4. Conclusions

The advanced chemical and microremains analyses of ceramic pans from the Ustie na Drim site have provided multiple evidence of their artifact use in the past. The location of the sampled material in pits on the pan surface and the character of the mass directly joined with the artifact surface reduces the possibility of contamination. Overall, the record is fragmentary; however, each of the methods used contributed to answering the basic question of what was usually prepared for a meal in this kind of pottery. Concerning the stratigraphic position of these artifacts, it was possible to determine their age by relative chronology to around 5200 BC. Two samples from the surface of the pans were dated by AMS ^{14}C . Both radiocarbon dates were probably affected by an intake of old carbon from the environment. Considering the estimated reservoir effect of Lake Ohrid, both dates indicate an origin for the organic mass within the period of functional use of the ceramic pans. Since radiocarbon dates are older than the relative chronology of pans, we can exclude any post-depositional contamination by material from a later archaeological period. The most relevant result was given by the advanced chemical analysis. The main compound that occurred in all samples is cholesterol. A major source of cholesterol is animal fat and meat (its presence was proved by immunological test). Recent data indicate the amount of cholesterol in meat was roughly 75 mg/100 g (fatty parts like liver, brains, etc., contain a much greater content, up to several hundred milligrams per 100 g) [78]. It should be noted that the concentration of cholesterol in the samples of organic residues from the ceramic pans' pits was significantly higher than in the reference samples, a fact that excludes the possibility of cross-contamination of a pan's pit by the surrounding material at the storage location. The presence of denatured proteins in the ceramic pan was also confirmed using an ELISA. Based on the results, we suppose that the analyzed ceramic pans from Ustie na Drim were used for the preparation of meals containing meat from common livestock in combination with cereals and wild plants.

Supplementary Materials: The following are available online, Figure S1: Total ion current (TIC) chromatogram of sample KE4-2 (green line; inner edge: close upper part, baked layer) and KE4-5 (orange line; edge: the reference sample). Table S1: Table of the most significant compound detected in sample KE4-2.

Author Contributions: Conceptualization, J.B. (Jaromír Beneš) and L.K.; methodology, J.B. (Jaromír Beneš), L.K., J.P., J.K., and K.B.; formal analysis, P.B., L.R., and V.V.; investigation, J.B. (Jaromír Beneš), L.K., J.P., J.K., K.B., and M.P.; resources, J.B. (Jaromír Beneš), J.K., T.M., and K.B.; data curation, J.K., L.K., J.P., and K.B.; writing—original draft preparation, J.B. (Jaromír Beneš), V.T., K.B., J.K., J.P., N.A., A.F., V.V., M.P., L.R., and L.K.; writing—review and editing, J.B. (Jaromír Beneš), V.T., K.B., J.K., J.P., N.A., J.B. (Jiří Bumerl), A.F., T.M., V.V., M.P., P.B., L.R., and L.K.; supervision, J.B. (Jaromír Beneš) and L.K. All authors have read and agreed to the published version of the manuscript.

Funding: OP RDE: MEYS (Reg. No. CZ.02.1.01/0.0/0.0/16_019/0000728), the Grant Agency of Czech Republic (17-17346S), Ministry of Education, Youth and Sports of the Czech Republic

(CZ.1.05/2.1.00/19.0377), Institutional Project of the University of South Bohemia (IP 2019-2020/36) and ERDF/ESF (No. CZ.02.1.01/0.0/0.0/17_048/0007378).

Institutional Review Board Statement: Not applicable.

Informed Consent Statement: Not applicable.

Data Availability Statement: The data presented in this study are available on request from the corresponding author. The data are not publicly available due to the privacy policy of the author's institution.

Acknowledgments: This publication was supported by the project "Ultra-trace isotope research in social and environmental studies using accelerator mass spectrometry", Ministry of Education, Youth and Sports of the Czech Republic OP RDE: MEYS (No. CZ.02.1.01/0.0/0.0/16_019/0000728), the Grant Agency of Czech Republic (17-17346S), Ministry of Education, Youth and Sports of the Czech Republic (CZ.1.05/2.1.00/19.0377), ERDF/ESF "Arteca: Advanced physical-chemical methods of research and protection of cultural and artistic heritage" (No. CZ.02.1.01/0.0/0.0/17_048/0007378) and by the Institutional Project of the University of South Bohemia, IP 2019-2020/36 "The Support of Summer Schools at the Faculty of Science".

Conflicts of Interest: The authors declare no conflict of interest.

Sample Availability: Studied samples are not available.

References

1. Schiffer, M.B. *Formation Processes of the Archaeological Record*; University of Utah Press: Salt Lake City, UT, USA, 1996.
2. Rösch, M. Pollen analysis of the contents of excavated vessels—Direct archaeobotanical evidence of beverages. *Veg. Hist. Archaeobotany* **2005**, *14*, 179–188. [[CrossRef](#)]
3. Romanus, K.; Baeten, J.; Poblome, J.; Accardo, S.; Degryse, P.; Jacobs, P.; De Vos, D.; Waelkens, M. Wine and olive oil permeation in pitched and non-pitched ceramics: Relation with results from archaeological amphorae from Sagalassos, Turkey. *J. Archaeol. Sci.* **2009**, *36*, 900–909. [[CrossRef](#)]
4. Preusz, M.; Jan, T.; Vilímek, J.; Enei, F.; Preusz, K. Chemical profile of organic residues from ancient amphoras found in Pyrgi. *J. Archaeol. Sci. Rep.* **2019**, *24*, 565–573.
5. Spiteri, C.; Belser, M.; Crispino, A. Preliminary results on content analysis of early bronze age vessels from the site of Castelluccio, Noto, Sicily. *J. Archaeol. Sci. Rep.* **2020**, *31*, 102533. [[CrossRef](#)]
6. Manhita, A.; Martins, S.; Gomes da Silva, M.; Lopes, M.C.; Barrocas Dias, C. Transporting olive oil in roman times: Chromatographic analysis of dressel 20 amphorae from Pax Julia Civitas, Lusitania. *Chromatographia* **2020**, *83*, 1055–1064. [[CrossRef](#)]
7. Rageot, M.; Mötsch, A.; Schorer, B.; Gutekunst, A.; Patrizi, G.; Zerrer, M.; Cafisso, S.; Fries-Knoblach, J.; Hansen, L.; Tarpini, R.; et al. The dynamics of early celtic consumption practices: A case study of the pottery from the Heuneburg. *PLoS ONE* **2019**, *14*, 1–29. [[CrossRef](#)]
8. Rösch, M. Evaluation of honey residues from iron age hill-top sites in southwestern Germany: Implications for local and regional land use and vegetation dynamics. *Veg. Hist. Archaeobotany* **1999**, *8*, 105–112. [[CrossRef](#)]
9. Ondrkál, F.; Peška, J.; Jagošová, K.; Sokolovská, D.; Kučera, L. The cult-wagon of liptovský hrádk: First evidence of using the urnfield cult-wagons as fat-powered lamps. *J. Archaeol. Sci. Rep.* **2020**, *34*, 102579. [[CrossRef](#)]
10. Kvavadze, E.; Boschian, G.; Chichinadze, M.; Gagoshidze, I.; Gavagnin, K.; Martkoplshvili, I.; Rova, E. Palynological and archaeological evidence for ritual use of wine in the kura-araxes period at aradeti orgora (georgia, caucasus). *J. Field Archaeol.* **2019**, *44*, 500–522. [[CrossRef](#)]
11. Bami, M.N. *The Diffusion of Neolithic Practices from Anatolia to Europe. A Contextual Study of Residential Construction, 8,500–5,500 BC Cal*; BAR International Series 2838; BAR Publishing: Oxford, UK, 2017.
12. Beneš, J. *Počátky Zemědělství ve Starém Světě: The Origins of Agriculture in the Ancient World*; Episteme: České Budějovice, Czech Republic, 2018.
13. Whittle, A.W.R. *Europe in the Neolithic: The Creation of New Worlds*; Cambridge University Press: Cambridge, UK, 1996.
14. Fowler, C.; Harding, J.; Hofmann, D. *The Oxford Handbook of Neolithic Europe*; Oxford University Press: Oxford, UK, 2015.
15. Matlová, V.; Roffet-Salque, M.; Pavlu, I.; Kyselka, J.; Sedlarova, I.; Filip, V.; Evershed, R.P. Defining pottery use and animal management at the neolithic site of bylany (czech republic). *J. Archaeol. Sci. Rep.* **2017**, *14*, 262–274. [[CrossRef](#)]
16. Whelton, H.L.; Roffet-Salque, M.; Kotsakis, K.; Urem-Kotsou, D.; Evershed, R.P. Strong bias towards carcass product processing at Neolithic settlements in northern Greece revealed through absorbed lipid residues of archaeological pottery. *Quat. Int.* **2018**, *496*, 127–139. [[CrossRef](#)]
17. Charters, S.; Evershed, R.P.; Quye, A.; Blinkhorn, P.W.; Reeves, V. Simulation experiments for determining the use of ancient pottery vessels: The behaviour of epicuticular leaf wax during boiling of a leafy vegetable. *J. Archaeol. Sci.* **1997**, *24*, 1–7. [[CrossRef](#)]
18. Dudd, S.N.; Regert, M.; Evershed, R.P. Assessing microbial lipid contributions during laboratory degradations of fats and oils and pure triacylglycerols absorbed in ceramic potsherds. *Org. Geochem.* **1998**, *29*, 1345–1354. [[CrossRef](#)]

19. Gregg, M.W.; Slater, G.F. A new method for extraction, isolation and transesterification of free fatty acids from archaeological pottery. *Archaeometry* **2010**, *52*, 833–854. [[CrossRef](#)]
20. Evershed, R.P.; Arnot, K.I.; Collister, J.; Eglinton, G.; Charters, S. Application of isotope ratio monitoring gas-chromatography mass-spectrometry to the analysis of organic residues of archaeological origin. *Analyst* **1994**, *119*, 909–914. [[CrossRef](#)]
21. Kučera, L.; Peška, J.; Fojtík, P.; Barták, P.; Kučerová, P.; Pavelka, J.; Komárková, V.; Beneš, J.; Polcerová, L.; Králík, M.; et al. First direct evidence of broomcorn millet (*panicum miliaceum*) in central Europe. *Archaeol. Anthropol. Sci.* **2019**, *11*, 4221–4227. [[CrossRef](#)]
22. Oras, E.; Vahur, S.; Isaksson, S.; Kaljurand, I.; Leito, I. MALDI-FT-ICR-MS for archaeological lipid residue analysis. *J. Mass Spectrom.* **2017**, *52*, 689–700. [[CrossRef](#)] [[PubMed](#)]
23. Kučera, L.; Peška, J.; Fojtík, P.; Barták, P.; Sokolovská, D.; Pavelka, J.; Komárková, V.; Beneš, J.; Polcerová, L.; Králík, M.; et al. Determination of milk products in ceramic vessels of corded ware culture from a late eneolithic burial. *Molecules* **2018**, *23*, 3247. [[CrossRef](#)]
24. Hammann, S.; Cramp, L.J.E. Towards the detection of dietary cereal processing through absorbed lipid biomarkers in archaeological pottery. *J. Archaeol. Sci.* **2018**, *93*, 74–81. [[CrossRef](#)]
25. Liu, L.; Wang, J.; Rosenberg, D.; Zhao, H.; Lengyel, G.; Nadel, D. Fermented beverage and food storage in 13,000 y-old stone mortars at Raqefet cave, Israel: Investigating natufian ritual feasting. *J. Archaeol. Sci. Rep.* **2018**, *21*, 783–793. [[CrossRef](#)]
26. Liu, L.; Wang, J.; Liu, H. The brewing function of the first amphorae in the neolithic yangshao culture, north China. *Archaeol. Anthropol. Sci.* **2020**, *12*, 1–15. [[CrossRef](#)]
27. Stojanovski, D.; Živaljević, I.; Dimitrijević, V.; Dunne, J.; Evershed, R.P.; Balasse, M.; Dowle, A.; Hendy, J.; McGrath, K.; Fischer, R.; et al. Living off the land: Terrestrial-based diet and dairying in the farming communities of the Neolithic Balkans. *PLoS ONE* **2020**, *15*, e0237608. [[CrossRef](#)]
28. Pavelka, J.; Smejda, L.; Hynek, R.; Hrdlickova Kuckova, S. Immunological detection of denatured proteins as a method for rapid identification of food residues on archaeological pottery. *J. Archaeol. Sci.* **2016**, *73*, 25–35. [[CrossRef](#)]
29. Pavelka, J.; Smejda, L.; Kučková, Š.; Menšík, P. Challenge to molecular archaeology - sediments contaminated by allochthonous animal proteins. *J. Liq. Chromatogr. Relat. Technol.* **2020**, *43*, 19–20. [[CrossRef](#)]
30. Pietra, F.; Baldwin, J.E.; Williams, R.M. *Biodiversity and Natural Product Diversity*; Elsevier Science: London, UK, 2002.
31. Casanova, E.; Knowles, T.D.J.; Williams, C.; Crump, M.P.; Evershed, R.P. Practical considerations in high-precision compound-specific radiocarbon dating: Eliminating the effects of solvent and sample cross-contamination on accuracy and precision. *Anal. Chem.* **2018**, *90*, 11025–11032. [[CrossRef](#)] [[PubMed](#)]
32. Bayliss, A.; Marshall, P. Confessions of a serial polygamist: The reality of radiocarbon reproducibility in archaeological samples. *Radiocarbon* **2019**, *61*, 1143–1158. [[CrossRef](#)]
33. Bayliss, A.; van der Plicht, J.; Bronk, R.C.; McCormac, F.G.; Healy, F.; Whittle, A. Towards generational time-scales: The quantitative interpretation of archaeological chronologies. In *Gathering Time: Dating the Early Neolithic Enclosures of Southern Britain and Ireland*; Whittle, A., Healy, F., Bayliss, A., Eds.; Oxbow Books: Oxford, UK, 2011; pp. 17–59.
34. Philippsen, B. Hard water and old food. The freshwater reservoir effect in radiocarbon dating of food residues on pottery. *Doc. Praehist.* **2015**, *42*, 159–170. [[CrossRef](#)]
35. Wagner, B.; Reicherter, K.; Daut, G.; Wessels, M.; Matzinger, A.; Schwalb, A.; Spirkovski, Z.; Sanxhaku, M. The potential of lake ohrid for long-term palaeoenvironmental reconstructions. *Palaeogeogr. Palaeoclimatol. Palaeoecol.* **2008**, *259*, 341–356. [[CrossRef](#)]
36. Beavan-Athfield, N.; McFadgen, B.; Sparks, R. Environmental influences on dietary carbon and ¹⁴C ages in modern rats and other species. *Radiocarbon* **2001**, *43*, 7–14. [[CrossRef](#)]
37. Bronk Ramsey, C. Bayesian analysis of radiocarbon dates. *Radiocarbon* **2009**, *51*, 337–360. [[CrossRef](#)]
38. Reimer, P.J.; Austin, W.E.N.; Bard, E.; Bayliss, A.; Blackwell, P.G.; Bronk Ramsey, C.; Butzin, M.; Cheng, H.; Edwards, R.L.; Friedrich, M.; et al. The intcal20 northern hemisphere radiocarbon age calibration curve (0–55 cal kBP). *Radiocarbon* **2020**, *62*, 725–757. [[CrossRef](#)]
39. Bozarth, S.R. Classification of opal phytoliths formed in selected dicotyledons native to the great plains. In *Phytolith Systematics*; Springer: Boston, UK, 1992; pp. 193–214.
40. Neumann, K.; Strömberg, C.A.E.; Ball, T.; Albert, M.R.; Vrydaghs, L.; Cumming, L.S. International code for phytolith nomenclature (ICPN) 2.0. *Ann. Bot.* **2019**, *124*, 189–199. [[CrossRef](#)]
41. Reichert, E.T. *The Differentiation and Specificity of Starches in Relation, to Genera, Species*; Carnegie Institution of Washington: Washington, DC, USA, 2013.
42. Velišek, J.; Koplík, R.; Cejpek, K. *The Chemistry of Food*; John Wiley & Sons: Hoboken, NJ, USA, 2020.
43. Henry, A.G.; Hudson, H.F.; Piperno, D.R. Changes in starch grain morphologies from cooking. *J. Archaeol. Sci.* **2009**, *36*, 915–922. [[CrossRef](#)]
44. Crowther, A. The differential survival of native starch during cooking and implications for archaeological analyses: A review. *Archaeol. Anthropol. Sci.* **2012**, *4*, 221–235. [[CrossRef](#)]
45. Barton, H. Starch residues on museum artefacts: Implications for determining tool use. *J. Archaeol. Sci.* **2007**, *34*, 1752–1762. [[CrossRef](#)]
46. Yang, X.Y.; Yu, J.C.; Lü, H.Y.; Cui, T.X.; Guo, J.N.; Ge, Q.S. Starch grain analysis reveals function of grinding stone tools at Shangzhai site, Beijing. *Sci. China Ser. D Earth Sci.* **2009**, *52*, 1164–1171. [[CrossRef](#)]

47. Liu, L. A long process towards agriculture in the middle yellow river valley, China: Evidence from macro- and micro-botanical remains. *J. Indo-Pac. Archaeol.* **2015**, *35*, 3. [[CrossRef](#)]
48. Bucchi, A.; Burguet-Coca, A.; Expósito, I.; Aceituno Bocanegra, F.J.; Lozano, M. Comparisons between methods for analyzing dental calculus samples from El Mirador cave (Sierra de Atapuerca, Spain). *Archaeol. Anthropol. Sci.* **2019**, *11*, 6305–6314. [[CrossRef](#)]
49. Yang, X.; Zhang, J.; Perry, L.; Ma, Z.; Wan, Z.; Li, M.; Diao, X.; Lu, H. From the modern to the archaeological: Starch grains from millets and their wild relatives in China. *J. Archaeol. Sci.* **2012**, *39*, 247–254. [[CrossRef](#)]
50. Liu, L.; Kealhofer, L.; Chen, X.; Ji, P. A broad-spectrum subsistence economy in neolithic inner mongolia, China: Evidence from grinding stones. *Holocene* **2014**, *24*, 726–742. [[CrossRef](#)]
51. Valentini, Q.; Favaretto, S.; Miola, A.; Sostizzo, I. Unknown and known quaternary non pollen palynomorphs from sediments analysed in the Laboratory of Palynology, University of Padua Italy. *Palyno-Bulletin* **2006**, *2*, 65–66.
52. Kvavadze, E. Non pollen palynomorphs as an important object for solution of archaeological problems. In *Proceedings of 3th International Workshop on Quaternary Non-Pollen Palynomorphs*; Maritan, M., Miola, A., Eds.; University of Padova Press: Padova, Italy, 2008; pp. 34–37.
53. Kvavadze, E.; Kakhiani, K. Palynology of the paravani burial mound (early bronze age, Georgia). *Veg. Hist. Archaeobot.* **2010**, *19*, 469–478. [[CrossRef](#)]
54. Athanassiou, C.G.; Phillips, T.W.; Wakil, W. Biology and control of the khapra beetle, *trogoderma granarium*, a major quarantine threat to global food security. *Annu. Rev. Entomol.* **2019**, *64*, 131–148. [[CrossRef](#)] [[PubMed](#)]
55. Kislev, M.E.; Nadel, D.; Carmi, I. Epipalaeolithic (19000 BP) cereal and fruit diet at ohalo II, sea of galilee, Izrael. *Rev. Palaeobot. Palynol.* **1992**, *73*, 161–166. [[CrossRef](#)]
56. Kubiak-Martens, L. The plant food component of the diet at the late Mesolithic (Ertebolle) settlement at Tybrind Vig, Denmark. *Veg. Hist. Archaeobot.* **1999**, *8*, 117–127. [[CrossRef](#)]
57. Aranguren, B.; Becattini, R.; Lippi, M.M.; Revedin, A. Grinding flour in upper Palaeolithic Europe (25 000 years bp). *Antiquity* **2007**, *81*, 845–855. [[CrossRef](#)]
58. Revedin, A.; Aranguren, B.; Becattini, R.; Longo, L.; Marconi, E.; Lippi, M.M.; Skakun, N.; Sinitsyn, A.; Spiridonova, E.; Svoboda, J. Thirty thousand-year-old evidence of plant food processing. *Proc. Natl. Acad. Sci. USA* **2010**, *107*, 18815–18819. [[CrossRef](#)]
59. Morton, J.F. Cattails (*typha* spp.)—Weed problem or potential crop? *Econ. Bot.* **1975**, *29*, 7–29. [[CrossRef](#)]
60. Gott, B. Cumbungi, *Typha* species: A staple aboriginal food in southern Australia. *AAS* **1999**, *1*, 33–49.
61. Vencl, S. Žaludy jako potravina: k poznání významu sběru pro výživu v pravěku. *Archeol. Rozhl.* **1985**, *37*, 516–565.
62. Vencl, S. Acorns as food: Again. *Památ. Archeol.* **1996**, *87*, 95–111.
63. De Hingh, A.E. Food Production and Food Procurement in the Bronze Age and Early Iron Age (2000–500 BC). Ph.D. Thesis, Leiden University, Leiden, The Netherlands, 2000.
64. AKRM. *Arheoloska Karta Na Republika Makedonija Tom II (The Archaeological Map of The Republic of Macedonia)*; Makedonska Akademija Na Naukite I Umetnostite: Skopje, North Macedonia, 1996.
65. Kuzman, P. Praistoriskite palafitni naselbi vo Makedonija. In *Makedonija, Mileniumski-Kulturno Istorsiki Fakti I*; Kuzman, P., Dimitrova, E., Donev, J., Eds.; Media Print Makedonija and Universitet Evro-Balkan: Skopje, North Macedonia, 2013; pp. 298–429.
66. Todoroska, V. The pile dwelling settlement “Ustie na Drim”. In *Neolithic in Macedonia: New Knowledge and Perspectives, Centre for Prehistoric Research*; Naumov, G., Fidanovski, L., Eds.; Magnasken: Skopje, North Macedonia, 2016; pp. 41–53.
67. Benac, A. Ohridsko jezero i južna Pelagonija. Arheološki otkritija na počvata na Makedonija. *MANU* **2008**, *17*, 21–32.
68. Sanec, V.; Stamenova, M. Neolitskata naselba “Stranata” vo selo Angelci. In *Zbornik na trudovi*; Dukovski, V., Pavlovski, V., Lazarev, J., Dudeski, L., Eds.; Mašinski fakultet: Skopje, North Macedonia, 1989; pp. 9–63.
69. Sinadinovski, P. Docniot Neolit Vo Republika Makedonija. Master’s Thesis, St. Cyril’s Metodi University, Skopje, North Macedonia, 2019.
70. Léra, P. Vendbanimi i neolitit të vonë në Barç (Faza Barç II)/L’habitat du Néolithique récent à Barç (La phase Barç II). *Iliria* **1987**, *17*, 25–69. [[CrossRef](#)]
71. Benac, A. *Praistorija jugoslavenskih zemalja II, Neolitsko doba*; Akademija nauke i umetnosti Bosne i Hercegovine: Sarajevo, North Macedonia, 1979; pp. 363–472.
72. Tsirtsoni, Z. Chapter 1: The chronological framework in Greece and Bulgaria between the late 6th and the early 3rd millennium BC, and the “Balkans 4000” project. In *The Human Face of Radiocarbon: Reassessing Chronology in Prehistoric Greece and Bulgaria, 5000–3000 Cal BC*; MOM Éditions: Lyon, France, 2016. [[CrossRef](#)]
73. Coil, J.; Korstanje, M.A.; Archer, S.; Hastorf, C.A. Laboratory goals and considerations for multiple microfossil extraction in archaeology. *J. Archaeol. Sci.* **2003**, *30*, 991–1008. [[CrossRef](#)]
74. Li, M.; Yang, X.; Ge, Q.; Ren, X.; Wan, Z. Starch grains analysis of stone knives from Changning site, Qinghai Province, Northwest China. *J. Archaeol. Sci.* **2013**, *40*, 1667–1672. [[CrossRef](#)]
75. Messner, T.C.; Dickau, R.; Harbison, J. Starch grain analysis: Methodology and applications in the northeast. In *Current Northeast Paleoethnobotany II*; Hart, J.P., Ed.; University of the State of New York, State Education Department: Albany, NY, USA, 2008; pp. 111–128.
76. Pagán-Jiménez, J.R.; Rodríguez-Ramos, R.; Reid, B.A.; van den Bel, M.; Hofman, C.L. Early dispersals of maize and other food plants into the Southern Caribbean and Northeastern South America. *Quat. Sci. Rev.* **2015**, *123*, 231–246. [[CrossRef](#)]

-
77. Pavelka, J.; Kovačiková, L.; Šmejda, L. Détermination d'espèces d'animaux domestiques à partir d'un échantillon néolithique grâce au test Elisa. *Comptes Rendus Palevol* **2011**, *10*, 61–70. [[CrossRef](#)]
 78. Dinh, T.T.N.; Thompson, L.D.; Galyean, M.L.; Brooks, J.C.; Patterson, K.Y.; Boylan, L.M. Cholesterol content and methods for cholesterol determination in meat and poultry. *Compr. Rev. Food. Sci Food Saf.* **2011**, *10*, 269–289. [[CrossRef](#)]

Article

Secret Recipe Revealed: Chemical Evaluation of Raw Colouring Mixtures from Early 19th Century Moravia

Klára Jagošová¹, Martin Moník², Jaroslav Kapusta², Radka Pechancová¹, Jana Nádvorníková¹, Pavel Fojtík³, Ondřej Kurka¹, Tereza Závodná¹, Petr Bednář¹, Lukáš Richtera⁴ and Lukáš Kučera^{1,*}

¹ Department of Analytical Chemistry, Faculty of Science, Palacký University, 17. listopadu 12, 77900 Olomouc, Czech Republic

² Department of Geology, Faculty of Science, Palacký University, 17. listopadu 12, 77900 Olomouc, Czech Republic

³ Institute of Archaeological Heritage Brno, v.v.i.-workplace Prostějov, Tetín 8, 79601 Prostějov, Czech Republic

⁴ Department of Chemistry and Biochemistry, Mendel University in Brno, Zemědělská 1, 61300 Brno, Czech Republic

* Correspondence: lukas.kucera@upol.cz

Abstract: An archaeological excavation in Prostějov (Czech Republic) revealed a workshop of a local potter with colourless, pink, and blue powders presumably used to produce faience/surface decoration. A comprehensive analytical study, which combined elemental and molecular analysis techniques, was performed to shed light on the chemical composition of these unique findings. Scanning electron microscopy with energy dispersive X-ray spectroscopy (SEM EDX), inductively coupled-plasma mass spectrometry (ICP MS), flow injection analysis (FIA) with electrospray ionisation mass spectrometry (ESI MS), laser desorption ionisation mass spectrometry (LDI MS), and Raman spectroscopy were applied to reveal the elemental composition of the powders and identify the colouring agents in the pink and blue powders. The colouring agents in the pink powder were probably iron and the agent in the blue powder is Prussian blue. On top of that, it was also possible to determine the organic additives in these powders through pyrolysis gas chromatography with mass spectrometric detection (Py GC/MS), atmospheric solids analysis probe ion mobility mass spectrometry (ASAP IM MS), and LDI MS. The organic constituents were identified as plant resin, beeswax, and fats. These results point to the preparation of faience/pigment mixtures as oil paint.

Keywords: Faience; direct mass spectrometry; elemental analysis; inorganic pigments; mass spectrometry; organic additives



Citation: Jagošová, K.; Moník, M.; Kapusta, J.; Pechancová, R.; Nádvorníková, J.; Fojtík, P.; Kurka, O.; Závodná, T.; Bednář, P.; Richtera, L.; et al. Secret Recipe Revealed: Chemical Evaluation of Raw Colouring Mixtures from Early 19th Century Moravia. *Molecules* **2022**, *27*, 5205. <https://doi.org/10.3390/molecules27165205>

Academic Editors: Erika Ribechini, Maria Perla Colombini and Jeannette Jacqueline Lucejko

Received: 11 July 2022

Accepted: 14 August 2022

Published: 15 August 2022

Publisher's Note: MDPI stays neutral with regard to jurisdictional claims in published maps and institutional affiliations.



Copyright: © 2022 by the authors. Licensee MDPI, Basel, Switzerland. This article is an open access article distributed under the terms and conditions of the Creative Commons Attribution (CC BY) license (<https://creativecommons.org/licenses/by/4.0/>).

1. Introduction

The chemical analysis of glazed pottery findings remains a big challenge because of usually minute amounts of unique samples available for analysis, the complexity of the matrix, and the transformation of the individual components during manufacturing processes. Many comprehensive studies on archaeological glazed pottery have been carried out combining microinvasive and non-invasive analytical techniques [1–10]. The main goal of these studies was to reveal the composition of the ceramic matrix, determine the colouring agents and additives in the glazed layers (faience), reconstruct the manufacturing technology, and estimate the provenance of the pottery. Electron microscopy combined with energy dispersive X-ray spectroscopy (SEM-EDX) and X-ray fluorescence spectrometry are often the methods of choice for the determination of elemental composition. The disadvantage of SEM-EDX and XRF is their lower sensitivity. Due to this limitation, ICP-MS is preferred when the pattern of trace elements needs to be determined. For the analysis of cross-sections, it is advantageous to use laser ablation coupled with ICP-MS since it has a suitable resolution (i.e., tens of micrometres) [3,6,11–13]. Among

other techniques of elemental analysis, thermal ionisation mass spectrometry [7,8], secondary ion mass spectrometry [14], particle induced X-ray or gamma ray spectroscopy [4,5], X-ray diffraction [1,9], laser induced breakdown spectrometry [15], neutron activation analysis [16] or X-ray photoelectron spectrometry [17] have been applied for glaze/faience analyses. Methods of molecular spectroscopy, such as Raman spectroscopy or infrared spectroscopy, are often utilised for the determination of the mineralogical structure of studied materials [18,19]. Until the present day, no study revealed the complete manufacturing technologies of faience production since only final products or fragments are available for physicochemical analysis using modern analytical techniques. The reason is the thermal degradation of organic additives during the firing of faience on ceramics. It should be noted that Zaremba et al. [20] observed the emission of CO₂ and ammonia during the thermal analysis of the glazed and underglazed layer of the faience Ptolemaic bowl. They assumed that the evolved gases were decomposition products of organic matter trapped in the pores of the object. However, even in this case, it was not possible to determine the original organic additives.

The technique of faience was applied to Moravian pottery (Czech Republic) from the 16th century onwards [21,22]. It consists of applying a glassy layer on fired sherd to make it harder, impenetrable, and easier to paint on. It was brought to the Czech lands by Anabaptists in the 16th century, probably from southern Germany, and remained in use after their expulsion from Bohemia and Moravia (1622 AD) after the Battle of White Mountain 1620 AD [21]. In 2017, a rescue archaeological excavation in Vodní ulice Street (*Wassergasse*) in Prostějov (Moravia, Czech Republic) discovered the house of pottery master Jan Skřivánek, born in 1773 and active in Prostějov after 1802 [23]. Three powder samples were found inside preparative ceramic vessels, i.e., colourless/white (sample 1), pink (sample 2), and blue (sample 3) powders (Figure 1).



Figure 1. From the left: colourless, pink, and blue powders.

The aim of the presented study is to identify the inorganic and organic components of the powders since their recipes were kept secret and formed a part of the “arcane” knowledge of folk alchemists [21]. Although a number of recipes for such powders are known to historians, *ibid.*, these were also often written in “secret” language so that no other pottery master could make use of them. In this way, this study helps to decode this language and understand the beginning part of the manufacturing process of faience. Untargeted analyses of powders were performed by ASAP-MS with ion mobility (IM), FIA/ESI-MS, Py-GC/MS, LDI-MS, and Raman spectroscopy. For elemental composition, SEM-EDX and semiquantitative ICP-MS analyses were performed. To the best of our knowledge, this is the first-time the analysis of raw faience materials has been conducted by modern instrumental analytical techniques.

2. Results

The morphological characterisation of inorganic grains of particular minerals was performed using SEM/EDX (Table 1). Based on the morphology of fragments observed

with SEM and their chemical composition, the colourless powder is formed by crushed glass, one of the components of a so-called *frit* (Figure 2a) [24]. In practice, it is later mixed with water and colourants and applied to the pottery surface before the second firing. Some fragments are enriched in Pb (EDX analyses 1, 2, and 4 in Table 1 and Figure 2a,b), ranging from 6 wt% to 18 wt% of PbO while others (analysis 3) are almost pure silica. Sulphur is present in small quantities (<0.3 wt% of SO₃) in all analysed samples, probably linked with the Pb mineral (galena). A variability in chemical composition within single pieces of crushed glass/frit was observed (Figure 2b), indicating the mixing of several types of glass. Notably, a high amount of lead in various forms was confirmed by LDI-MS as well. The signals of clusters with different elemental compositions dominate the LDI-MS spectra in both ionisation modes (see Supplementary Material Figures S1–S3).

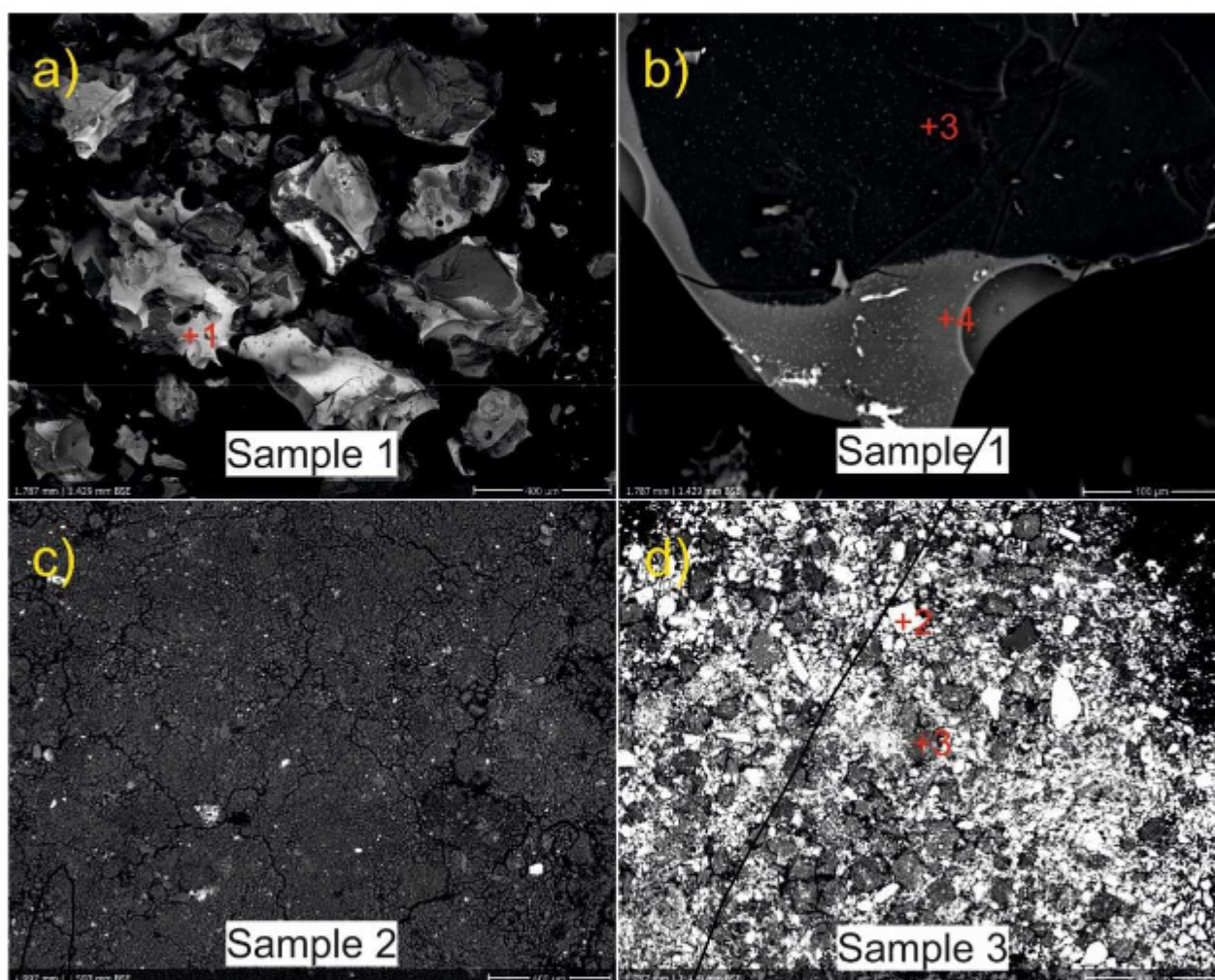


Figure 2. BSE images of the powders encountered in Vodní ulice Street. Crushed glass or frit (a,b) composed of glass of variable chemistry, pink powder (c), and blue powder (d). The numbers in red indicate the points of SEM-EDX analysis and correspond to the numbers of analyses in Table 1.

The pink-coloured powder turned out to be very fine-grained (Figure 2c) so only “bulk” SEM-EDX analysis was performed. Apart from the predominant SiO₂ and Al₂O₃ oxides, we encountered CaO, PbO, and K₂O in the mixture; (hydr)oxides of P₂O₅, FeO, TiO₂, MgO, and Na₂O, together with SO₃, were present in amounts < 1 wt%. The blue powder comprises abundant baryte crystals (EDX analyses), a common additive in faience manufacture which served as flux, increased the brilliancy of the glaze, and reduced the number of bubbles during melting [24,25]. The remaining matter also contains SiO₂, Al₂O₃, PbO, and FeO, and in lesser or trace amounts CaO, P₂O₅, MgO, SrO, or Na₂O as well. With

regard to the manufacturing technology, the addition of Pb both in the crushed glass and in the two coloured powders is obvious. The slightly elevated values of K₂O and Na₂O indicate that we have mixtures for lead glazes with low amounts of alkalis [3]. Though elevated, the amounts of Pb (wt% from SEM-EDS) in the powders from Prostějov are still much lower than in Modern Age glazes published by Tite et al. or Gregerová et al. [3,22]; therefore, it can be assumed that another Pb-rich mixture, not found during excavation, was added. Lead was probably available in the form of litharge (PbO), either a secondary mineral from outcrops of galena ores, or a by-product from smelting (lead-) silver ores [26]. Similar to baryte, litharge served as a flux in glazes, increasing their brilliance, smoothness, density, and resistance to cracking [3,14]. Its disadvantage was the release of lead in meals, resulting in higher Pb-intake by the early Modern Age population, with potentially poisonous effects [27,28]. Most of the analysed mixtures, especially the pink powder and crushed glass, contain small amounts of P₂O₅, CaO, and MgO, but their amounts are lower than in the Anabaptist pottery from Strachotín (Moravia) where the use of bone ash from calcined bones or antlers was conjectured [22]. As it stands, the mixtures from Prostějov would probably result in translucent rather than opacified glazes. Only the joint presence of TiO₂, SO₃, and FeO in the pink powder may potentially indicate the use of titanium oxide opacifiers, manufactured by soaking ilmenite (FeTiSiO₃) in green vitriol, i.e., ferrous sulphate (FeSO₄).

Table 1. EDX results of the three samples in wt%.

No. of Analysis	Sample	Na	Mg	Al	Si	P	S	K	Ca	Ti	Fe	Sr	Ba	Pb	Sum	Other Minerals
1	#1	0.98	0.17	8.52	65.21	0.05	0.22	2.42	0.22	ND	0.94	ND	0.27	11.76	90.76	quartz
2	#1	0.85	0.27	6.40	66.54	0.05	0.15	1.87	0.27	ND	1.30	ND	ND	18.13	95.82	
3	#1	0.36	0.28	0.62	101.83	0.42	0.43	0.11	0.05	ND	0.05	ND	ND	0.13	104.26	
4	#1	1.37	0.69	9.21	75.92	0.54	0.65	2.16	0.33	1.45	1.70	ND	ND	6.59	100.62	
1 (bulk)	#2	0.26	0.60	20.95	38.58	1.39	1.31	1.69	4.21	0.69	0.60	ND	ND	1.97	72.24	baryte, Na-feldspar, chlorite, and aluminosilicate
1 (bulk)	#3	0	0	4.23	9.17	0	8.51	0.04	0.83	ND	1.33	0.19	20.34	9.22	53.84	Quartz and aluminosilicate
3 (bulk)	#3	0.03	0.32	21.92	33.99	2.67	1.11	1.08	4.22		7.85	0.67	0.27	8.21	82.34	
2 (baryte)	#3						17.81		0		0	0	52.60	0	70.40	
4 (baryte)	#3	0	0	0			27.83	0	0		0	0	56.26	0	84.09	

In addition to SEM-EDX, ICP-MS analyses were performed to obtain an exact concentration of elements in the studied powders and reveal the colour origin (Table 2). One of the most common red pigments used in glazes/faience was hematite α -Fe₂O₃ (or maghemite γ -Fe₂O₃) which causes red to brown shades depending on the conditions during firing. The red hue was achieved under oxidising conditions at a temperature higher than 700 °C [29]. Red glazes were also achieved by the use of other minerals, for example, cuprite Cu₂O, crocoite (PbCrO₄), or red lead (Pb₃O₄) [29–31]. Based on the results of the ICP-MS analysis, though, we hypothesise that the colouring agent in the pink powder was Fe found in concentrations of 0.50 mg·g⁻¹, probably in the form of hematite. Copper, e.g., in the form of cuprite or copper nanoparticles, was also used as a red colourant in historical glassmaking [32,33], but the amount of Cu used in such cases was about 100x greater than in the red powder from Prostějov (0.26 mg·g⁻¹, Table 2).

Table 2. ICP-MS results in mg·g⁻¹.

Sample	P	S	Ca	Na	Mg	Al	Si	K	Ti	V	Mn	Fe	Cu	Zn	Ga	Sr	Sn	Sb	Ba	Hg	Pb
1	0.3	0.6	<LOD	34.6	0.8	32	317	5.2	0.86	0.02	0.02	2.0	0.08	0.01	0.02	0.02	0.44	0.01	0.3	<LOD	6
2	3.2	3.3	4.4	1.1	1.3	51	223	4.0	0.07	0.03	0.01	0.5	0.26	0.02	0.22	0.15	0.02	0.05	4.3	0.01	35
3	0.6	14.0	14.0	1.2	0.6	11	101	0.9	0.04	0.03	0.03	4.0	0.13	0.10	4.84	3.52	0.17	0.10	86.0	0.43	232

Py-GC/MS analysis revealed the presence of organic additives in the pink faience powder, i.e., diterpene resin acids of the abietane and pimarane types (Figure 3a). Abietic acid, dehydroabietic acid, pimaric acid, and levopimaric acid are significant components of resins produced by conifers (gymnosperms), e.g., pine (*Pinus*), larch (*Larix*), spruce (*Pices*),

and fir (*Abies*). [34,35]. ASAP-IM-MS did not allow the separation of individual resin acid isomers but confirmed the presence of the resin as a sum of all isomers. A compound with m/z 301.2145 ($C_{20}H_{29}O_2^+$) corresponds to the structure of protonated dehydroabietic acid with the deviation from theoretical mass (dtm) of -2.3 mDa. The fragmentation spectra of dehydroabietic acid in the pink powder and in the standard are presented in Figure 3b,c, respectively. In addition to the signals belonging to the resin, the signals at m/z 463.4858, 491.5186, and 519.5491 correspond to the ions of molecular formula $C_{32}H_{63}O_1^+$, $C_{34}H_{67}O_1^+$, $C_{36}H_{71}O_1^+$ with dtm -2.1 , -0.6 and -1.4 mDa, respectively (for fragmentation spectra see Supplementary Material Figures S4–S6). Those signals were assigned as thermal/ion fragments of beeswax components based on a comparison with the mass spectrum of a standard of beeswax. As further evidence of beeswax presence, we also identified molecule $C_{42}H_{83}O_2^+$ (619.6393 Da) with dtm -0.8 mDa as an ester of palmitic acid, which is a typical component of beeswax [36] (for fragmentation spectra see Supplementary Material Figure S7). In addition, diglycerols also were found with m/z 607.5640 ($C_{39}H_{75}O_4^+$; dtm -2.5 mDa; distearoyl glycerol, SS), 579.5327 ($C_{37}H_{71}O_4^+$; dtm -2.5 mDa; palmitoyl-stearoyl glycerol; PS), and 551.4991 ($C_{35}H_{67}O_4^+$; dmt -4.8 dipalmitoyl glycerol, PP). (for fragmentation spectra see Supplementary Material Figures S8–S10). Those compounds are present in high concentrations in fatty materials (originating from both plants and animals) [36]. The pink powder was probably prepared in a similar way as pigments for traditional oil paintings. According to Slánský, the preparation of traditional oil paints includes pigment(s) and oil as main components with the frequent presence of resin, wax, or balms [37].

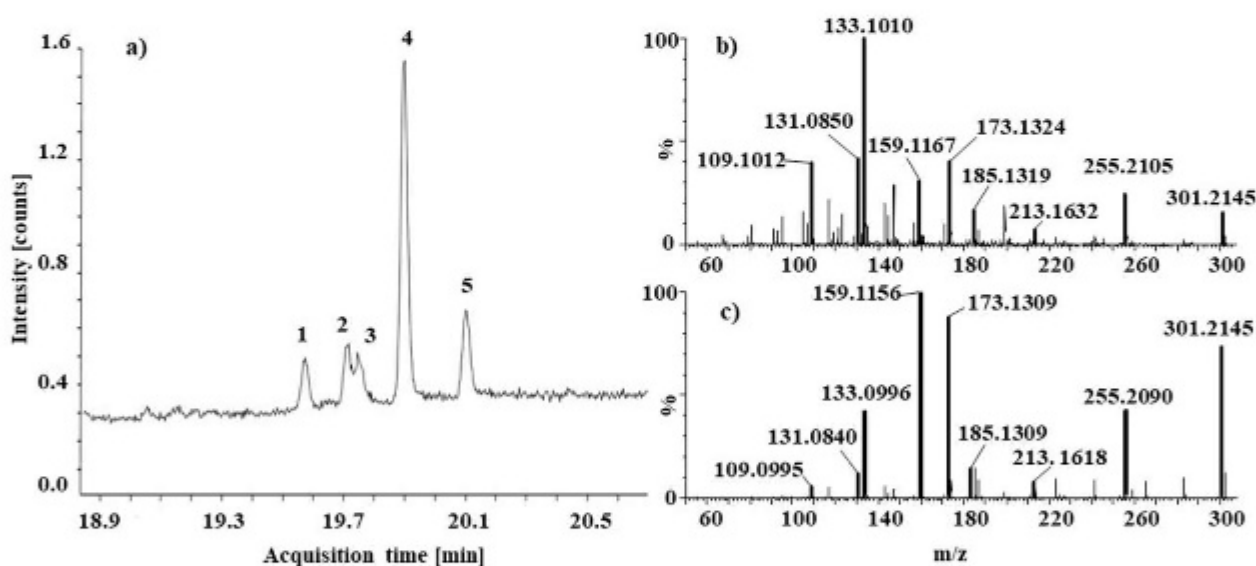


Figure 3. Pyrogram of the pink powder (1: pimaric acid TMS, 2: isopimaric acid TMS, 3: unknown compound, 4: dehydroabietic acid TMS, and 5: abietic acid TMS) (a); ASAP IM MS fragmentation spectra of compound m/z 301.2152 in pink powder (collision energy 20 V) (b) and in the standard of dehydroabietic acid (collision energy 20 V) (c).

The blue colour in glaze making is normally achieved by the addition of Cr, Co, or Cu [11,26,38], but none are present in the powder from Prostějov–Vodní ulice Street. According to the ICP-MS results, the bulk of the blue powder contained an increased amount of iron (approximately $4 \text{ mg}\cdot\text{g}^{-1}$) which could be the source of the blue colour as hexacyanoferrate pigment $\text{Fe}_4[\text{Fe}(\text{CN})_6]_3$, commonly known as Prussian blue. The presence of PB was consequently identified and proved by the means of FIA/ESI-MS and Raman spectroscopy. The FIA/ESI-MS spectrum of PB standard contained the most intense signals of $[\text{Fe}(\text{CN})_3]^-$ at m/z 133.9443 Da (Figure 4a). In the spectrum of the blue powder, this signal was found as well (m/z 133.9434), with dtm -0.8 mDa (Figure 4b). These results were consequently supported by Raman spectra of the reference material and

sample (see Figure 4c). Four significant signals were found in Raman spectra, i.e., 2154, 2090, 527, and 275 cm^{-1} . The vibration at 2154 cm^{-1} corresponds to $\nu(\text{C}\equiv\text{N})$ stretching vibration and [Fe(II), Fe(III)] vibrational state. This peak is followed by a shoulder of a characteristic CN^- vibration, and signal at 2090 cm^{-1} that corresponds to the $\nu(\text{C}\equiv\text{N})$ stretching vibration of the [Fe(II), Fe(III)] state. The remaining two signals at 527 and 275 cm^{-1} refer to Fe–C stretching vibrations of the lattice and Fe–CN–Fe bond deformation vibrations, respectively [39]. Note that the high concentration of sulphur, which was found in the sample of blue powder by SEM-EDX and ICP-MS (Tables 1 and 2), points to the traditional preparation of PB, i.e., the usage of green vitriol ($\text{FeSO}_4 \cdot 7 \text{H}_2\text{O}$) and dried cattle blood as the source of cyano or/and ferrocyanide groups [29]. The problem with PB, though, is that it would probably not have survived the sintering process in glaze melts. In oxidising conditions, the ferrocyanide bonds would have broken and disassembled (and likely oxidised) into Fe^{3+} . We assume that in reduction conditions, PB possibly formed Fe^{2+} which can cause the aqua blue colour of the glaze. [29]. It would seem that the potter from Prostějov manufactured a mixture based on Prussian blue which he ultimately did not achieve but was left with a perfectly viable alternative. Throughout the 18th century, PB was not used for pottery glazes from other parts of the world either, as it was mostly used for paintings [26]. According to Černohorský, the blue powder could be utilised for decorative purposes after the second firing. This decorative technique was well known in the Moravia region since approximately the 1760s and was known under the German term *Überglasumalerei* [21]. In the findings of Anabaptist faience from 17th century Hungary, another blue colourant based on $\text{CoO} + \text{As}_2\text{O}_3$, FeO , and NiO was used [1]. This was applied on tin-based glazes whereas Prostějov potter Jan Skřivánek either manufactured lead glazes (see Table 1) or his tin mixtures were not found during excavation.

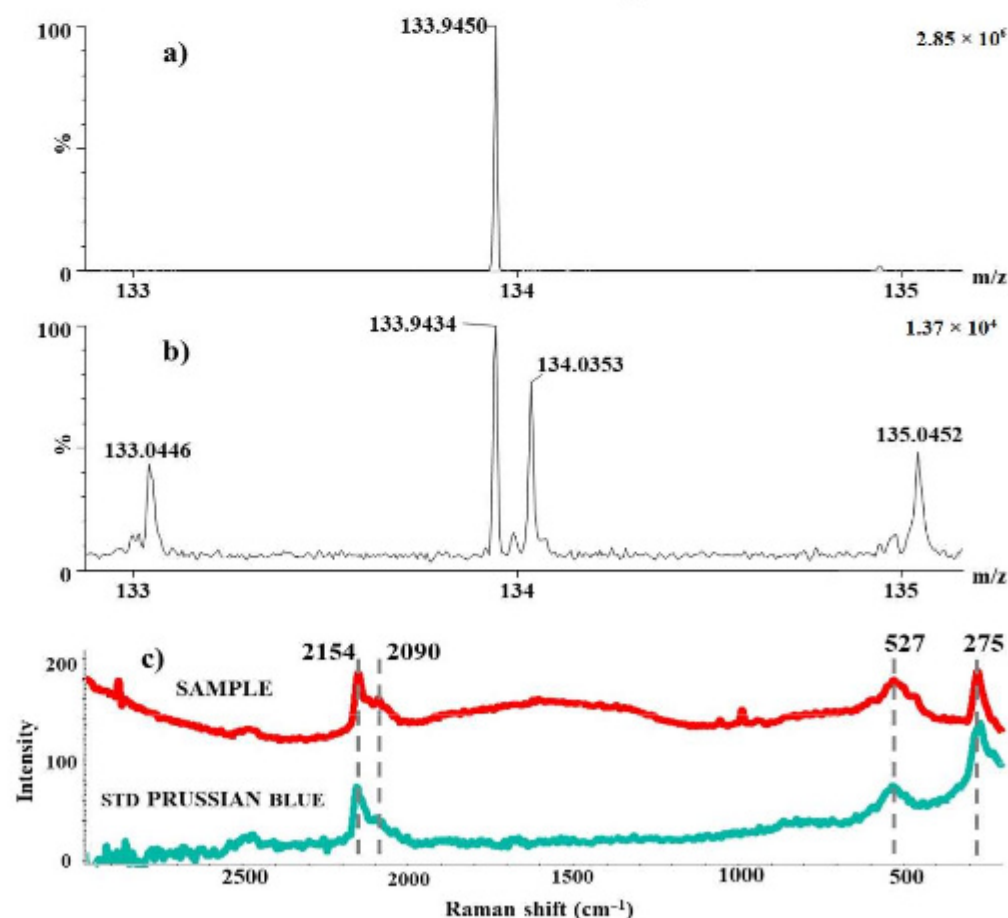


Figure 4. MS spectrum of the PB standard (a), MS spectrum of analysis of the blue powder (b), Raman spectrum of the blue powder, and the PB standard (c).

Analysis of the organic binders in blue powder was performed by ASAP-IM-MS and LDI-MS. The content of organic additives was substantially lower in this sample compared to the sample of the pink powder. In the blue powder, we identified only the same diglycerols as in the case of the pink powder, SS, SP, and PP with *dm* 1.2, 1.2, and 1.3 mDa, respectively (for fragmentation spectra see Figures S11–S13). The LDI-MS in the negative ionisation mode detected three common fatty acids, i.e., palmitic, stearic, and oleic acid in the blue faience powder, further confirming the presence of fatty material in the faience materials (see Figures S14 and S15). We hypothesise that the blue mixture also was prepared similarly to oil paints. None of the aforementioned compounds were found in colourless powder.

3. Materials and Methods

3.1. Chemicals

Abietic acid (Lachema, Brno, Czech Republic), acetone (HPLC grade $\geq 99.8\%$, Fisher Scientific, Waltham, MA, USA), acetonitrile (Honeywell, Charlotte, NC, USA), dehydroabiatic acid (Sigma Aldrich, St. Louis, MI, USA), hydrochloric acid (Analaure, 34–37%, Analytika, Praha, Czech Republic), hydrofluoric acid (Analaure, 48%), leucine enkephalin (HPLC $\geq 95\%$, Sigma Aldrich), methanol (LC-MS $\geq 99.9\%$, Honeywell), Mili-Q water (Merc), nitric acid (Analaure, 67–69%), N,O-Bis(trimethylsilyl)trifluoroacetamide (BSTFA) ($\geq 99.0\%$, Sigma Aldrich), Prussian blue (laboratory prepared), red phosphorus (Sigma Aldrich) for the mass calibration of LDI-MS), sodium formate for the TOF calibration (prepared by mixing 100 μL 0.1 M sodium hydroxide (Fluka, Buchs, Switzerland) with 200 μL 10% formic acid (99–100%, Analaure Normapur) and diluted with a mixture of acetonitrile/water (80:20, *v/v*), and sodium hydroxide (Penta, p.a., Brno, Czech Republic) were used.

3.2. Scanning Electron Microscopy–Energy Dispersive X-ray Spectrometry (SEM/EDX)

Raw faience materials were mounted on carbon foil, carbon coating (25 nm), analysed with SEM-EDX (JEOL JXA-8600), and the chemical composition of single minerals or fragments of glass were established. In other instances, and in the case of the very fine-grained pink powder, “bulk” analyses were performed by targeting a larger area to determine the composition of the whole mixture. The conditions of analysis were set as follows: accelerating voltage 15 kV, beam current 10 nA, beam diameter 1–5 μm , and counting time 60 s per spectrum. Acquired spectra were quantified by IdFix software (remX GmbH) and the following set of standards: albite (Na), diopside (Mg, Ca), microcline (Si, Al, K), apatite (P), barite (Ba, S), ilmenite (Ti, Fe), strontianite (Sr), and lead metal (Pb).

3.3. Inductively Coupled Plasma–Mass Spectrometry (ICP-MS)

A microwave digestion unit MLS 1200 Mega (Milestone, Italy) was employed for sample mineralisation. Prior to the mineralisation step, the powder samples were manually milled and homogenised. Subsequently, approximately 20 mg of homogenised samples were digested with a mixture of concentrated HNO_3 (1 mL), HCl (3 mL), and HF (0.125 mL) according to a seven-step digestion program consisting of 2 min at 250 W, 2 min at 0 W, 5 min at 400 W, 2 min at 0 W, 2 min at 500 W, 2 min at 0 W, and 6 min at 600 W. After digestion and cooling, the samples were diluted with deionised water to 10 mL, transferred into polypropylene tubes and stored at 4 °C until ICP-MS analysis. Blank samples were prepared by digestion of the mixture of acids but without the presence of the sample.

All measurements were carried out using an inductively coupled plasma mass spectrometer 7700x ICP-MS (Agilent Technologies, Tokyo, Japan), fitted with an ASX-520 autosampler, a MicroMist concentric nebuliser, a cooled Scott-type double pass spray chamber, and an octopole reaction cell operating in Helium mode to overcome spectral interferences. The instrumental conditions for the semi-quantitative analysis of selected isotopes (up to 70 elements) by ICP-MS were set as follows: RF power of 1600 W, plasma gas Ar flow rate of 15.0 $\text{L}\cdot\text{min}^{-1}$, an auxiliary gas Ar flow rate of 0.61 $\text{L}\cdot\text{min}^{-1}$, nebuliser

gas Ar flow rate of $0.36 \text{ L}\cdot\text{min}^{-1}$, collision gas He flow rate of $5 \text{ mL}\cdot\text{min}^{-1}$ (He mode) or $0 \text{ mL}\cdot\text{min}^{-1}$ (No Gas mode). All ICP-MS analyses were performed in six replicates. Obtained data were evaluated in MassHunter (Agilent Technologies, Palo Alto, CA, USA).

3.4. Pyrolysis–Gas Chromatography/Mass Spectrometry (Py-GC/MS)

Gas chromatographic analysis was carried out on an Agilent 8890 coupled to a mass detector Agilent 5977B (Agilent, Santa Clara, CA, USA). Pyrolysis of samples was performed with a multi-shot pyrolyzer EGA/PY-3030D (Frontier Lab, New Ulm, MN, USA) at $500 \text{ }^{\circ}\text{C}$ for 0.5 min. A capillary column Ultra Alloy UA5(MS/HT), $30 \text{ m} \times 0.25 \text{ mm} \times 0.25 \text{ }\mu\text{m}$ (Frontier Laboratories Ltd., Fukushima, Japan) was operated with helium as a carrier gas at a constant flow rate of $1 \text{ mL}\cdot\text{min}^{-1}$. The oven program was as follows: $50 \text{ }^{\circ}\text{C}$ for 4 min followed by a $20 \text{ }^{\circ}\text{C}/\text{min}$ ramp to a final temperature of $320 \text{ }^{\circ}\text{C}$ and held for 15 min. The total run time was 32.50 min. The injection was performed in a split mode with a 60:1 split ratio. MassHunter Qualitative Analysis software (Agilent Technologies, Palo Alto, CA, USA) was used for data evaluation. A microsample of the potter's pink powder was put into a pyrolyzer cup. Derivatisation was carried out with $2 \text{ }\mu\text{L}$ of BSTFA prior to Py-GC/MS analysis.

3.5. Direct Mass-Spectrometric Analysis

ASAP-IM-MS and FIA/ESI-MS analyses were performed on Synapt G2-S (Waters, Milford, MA, USA) equipped with an atmospheric solid analysis probe (ASAP) and electrospray ionisation (ESI) source, a hybrid QqTOF mass analyser, and an ion mobility cell (TriWave). Exact masses of analytes were obtained by correction to the mass of leucine enkephalin (556.2771 Da) at a concentration of $2 \text{ ng}\cdot\text{mL}^{-1}$ in water/ACN 80/20 (*v/v*) with 0.1% formic acid, which was measured during each run. Data acquisition and processing were performed by MassLynx (Waters, Manchester, UK). LDI-MS analyses were done using a high-resolution tandem mass spectrometer Synapt G1 equipped with a Q-TOF analyser and vacuum MALDI ion source (Waters). Obtained spectra were treated using MassLynx 4.2. In all cases, the TOF analyser was set to resolution mode (V-mode).

3.5.1. Atmospheric Solids Analysis Probe Ion Mobility Mass Spectrometry (ASAP-IM-MS)

Analyses of the three powders were performed by means of ASAP-IM-MS. This ionisation technique utilises a stream of hot nitrogen to evaporate analytes deposited on a glass capillary tube and ionises them in corona discharge [40]. Since this approach does not require extensive sample preparation, samples were prepared in a form of acetone suspension ($5 \text{ mg}\cdot\text{mL}^{-1}$) that was introduced into an open-ended glass capillary by capillary elevation. After evaporation of the solvent, roughly $10 \text{ }\mu\text{g}$ of the solid sample was subjected to analysis. The glass capillary was transferred to the mass spectrometer ion source and the analytes were evaporated by a stream of nitrogen and finally reached the temperature of $600 \text{ }^{\circ}\text{C}$. Evaporated analytes were subsequently ionised in the plasma created by a corona discharge, and the ionised species were additionally separated according to their shape, size, and charge in the ion mobility cell. The experimental conditions were set as follows: Ionisation mode positive, analysis time 3 min, trap collision energy 4 eV, transfer collision energy 2 eV, source temperature $100 \text{ }^{\circ}\text{C}$, sampling cone 80 V, corona current $2 \text{ }\mu\text{A}$, nitrogen flow rate $500 \text{ L}\cdot\text{h}^{-1}$, nitrogen temperature of $500\text{--}600 \text{ }^{\circ}\text{C}$, IM wave velocity of $550 \text{ m}\cdot\text{s}^{-1}$, IM wave height of 40 V, and helium drift gas. The parameters for the fragmentation experiments were as follows: LM resolution 15, and transfer collision energy (transfer CE) values are listed in Supplementary Material Figures S4–S13 for each compound.

3.5.2. Flow Injection Analysis Electrospray Ionisation Mass Spectrometry (FIA/ESI-MS)

FIA/ESI-MS was utilised for the analysis of the decomposed blue pigment in an alkaline solution. Sample preparation and method parameters were adopted from [41]. The parameters were set as follows: Ionisation mode negative, capillary voltage 2.30 kV, sampling cone 30 V, analysis time 2 min, trap collision energy 4 V, transfer collision energy

2 V, source temperature: 120 °C, desolvation gas 250 °C at a rate of 360 L·h⁻¹, nebuliser 6 bar, mass range 50–600 Da, and scan time 1 s. A mixture of methanol and water (1:1, v/v) at a flow rate of 0.075 mL·min⁻¹ was used as a mobile phase, and 5 µL of the sample was injected.

The sample of standard Prussian Blue (PB, synthesised in our laboratory by mixing a solution of 1 M iron(III) chloride with a 1 M solution of a hexacyanoferrate(II) salt) was prepared at a concentration of 0.05 mg·mL⁻¹ in 0.04 M solution of NaOH. The decomposition was supported by sonification in an ultrasound bath at laboratory temperature in sweep mode for 30 min. The blue powder sample was decomposed in the same way, i.e., approximately 2.5 mg were weighed and dissolved in 10 mL of 0.04 M NaOH. A blank sample was prepared from a 0.04 M solution of NaOH. All samples were diluted ten times and filtered with syringe filters before injection into the system.

3.5.3. Laser Desorption-Ionisation Mass Spectrometry (LDI-MS)

Raw faience materials were fixed on a standard stainless steel MALDI plate using double-sided tape (Ulith, Prague, Czech Republic) and the MALDI plates were inserted into the MALDI chamber for analysis. Mass calibration for the LDI-MS experiments was done by the measurement of red phosphorus which was deposited as acetone suspension (10 mg·mL⁻¹) on a selected position on the MALDI plate. Samples were analysed in both positive and negative ionisation modes without the application of a matrix. Parameters of LDI-MS were set as follows: sample plate 10 V, hexapole bias 10, source gas flow 0 mL·min⁻¹, trap collision energy 6 eV, cooling gas flow 10 mL·min⁻¹, transfer collision energy 4 eV, laser energy 500 (arb), trap gas flow 1.5 mL·min⁻¹, and laser firing rate 200. Manual laser aiming was used.

3.6. Raman Spectroscopy

Raw faience materials were analysed using a DXR2 Raman microscope (Thermo Scientific, Waltham, MA, USA). The parameters were as follows: laser wavelength 785 nm, laser power 1 mW, aperture 50 mm slit, collect exposure time 2 s, and 16 sample exposures. 16. Omnic 9 (Thermo Scientific, Waltham, MA, USA) was used for data evaluation.

4. Conclusions

Modern analytical techniques were used to evaluate historical raw faience materials. The colouring agent in the pink powder was probably iron in the form of Fe₂O₃. The colourant in blue powder is Prussian blue. To the best of our knowledge, this is the first evidence of PB in faience materials. Additionally, Py-GC/MS and ASAP-IM-MS determined constituents of plant resin, beeswax, and fats in the pink powder. The blue powder contained only fat constituents (according to ASAP-IM-MS and LDI-MS). Both coloured powders were probably prepared in a manner also used for the preparation of oil paints [37]. The colourless powder consists of various glass materials, lead as the glaze-forming ingredient, and possibly opacifiers. An obvious difference is observable between the technology used by Hungarian Anabaptists from the 17th century [1] and the potter from early 19th century Prostějov, especially regarding the glazes and blue colour, but it is possible that some parts of the glaze mixture from Prostějov are missing. Some minerals present in the potter's powders, or crushed glass, must have been imported from other parts of Moravia, Silesia, Bohemia, or elsewhere. Baryte (BaSO₄), the source of Ba in the blue powder, is known from several polymetallic ore deposits in the Bohemian Massif such as Horní Benešov, Zlaté Hory (then Zuckmantel) in Silesia (83 km from Prostějov [42]) or the suburbs of Jihlava (110 km) in the Bohemian-Moravian Highlands. The latter two sources comprise galena mineralisation [42,43], a possible source of Pb in the pink and blue powders and the crushed glass. As major mining activities around Jihlava occurred in the Middle Ages, the deposits from Zlaté Hory (or elsewhere) are more likely to be the sources [42] to have supplied the pottery masters in Prostějov. This seems more likely, as Zlaté Hory was a traditional source of chalcopyrite and other Cu-ores [44], potential

colourants of the analysed pink powder. Apart from Zlaté Hory, a possible source of the lead (litharge) is the deposit at Příbram-Zlaté hory, a major source of Central European lead and silver in the 19th century [45], albeit somewhat distant from Prostějov (225 km). If green vitriol (FeSO_4) was indeed used in the glaze mixtures, it could have been acquired from any pit water of the mentioned deposits (i.e., Zlaté Hory or another). To the best of our knowledge, this is the first study describing the composition of raw faience materials by modern analytical techniques and the obtained results help to understand the early part of the manufacturing process in the Central European region.

Supplementary Materials: The following supporting information can be downloaded at: <https://www.mdpi.com/article/10.3390/molecules27165205/s1>, Figure S1: LDI-MS spectra of the pink powder in positive ion mode, Figure S2: LDI-MS spectra of the blue powder in positive ion mode, Figure S3: LDI-MS spectra of the blue powder in negative ion mode (full range), Figure S4: MS/MS spectra of 463.4858 Da in pink powder, Figure S5: MS/MS spectra of 491.5186 Da in pink powder, Figure S6: MS/MS spectra of 519.5491 Da in pink powder, Figure S7: MS/MS spectra of 619.6385 Da in pink powder (a) and beeswax (b), Figure S8: MS/MS spectra of 551.4991 Da in pink powder, Figure S9: MS/MS spectra of 579.5327 Da in pink powder, Figure S10: MS/MS spectra of 607.5640 Da in pink powder, Figure S11: MS/MS spectra of 551.4991 Da in blue powder, Figure S12: MS/MS spectra of 579.5327 Da in blue powder, Figure S13: MS/MS spectra of 607.5677 Da in blue powder, Figure S14: LDI-MS spectra of the blue powder in negative ion mode (zoomed range 250–270 Da; lock-mass correction using PbO_2H^- clusters), Figure S15: LDI-MS spectra of the blue powder in negative ion mode (zoomed range 280–290 Da; lock-mass correction using PbO_2H^- clusters).

Author Contributions: Conceptualisation, L.K., K.J. and P.F.; methodology, L.K., K.J., R.P., J.N., P.B., J.K. and T.Z.; data curation, L.K., M.M., J.K. and P.B.; investigation, K.J., M.M., L.K. and P.F.; resources, P.F.; writing—original draft preparation, L.K., M.M. and K.J.; writing—review and editing, O.K. and L.R.; visualisation, K.J., R.P. and L.K.; supervision, L.K. and P.B.; All authors have read and agreed to the published version of the manuscript.

Funding: This research was funded by ERDF/ESF (No. CZ.02.1.01/0.0/0.0/17_048/0007378) and Palacký University (IGA_PrF_2022_023).

Institutional Review Board Statement: Not applicable.

Informed Consent Statement: Not applicable.

Data Availability Statement: The data presented in this study are available on request from the corresponding author. The data are not publicly available due to the privacy policy of the author's institution.

Acknowledgments: This publication was supported by the project ERDF/ESF “Arteca: Advanced physical-chemical methods of research and protection of cultural and artistic heritage” (No. CZ.02.1.01/0.0/0.0/17_048/0007378) and by the Institutional Project of the Palacký University (IGA_PrF_2022_023).

Conflicts of Interest: The authors declare no conflict of interest.

References

1. Bajnóczi, B.; Nagy, G.; Tóth, M.; Ringer, I.; Ridovics, A. Archaeometric characterization of 17th century tin-glazed Anabaptist (Hutterite) faience artefacts from North-East-Hungary. *J. Archaeol. Sci.* **2014**, *45*, 1–14. [CrossRef]
2. Ma, H.; Henderson, J.; Evans, J. The exploration of Sr isotopic analysis applied to Chinese glazes: Part two. *Archaeometry* **2016**, *58*, 68–80. [CrossRef]
3. Tite, M.S.; Shortland, A.J.; Schibille, N.; Degryse, P. New data on the soda flux used in the production of Iznik glazes and Byzantine glasses. *Archaeometry* **2016**, *58*, 57–67. [CrossRef]
4. Bouquillon, A.; Castaing, J.; Barbe, F.; Paine, S.R.; Christman, B.; Crépin-Leblond, T.; Heuer, A.H. Lead-glazed rustiques figulines (rustic ceramics) of Bernard Palissy (1510–90) and his followers. *Archaeometry* **2017**, *59*, 69–83. [CrossRef]
5. Bouquillon, A.; Castaing, J.; Barbe, F.; Crepin-Leblond, T.; Tilliard, T.; Paine, S.R.; Christman, B.; Heuer, A.H. French decorative ceramics mass-produced during and after the 17th century: Chemical analyses of the glazes. *Archaeometry* **2018**, *60*, 946–965. [CrossRef]

6. Shen, J.Y.; Henderson, J.; Evans, J.; Chenery, S.; Zhao, F.Y. A study of the glazing techniques and provenances of Tang Sancai glazes using elemental and lead isotope analyses. *Archaeometry* **2019**, *61*, 358–373. [[CrossRef](#)]
7. Shen, J.Y.; Ma, H.; Henderson, J.; Evans, J.; Chenery, S.; Wang, F.; Wen, R. Chemical and strontium isotope analysis of Yaozhou celadon glaze. *Archaeometry* **2019**, *61*, 1039–1052. [[CrossRef](#)]
8. Ma, H.; Wood, N.; Doherty, C.; Zheng, J.; Zhou, G.; Duan, H. New insights into the calcium flux used in ancient Longquan and Yue kilns based on strontium isotopic compositions. *Archaeometry* **2019**, *61*, 342–357. [[CrossRef](#)]
9. Zhou, X.Q.; Cui, J.F.; Ren, X.Y.; Wang, Q.Q.; Du, W.; Du, Z.W.; Liu, X.Y. The earliest high-fired glazed ceramic in China: Evidence from a glazed ceramic sample from the Lajia site, Qinghai province. *Archaeometry* **2019**, *61*, 588–599. [[CrossRef](#)]
10. Ting, C.; Lichtenberger, A.; Raja, R. The technology and production of glazed ceramics from Middle Islamic Jerash, Jordan. *Archaeometry* **2019**, *61*, 1296–1312. [[CrossRef](#)]
11. Mangone, A.; De Benedetto, G.; Fico, D.; Giannossa, L.; Laviano, R.; Sabbatini, L.; van der Werf, I.; Traini, A. A multianalytical study of archaeological faience from the Vesuvian area as a valid tool to investigate provenance and technological features. *New J. Chem.* **2011**, *35*, 2860–2868. [[CrossRef](#)]
12. Neff, H. Analysis of Mesoamerican Plumbate Pottery Surfaces by Laser Ablation-Inductively Coupled Plasma-Mass Spectrometry (LA-ICP-MS). *J. Archaeol. Sci.* **2003**, *30*, 21–35. [[CrossRef](#)]
13. Tanasi, D.; Brunelli, D.; Cannavò, V.; Levi, S. Archaeometric characterization of prehistoric pottery from Baħrija, Malta. *J. Archaeol. Sci. Rep.* **2019**, *27*, 101938. [[CrossRef](#)]
14. Medeghini, L.; Fayek, M.; Mignardi, S.; Coletti, F.; Contino, A.; De Vito, C. A provenance study of Roman lead-glazed ceramics using lead isotopes and secondary ion mass spectrometry (SIMS). *Microchem. J.* **2020**, *154*, 104519. [[CrossRef](#)]
15. Kuzmanovic, M.; Stancalie, A.; Milovanovic, D.; Staicu, A.; Damjanovic-Vasilic, L.; Rankovic, D.; Savovic, J. Analysis of lead-based archaeological pottery glazes by laser induced breakdown spectroscopy. *Opt. Laser Technol.* **2021**, *134*, 106599. [[CrossRef](#)]
16. Spataro, M.; Mommsen, H.; Villing, A. Making pottery in the Nile Delta: Ceramic provenance and technology at Naukratis, 6th–3rd centuries BC. *Archaeol. Anthropol. Sci.* **2019**, *11*, 1059–1087. [[CrossRef](#)]
17. Wang, Y.; Yu, S.; Tong, M.; Wang, W.; Yang, X. Deciphering the formation mechanism of ancient Jun wares copper red and blue glazes. *J. Cult. Herit.* **2021**, *48*, 29–35. [[CrossRef](#)]
18. Toffolo, M.; Klein, E.; Elbaum, R.; Aja, A.; Master, D.; Boaretto, E. An early Iron Age assemblage of faience beads from Ashkelon, Israel: Chemical composition and manufacturing process. *J. Archaeol. Sci.* **2013**, *40*, 3626–3635. [[CrossRef](#)]
19. Marco de Lucas, M.C.; Moncada, F.; Rosen, J. Micro-Raman study of red decorations in French faïences of the 18th and 19th centuries. *J. Raman Spectrosc.* **2016**, *37*, 1154–1159. [[CrossRef](#)]
20. Zaremba, M.; Trzciniński, J.; Rogulska, M.; Kaproń, G.; Welc, F.; Południkiewicz, A. A Multiproxy Approach to the Reconstruction of an Ancient Manufacturing Technology: A Case Study of a Faience Ptolemaic Bowl from Tell Atrib (Nile Delta). *Minerals* **2020**, *10*, 785. [[CrossRef](#)]
21. Černohorský, K. *Moravská Lidová Keramika*, 1st ed.; J. Otto: Prague, Czech Republic, 1941; p. 284.
22. Gregerová, M.; Hložek, M.; Kuljovská, Z. Mikropetrografické a petrochemické rozborov novověké glazované keramiky z lokality Strachotín. *Geol. Výzk. Mor. Slez.* **2006**, *2007*, 95–100.
23. Fojtik, P. Prostějov (okr. Prostějov), fig. 47–50. *Přehl. Výzk.* **2017**, *58*, 243–244.
24. Dodd, A. *Dictionary of Ceramics*, 3rd ed.; The University Press: Cambridge, UK, 1994; p. 371.
25. Ebinu, A.I.; Olanrewaju, Y.A.; Ogolo, O.; Adetunji, A.R.; Onwualu, A.P. Barite as an industrial mineral in Nigeria: Occurrence, utilization, challenges and future prospects. *Heliyon* **2021**, *7*, e07365. [[CrossRef](#)]
26. Eastaugh, N.; Walsh, V.; Chaplin, T.; Siddall, R. *The Pigment Compendium: A Dictionary and Optical Microscopy of Historical Pigments*, 1st ed.; Elsevier: Amsterdam, The Netherlands, 2004; p. 499.
27. Vodičková, N. Taxonomic and Individual Differentiation of Burned and Unburned Bones Using X-ray Fluorescence (XRF). Diploma Thesis, University of West Bohemia, Plzeň, Czech Republic, 2017; p. 83.
28. Rasmussen, K.L.; Milner, G.R.; Delbey, T.; Ivalu Jensen, L.K.; Witte, F.; Rehren, T.; Kjaer, U.; Grindler-Hansen, P. Release of lead from Renaissance lead-glazed ceramics from southern Denmark and northern Germany: Implications from acetic acid etching experiments. *Herit. Sci.* **2022**, *10*, 63. [[CrossRef](#)]
29. Cartechini, L.; Miliani, C.; Nodari, L.; Rosi, F.; Tomasin, P. The chemistry of making color in art. *J. Cult. Herit.* **2021**, *50*, 188–210. [[CrossRef](#)]
30. Gliozzo, E. Pigments—Mercury-based red (cinnabar-vermilion) and white (calomel) and their degradation products. *Archaeol. Anthropol. Sci.* **2021**, *13*, 210. [[CrossRef](#)]
31. Colomban, P. Rocks as blue, green and black pigments/dyes of glazed pottery and enamelled glass artefacts: A review. *Eur. J. Mineral.* **2013**, *25*, 863–879. [[CrossRef](#)]
32. Freestone, I.C. Composition and microstructure of early opaque red glasses, early vitreous materials. *Br. Mus. Occas. Pap.* **1987**, *56*, 173–191.
33. Gedzevičiūtė, V.; Welter, N.; Schüssler, U.; Weiss, C. Chemical composition and colouring agents of Roman mosaic and millefiori glass, studied by electron microprobe analysis and Raman microspectroscopy. *Archaeol. Anthropol. Sci.* **2009**, *1*, 15–29. [[CrossRef](#)]
34. Reitner, J.; Thiel, V. *Encyclopedia of Geobiology*, 1st ed.; Springer: Berlin/Heidelberg, Germany, 2011; pp. 25–28.
35. Keeling, C.; Bohlmann, J. Diterpene resin acids in conifers. *Phytochemistry* **2006**, *67*, 2415–2423. [[CrossRef](#)]
36. Colombini, M.; Modugno, F. *Organic Mass Spectrometry in Art and Archaeology*, 1st ed.; Wiley: Oxford, UK, 2009; pp. 97–100.

37. Slánský, B. *Technika malby I. Díl, Malířský a conservační materiál*, 1st ed.; Státní Nakladatelství Krásné Literatury, Hudby a Umění: Prague, Czech Republic, 1953; p. 141.
38. Gu, Z.; Kenoyer, J.; Yang, Y. Investigation of ancient Harappan faience through LA-ICP-AES and SR- μ CT. *J. Instrum.* **2016**, *11*, C04001. [[CrossRef](#)]
39. Moretti, G.; Gervais, C. Raman spectroscopy of the photosensitive pigment Prussian blue. *J. Raman Spectrosc.* **2018**, *49*, 1198–1204. [[CrossRef](#)]
40. McEwen, C.; McKay, R.; Larsen, B. Analysis of Solids, Liquids, and Biological Tissues Using Solids Probe Introduction at Atmospheric Pressure on Commercial LC/MS Instruments. *Anal. Chem.* **2005**, *77*, 7826–7831. [[CrossRef](#)] [[PubMed](#)]
41. Pauk, V.; Havlíček, V.; Papoušková, B.; Sulovský, P.; Lemr, K. Simultaneous identification of historical pigments Prussian blue and indigo in paintings by electrospray mass spectrometry. *J. Mass Spec.* **2013**, *48*, 927–930. [[CrossRef](#)]
42. Fojt, B.; Hladíková, J.; Kalenda, F. Zlaté Hory ve Slezsku: Největší rudní revír v Jeseníkách, Část 2.: C. Geologie D. Mineralogie E. Geochemie stabilních izotopů. *Acta Mus. Morav. Sci. Geol.* **2001**, *86*, 3–58.
43. Sejkora, J.; Kouřimský, J. *Atlas Minerálů České a Slovenské Republiky*, 1st ed.; Academia: Prague, Czech Republic, 2005; p. 376.
44. Starý, J.; Kavina, P.; Vaněček, M.; Sitenský, I. *Surovinové Zdroje České Republiky: Nerostné Suroviny*; Ministerstvo Životního Prostředí & Česká Geologická Služba–Geofond: Prague, Czech Republic, 2005; p. 213.
45. Kunický, Z.; Vurm, K. *700 Let Hutnictví Stříbra a Olova na Příbramsku (1311–2011), 225 Let Stříbrné Hutě—Kovohutí Příbram (1786–2011): 700 Years Anniversary of Příbram's Metallurgy (1311–2011), 225 Years Anniversary of Silver Smelting Works—Kovohutě Příbram (1786–2011)*; Kovohutě Příbram: Příbram, Czech Republic, 2011; p. 212.

See discussions, stats, and author profiles for this publication at: <https://www.researchgate.net/publication/330080924>

Some Remarks on Amber Usage Tradition and Amber Provenance in the Interfluve of Nemunas and Daugava Rivers in the Migration Period

Article · January 2019

CITATIONS

7

READS

205

2 authors:



Audronė Bliujienė
Klaipėda University

54 PUBLICATIONS 234 CITATIONS

[SEE PROFILE](#)



Lukáš Kučera
Palacký University Olomouc

41 PUBLICATIONS 212 CITATIONS

[SEE PROFILE](#)

STUDIA
BARBARICA

STUDIA BARBARICA



PROFESOROWI ANDRZEJOWI KOKOWSKIEMU
W 65. ROCZNICĘ, URODZIN
FOR PROFESSOR ANDRZEJ KOKOWSKI
ON HIS 65TH BIRTHDAY

TOM I

REDAKCJA
BARBARA NIEZABITOWSKA-WISNIEWSKA
PIOTR FLUCZKIEWICZ
SYLWESTER SADOWSKI
MAGDA STASIAK-CYRAN
MICHAŁ ERDRICH



LUBLIN 2018



ARCHEOLOG TO NIE ZAWÓD – TO CHARAKTER
 ARCHAEOLOGIST IS AIL ABOUT CHARACTER, NOT CAREER

12	TABUJA GRATULATORIA	42	KACIWI ŻUREKA ZŁOTOWSKIE KORZENIE ZŁOTOW ROOTS
14	SUBIEKTYWNY WYBÓR FAKTÓW Z ŻYCIA I KARIERY NAUKOWEJ PROFESORA ANDRZEJA KOKOWSKIEGO REKĄ UCZNIÓW SPISANY, PRZEZ RODZINĘ ZAACEPTOWANY ORAZ BIEŻĄCO ILLUSTROWANY	48	ZORA KOWALCZUK-BUKOMONA TU, W ZŁOTOWIE, WSZYSTKIO SIĘ ZACZEŁO. EVERYTHING BEGAN HERE IN ZŁOTOW.
15	A SUBJECTIVE SELECTION OF FACTS FROM THE LIFE AND CAREER OF PROFESSOR ANDRZEJ KOKOWSKI, MADE BY HIS STUDENTS, ACCEPTED BY HIS FAMILY, AND RICHLY ILLUSTRATED	56	BIRUKIRAHÁ PRAC PROF. DR HAB. ANDRZEJA KOKOWSKIEGO – 100 ROKU 2017 BIRUKIRAHÁ OF PROF. ANDRZEJ KOKOWSKI PUBLICATIONS – 100. 2017
		64	TACHELUSZ WISNIEWSKI JAMAMUT 102 – KRÓTKA HISTORIA Z PROFESOREM ANDRZEJEM KOKOWSKIM W TLE "MAMMOTH 102" – A SHORT STORY WITH PROFESSOR ANDRZEJ KOKOWSKI IN THE BACKGROUND
		68	ANNA HUCHNIA, Bartłomiej Bauritok WREKAD PROF. ANDRZEJA KOKOWSKIEGO W BADANIA NAD NEOLITEM, EPOKĄ BRĄZU ORAZ WCZESNĄ I ŚRODKOWĄ EPOKĄ ŻELAZA THE REVELATION OF PROFESSOR ANDRZEJ KOKOWSKI TO THE STUDY OF THE NEOLITHIC, THE BRONZE AGE, AND EARLY AND MIDDLE IRON AGE
		86	MAREK FIŁCZYK SŁÓW KIŁKA O ANDRZEJA KOKOWSKIEGO ZAANGAŻOWANIU W BADANIA NAD WCZESNĄ ŚREDNIOWIECZEM I ICH POPULARYZACJĄ A FEW WORDS ABOUT ANDRZEJ KOKOWSKI'S INVOLVEMENT IN THE RESEARCH ON EARLY MIDDLE AGES AND ITS POPULARIZATION
		102	JOY KAKOSZKON MOI TRZYDZIEŚTY PIERWSZY POWOŁO DO DUMY Z MIESZKANIA W KRAINIE GOTÓW MY THIRTY FIRST REASON TO BE PROUD OF DWING IN THE LAND OF GOTHES
		106	TOMASZ ŻYMC MY Z KRAINY GOTÓW US FROM THE LAND OF GOTHES
		110	PIETRI LIGORZINSKI LUDZIE, LUDZIE, JAK TEN CZAS LEG, TO NIE DO WIARY WPROST. PEOPAN, PEOPAN, FOLK, THE TIME FLIES IT'S SURELY UNBELIEVABLE.
		114	ANNA HUCHNIA, Bartłomiej Bauritok HRUBESZÓW: OPowieść O MAŁYM MUZEUM – WSPÓTRACA PROFESORA ANDRZEJA KOKOWSKIEGO Z HRUBESZÓWSKIM MUZEUM I WIOSKĄ GOTÓW W MASOWIECZU HRUBESZÓW: THE STORY ABOUT SMALL MUSEUM – COOPERATION BETWEEN PROFESSOR ANDRZEJ KOKOWSKI, MUSEUM IN HRUBESZÓW, AND GOTHS VILLAGE IN MASOWIECZ
		128	MARZELINA WYŻYŃSKA O SPOTKANIACH Z JUBILATEM W ROMISCH-GERMANISCHE KOMMISSION MENSCH ZUSAMMENHÖRREN MIT DER LUTLAS IN DER ROMISCH GERMANISCHEN KOMMISSION





KULTURA WIELBARSKA I GRUPA MASŁOMEŃKA WIELBARK CULTURE AND MASŁOMEŃCZ GROUP

- 138 ANNA STROBA, PIKARSKA STROBA
UWAGI NA TEMAT PRODUKCJI BRANSOLET TAŚMOWATYCH
I ZWIĄZEK A 95 ZDEBIONYCH FOJAMÓW Z METALI SZLACHTNYCH
NA PRZYKŁADZIE ZBIORYCH Z GROBU KULTURY WIELBARSKIEJ W BRZYMIE,
STAN 7, POW. PUCKI
- 138 VICTORIA STROBA, PIKARSKA STROBA
GOLD RINGS FROM PUPKI IN PODLASIE.
SOME REMARKS ON THE CONNECTIONS BETWEEN THE WIELBARK CULTURE
AND SCANDINAVIA AT THE CLOSE OF THE EARLY AND IN THE BEGINNINGS
OF THE LATE ROMAN PERIOD
- 188 DANIEL ZWIERSKI
W JAKIM CELU POWTÓRNIŃIE OTWIERANO GROBY NA CMENTARZYSKACH
LUDNOŚCI KULTURY WIELBARSKIEJ W WIELKOPOLSCE?
ROZWAŻANIA NA PODSTAWIE NEKROPOLI W KOWALEWKU,
POW. GIBORNIKI
- 202 OMERGAŁ C. MIWAŁIKIEWICZ, BOŻENA A. TRWAŁKA, OUBKIRITI BOUTIKK
ПОХОРОНЕННЯ РЕАБІЛІТАЦІЙНОЇ КВАЛІТАТИ БІЛІ
С. САНКЦІЯМИ НА ПІРЕННІЛІННІ
- 212 MICHAEL BRONCH
WHERE DOES THE BRONZE COME FROM?
- 222 JACZEK SZCZUBIAK, ANNA SZCZUBIAK, PAWEŁ DĘBICKI, BOŻENA KWATKOWSKA
KONDYCJA BIOLOGICZNA LUDNOŚCI POCHOWANEJ
NA CMENTARZYSKU W MASŁOMEŃCZU (II–IV W. N.E. – STAN. 15)

KULTURA PRZEWORSKA PRZEWORSK CULTURE

- 258 HAJNA DZIEDZIWIŃSKA
OSADNICTWO OKOLIC GIEBLIETOWA W OKRESIE RZYMSKIM
- 252 JEWANA ZACHARWA-TALISA
SYMBOLICZNY CZY CZĄSTKOWY? NIETYPOWY OBIEKT
Z CMENTARZYSKA KULTURY PRZEWORSKIEJ
W MICHAŁOWICACH, POW. KAZIMIERSKI
- 266 MARIA SIŚKAK-OBYDAN
GROB WOJOWNIKA Z BISKOWIC, POW. KRASNIKI
– NOWE DANE DO STUDIÓW NAD ROZWOJEM KULTURY PRZEWORSKIEJ
NA LUBELSZCZYZNIE
- 282 JACZEK SZCZUBIAK
ANALIZA ANTRPOLOGICZNA SZCZĄTKÓW KOSTNYCH
Z GŁĘBOKIEGO GROBU POPĘTNIWIEGO KULTURY PRZEWORSKIEJ
ODKRYTEGO W BISKOWICACH – GM. ANSOTÓL, POW. KRASNIKI
- 288 KATARZYNA CZARNECKA
ZAPORĘCZONY KOWAL – RECYCLING W KUŹNI.
CIEKAWY ZNALEZISKO OKOLIC SKRZYŃKI
Z CMENTARZYSKA KULTURY PRZEWORSKIEJ W GARGOŁINIE
- 296 ANNA LABOW-KUS, RENATA MAJTYMA-SZULCJO
ŻELCIE „WIESZADEŁKA” Z OKRESU RZYMSKIEGO Z CMENTARZYSKA W GAŁC,
POW. PRZEWORSKI
- 308 JEWANA DZIEDZIWIŃSKA-CZEPIK, SIEWESTER CZEPIK
DWA OBIEKTY Z TZW. CERAMIKĄ PSEUDOŚREDNIOWIECZNA
ZE STANOWISKA NR 9 W ZAMOJSKACH, POW. JAROSŁAWSKI



BAŁTOWIE
THE BALTS

322	WIKTICH NAJWIKSZE EINE VERGESSENE FUNDKATEGORIE: EISERNE HUFEISENFIBELN DER RÖMISCHEN KAISERZEIT AUS MASLZEN
332	BEPIECZKOŃCZYŃCWA LEWAĆ PIERWSZA OSTRZĄ ZŁOŻONA POLAMI EWAMI Z ZIEMI POLSKICH, ALBO O RĄDZIŚCIE PRZYŃCĄCĄJ Z BYGŁA, ARCHEOLOGICZEM
354	TERESA ŚWIAŁCZAK BADANIA TECHNOLOGICZNE OSTRZĄI EMALOWANEJ Z JANÓWKA PROBA OKREŚLENIA WZHOJZENIA
364	DAŠA BAIGIŖE-ROZELL GLASS BEADS OF THE CALATIS TYPE IN WEST LITHUANIAN CEMETERIES
380	MIRSKAWI RUDNICKI, NICHAIKINA SMORTSOVA NOWE ZNALEZISKO ZAPISKI CYKADRYWATEJ Z TERENU POBYWYSPU SĄWBIJSKIEGO
392	AUDRONSĖ BUIŠIENĖ, LUKAS KLČBA SOME REMARKS ON AMBER USAGE TRADITION AND AMBER PROVENANCE IN THE INTERFLUVE OF NEMUNAS AND DAUGAVA RIVERS IN THE MIGRATION PERIOD

EUROPA WSCHODNIA
EASTERN EUROPE

410	194 O-HOCHZWEISER JEDEN TZEIEN Z ZVGA... W KOSZARACH BEVA FOUL SEVERAL REMARKS ON METAL BRACELETS FROM CHILD GRAVES OF THE LATE SCYTHIAN CULTURE
442	ŁUKAS KRUPNIK, ANASTASIA STOWSIKA FIBULAE IN THE CEMETERY OF NEJZAC ALEKSANDR LABAREK, ELŻAŻA A. HARTLIKOWA EIN NEUER GOTISCHER FUNDKOMPLEX AUS DEM GRÄBERFELD VON DORF LUCISTOE
456	ROSTISLAW TERLUKOWSKI, CEYLANOVI ZHAROVA WEAPONS OF THE MUTIN WARRIOR CEMETERY BORIS MACHOULOV RING-SHAPED PENDANTS 'WITH DUCKS' OF CHERNYAKHOV CULTURE
480	MICHAEL V. LEIBERTZ, FRANKFURT-SCHULZTE ZU EINER GRUPPE UNGEWÖHNLICHER GRÄBERFELDER DER ČERNJACHOV-KULTUR
492	O. V. PETRUSKAS GLASBECHER VOM TYP EGERS 230 IN DER ČERNJACHOV-KULTUR ZUR RELATIVEN CHRONOLOGIE
502	OLEGA GORIKOVA DOUBLE-PLATE FIBULA FROM A WARRIOR'S GRAVE OF THE ČERNYAKHOV – SÄNTANA-DE-MUREŞ CULTURE CEMETERY IN KOMANIČI: A MAN'S BROOCH WHICH GAVE RISE TO A WOMEN'S FASHION OR A WOMAN'S GIFT?
512	СВЕТЛА ТРАКЦІЎ ЛЫСКО-ДАТЕЦКАЯ ПУТІЦА ПАМІТНІКОВ ФІНАВА ЧЕРНЬКОЎСКОЙ КУЛЬТУРЫ. В ВЕРХОВЬЯХ П. СЕРПІ (КВІЦКАЎ ОБА, ПОВІСЦІЎ)
536	НІКОЉА ДИВІЉАЦКА, АНЖЕЉА РУКЧІЉОВ УКРЕПЕЊЕ ПЕМЕННЕ НАКОЉЕЧКА КІ ЦІЉЕЉО ДАЉІ КРЕПЉЕНІЯ, БІТОВЕДІЉШЕ ВО 2–3 БЕКАХ НА БІЉТОКЕ ЕВРОПЫ
564	ANASTASIA M. OBOLENSKIJA О ЗАХІСЦІХ КУВАКАХ УКРАЇНЕНІЯ С БІБІМІНТОЇЇ ЭМАЉАНО БІЉТОКЕВІЉНОЇСКОЇ СТУЇЯ ІАЉІ П. АМЕРІКАЇ
570	СВЕТЛА ТРАКЦІЎ ЛЫСКО-ДАТЕЦКАЯ ПУТІЦА ПАМІТНІКОВ ФІНАВА ЧЕРНЬКОЎСКОЙ КУЛЬТУРЫ. В ВЕРХОВЬЯХ П. СЕРПІ (КВІЦКАЎ ОБА, ПОВІСЦІЎ)
570	НІКОЉА ДИВІЉАЦКА, АНЖЕЉА РУКЧІЉОВ УКРЕПЕЊЕ ПЕМЕННЕ НАКОЉЕЧКА КІ ЦІЉЕЉО ДАЉІ КРЕПЉЕНІЯ, БІТОВЕДІЉШЕ ВО 2–3 БЕКАХ НА БІЉТОКЕ ЕВРОПЫ
592	ANASTASIA M. OBOLENSKIJA О ЗАХІСЦІХ КУВАКАХ УКРАЇНЕНІЯ С БІБІМІНТОЇЇ ЭМАЉАНО БІЉТОКЕВІЉНОЇСКОЇ СТУЇЯ ІАЉІ П. АМЕРІКАЇ
618	ANASTASIA M. OBOLENSKIJA О ЗАХІСЦІХ КУВАКАХ УКРАЇНЕНІЯ С БІБІМІНТОЇЇ ЭМАЉАНО БІЉТОКЕВІЉНОЇСКОЇ СТУЇЯ ІАЉІ П. АМЕРІКАЇ
648	ANASTASIA M. OBOLENSKIJA О ЗАХІСЦІХ КУВАКАХ УКРАЇНЕНІЯ С БІБІМІНТОЇЇ ЭМАЉАНО БІЉТОКЕВІЉНОЇСКОЇ СТУЇЯ ІАЉІ П. АМЕРІКАЇ
670	ANASTASIA M. OBOLENSKIJA О ЗАХІСЦІХ КУВАКАХ УКРАЇНЕНІЯ С БІБІМІНТОЇЇ ЭМАЉАНО БІЉТОКЕВІЉНОЇСКОЇ СТУЇЯ ІАЉІ П. АМЕРІКАЇ
680	NOTA OD REDAKCJI / A NOTE FROM THE EDITORS
681	WYKAZ SKRÓTÓW / ABBREVIATIONS





AUDRONE BLIJIJENE,
LUKAS KUČERA

SOME REMARKS ON AMBER USAGE TRADITION AND AMBER PROVENANCE IN THE INTERFLUVE OF NEMUNAS AND DAUGAVA RIVERS IN THE MIGRATION PERIOD

Audrone Blujene
Kaipeda University
Institute of the Balts, Sea Region History and Archaeology
Hersloko Miesto Street 84
LT-82004 Kaipėda
audrone.blujene@gmail.com

Lukas Kučera
Regional Centre of Advanced Technologies and Materials
Department of Analytical Chemistry, Faculty of Science
Palačků University in Olomouc
Č. 779 00, Olomouc
lukas.kucera@upol.cz

of Emperor Nero (*Nero Claudius Drusus Germanicus*, 54–68) around year 60–61/62. The amber wearing tradition did not change at the end of the 1st century AD, as briefly described by Publius Cornelius Tacitus (55/58–116/120) around the year 98 in his book *De origine et situ Germanorum* (Concerning the Origin and Situation of the Germans) commonly referred as *Germanica*. (Tacitus § 45). Furthermore, for Tacitus description of amber or *glaesum* (*glacsum*) formation, its quality and gathering manner was the reason to mention amber gatherers – the *Aestiorum* gentes. Nowadays researchers often link Aestii with the western Balts or the inhabitants of the southern and eastern Baltic regions. Tacitus wrote that Aestii did not use amber for themselves, they just gathered crude amber, passed it on unworked, and they were astonished at the price they got for it (Tacitus § 45). Until the end of the 2nd century AD, only seventeen sites (cemeteteries, hill-forts and settlements) with single amber artefacts are known in Lithuania from this period. Amber in graves and habitation sites slowly begins to increase in the interfluvium between Ne-

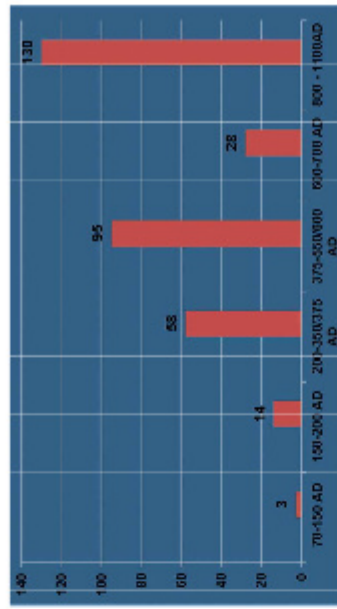


Fig. 1. Number of the artefacts (conspicuous, non-theriacal and bifurcated) containing amber. After: A. Blujene 2016, Appendix B-C-E

INTRODUCTION

Enormous changes in the territory between the Nemunas in the south and the Daugava in the north were already noticeable during the early Migration Period. The new evidence from recent research shows the changes in the inner settlement structure and network of settlements all over the territory of the Balts from the end of the 4th century AD to the beginning of the 5th century AD in the interfluvia of Nemunas and Daugava rivers (A. Blujene 2013, maps IV–VI).

The amber wearing tradition in the region between the Nemunas and Daugava rivers was under constant changes (Fig. 1). Amber artefacts are extremely rarely found in Lithuania and even in the entire eastern region with burial sites dated to the times of Pliny the Elder (*Genius Pinus Secundus* 33/24–79), when he in his great work *Natural History* (*Naturalis Historiae*) described specially to the southeaster Baltic Sea coast to bring amber back to Rome (Pliny, book XXVII, § 45). This mission was organized during the reign

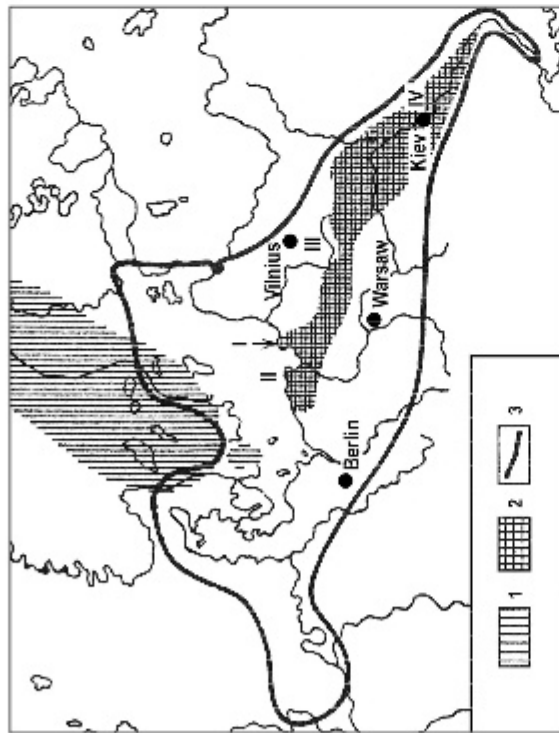
of Emperor Nero (*Nero Claudius Drusus Germanicus*, 54–68) around year 60–61/62. The amber wearing tradition did not change at the end of the 1st century AD, as briefly described by Publius Cornelius Tacitus (55/58–116/120) around the year 98 in his book *De origine et situ Germanorum* (Concerning the Origin and Situation of the Germans) commonly referred as *Germanica*. (Tacitus § 45). Furthermore, for Tacitus description of amber or *glaesum* (*glacsum*) formation, its quality and gathering manner was the reason to mention amber gatherers – the *Aestiorum* gentes. Nowadays researchers often link Aestii with the western Balts or the inhabitants of the southern and eastern Baltic regions. Tacitus wrote that Aestii did not use amber for themselves, they just gathered crude amber, passed it on unworked, and they were astonished at the price they got for it (Tacitus § 45). Until the end of the 2nd century AD, only seventeen sites (cemeteteries, hill-forts and settlements) with single amber artefacts are known in Lithuania from this period. Amber in graves and habitation sites slowly begins to increase in the interfluvium between Ne-

THE RAW AMBER SOURCES IN THE INTERFLUVE OF NEMUNAS AND DAUGAVA RIVERS AND EUROPE

Formation of Baltic amber begins tens of millions of years back in Fennoscandia or the southern regions of the present-day Scandinavia and nearby territories of the bed of the Baltic Sea (the formation of the Baltic Sea began only 13 thousand years ago), where subtropical pine (conifer) forests grew more than 55 million years ago. Due to the different processes and climate warming these pines produced excessive amounts of resin (today there is no one type of pine which had similar characteristics to those of the fossil trees). The resin dropped to the forest ground and then was embedded into the local sediments, compressed by the overlying deposits, and in time became fossilized (V. Katina 1971; B. Kosmowska-Czeramowicz 1996; W. Weitschat 2000; A. Grigelis 2001). The transformation of the resin into amber continued when it was re-deposited

into secondary sedimentary deposits together with rock material, gravel and sand from Fennoscandia, because Fennoscandia was drained by a river system called 'Eridanos', which flew into the Eocene Sea. The place of re-deposited amber coincides with the present day Bay of Gdańsk and Sambian Peninsula (or Samland; now the Kaliningrad region of Russia). All these sediments were washed out and deposited as amber in flat sea sands or in the so-called 'blue earth', which is made up of maritime sediments from the Eocene and Oligocene Epochs. But the area of distribution of amber bearing sediments is much larger than the Bay of Gdańsk and the Sambian Peninsula (Fig. 2). In this regard, there are some differences in the age of amber bearing sediments (N. P. Lukashina, G. S. Kharin 1999, 29–30, Tab. 1).

■ Fig. 2. Area of the distribution of Baltic amber-bearing sediments:
 1 - primary amber deposits in Fennoscandia; 2 - amber from Eocene deposits; 3 - boundary of distribution of re-deposited amber.
 P - Sambia Kaliningrad oblast, Russian amber sites; C - Chłapowo Plesko, Baltic; B - Gornio (Belarus) site; F - Obolovno-Osare (Ukraine) site. Areas indicate Symbian Peninsula. Map redrawn after V. Katina, 1976, fig. 12.



The biggest known Baltic amber-bearing layers are still in the northwestern part of the Sambia Peninsula near Jantarny (in Kaliningrad region; formerly *Pravenskoen* in Eastern Prussia) (Fig. 2). One cubic meter of 'blue earth' contains from 0.5 to 2.5 kilograms per $1m^3$ (A. Grigelis 2001, 39). These amber bearing sediments belong to the Aestii or people of the Dollkeim-Kovrovo Culture in the Roman and Migration Periods. Drifted amber transported by sea currents and amber from waterlogged lagoons, was and still is available on the Lithuanian and southwestern Latvian coasts. In Lithuania amber is also found in the northern part of Curonian Lagoon. The amber was brought and deposited here in Holocene when in time of Littorina Sea (the stage of formation of the Baltic Sea) the islands of Curonian Spit were being formed (V. Katina 1971, fig. 13; A. Grigelis 2001, fig. 1, 4B).

The amber was collected in the Vistula Spit, the Vistula Delta and Gdansk Bay (B. Kosmowski-Ceranasowicz, T. Pietrzak 1985, fig. 6) and was

retrieved in especially large quantities in the Lower Zulawy at the late Neolithic Period. In northeastern Poland, amber was scooped up in the lakes by the people of the Bogaczewo culture and later on by the Oleztyń Group people (A. Bitner-Wroblewska 2000, 155). Nowadays, amber is mined using hydraulic-extraction methods in the Żuławy Gdańskie (T. Pietrzak 2002, 14).

The re-deposited amber, occurs naturally at the Frisian Islands in the southwest to the Gulf of Riga and Saaremaa island in the northeast. Succinite may also be found on inland sites in Poland (in the valley of the Narew and the Western Bug Rivers, and the region of the Mazurian Lakes), Germany (deposits in Bitterfeld, near Halle) as well as in southwestern Ukraine and western Belarus (V. Katina 1971, 140–145, fig. 13; W. Weitschat 2000, 24–46; M. Ols 2012, 47–56, fig. 1; V. M. Matsui, E. P. Belichenko 2011, 49–51).

This short overview of the Baltic amber (succinate) spread clearly indicates, that the Aestii or

western Balts had raw amber sources of distinctive wealth in the vast area of the Baltic amber distribution. Certainly, the geographical position of each ethnocultural group in the West Baltic world give distinctive access to the raw amber

sources. Ipsa facta distinctive wealth of amber source determined different traditions of amber usage, possibilities merchandise in regional and long-distance exchange in raw amber and ready-made artefacts.

NEW APPROACH TO DETERMINING THE AMBER ORIGIN FROM THE PROVENANCE OF THE BALTIC AMBER (SUCCINATE) SOURCES

The Baltic amber can be simply described as organic material containing roughly 80% of carbon, 10% of oxygen and 10% of hydrogen. Amber contains also traces of other elements, such as copper, iron, sodium, calcium, manganese, vanadium, lead, aluminium, nitrogen and sulphur (K. B. Anderson, R. E. Witans 1991; S. Z. Chen, D. B. Lu 2006). During recent years, a lot of analytical techniques have been used for the characterization of chemical composition of amber to determine its origin. Among them Raman spectroscopy, X-ray diffraction, scanning electron microscopy, gas chromatography-mass spectrometry and liquid chromatography-mass spectrometry are the most frequent (P. Vandenberghe 2003; A. Matyszewska, M. Czaja 2002; I. Pakutinskienė 2007; J. T. Senfale, S. R. Larter 1988; G. I. Traiack 2012; M. Havelcova 2016). Perhaps the most popular method for determination of amber origin is infrared spectroscopy (IR). It was suggested to allow an estimation whether an amber belongs to vicinity of Baltic Sea or not (presence of so called 'Baltic shoulder'; 1100–1250 cm^{-1}) (C. W. Beck 1964). Although this technique gives possibility to discern Baltic amber from other fossil resins, but it does not allow a further (geographical) classification of amber samples.

The ability of IR spectroscopy to distinguish among ambers found on Lithuanian coast, scooped in Mazurian Lakes region and other Baltic seacoast regions is very limited. The discrimination of non-Baltic ambers can be sometimes misleading due to the presence of small amount of succinic acid in them, e.g. gedanite (E. C. Steut 1995), romanite (I. D. van der Werf 2014) and goettschite (S. Yamamoto 2006). A pine resin has achieved a stiff state through oxidation, action

of micro-organisms and fossilization processes. Additionally, resin of pine trees was exposed to different temperature and weather conditions. It resulted in a variety of its chemical and physical properties depending on its chemical composition. Small but characteristic variations in chemical composition (profile of particular chemical compounds present in amber) can help to distinguish the origin of amber. For a more detailed chemical characterization of amber a new method was designed in laboratory of Department of Analytical chemistry, Palacký University in Olomouc, Czech Republic. It is based on Laser Desorption/Ionization High Resolution Tandem Mass Spectrometry (LDI-MS) combined with multivariate statistics (i.e. principal component analysis, PCA) orthogonally projection to latent structure discriminant analysis, OPLS-DA. Although LDI-MS is a destructive analytical technique, the required amount of amber sample for analysis by LDI-MS is lower than a head of a conventional pin (about 4 mg). The principle of LDI-MS method is desorption/ionization of compounds from amber micro-sample using a pulsed laser and acceleration of ionized molecules to mass spectrometer where their mass (more precisely, mass to charge ratio, m/z) is measured. The obtained mass spectrum of amber contains thousands of signals due to huge number of present (ionisable) compounds. Such a huge number of signals is not directly manageable and here benefit of advanced statistics is utilized. We have applied PCA to display what samples are similar from the chemical point of view (and would belong to a group of the same origin) and what samples differ significantly. Some features of the data are interpretable in relation to geographical distribution

of samples but a more detailed characterization of more amber samples is now in progress to understand in deep the relation between chemical

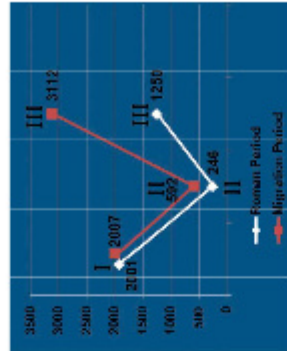
composition and amber formation circumstances and optimize the proposed method.

AMBER USAGE TRADITIONS IN THE MIGRATION PERIOD

The amount of amber artefacts and raw amber in graves increased significantly in Lithuania from the 5th to the first half of the 6th century AD compared with the Late Roman Period (Fig. 1, 3; Table 1). Besides this, amber beads spread all over Lithuania and in some parts of the southern Latvia. On the other hand, the analyses of Migration Period settlement structure show the partial decline of the cultural landscape and decrease in the number of sites and simultaneously of the population (A. Blujienė 2013, maps V–VI). At the beginning of Migration Period the climate became colder and primarily this factor might be the reason of previous settlement structure transformation. At 536–537 AD a short-term and sudden cooling of the climate was observed in the northern hemisphere after volcanic eruption. Archaeological, dendrochronological and pollen data reveal that this event caused crop failure and demographic catastrophe (M. Axboe 2001, 129–135, fig. 3; B. E. Berglund 2003, 9–10, fig. 1; P. Lagerås 2013, 82, fig. 4; A. Tvaari 2014,

beads, silver as a raw metal, and ornaments produced from this precious metal (L. Vaitkušienė 1981, Table 1; A. Astrauskas 1998, 21, Table 34; V. Šimėnas 2006, 93–95; A. Blujienė 2013, 556–561, fig. 386). The biggest portion of the archaeological sites with amber cluster are linked to the different routes of access to the territory of Lithuania in four main areas (Fig. 4I–IV). If we compare the amber wearing tradition during the Roman and Migration Period, it can be seen that if we have approximately the same amount of researched graves of both periods. The number of graves containing amber increased 2–4 times and the number of amber beads in graves by 2–5 times in the Migration Period (Fig. 3; Table 1). In the Roman Period the biggest amount of amber artefacts is known from the western part of Lithuania, and in the Migration Period it is known from the region of Nemunas River

Fig. 3. Comparison of the amount of amber artefacts found in the Roman Period burial sites and graves and total sites and graves of the Migration Period I – total amount of researched graves; II – graves containing amber; III – total amount of amber in graves. After: Blujienė 2013, Table 2, for data see Table 1.



delta sites, and even Eastern Lithuania. In both regions, the Migration Period graves contained the longest and most fashionable necklaces strung from several to 60 and more amber beads (Fig. 4II–III; 5:4–7; Table 1). The new concentration of amber artefacts could be seen in Eastern

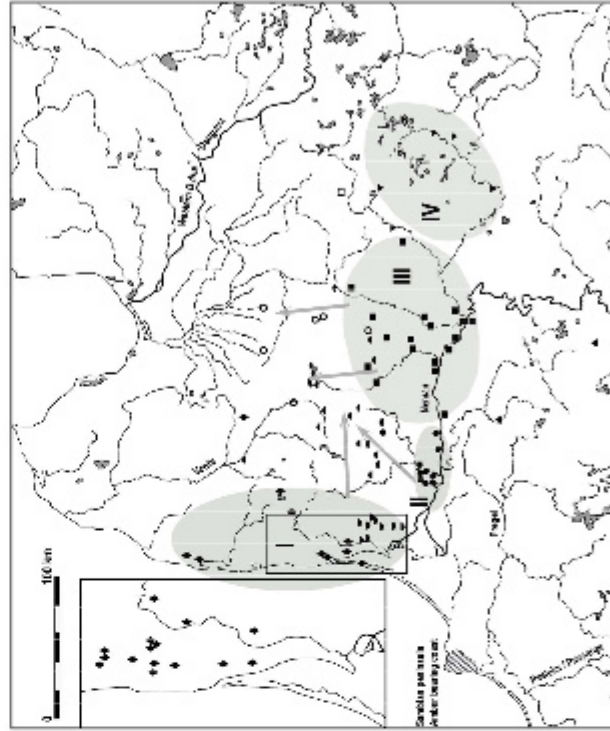


Fig. 4. Spread of amber artefacts in Lithuania and southwestern Latvia from the 5th to the first half of the 6th century and amber concentration in Lithuania. I – Lithuanian and southwestern Latvia coast; II – the Nemunas delta; III – Central Lithuania; IV – Eastern Lithuania. After: A. Blujienė 2013, fig. 67, with current additions.

Table 1. Approximate quantity of amber artefacts in the more comprehensively researched cemeteries dated from the end of the 2nd century AD to the first half of the 6th century AD (A. Blujienė 2013, Appendix B, Table 2).

Region in Lithuania	Number of cemeteries	Total number of researched graves	Number of graves containing amber artefacts	Total amount of amber artefacts
Roman Period				
Western Lithuania	24	548	142	802
Nemunas River delta region	6	208	52	175
Samogitia and Northern Lithuania	7	203	9	37
Central Lithuania	7	~1039	~40	~80
Eastern Lithuania	3	33	3	56
Migration Period				
Western Lithuania	9	411	122	469
Nemunas River delta region	4	108	76	691
Samogitia and Northern Lithuania	11	794	154	319
Central Lithuania	8	775	228	1369
Eastern Lithuania	6	58	12	264



Fig. 3. Migration Period amber artefacts found in Lithuania.
 1 – necklace of amber, glass and glass paste beads from Būdikiai (Švenčionys district, Eastern Lithuania);
 2 – beads from Užsėdai (Kretingė district, Western Lithuania);
 3 – necklace, strap finds; 4 – necklace from Žuikūnai (Vilnius district, Eastern Lithuania);
 5 – beads from grave 1-45 – necklaces from Vidugalių (Šilutė district, the Nemunas river delta region);
 6-7 – necklaces from women's graves 51 and 21 found at the Hraikųgala cemetery (Klaipėda district, Central Lithuania);
 8 – pendant of natural amber lump from a woman's grave 64 at the Ulpūkiai cemetery; 9 – spindle whorl from a woman's grave; 10 – the Dyvilai cemetery (Majūpių district, Western Lithuania);
 11 – bracelet from Užsėdai (Kretingė district, Western Lithuania).
 After: V. Štremas 2000, fig. 38-47; A. Blujana 2005, fig. 95-98; Lithuanian National Museum, Department of Archaeology 48, 200, 101, 20, catalogue cards.⁴⁶

Table 2. List of amber samples analysed by LDMMS (developed by L. Kuzon).

Archaeological site	Coordinates (X,Y)	Context	Number (MLM)	Type of amber samples	Position in PCA score plot (LDMMS)
Ulpūkiai cemetery	X320933; Y0204138	grave 86	62010	biconical bead	n.d.
		stray find P_24	63271	step cut bead	n.d.
		grave 66	54897	raw amber	strip-mine
		horse grave 101	55033	pendant fragment	strip-mine
		grave 50	-	bead fragment	seacoast
		stray find P13	55148	step cut bead	strip-mine
		stray find P14	55164	raw amber	strip-mine
		stray find P30	62646	cylindrical bead	strip-mine
		stray find P19	62238	raw amber	seacoast
Rožonai-Zeigal settlement	X192054; Y0193078	stray find L207	P22196	raw amber	seacoast
		P1 Q1a-B-9	P22191/94	raw amber	seacoast
		P1 Q1E-1	P22191/75	raw amber	strip-mine
Būdikiai cemetery	X320956; Y0203350	grave 19	47743	biconical bead	seacoast
		cremation grave 36	47829	biconical bead	seacoast
		stray find P48	48031	conical bead	seacoast
		grave 87	48235	-	strip-mine
Vidugalių cemetery	X320685; Y0194304	grave 22	-	Ratovian type bead	strip-mine
		grave 14	32295	Ratovian type bead	n.d.
		grave 17	32786	biconical bead	n.d.
		grave 19	32818	biconical bead	seacoast
Janany strip-mine	-	strip-mine	-	raw amber	-
Juodkrantė	-	seacoast	-	raw amber	-

Lithuania (Fig. 41V; 51; Table 1). A few amber beads also appear in the grave assemblages from the region of the rivers Nevezis-Daugava and Jūra, the Samogitian (present-day ethnographic region of Lithuania). In Western Lithuania the amber usage tradition was different. The amber was

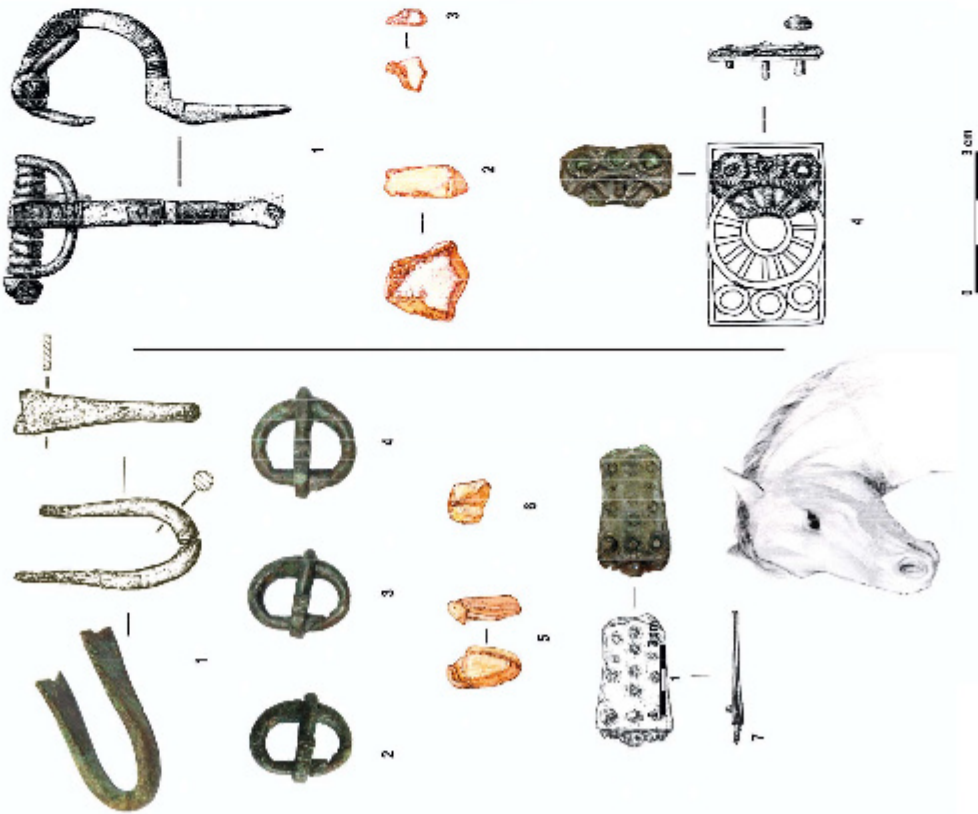
found not only in human graves, but sometimes raw amber pieces were placed into horse offerings (fitted horse parts, mostly head or head and legs) buried together with a human or separately (Fig. 6). In Western Lithuania, during the 5th century to the first half of the 6th century AD amber spindle whorls started to be found more often. Also the tradition of placing single raw amber bits noticeably increases. At Užpelkiai cemetery, in woman's grave 84 (the age of 30-40), a specially selected bit of raw amber with a natural

opening was found close to the woman's waist on the left side. It seems that a sash was attached through the opening creating a pendant (Fig. 55). The context of the find clearly shows that the amber bit was used as a pendant and as an apotropaic amulet.

The amber replaced beads of glass and other materials in a lot of cases. Glass beads in the Migration Period are found much more rarely than before (Fig. 56). Therefore, there was a flourishing period of the amber-wearing tradition in the 5th and the first half of the 6th century. Never before was amber worn on such a scale. It was the 'golden age' of amber.

It is impossible to answer the question if the amber found in the graves was a prestigious artefact, because amber value in a grave

Fig. 6. The early Migration Period cemetery in Užpelkiai (Kretinga district), near the road and horse-riding site from A. Blujienė's excavations in 1997. Drawing: Vydasius Tekelekas. Photos: A. Blujienė.



can be interpreted in the context of all the grave goods. Therefore, the quantity and quality of amber beads (e.g. lathe-turned, particular shaped beads) in combination with rare silver ornaments, weapon sets, other rare artefacts and horses could provide the information about the value of grave assemblages and indicate the social status (Fig. 6).

AMBER BEAD SPREAD AND POSSIBLE PLACES OF BEAD PRODUCTION

Amber from archaeological sites of the Western Lithuania and raw amber from the coast were analysed by LDI-MS. The list of studied samples is shown in Table 2.

The Fig. 7 shows the PCA Score Plot of two groups of archaeological samples and two groups of raw amber samples. The total segregation of raw amber samples from strip-mine (Palmnicken in former East Prussia in Sambian Peninsula, currently Kaliningraskaja oblast, Russian Federation) and sea-coast (Lithuania) can be seen in Fig. 7A. Certain distribution of these samples with respect to different localities can be observed mainly in the direction of the first component axis (first component explains 59.2% of variation in data; cumulative proportion of variance of first two principal component explain 82.1% of data). The archaeological amber samples Romai-Zeigiai settlement (in Kretinga district) distance from the sea coast 3.1 km, and distance from Jantarny mines about 123 km) and Baudužiai cemetery in Klaipėda city (distance from the sea coast 3.2 km, and distance from Jantarny mine about 115 km) are shown in Fig. 7B. From these preliminary results (PCA Score plots) we can suppose that all amber samples were not from only one location. The majority of studied amber samples from Romai-Zeigiai settlement is situated in PCA Score plot in region of sea-coast amber samples. Baudužiai cemetery amber samples are conversely placed in PCA region of strip-mine samples. In this case, it is necessary to count with other amber strip-mines than Jantarny (e.g. Lukstas Lake) and sea current from Sambia peninsula sea-coast (transport from Jantarny strip-mine). The amber samples from Užpelkiai cemetery in Kretinga region (distance to the sea coast 4.6 km, distance to the Jantarny strip-mine about 135 km; twenty samples of different types amber beads and raw amber was investigated) and Vidgirių cemetery in Pagėgių municipality (distance from the Lithuanian sea coast 50 km, and distance from Jantarny strip-mine about 120 km) are distributed throughout the chart area (data not shown) amber was used from more than one location (Ta-

ble 2). Three *Bassonia* type beads and one *Pseudonidulium* type bead were investigated. All studied beads fall into the PCA area of strip-mine region.

The *Bassonia* amber bead types (beads are named after their find-spot, not far from Lublin in Poland) makes up the biggest part of found beads in the region from the time-period 5th to the beginning of 6th century AD. Plenty of the *Bassonia* beads are known from the region of Nemunas River delta and Central Lithuanian cemeteries (Fig. 5:4–7). The *Bassonia* beads are varied in shapes, in their producing technology (semi-lathed and lathe-turned) and some of them are with incised linear decoration or deep grooves. These types of beads have been spread across Central Europe, the Middle Danube, the central Balkans, southern Scandinavia, Bornholm and Ohland islands, Pomerania, the Sambian Peninsula, and other sites of the Baltic lands (P. Włodowicki 1990, 101–133; R. V. Sidrys 1994: 35–37; fig. 6; A. Maatjykovs 2001, 342–358; fig. 1–9; V. Ivanušević *et alii* 2006, fig. 51: 58; 59; 62; 65; A. Blujienė 2011, 213–224). It is a pity that in most

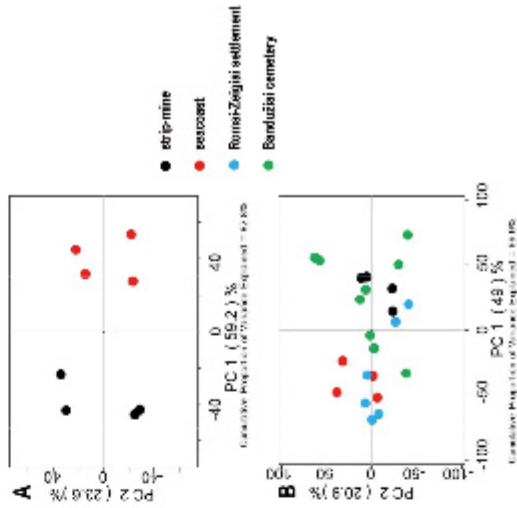


Fig. 7. The PCA score plot of raw amber samples from strip-mine and sea-coast (A) and archaeological amber samples from Romai-Zeigiai settlement and Baudužiai cemetery (B).



cases, for many reasons, it is not clear where certain amber beads were crafted. Semi-lathed and lathe-turned amber beads of the end of the Roman and Migration Periods might be imported from the amber workshops where the turning technology in manufacturing was known and certain mechanical devices, such as pottery wheel (lathe) or a device that move consistently in one direction was used. Technological research on the Wielbark culture's pottery showed that already by the second half of the 2nd century, wheel-made pottery was manufactured in local workshops (M. Natuniewicz-Szkuła, 2005, 58–67). However, in Lithuania, local wheel-made pottery appears much later, only in the 10th to 11th centuries (A. Bliujienė 2011, 92–93). In the second half of the 2nd century, the Wielbark culture amber craftsmen adopted the lathe technology from masters who had worked in the workshops of the Roman Empire (J. Wielewolski 1980, 178). At the beginning of the 3rd century AD, the lathe technology has been adopted by the amber craftsmen of the Dollkeim-Kovrovo culture. Obviously, the lathe was appropriated from the Wielbark culture, because at that time on the Sambian Peninsula several forms of lathed amber beads originate. In the amber workshops of the Przeworsk culture, semi-lathed and lathe-turned beads were crafted and the lathe was known from the second half of the 2nd century. The Przeworsk culture amber workshops (e.g. Konary, Swłocza and Jacewo site 4 in Poland) fell out of use in the middle of the 5th century AD (A. Cofia-Broniewska 1999, 178; A. Gruszczynska 1999, 183–188, fig. 6). Perhaps, a portion of the beads might be produced in workshops that might be operating in the territory of the Dollkeim-Kovrovo culture in Sambian Peninsula.

Even if very few the *Baionia* type beads were analysed by LDI-MS, some conclusions could be proposed. The ready-made beads come to Lithuania from Sambian Peninsula workshops or were produced somewhere in Europe. A confirmation or rejection of this hypothesis could be done after more comprehensive analyses of raw and ready-made beads. However, it seems, the perfectly lathe-turned step cut amber beads found

2011; A. Bliujienė *et alii* 2017). With time, a crisis of geopolitical system escalated and exchange networks collapsed. After the main part of crisis, only bi-conical, spherical hand-made semi-lathe turned amber beads are found in the interfluvial be-

tween the rivers Nemunas and Daugava. The single amber beads appear occasionally in burial assemblages dated between the late 6th and the 9th centuries AD.

CONCLUSIONS

There was a flourishing period in amber-wearing traditions in the region between the rivers Nemunas (Neman) and Daugava (Western Dvina) in the Migration Period, compared with the Roman Period. A lot of archaeological sites contain amber and many amber beads were deposited in graves. We suppose that the people who inhabited the interfluvial of Neman (Memel) and Daugava (Western Dvina) in the West of Lithuania owned raw amber sources in the Migration Period.

Amber artefacts from archaeological sites of Western Lithuania, raw amber from the seacoast and strip-mine were analysed by LDI-MS. From obtained results we can supposed, that amber was used from more than one location. It could be said that the amount of this commodity varies through the time in the region. The most popular lathe-turned and semi-lathe turned amber beads were characteristic to the early and first part of the Late Migration Period rather drastically disappeared from sites of eastern Baltic region between the first quarter of the 6th century to the mid. of the 6th century AD. This disappearance of amber from graves was connected with vanishing of silver ornaments.

ACKNOWLEDGEMENTS

The authors gratefully acknowledge the support of the Research Council of Lithuania (grant number LIP-1998/2016), the Czech Science Foundation (project 17-17346S) and Ministry of Education, Youth and Sports of the Czech Republic (project LO1305). We express our thanks to PhD Jonas

Stankus and PhD Valdemaras Simėnas for giving us the possibility to investigate amber beads from Bandžiūnai and Vėdgiriai cemeteries, and the Lithuanian Minor History Museum in Klaipėda, for providing amber samples for this study.

SOURCES

FLAN THE ELDER

1994. *National History*, Vol. X, Libri XXXVI–XXXVII. With an English Translation in Ten Volumes. Trans. E. D. Eichholz. London, Cambridge, Mass.

TACTILS

1979. *Germans*. In: *The Earliest Beginnings and the Land of the Germans*. Tacitus, in the volumes, vol. 1. Trans. M. Hutton, revised E. H. Warmington. Harvard University Press.

BIBLIOGRAPHY

- ANDERSON, K. B., WINDAS, R. E.
1994. *Nature and Fate of Natural Resins in the Geosphere*. *Evolution of Pyrolysis-Gas Chromatography Mass Spectrometry for the Analysis of Natural Resins and Resinites*, Anal Chem 65, 2021–2028.
- ASTRABODAS, A.
1998. *Merrys de benromerens (Il m. pasbaga - V. a.) Daktaro disertacija. Humanitariniai mokslai (Klasikos ir Istorijos)*. Vilnius, Lithuanian National Library, Department of Manuscripts, I. 322–736. Vilnius.
- AVRIE, M.
2001. *Amulet Pendant and Dorsalend Scar. On the Function of the Gold Breviaris and a Possible Motivation of the Large Gold Hoards*. In: B. Magyus (ed.), *Roman Gold and the Development of the Early Germanic Kingdoms. Aspects of technical, socio-political, socio-economic, artistic and intellectual development, A.D. 1–500 Symposium in Stockholm 14–16 November 1997*. Konferencijų su. Stockholm, 119–125.
- BECK, C. W., WILBER, E., MIRET, S.
1994. *Infrared Spectra and the Origin of Amber*. *Nature* 370, 18 January 1994, 267–267.
- BERGLUND, R. E.
2009. *Human Impact and Climate Changes synchronous and causal link?*. *Quaternary International* 195, 7–12.
- BURNARD, R. E.
2009. *Early Migration Period to the Macarurian Late Iron Age or Reality?* In: M. Măciuş, T. W. Grătară (eds.), *Die spätantische Kaiserzeit und die frühe Völkerwanderungszeit in Mittel- und Osteuropa*, Lidda, 131–147.
- BULJEVIC, A.
2001. *Northern Gold Amber in Lithuania (c. 200 to c. 700)*. In: F. Curtis (ed.), *East Central and Eastern*

- BLUJNE, A., CURIA, F.
2011. *Exotic Lands, Quasiotic Friends: Eastern Lithuania and the Carpathian Basin in Late Antiquity and the Early Middle Ages (ca. 380 to ca. 620)*. *Medieval Archaeology* 55, 29–46.
- BULJEVIC, A., STEVANIĆ, V., SEDIĆ, E., GRIZAN, G.
2017. *Concentration of Authority and Power in East Lithuania, between Tinnang Lake and the Middle Reaches of the Žemaitė River during the Migration Period*. *Journal of Estonian Archaeology* 11.2, 2017 in print (doi: 10.31063/jaech.2017.1).
- CHEN, S. Z., LI, D. B.
2006. *Starry sampling introduction with electothermal vaporization for multi-element analysis of amber by ICP-AES*. *Atom Spectroscopy* 27, 128–133.
- COCHRAN, B. G.
1999. *Amber in the material culture of the communities of the region of Kolaria during the Roman period*. In: B. Kosmowska-Ceranowska, H. Paner (eds.), *Investigations into Amber. Proceedings of the International Symposium, Baltic Amber and other Fossil Resins 1997 Upps Guldrens - 1997 Gdańsk 2-6 September 1997*. Gdańsk, 157–175.
- GRIGELIS, A.
2001. *Outline of Geology of Amber-Bearing Deposits in the Sakabala Province*. *Acta Academiae Artium Vilnensis* 24, 35–40.
- GRUCIŲNINKA, A.
1999. *Amber-workers of the fourth and fifth centuries AD from Smilga near Raseiniai*. In: B. Kosmowska-Ceranowska, H. Paner (eds.), *Investigations into Amber. Proceedings of the International Symposium, Baltic Amber and other Fossil Resins 1997 Upps Guldrens - 1997 Gdańsk 2-6 September 1997*. Gdańsk, 163–191.

(eds.), *International Connections of the Barbarians of the Carpathian Basin in the 4th century AD*. *Proceedings of the international conference held in 1999 in Assisi and Nyingshian*, Debrecen, 341–361.

MATUSZEWSKA, A., CZYJA, W.
2002. *Aromatic compounds in molecular phase of Baltic amber pyrolysis: fluorescence analysis*. *Talanta* 56, 1049–1059.

MCCURRY, M., BOUTIER, G., CAFFI, M. A., COOK, E. R., HOPPER, K., HUNTERS, P., LIU, T., MANNING, S. W., MANNING, F. A., MOORE, A. F. M., NICKLISCH, K., TEGEL, W.
2002. *Climate Change during and after the Roman Empire: Reconstructing the Peak from Scientific and Historical Evidence*. *Journal of Interdisciplinary History* XIII.2 (Autumn), 199–220.

MAZUR, V. M., BELCHENKO, E. P.
2011. *Mining, processing and trade in amber from Palaeolithic age till the Middle ages in the territory of russia-day/Ukraine*. In: Z. V. Korjajeva (ed.), *Trade routes of amber. Materials of the international Research and practice conference*, Kaliningrad, 2011, 45–54.

OTS, M.
2012. *The Significance of Deposits of Natural Amber in Estonia in the Context of Early Metal Age Society*. In: A. Blüggens (ed.), *People at the Crossroads of Space and Time (Footprints of Societies in Ancient Europe)*, Arch. Bohica 37.1, 46–59.

NATUKIEWICZ-SEREA, M.
2005. *Mazowskie wykopaliska przy ujściu kieda z cennymi - zabytkami kultury w Wieliczce kolo Elblaga*. *Prace i Sprawozdania Instytutu Archeologii i Etnologii Uniwersytetu Warszawskiego* 2, 38–47.

PHILIPSEN, I., KJERSFELD, J., KJERSFELD, P., SEVASTIANE, J., KAFERA, A.
2007. *Analytical characterization of Baltic amber by FTIR, XRD and SEM*. *The Canadian J Anal Sci Spectroscopy* 51, 297–304.

PETRAK, T.
2012. *Wielobismowe hurztywno na Krupach i w innych regionach Polski. Zdziedziczy i dawne kopie kopie i dziedziczy. Gd polska przez Krupie do Krupie*. In: Biblioteka kurpiowska im. Sieda Konwya 2, Lotka, 13–22.

QUEST, D.
2009. *Communication, Migration, Mobility and Trade. Exploratory Models for Exchange Processes from the Roman Iron Age to the Viking Age*. In: D. Quest (ed.), *Foreigners in Early Medieval Europe. Thematic Monographs BZGM 78*, 1–26.

HAWELDZA, M., MACHONIC, V., LINDAROVA, M., LADAK, L., PRICHISTAL, A., DVOŘAK, Z.
2006. *Vibrational spectroscopy with chromatographic methods in molecular analysis of Mesozoic amber inclusions (Czech Republic)*. *Microchimica* 1348, 152–166.

HANČEK, V., KAZANSKI, M., MASTYŃSKA, A.
2006. *Les nécrópolis de l'Antiquité et l'époque des Grandes Migrations*. Monographies. Centre de recherches historiques et d'histoire et civilisation de Byzance 24, Paris.

YAMAMOTO, S., OTTO, A., ERDARBEI, G., SIMONET, R. R. T.
2006. *The mineral-pyroclastic pyroclastic in volcanic and mineral-pyroclastic pyroclastic pyroclastic*. *Ber Palaebot Paläontol* 146, 47–49.

KARTUSI, V. (KOSTIHEC, B.)
1971. *Amber / Antarevossye otdelnoš Džnoj Próbital, In: Trudy, vyposk an. Upravleniya geologii pri Sovershenno Ministerstva Litovskio SSR, VII t.* *Amber in mineralogical and geochemical investigations of the Lithuanian Republic*. In: *Upravnenie resourc pri Centre minncipal. Antroclat. CCC, Buhavoc.*

KOSMOWSKA-CERANOWICZ, B.
1996. *Beustein - die Lagerstätte und ihre Entstehung*. In: M. Gamszowski, B. Stalla (eds.), *Beustein - Trümp der Götter. Katalog der Ausstellung des Deutschen Bergbau-Museum Bochum im Zusammenhang mit dem 60-jährigen Jubiläum des Museums Bochum*. Bochum, 61–68.

KOSMOWSKA-CERANOWICZ, B., PETRAK, T.
1985. *Z dziejów najnowszej wiedzy o znaleziskach iverztywno i ich prezentacji na przykładzie wykopu w wojewodztwie*. *Prace Muzeum Ziemi* 37, 47–60.

LADAR, P.
2005. *Medieval colonization and abandonment in the south Swedish uplands: a review of settlement and land use dynamics inferred from the pollen record*. *Arch. Bohica* 30, 77–90.

LUKASINA, N. P., RIJARD, G. S.
1999. *Criteria for the Recognition of the Prussian Silesia (Prussia and Prussian Horizon)*. In: B. Kosmowska-Ceranowska, H. Paner (eds.), *Investigations into Amber. Proceedings of the International Interdisciplinary Symposium, Baltic Amber and Other Fossil Resins 1997 Upps Guldrens - 1997 Gdańsk 2-6 September 1997*. Gdańsk, 37–43.

MASTYŃSKA, A. V.
2001. *Amber beads with incised linear decoration in the Great Migration Period*. In: V. Ivančević, V. Kulskir

- SEMPLE, J. T., LAWTER, S. R.
1988 *The geochemistry of caninera-1. Evaluation of spectral fluorescence of a series of modern resins and fossil resinsites*, Organic Geochemistry 13, 973–986.
- SIGRYS, R. V.
1994 *Gintaro įspėis senyvi ir višierinių geležies surišimas*, In: A. Auštinskas, M. Bertakis (eds.), *Vidurio Lietuvos archeologija. Etnoarcheologiniai tyrimai*, Vilnius, 28–46.
- SCOTT, E. C., BECK, C. W., KOBAYASHI-CODRANOVIC, B.
1995 *Gedantė and gedantė-sucrimė*, Acta Sym Ser 077, 130–148.
- ŠIMONAS, V.
2006 *Etnoarcheologiniai tyrimai Vakarų Lietuvoje pirmąją mūsų eros infliuzinimo uolūryje*, Vilnius.
- TRUČKÁ, G. L., TROCKO, E. D., LITERSKIJ, S. C., RAGU, G. L.
2013 *IC-MS and FT-IR characterization of amber artifacts*, Central European Journal of Chemistry 10, 1882–1889.
- TVALIB, A.
2014 *The impact of the climate catastrophe of 507–507 and in Estonia and neighbouring areas*, Journal of Estonian Archaeology 48.1, 30–46.
- VAMKASHEINÉ, L.
1995 *Šaldražių senovės Lietuvoje*, Vilnius.
- VANDERBEELE, P., CHIVALDIN, D. M., EDWARDS, H. G. M., MOENS, L.
2009 *Resin spectroscopy of different types of Mexican copal resins*, Spectrochimica Acta Part A: Molecular and Biomolecular Spectroscopy 59, 2221–2229.
- VAN DER WEGE, J. D., ARESTA, A., TRUČKÁ, G. L., RAGU, G. L., PALAMANGI, F., SABBATINI, I.
2014 *A quartz non-destructive approach for amber post-glacial provenience assessment based on broad space solid-phase microextraction gas chromatography-mass spectrometry*, Talanta 119, 485–498.
- WEISCHAT, W.
2000 *Die Elfenbein im Bernstein. Beitrag zum Infusionsverhalten der Dendroideen*, In: U. Eichson (ed.), *Bernsteinmuseum Ralswiek-Daunharden, Ralswiek-Daunharden*.
- WIELOWEJSKI, J.
1980 *Główny ciałek burzliwiny w ranach Coarctator Rzynowego, Wroclaw*.
- WIELOWEJSKI, P.
1990 *Skarb burzliwiny z podziemi obrzeży rezerwanego od 1979 w miejscowości Balamon, wś. Lalelelat, France*, Museum Ziemi 14, 101–103.





NOTA OD REDAKCJI

Przygotowując do druku dwutomową Księgę poświęconą Profesorowi Andrzejowi Kokowskiemu przyjęliśmy następujące zasady:

- łacińską transliterację cyrylicy zgodną z normą międzynarodową ISO 9 we wszystkich tekstach w językach polskim, angielskim i niemieckim
- w tekstach w językach polskim, angielskim i niemieckim nie transliterowano jedynie nazw własnych kultur, krain geograficznych i rzek pozostawiając zapis powszechnie stosowany w każdym z tych języków
- w tekstach w językach polskim, angielskim i niemieckim wszystkie cyryliczne pozycje bibliograficzne zapisano w postaci transliterowanej, umieszczając poniżej także zapis oryginalny
- w tekstach w językach polskim i rosyjskim nazwy jednostek administracyjnych Polski, Rosji i Ukrainy (np. powiatów, województw, rajonów, obłast) zapisano w formie przymiotnikowej, obowiązującej w tych krajach

A NOTE FROM THE EDITORS

When preparing this two-volume Festschrift for Professor Andrzej Kokowski we have adopted the following rules:

- Latin transliteration of the Cyrillic script following the international norm ISO 9 in all the texts in Polish, English and German
- in the Polish, English and German texts, only the proper names of cultures, geographical places and rivers were not transliterated, leaving the commonly used notation in each of the languages in question
- in the Polish, English and German texts all the Cyrillic bibliographical entries were transliterated, leaving the original notation below
- in the Polish and Russian texts, the names of administrative units of Poland, Russia and Ukraine (e.g. districts, voivodships, regions and oblasts) were written in the adjectival form which is in force in the respective countries

- w tekstach w językach angielskim i niemieckim, w tym w streszczeniach w tych językach, nazwy jednostek administracyjnych Polski, Rosji i Ukrainy zapisano w formie rzeczownikowej, podając także, najczęściej przy pierwszym użyciu, oryginalny zapis cyryliczny nazw rosyjskich i ukraińskich
- w tekstach w języku polskim nazwy jednostek administracyjnych Rosji i Ukrainy zapisano w formie rzeczownikowej, podając także, najczęściej przy pierwszym użyciu, oryginalny zapis cyryliczny
- w skróconym zapisie nazw państw, z małymi wyjątkami, zastosowano zalecany, dwuliterowy kod ISO (ISO 3166 alpha-2).

Oczywiście w uzasadnionych wypadkach pozwoliliśmy sobie na pewne odstępstwa od powyższych reguł.

Redakcja

WYKAZ SKRÓTÓW ABBREVIATIONS

- AA >> Acta Archaeologica
 AAC >> Acta Archaeologica Carpathica
 AarbKob >> Aarbøger for Nordisk Oldkyndighed og Historie
 AAustr >> Archaeologia Austriaca
 ActaArchHung >> Acta Archaeologica Academiae Scientiarum Hungaricae
 ActaPraehistA >> Acta Praehistorica et Archaeologica
 AIBB >> Archäologie in Berlin und Brandenburg
 AIHV >> Annales du Congrès de l'Association Internationale pour l'Histoire du Verre⁷, Liège
 AL >> Archaeologia Litwana
 APolski >> Archeologia Polski
 APŚ >> Archeologia Polski Środkowoschodni, Lublin
 Arbeitsber. Bodendenkmalpf. Brandenburg >> Arbeitsberichte zur Bodendenkmalpflege in Brandenburg
 ArbBerStsch >> Arbeits- und Forschungsberichte zur Sächsischen Bodendenkmalpflege
 ArchBaltica >> Archaeologia Baltica
 Arch. Korbl. >> Archäologisches Korrespondenzblatt
 ABozbl >> Archeologický Rozhledy
 BARIntSer >> British Archaeological Reports, International Series, Oxford
 Beiträge zu römischer und barbarischer Bewaffnung >> C. von Carnap-Bornheim (ed.), Beiträge zu römischer und barbarischer Bewaffnung in den ersten vier nachchristlichen Jahrhunderten. Akten des 2. Internationalen Kolloquiums in Marburg a. d. Lahn, 20. bis 24. Februar 1996. Veröffentlichungen des Vorgeschiedlichen Seminars Marburg, Sonderband 8, Marburg-Lublin 1994
 BERGG >> Bericht der Römisch-Germanischen Kommission
 FAZ >> Ethnographisch-Archäologische Zeitschrift

- Europa barbarica >> P. Luczkiewicz, M. Gładysz, Jucisiska, M. Juszcinski, B. Nierzbittowska, S. Sadowski (eds.), Europa barbarica. Czwarty wiek archeologii w Madrycie, Monumenta Studia Gothica IV, Lublin 2005
 FPP >> Folia Praehistorica Posnaniensia
 Gacrl i ich spisy >> W. Nowakowski (ed.), Gacrl i ich spisy na Pomorzu. Materiały z konferencji „Gacrl na Pomorzu Środkowym”, Koszalin 28–29 października 2005, Koszalinские Зeszyty Musealne, Seria A: Studia Archaeologica Pomorania II, Koszalin 2006
 HS >> Hersenskiej Sbornik / Херсонский Сbornik (=XC)
 100 Jahre Fibelformen >> I. Kunov (ed.), 100 Jahre Fibelformen nach Oscar Almgren, Internationaler Arbeitskongress 25.–28. Mai 1997 Kitzbühel, Land Brandenburg, Forschungen zur Archäologie im Land Brandenburg 5, Wernsdorf 1998
 IAK >> Investit Imperatoris Archeologische-Kommission / Историческое Исследовательское Комитет (=IAK)
 InvArch >> Inventaria Archaeologica, Polone
 JbRGZM >> Jahrbuch des Römisch-Germanischen Zentralmuseums Mainz
 Kontakt-Kooperation-Konflikt >> C. von Carnap-Bornheim (ed.), Kontakt – Kooperation – Konflikt. Internationales Kolloquium des Vorgeschiedlichen Seminars der Philipps-Universität Marburg, 22.–26. Februar 1996, Neumünster 2003
 Kontakty pomadregionalne... >> M. Fudziński, H. Paner (eds.), Kontakty pomadregionalne kultury wielbarzkiej, Przemiany kulturowe w okresie wpływów rzymskich na Pomorzu, Gdańsk 2015
 KSIA >> Krakkie sobiecia Instituta archeologii / Краккие сoбoеcia Иститута Археологического (=KSIA)

- Kultura bogactwa** ⇨ A. Bitner-Wroblewska (ed.), *Kultura bogactwa w 20 lat później. Materiały z konferencji*, Warszawa, 26–27 marca 2013, Seminarium Bałtyckie 1, Warszawa 2007
- Kultura wielborska** ⇨ J. Gurba, A. Kokowski (eds.), *Kultura wielborska w rafałowskim okresie rzymskim*, t. I 1988, II 1989, Lublin
- KZM** ⇨ Koszalińskie Zeszyty Muzealne
- LA** ⇨ Lietuvos archeologija
- MAIET** ⇨ *Материалы по археологии, истории и этнографии Таврии (= MAIET)*, под редакцией Тарана / *Материалы по археологии, истории и этнографии Таврии (= MAIET)*, Симферополь-Керчь / Симферополь-Керчь
- MANH** ⇨ Materiały Archeologiczne Nowej Huty
- MatArch** ⇨ Materiały Archeologiczne
- MIA** ⇨ *Материалы и исследования по археологии СССР (=MIA)*, Москва / *Материалы и исследования по археологии СССР (=MIA)*, Москва / *Материалы и исследования по археологии СССР (=MIA)*, Москва
- MonArch, Barbica** ⇨ Monumenta Archaeologica Barbica, Kraków-Warszawa
- Mon. Stud. Gothica** ⇨ A. Kokowski (ed.), Monumenta Studia Gothica, Lublin
- Mongraphien RGZM** ⇨ Monographien des Römisch-Germanischen Zentralmuseums, Mainz
- MSROA** ⇨ Materiały i Sprawozdania Rzeszowskiego Ośrodka Archeologicznego
- MS** ⇨ *Материалы Староżytне*, Warszawa
- MSW** ⇨ *Материалы Староżytне i Wczesноśrednio-wieczne*, Warszawa
- Nachrichtl.Vorzeit** ⇨ *Nachrichtenblatt für deutsche Vorzeit*
- Nowe materiały kultury wielborskiej** ⇨ M. Fudziński, H. Pauer (eds.), *Nowe materiały i interpretacje. Stan dyskusji na temat kultury wielborskiej*, Gdańsk 2007
- Officina archaeologica optima** ⇨ W. Nowakowski, A. Szeda (eds.), *Officina archaeologica optima. Studia oformowane Jerzemu Okuliczakowi-Kaczorynowi w siedemdziesiąty rocznicę urodzin*, Swiatowit Supplement Series P: Prehistory and Middle Ages VII, Warszawa 2003
- Orbis Barbarorum** ⇨ J. Andrzejowski, C. van Carnap-Bornheim, A. Cielinski, B. Kontny (eds.), *Orbis Barbarorum. Studia ad archaeologiam Germanorum et Baltorum temporibus*
- Importi Bonant perizoonitir Adalberto Nowakowski dedicata*, MonArch, Barbica, Series Gemina VI, Warszawa-Schleswig 2017
- PamA** ⇨ *Pamiętki Archeologiczne*
- PArch** ⇨ *Przegląd Archeologiczny*
- PMMAE** ⇨ *Prace i Materiały Muzeum Archeologicznego i Etnograficznego w Łodzi, Seria Archeologiczna*
- Pogranicze trzech światów* ⇨ W. Nowakowski, A. Szeda (eds.), *Pogranicze trzech światów. Kontakty kultur przeworskiej, wielborskiej i bogactwańskiej w świetle materiałów z badań i poszukiwań archeologicznych*, Swiatowit Supplement Series P: Prehistory and Middle Ages XIV, Warszawa 2006
- PomAnt** ⇨ *Pomerania Antiqua*
- Prussia** ⇨ *Sitzungsberichte der Altertumsgesellschaft Prussia*, Zeitschrift für Heimatkunde
- PZ** ⇨ *Prähistorische Zeitschrift*
- RArch** ⇨ *Recherches Archéologiques*
- RA** ⇨ *Российская археология / Российская археология (=RA)*
- RB** ⇨ *Rocznik Białostocki*
- RGA** ⇨ J. Hoops, I-IV (ed.), *Reallexikon der Germanischen Altertumskunde*, Straßburg 1911–1919;
- H. Beck, D. Gieseler, H. Steiner (eds.), *Reallexikon der Germanischen Altertumskunde*, Berlin, New York
- RGF** ⇨ *Römisch-Germanische Forschungen*, Berlin-Letzgig-Mainz
- SA** ⇨ *Советская археология / Советская археология (=CA)*
- Saalhb** ⇨ *Saalburg-Jahrbuch*
- SAI** ⇨ *Archeologia SSSI, Stud Archaeologicznych Instytutow / Stud Archaeologicznych Instytutow (=CAI)*, Moskwa / *Материалы и исследования по археологии (=CAI)*, Moskwa / *Материалы и исследования по археологии (=CAI)*, Moskwa
- SCIVA** ⇨ *Studia et ceriectari de istorie veche și arheologie*
- SGD N.F.** ⇨ *Schriften der naturforschenden Gesellschaft in Danzig N.F.*
- SilAnt.** ⇨ *Silesia Antiqua*
- Slova** ⇨ *Slavenska Archeologia*
- Spisy Brno** ⇨ *Spisy Archeologickeho Ustavu AV CR Brno*, Brno

SprArch. ⇨ *Sprawozdania Archeologiczne*

StudArch ⇨ *Studia Archeologicae, Wrocław*

Studia Gothica ⇨ A. Kokowski (ed.), *Studia Gothica*, Lublin

Stud.Sachsenforsch. ⇨ *Studien zur Sachsenforschung*

Stud. Zvěsti ⇨ *Studijné Zvěsti Archeologickeho Ustavu SAV (Slovenskej Akademie Vedy)*

Terra Barbarica ⇨ A. Urbanik, R. Prochoc-wicz, J. Jakubczyk, M. Levada, J. Schuster (eds.), *Terra Barbarica. Studia oformowane Magdalena Murczyńskiej w 65. rocznicę urodzin*, Monumenta Archaeologica Barbica, Series Gemina, II, Łódź-Warszawa 2010

WA ⇨ *Wiadomości Archeologiczne*

ZNUJ PA ⇨ *Zeszyty Naukowe Uniwersytetu Jagiellońskiego, Prace Archeologiczne, Kraków*

БГУ ⇨ *Брянский Государственный университет*

ВГУ ⇨ *Воронежский Государственный университет*

ГИМ ⇨ *Государственный Исторический музей, Москва*

ИАК ⇨ *Известия Императорской Археологической Комиссии (=IAK)*

ИА РАН ⇨ *Институт археологии Российской академии наук*

ИИМК РАН ⇨ *Институт истории материальной культуры Российской академии наук*

КВЭЭ ⇨ *Киево-Ватиканская археологическая экспедиция*

КСИА ⇨ *Краткие сообщения Института археологии (=KSIA)*

МАИЭТ ⇨ *Материалы по археологии, истории и этнографии Таврии (=МАИЭТ)*

МЭП ⇨ *Музей-заповедник «Кремлёвский полъ», Тува*

МИА ⇨ *Материалы и исследования по археологии СССР, Москва (=MIA)*

ММ ⇨ *Музей Москвы*

МНИИЭИЭ ⇨ *Мордовский научно-исследовательский институт языка, литературы истории, этнографии*

РА ⇨ *Российская археология (=RA)*

СА ⇨ *Советская археология (=SA)*

САИ ⇨ *Своа археологических источников (=SAI)*

ХС ⇨ *Херсонесский Сборник (=HS)*

БГУ ⇨ *Брянский Государственный университет*

ВГУ ⇨ *Воронежский Государственный университет*

ГИМ ⇨ *Государственный Исторический музей, Москва*

ИАК ⇨ *Известия Императорской Археологической Комиссии (=IAK)*

ИА РАН ⇨ *Институт археологии Российской академии наук*

ИИМК РАН ⇨ *Институт истории материальной культуры Российской академии наук*

КВЭЭ ⇨ *Киево-Ватиканская археологическая экспедиция*

КСИА ⇨ *Краткие сообщения Института археологии (=KSIA)*

МАИЭТ ⇨ *Материалы по археологии, истории и этнографии Таврии (=МАИЭТ)*

МЭП ⇨ *Музей-заповедник «Кремлёвский полъ», Тува*

МИА ⇨ *Материалы и исследования по археологии СССР, Москва (=MIA)*

ММ ⇨ *Музей Москвы*

МНИИЭИЭ ⇨ *Мордовский научно-исследовательский институт языка, литературы истории, этнографии*

РА ⇨ *Российская археология (=RA)*

СА ⇨ *Советская археология (=SA)*

САИ ⇨ *Своа археологических источников (=SAI)*

ХС ⇨ *Херсонесский Сборник (=HS)*

Mikulovice

Pohřebiště starší doby bronzové na Jantarové stezce
Early Bronze Age Cemetery on the Amber Road

Michal Ernée, Michaela Langová et al.

Laura **Arppe** (*LA*), Petr **Bednář** (*PB*), Daniel **Berger** (*DB*), Gerhard **Brügmann** (*GB*), Jarmila **Bíšková** (*JB*),
Jan **Cvrček** (*JC*), Sylva **Drtíková Kaupová** (*SDK*), Michal **Ernée** (*ME*), Vanessa **Fairbank** (*VF*),
Jan **Frolík** (*JF*), Volker **Heyd** (*VH*), Ladislava **Horáčková** (*LH*), Ludmila **Kaňáková** (*LK*),
Jiří **Kmošek** (*JK*), Petr **Kočár** (*PK*), Romana **Kočárová** (*RKo*), Šárka **Křížová** (*SK*), Lukáš **Kučera** (*LKu*),
René **Kyselý** (*RK*), Michaela **Langová** (*ML*), Martin **Mihaljevič** (*MM*), Kamila **Moravcová** (*KM*),
Ernst **Pernicka** (*EP*), Petra **Stránská** (*PS*), Radko **Sedláček** (*RS*), Jiří **Šura** (*JSu*), Jarmila **Švédová** (*JSv*),
Lenka **Vargová** (*LV*), Petr **Velemínský** (*PV*), Kateřina **Vymazalová** (*KV*), Eliška **Zazvonilová** (*EZ*)

Praha 2020



Technical Editor

Ivana HERGLOVÁ, herglova@arup.cas.cz

Type-setting, Layout

Agama® poly-grafický ateliér, s. r. o., Na Výši 424/4, 150 00 Praha 5, Czech Republic, agama@agamaart.cz
Cover design Michal ERNÉE, Irena MACHÁČKOVÁ

Print

TNM PRINT s. r. o., Czech Republic

Tato kniha je publikačním výstupem grantu GAČR č. GA16-14855S „*Mobilita a sociální status populace časně doby bronzové na jantarové stezce. Výpověď pohřebiště v Mikulovicích*“.

Vydání této publikace bylo finančně podpořeno cenou AV ČR Praemium Academiae, kterou obdržel M. Ernée v roce 2019.

© Authors 2020

© Institute of Archaeology of the Czech Academy of Sciences, Prague; Prague 2020

Vydává Archeologický ústav Akademie věd České republiky, Praha, v. v. i.

Published by the Institute of Archaeology of the Czech Academy of Sciences, Prague

Registrováno pod ev. č. MK E 4240

Redakce — Office: Letenská 4, CZ 118 01 Praha 1, tel.: +420 257 014 382, e-mail: pamatky@arup.cas.cz

Rozšiřuje, informace o předplatném podává a objednávky přijímá:

Archeologický ústav AV ČR, v. v. i., Knihovna, Letenská 4, CZ 118 01 Praha 1, tel.: +420 257 014 415, +420 257 014 318, e-mail: knihovna@arup.cas.cz

Orders from abroad:

Mr. František Ochrana, LIBRARY, Letenská 4, Praha 1, CZ 118 01, Czech Republic, tel.: +420 257 014 415, e-mail: ochrana@arup.cas.cz

SUWECO CZ, s. r. o., Sestupná 153/11, Praha 6 - Liboc, CZ 162 00, Czech Republic, tel.: + 420 242 459 205, e-mail: suweco@suweco.cz

13.5. Chemická analýza vzorků jantaru

L. Kučera, P. Bednář

Rostlinné pryskyřice obecně tvrdnou fosilizačním procesem, který zahrnuje oxidační a polymerační reakce, působení tlaku a mikroorganismů. Tyto všechny procesy se navíc odehrávají při různých teplotách a povětrnostních podmínkách. Výsledkem je poté tuhá pryskyřice s různými chemickými a fyzikálními vlastnostmi, které jsou dány druhem rostliny, ze které pochází, geografickým původem a okolnostmi fosilizačního procesu. Nejznámější fosilní pryskyřicí je jantar. Malé, ale charakteristické rozdíly v chemickém složení jantaru mohou tedy pomoci určit geografickou oblast původu jantaru. Jantar můžeme popsat jako složitou směs organických a anorganických látek, která obsahuje přibližně 80 % uhlíku, 10 % kyslíku a 10 % vodíku. Dále jantar obsahuje stopové prvky jako např. měď, železo, sodík, vápník, mangan, vanad, olovo, hliník, dusík a síru (Anderson – Winans 1991; Chen – Lu 2006).

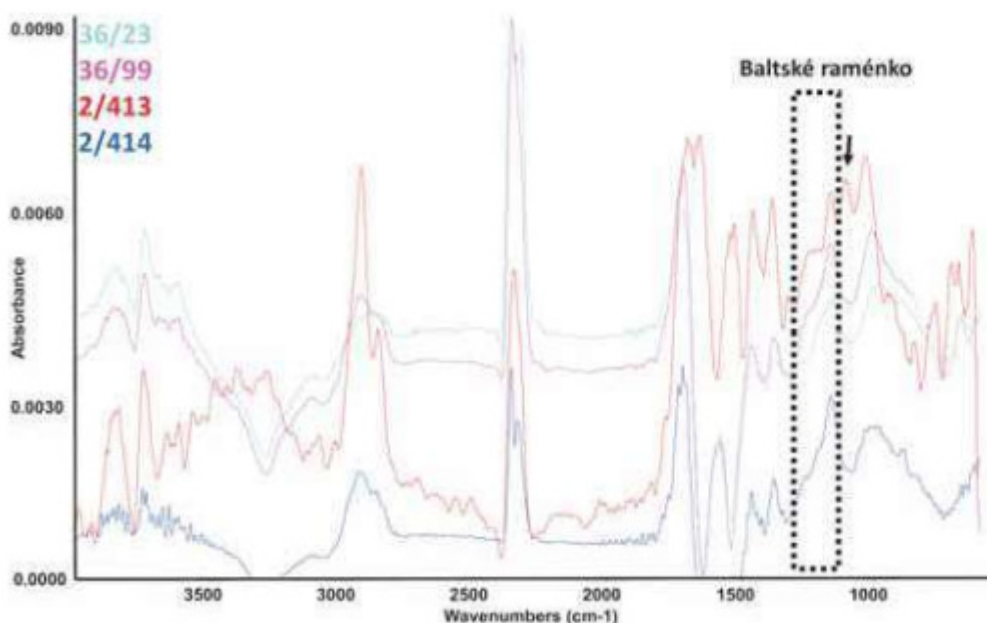
13.5.1. Použité metody, analyzovaný soubor a výsledky analýz

Rychlý vývoj instrumentální techniky v analytické chemii v posledních desetiletích umožnil výrazně rozšířit možnosti studia chemického složení jantaru, mimo jiné i pro účely určení jeho geografického původu. V literatuře se můžeme setkat s řadou spektrálních a separačních technik. Studovány byly možnosti použití Ramanovy spektroskopie, rentgenové krystalografie, elektronové mikroskopie, nukleární magnetické rezonance, plynové a kapalinové chromatografie ve spojení s hmotnostním spektrometrem (Vandenabeele et al. 2003; Matuszewska – Czaja 2002; Pakutinskiene et al. 2007; Senftle – Larter 1988; Truică et al. 2012; Havelcová et al. 2016). Zřejmě nejčastěji je však pro přiblížení původu jantaru používána infračervená spektrometrie s Fourier-

ovou transformací (FTIR). Dle dostupné literatury umožňuje tato technika například určit, zdali jantar pochází z blízkosti Baltského moře či nikoliv, a to na základě přítomnosti pásů známých jako „Baltské raménko“. Rozlišení baltského jantaru od jiných typů je založeno na hypotéze, že materiály z Pobaltí obsahují vysoký obsah kyseliny jantarové (až 8 %), jejíž signály se projevují v IR spektru ramenem ve výše uvedené oblasti vlnočtů $1110\text{--}1250\text{ cm}^{-1}$ (Beck – Wilbur – Meret 1964). Poznamenejme, že Baltský jantar je podle kyseliny jantarové (z angl. succinic acid) v některých literárních zdrojích nazýván Sukcinitem (Gough – Mills 1972). V určitých případech však může docházet ke špatnému určení ne-Baltského jantaru jako Baltský, což by mohlo být způsobeno přítomností určitého množství kyseliny jantarové ve vzorcích jantaru, např. gedanitu (Stout – Beck – Kosmowska-Ceranowicz 1995), romanitu (van der Werf et al. 2014) a goitschitu (Yamamoto et al. 2006). Ještě problematičtější může logicky být snaha o použití FTIR techniky pro podrobnější geografickou/geologickou klasifikaci například v rámci Baltských jantaru. Problematická je v této souvislosti zřejmě nízká selektivita techniky s ohledem na velké množství chemicky různých složek přítomných v jantaru. Na druhou stranu, zřejmou výhodou této techniky je její neinvazivnost – touto metodou je možno měřit vzorek přímo, prakticky bez jeho ovlivnění.

V této kapitole jsme testovali možnosti FTIR techniky pro analýzu a klasifikaci vzorků jantaru pocházejících z Litevského pobřeží, ruského povrchového dolu Jantarny, Mazurských jezer a z dalších regionů z oblasti Baltského moře. Pro detailnější charakterizaci jantaru jsme dále vyvinuli techniku založenou na jiném fyzikálně-chemickém principu, hmotnostní spektrometrii s laserovou desorpcí-ionizací (LDI-MS).

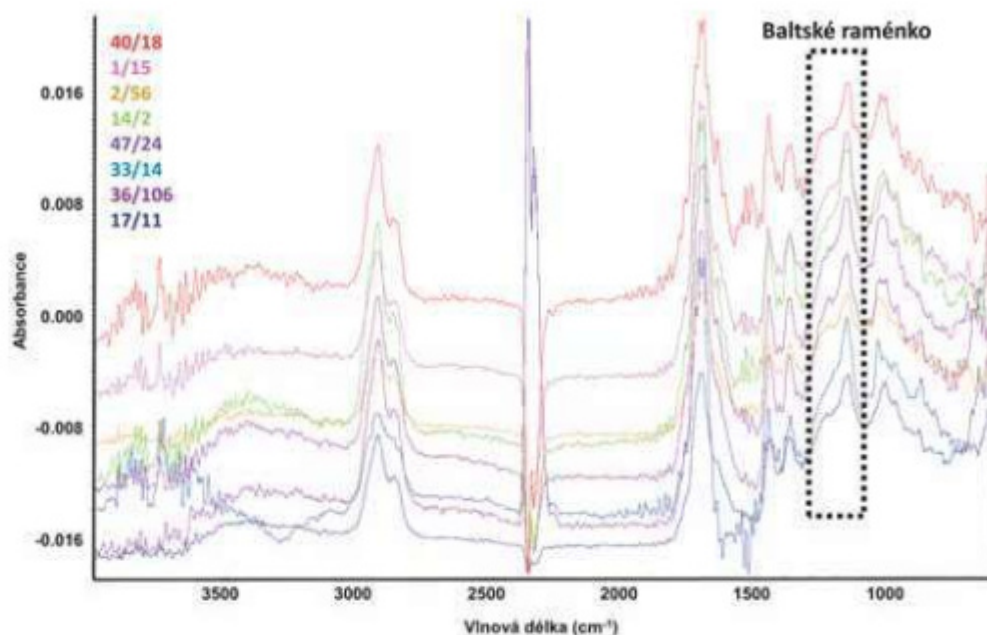
Metodou infračervené spektrometrie bylo analyzováno 41 jantarových artefaktů (tabula 68). Vzorky jantaru byly měřeny pomocí infračerveného (FTIR) spektrometru s Fourierovou transformací (FTIR spektrometru



Obr. 283. Mikulovice. Infračervená spektra analyzovaných jantarových rozřadovačů 2/413, 2/414, 36/23 a 36/99 z hrobů č. 2 a 36. Grafika L. Kučera. — **Fig. 283.** Mikulovice. Infrared spectrum of analysed amber spacers 2/413, 2/414, 36/23 and 36/99 from grave nos. 2 and 36. Graphic by L. Kučera.

Obr. 284. Mikulovice. Vybraná infračervená spektra studovaných vzorků jantaru. Grafika L. Kučera.

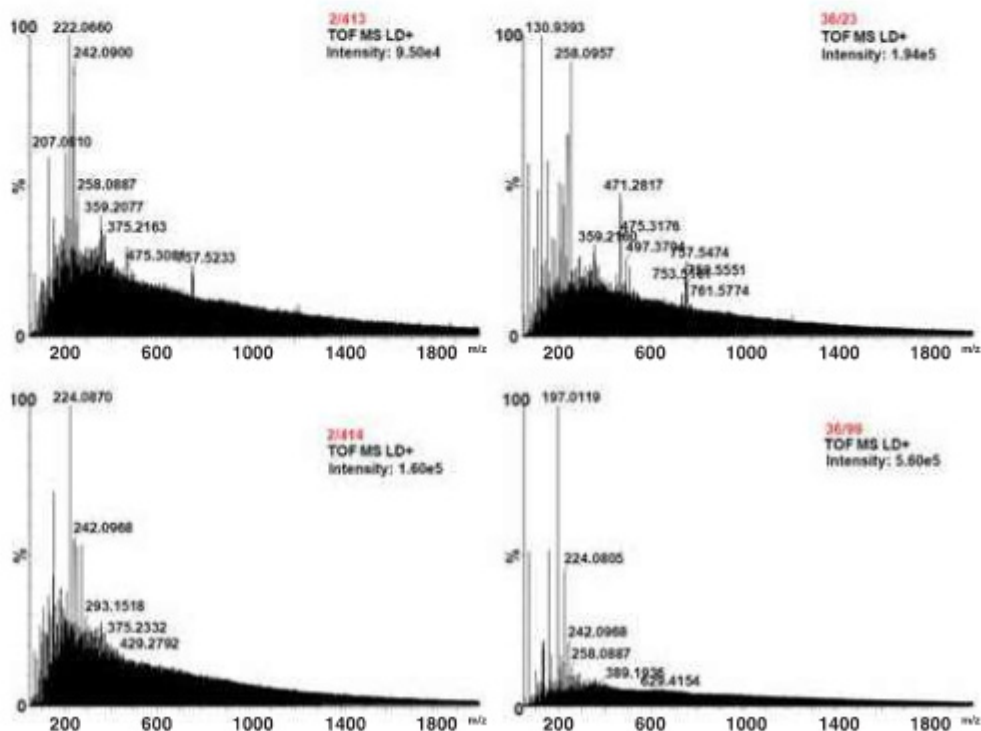
Fig. 284. Mikulovice. The selected infrared spectrum of the studied amber samples. Graphic by L. Kučera.



Nicolet 6700, Thermo-Nicolet) ve spektrálním rozsahu 4000–600 cm^{-1} . Byla použita technika zeslabené totální reflektance (ATR) a finální spektra byla získána akumulací 32 jednotlivých naměřených spekter. Spektra byla zpracována programem Omnic (Thermo Fisher Scientific). U všech vzorků jantaru analyzovaných technikou infračervené spektroskopie byl nalezen signál 1134–1142 cm^{-1} , na jehož základě a výše zmíněné hypotéze o rozdílech v obsahu jantarové kyseliny byly tyto vzorky přiřazeny do Baltské oblasti („Baltské jantary“). Mezi analyzovanými vzorky se nacházely čtyři rozřaďovače. U všech čtyř vzorků byly nalezeny signály náležející

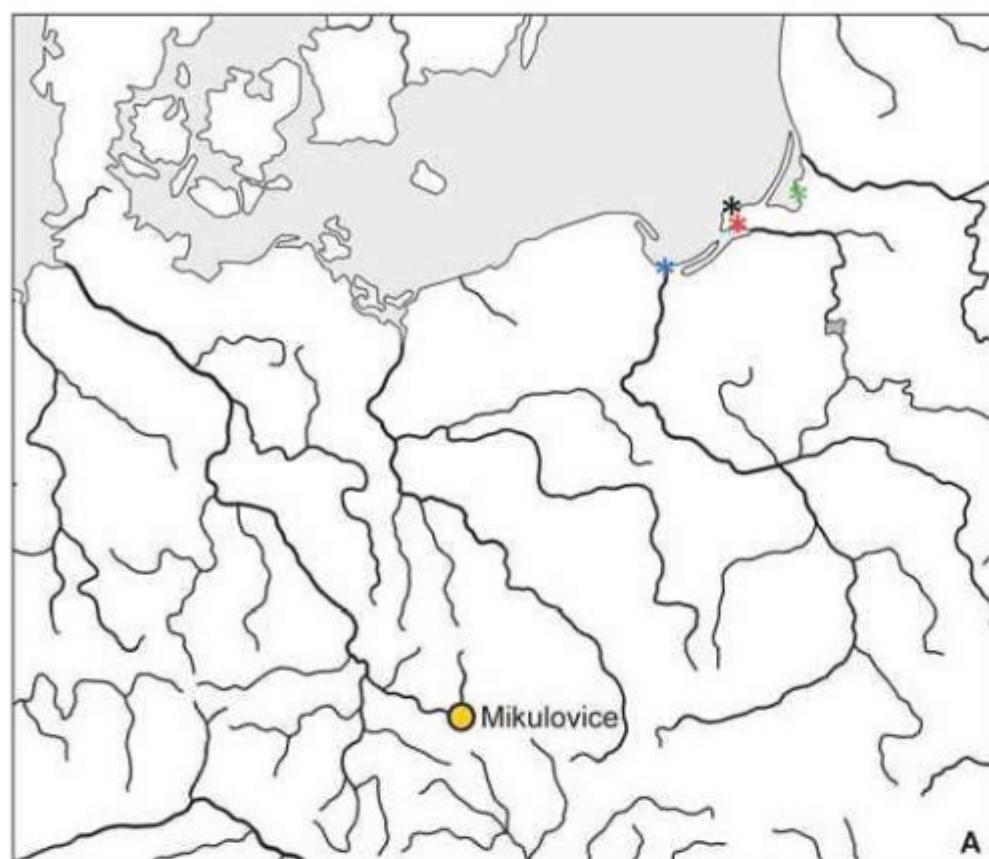
„baltskému raménku“ poukazující na baltský původ. Nicméně vzorek 2/413 (červená linka) se od ostatních vzorků lišil (signál 1104 cm^{-1} , vyznačeno šipkou; obr. 283). Tento rozdíl může mít spojitost s původem jantaru (regiony v oblasti Baltského moře). Na obr. 284 jsou zobrazena spektra vždy jednoho zástupce z každé analyzované skupiny – hrobu.

Pro podrobnější charakterizování jantaru byla na našem pracovišti vyvinuta nová metoda s využitím vysokorozlišujícího tandemového hmotnostního spektrometru s laserovou desorpce/ionizací (LDI-MS) v kombinaci s vícerozměrnou analýzou (analýza hlavních

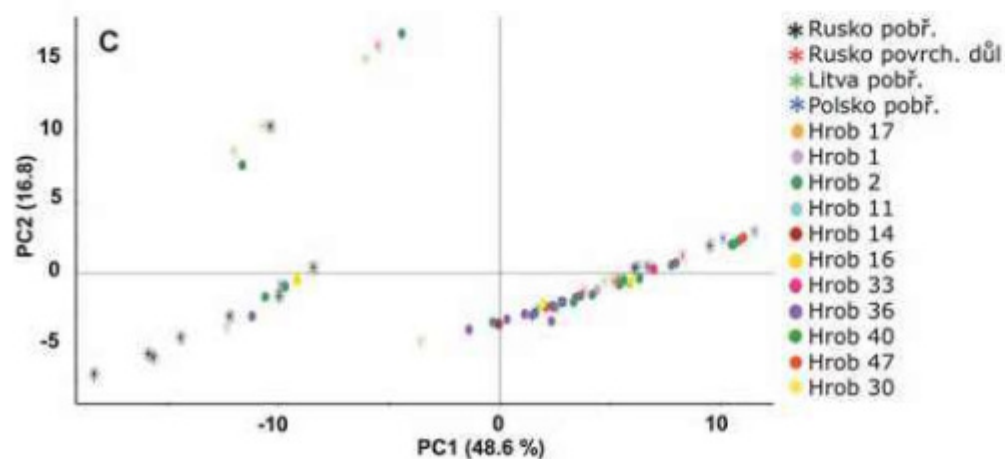
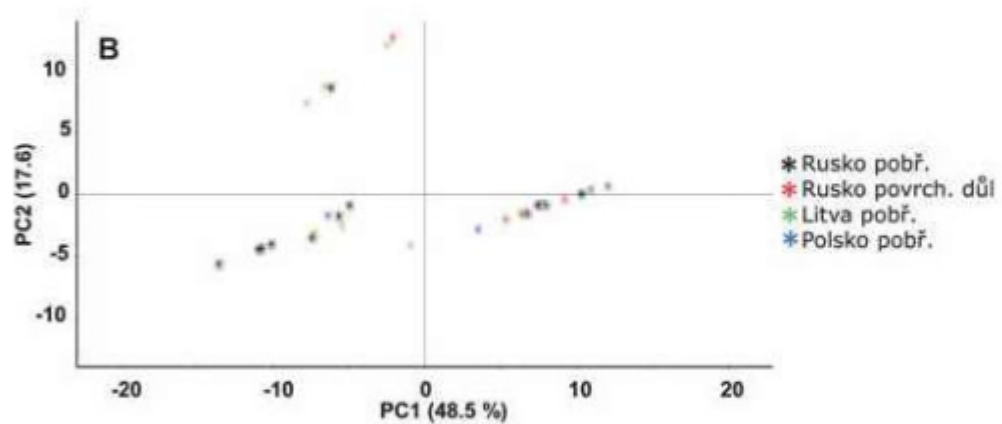


Obr. 285. LDI-MS spektra vzorků jantaru z analyzovaných rozřaďovačů 2/413, 2/414, 36/23 a 36/99. Grafika L. Kučera.

Fig. 285. LDI-MS spectrum of amber samples from analysed spacers 2/413, 2/414, 36/23 and 36/99. Graphic by L. Kučera.



Obr. 286. Mapa Baltské oblasti s označením lokalit jantaru z hlediska jejich těžby (A), PCA score plot vzorků surových jantarů pocházejících z těchto lokalit (B) a archeologických vzorků z lokality Mikulovice (C). Grafika L. Kučera. — **Fig. 286.** Map of the Baltic Region showing sites of amber from the perspective of their extraction (A), PCA score plot of samples of raw amber from these sites (B) and archaeological samples from the Mikulovice site (C). Graphic by L. Kučera.



Hrob	Č. vzorku	Konzerv.	Pozn.
2	2/29	ano	
	2/30	ano	
	2/56	ano	
	2/85	ano	
	2/78	ano	
	2/119	ano	
	2/127	ano	
	2/172	ano	
	2/199	ano	
	2/229	ano	
	2/253	ano	
	2/256	ano	
	2/283	ano	
	2/298	ano	
	2/343	ano	
	2/402	ano	
	2/409	ano	
	2/412	ano	
	2/413	ano	rozřadovač
	2/414	ano	rozřadovač

Hrob	Č. vzorku	Konzerv.	Pozn.
36	36/5	ano	
	36/23	ano	rozřadovač
	36/34	ano	
	36/99	ano	rozřadovač
	36/106	ne	
	36/118	ano	
	36/124	ano	
	36/130	ano	
	36/152	ano	
	36/159	ne	

Hrob	Č. vzorku	Konzerv.	Pozn.
1	1/15	ano	
11	11/13	ano	
14	14/2	ano	
16	16/28	ano	
	16/30	ano	
17	17/11	ne	
30	30/11	ne	
33	33/14	ne	
40	40/19	ne	
47	47/12	ano	
	47/24	ne	

Tabella 68. Mikulovice. Analyzované jantarové předměty.
Table 68. Mikulovice. Analysed amber artefacts.

komponent, PCA). I když je tato technika destruktivní, tak množství potřebné k analýze je menší než hlavička běžného špendlíku (zhruba 4 mg; 1 x 1 x 1 mm). Princip LDI-MS metody spočívá v desorpci/ionizaci látek ze vzorku pomocí pulzního laseru a následně akceleraci ionizovaných molekul do hmotnostního spektrometru, kde dochází k měření jejich přesné hmotnosti (přesněji poměru hmotnosti k náboji, m/z). Naměřené spektrum obsahuje velké množství (tisíce) signálů z důvodu přítomnosti velkého množství ionizovatelných látek (obr. 285). Tyto signály jsou vzhledem k velké selektivitě hmotnostní spektrometrie velmi dobře rozlišeny. Vzájemné porovnání jednotlivých signálů ve spektru mezi větším množstvím vzorků je obtížné a těžko přímo interpretovatelné a z toho důvodu byl využit potenciál pokročilého statistického zpracování dat. Analýza hlavních komponent (PCA) byla po převedení signálů ve spektrách na datovou matici použita pro necílené zobrazení rozdílů a podobností mezi jednotlivými vzorky. Předběžné výsledky LDI-MS analýzy surových jantarů z pobřeží Ruska (Donskoe), Litvy (Palanga) a Polska (Gdaňsk) a povrchového ruského dolu (Jantarny – obr. 286: A) poukázaly na chemickou podobnost vzorků ze stejné lokality a současně na rozdíly v sadách vzorků z pobřeží Polska a ruského povrchového dolu (segregace vzorků přibližně ve směru první komponenty, PC1, obr. 286: B). Vzorky z pobřeží Litvy a Ruska jsou v PCA Score plotu situovány v levé části a lze tedy uvažovat o jejich určité chemické podobnosti. Výjimkou jsou dva vzorky z ruského pobřeží a jeden vzorek z pobřeží Litvy, které jsou situovány v pravé části plotu. Tři vzorky z Polska jsou situovány na pravé straně PCA plotu (jeden na levé). Podobnou situaci můžeme pozorovat i u vzorků z ruského povrchového dolu (tři vzorky jsou situovány poměrně kompaktně na pravé straně PCA plotu a jeden je z hlediska PC1 v poloze mezi oběma skupinami. První a druhá hlavní komponenta popisuje 66,1 % variability v datech.

Pokud do toho statistického modelu implementujeme vzorky z archeologického průzkumu z lokality Mikulovice u Pardubic (provedeme společnou PCA analýzu na vzorcích rozřadovačů a mikulovických vzorků), můžeme stále pozorovat separaci ve směru první komponenty. Většina studovaných vzorků se nachází v klastru odpovídajícím lokalitám polského pobřeží a/nebo ruského povrchového dolu (obr. 286: C), ale několik vzorků spadá i do regionu pobřeží Litvy a Ruska. Jedná se o šest vzorků č. 2/78, 2/127, 2/199, 2/413, 16/30, 36/152.


13.5.2. Závěr

Na základě FTIR měření a přítomnosti „Baltského raménka“ ve spektru lze všechny studované jantary zařadit do oblasti Baltského moře. Na základě předběžných výsledků z LDI-MS měření a analýzy hlavních komponent pochází přibližně 85 % vzorků ze studované sbírky jantarů z oblasti polského pobřeží a/nebo ruského povrchového dolu (Gdaňský/Kaliningradský záliv). Zbýlých 15 % jantarových artefaktů pravděpodobně pochází z oblasti rusko-litevského pobřeží (Kurský záliv). Kombinace měření infračervenou spektrometrií a hmotnostní spektrometrií s laserovou desorpcí/ionizací se ukazuje být perspektivním nástrojem pro získání detailnějších informací o původu jantarů. Jde o předběžné výsledky, které budou doplňovány a zpřesňovány měřeními dalších vzorků. V současné době pracujeme na propojení dat z FTIR a LDI-MS a cross-validaci statistického modelu.¹³⁶

¹³⁶ Autoři by rádi poděkovali Grantové agentuře České republiky (projekt 17-17346S) za finanční podporu a dr. Sigitė Bagužaitė-Talačkienė (Palanga Muzeum, Litva) a Archeologickému muzeu v Gdaňsku za poskytnutí vzorků surových jantarů k analýze.

Article

Determination of Milk Products in Ceramic Vessels of Corded Ware Culture from a Late Eneolithic Burial

Lukáš Kučera ¹ , Jaroslav Peška ², Pavel Fojtík ³, Petr Barták ¹, Diana Sokolovská ¹, Jaroslav Pavelka ⁴, Veronika Komárková ⁵, Jaromír Beneš ⁵, Lenka Polcerová ⁶ , Miroslav Králík ⁶  and Petr Bednář ^{1,*} 

- ¹ Regional Centre of Advanced Technologies and Materials, Department of Analytical Chemistry, Faculty of Science, Palacký University, 17. listopadu 12, 779 00 Olomouc, Czech Republic; lukas.kucera@upol.cz (L.K.); petr.bartak@upol.cz (P.B.); dia.sokolovska@gmail.com (D.S.)
- ² Archaeological Centre Olomouc, U Hradiska 42/6, 779 00 Olomouc, Czech Republic; peska@ac-olomouc.cz
- ³ Institute of Archaeological Heritage Brno, Kaloudova 1321/30, 614 00 Brno, Czech Republic; pavfojtik@seznam.cz
- ⁴ Centre of Biology, Geoscience and Environmental Education, University of West Bohemia, Sedláčkova 15, 30614 Plzeň, Czech Republic; japedos@cbg.zcu.cz
- ⁵ Laboratory of Archaeobotany and Palaeoecology, Faculty of Science, University of South Bohemia, Na Zlaté stoce 3, 370 05 České Budějovice, Czech Republic; verokomar@seznam.cz (V.K.); benes.jaromir@gmail.com (J.B.)
- ⁶ Laboratory of Morphology and Forensic Anthropology (LaMorFA), Department of Anthropology, Faculty of Science, Masaryk University, Kotlářská 2, 611 37 Brno, Czech Republic; polcerova@seznam.cz (L.P.); mirekkralik@seznam.cz (M.K.)
- * Correspondence: petr.bednar@upol.cz; Tel.: +42-0585-6344-03

Received: 14 November 2018; Accepted: 4 December 2018; Published: 7 December 2018



Abstract: In this study, a soil from two ceramic vessels belonging to Corded Ware culture, 2707–2571 B.C., found in a cremation grave discovered in Central Moravia, Czech Republic, was analyzed using matrix-assisted laser desorption/ionization–mass spectrometry (MALDI–MS) combined with advanced statistical treatment (principal component analysis, PCA, and orthogonal projection to latent structures discriminant analysis, OPLS–DA) and by enzyme-linked immunosorbent assay (ELISA). MALDI–MS revealed the presence of triacylglycerols in both vessels. This analytical technique was used for the analysis of the soil content from archaeological ceramic vessels for the first time. Targeted ELISA experiments consequently proved the presence of milk proteins in both ceramic vessels. These results represent the first direct evidence of the use of milk or dairy products in the Eneolithic period in Moravian Corded Ware Culture and help to better understand the diet habits and living conditions of Eneolithic populations in Central Europe.

Keywords: ceramic vessels; laser desorption–ionization; mass spectrometry; milk; enzyme-linked immunosorbent assay; Eneolithic period; Corded Ware culture

1. Introduction

The analysis of human cremations from archaeological burials is a very important part of archaeological research that provides valuable information for a better understanding of former populations' habits. However, this research is difficult in general, especially because of a high level of bone fragmentation, size changes, thermal fractures and distortions, and possible artificial changes of bones related to burial rite habits [1–4]. In such a situation, explicit sex assessment, age estimation at death, population affinity, body size estimations, etc. are almost impossible. However, the obtained information can be completed by a detailed chemical characterization of graves' content accompanying

human remains (i.e., ceramic vessels containing certain material, residues of food, personal things, gifts, etc.).

Analysis of lipid residues present in ceramic vessels has already provided information about vessels' usage and former content. Analysis of isotope ratios of individual fatty acids adsorbed in prehistoric and medieval ceramics using gas chromatography–combustion–isotope ratio mass spectrometry (GC–C–IRMS) appeared to be an effective tool for the identification of fat origin [5,6]. The detection of milk residues in archaeological contexts was already described by many authors [7–10]. The oldest evidence of storage of milk products in pottery was described by Evershed et al. [11] (by using GC–C–IRMS). These authors analyzed more than 2000 archaeological samples from Near East and Southeastern Europe, and milk lipids were detected in a wide range of historical periods, from the seventh millennium B.C. The presence of milk lipids in ceramic vessels from the Neolithic period indicates milking skills and usage of dairy products in this period. Compared with the published studies dealing with the analysis of organic residues of milk adherent to the surface of a ceramic vessel or soaked into ceramics from Copper Age (Turkey [12]), Bronze Age (England [7]), and Iron Age sites (Netherlands [13], Scotland [9]), more ceramic vessels or shreds containing milk are found from the Neolithic period, e.g., ceramic vessels from Sweden [14], Anatolia [15], Slovenia [16], France [17], Switzerland [18], England [19,20], Germany, and Italy [21,22]. GC–C–IRMS is the method mainly used. However, there are some papers dealing with the detection of milk lipids in archaeological ceramics by direct temperature–resolved mass spectrometry and nanoelectrospray mass spectrometry [13,17]. Matrix-assisted laser desorption/ionization–mass spectrometry (MALDI–MS) has been used for the study of milk residues mainly in paintings, especially for the analysis of proteins after trypsin digestion and lipids [23–30]. Besides, MALDI–MS was used for proteomic analysis of a compact organic residue found inside a more than 4000-year-old container [7].

Another promising possibility for the exact determination of organic matrices (i.e., milk, etc.) is the utilization of immunological tests. In archaeological samples, thermostable native as well as modified (partially degraded) proteins are found. On the other hand, many factors limit antibody tests applicability when dealing with archaeological material. Possible cross-reactions [31,32], degradation of proteins resulting in antigen binding—nonspecific reactions in ELISA tests [33], and contamination from surrounding areas are the main risks that need to be kept in mind when analyzing non-collagenous proteins from human and other mammal samples of modern and ancient origin [34]. Nevertheless, following a proper experimental design including sufficient reference samples and a reasonable amount of native proteins in the organic residues under study, the commercially available ELISA kits can be used with an acceptable degree of reliability. This has been already shown by the analysis of animal proteins in Neolithic samples (i.e., detection of heat-stable species-specific muscle proteins) [35]. Besides, it is possible to utilize antibody tests targeted specifically to denatured proteins that provide reliable results with a high selectivity. A wide range of detection tests based on an immunological reaction that were developed for the identification of various components in heat-treated foods are commercially available today. This category of commercial tests is purposefully designed to work with degraded traces of biological tissues in the food industry and they are undergoing a rigorous evaluation of their ability to correctly detect the ingredients in processed food [36]. It can be emphasized that their suitability for archaeology has been already proven by the identification of damaged and denatured proteins in desiccated and partially carbonized organic residues from antiquity [37].

The usage of milk by prehistoric populations is problematic and still not well explained. Analysis of ancient DNA (aDNA) shows that almost all people at the time (i.e., populations living in (E)Neolith) failed to digest lactose in adult age [38–40]. Currently, in Europe, only a single mutation of the lactase gene, called 13910 * T, allowing to digest lactose in adulthood was found. This supports the idea of the spreading of this mutation from one area [41]. The 13910 * T mutation was mainly detected in samples from the Late Bronze Age and Hallstatt period [38–40]. The mutant allele allowing lactose digestion occurred in Europe even before the Bronze Age, but its geographical distribution is uneven

(e.g., in Scandinavia, where the hunter–gatherer economy prevailed, the mutant allele’s frequency in the population was 5% in the analyzed assemblage). The prevalence of the mutant allele allowing the digestion of lactose in contemporary humans is about 35%, and, in some North European populations, it is up to 90% in adults [42]. The milk of dairy animals as a complex admixture of many important nutrients—proteins, fats, minerals, vitamins, and others [43]—is a nutritionally beneficial food and after natural fermentation (without any complex cultural addition) it can be digested even by lactase activity-deficient people [44]. Based on the above-mentioned evidence, we hypothesize that milk served as food in Neolithic–Eneolithic Europe, but not in fresh form. To decrease the amount of lactose, milk processing could be used, i.e., fermentation and/or heating [44]. Therefore, molecular genetic event(s) in the evolution of lactase persistence in adults might be a secondary by-product of herding dairy animals. Anthropological reconstructions [45] showed that dairy product consumption and adoption by human cultures preceded the evolution of lactase persistency by thousands of years (milking came first, lactose digestion followed) [46]. Additionally, using milk in nutrition might have been important not only for nutritional purposes. For example, the fermented milk products might have positive health effects to gut microbiota during nomadic movements over long distances and in diverse environments [47]. Therefore, the direct detection of milk proteins and lipids in archeologically excavated vessels might be, in our opinion, a much better indicator of the time in prehistory of dairy product adoption for human persistence and economic strategies than any molecular genetic estimations of the evolution of lactase persistence.

In this contribution, the content of two archaeological ceramic vessels from a grave belonging to the Moravian Corded Ware culture was analyzed by matrix-assisted laser desorption/ionization–mass spectrometry (MALDI–MS) and enzyme-linked immunosorbent analysis (ELISA). To the best of our knowledge, this is the first time that MALDI–MS is used for the analysis of ancient milk fat residues from the soil content of ceramic vessels. Lipid profiling by MALDI–MS revealed the presence of milk residues in the bottom soil layers of the excavated vessels. The subsequent ELISA experiments confirmed the occurrence of milk proteins. Both methods thus mutually confirmed the presence of milk or dairy products in the investigated vessels. Information about the utilization of milk products in the Eneolithic period in Central Europe is of key importance for the description of the Eurasian population’s migration at that time and the expansion of lactase gene mutation.

2. Results

The soil extracts were analyzed by MALDI–MS, and the raw data were transferred to a statistical software and studied by PCA, HCA, and OPLS-DA. Figure 1 shows the score plots (PCA) of MALDI–MS data obtained by the analysis of acetone extracts of separated soil layers (for details see Experimental, Chapt. 3.2). A distinct segregation of the bottom samples (5th layer) from the upper ones (1st–3rd layer; 4th layer not considered) was observed in ceramic vessel no. 4. Each sample was measured in three chemical replications represented by three points of particular color (Figure 1A). A similar pattern could be observed in the soil extracts taken from vessel no. 5 (Figure 1B). Here, the 4th and 5th layer significantly segregated from the upper layers. Hierarchical clustering was used to study the similarity of specific layers. Figure 1C,D shows the dendrograms of the relationships between the soil extracts of ceramic vessels no. 4 and 5. Generally, the soil samples from the 4th and 5th layers of both ceramic vessels were located in separated clades (i.e., leaves 4 and 5 were dissimilar to other leaves, with the exemption of two measurements of layer 1 in vessel No. 4 that were probably due to a higher data dispersion visible in the related PCA plot). Both multivariate methods pointed out a significantly different composition of the bottom layer(s). MALDI–MS combined with multivariate statistics was thus a sufficiently selective tool to differentiate particular samples of soil based on variances in chemical composition. The first two components explained 61.7% (ceramic vessel no. 4) and 65.4% (ceramic vessel no. 5) of the variance in the data. Note that cumulative proportion of variance with third and fourth component explained 75.5% and 81.0% of the variance for ceramic vessel no. 4 and 75.5% and 79.9% of the variance for ceramic vessel no. 5, respectively (Supplement 4).

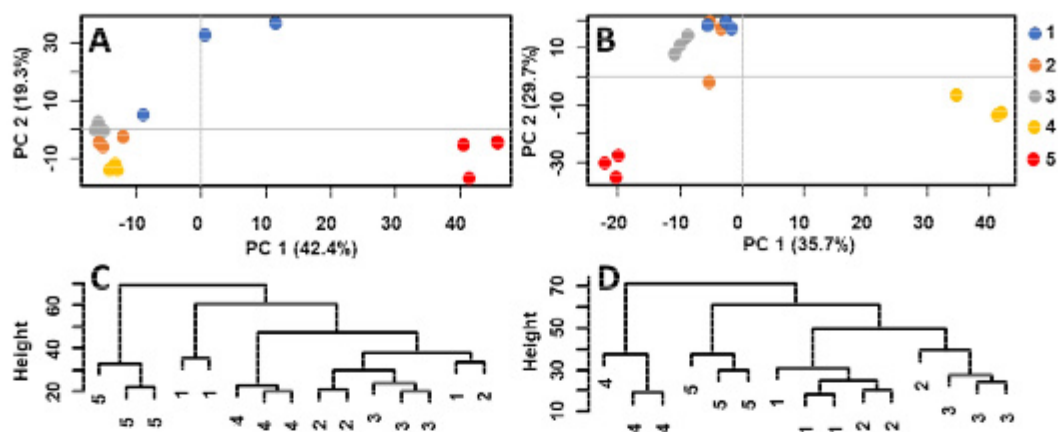


Figure 1. Score plots and dendrograms of MALDI-MS data measured in acetone extracts of five soil layers from ceramic vessels no. 4 (A,C) and no. 5 (B,D), respectively.

The following analysis of the data by OPLS-DA provided signals of significant markers describing the main differences between the upper and the bottom layers of soil in the vessels. Markers (i.e., compounds present in the bottom layer in significantly higher amounts than in the upper layer) with the highest variability and reliability at the same time were taken from a low-risk region of an appropriate S-plot (Supplement 5). For our purposes, the low-risk region was defined as a box with the following coordinates: $p[1] = 30\text{--}100\%$ and $p[2] = 75\text{--}100\%$ from the highest value on the x -axis and y -axis, respectively, as already reported [48]. Table 1 shows significant markers of the bottom soil layers taken from ceramic vessels no. 4 and no. 5. A manual inspection of appropriate MALDI mass spectra supported the significant differences in those signals, evidencing the functionality of the used OPLS-DA method. The most significant signals (taken from the appropriate S-plot) were observed in soil from pottery no. 5. (soil from the fifth, bottom layer compared to the first, upper layer). The differences between two adjacent signals corresponded to the CH_2 group homological increments (i.e., $\Delta m/z(1) = 687.4951\text{--}673.4808 = 14.0143$; $\Delta m/z(2) = 14.0163$; $\Delta m/z(3) = 14.0172$) and oxygen ($\Delta m/z(4) = 15.9721$). These signals corresponded to potassium adducts of triacylglycerols (TAGs). A good agreement of the theoretical mass of the proposed elemental compositions with the measured values was observed. Picariello, Sacchi, and Addeo studied TAGs in various (recent) animal fats (lard, tallow, and milk fat). Particular signals of TAGs were observed in the form of sodium adducts solely in the bovine milk sample and not in the other fatty materials (i.e., m/z 657.5, 685.5, 699.6, 715.6), and, after recalculation of the sodium adducts m/z values to the corresponding potassium ones, a good agreement with our signals was observed [49]. On the basis of this agreement, the markers found in the bottom soil layers of both ceramic vessels were attributed to organic residues of dairy products. Similar signals were observed in the bottom layer of the vessel no. 4. Note that other (higher) TAGs were also found in the spectra from ceramic vessel no. 4, i.e., m/z 829.7618, 855.7787, 925.7029, 939.7148, 953.7241, 967.7419, and from ceramic vessel no. 5, i.e., 829.7870, 835.5690, 879.5928, 923.6188, 951.6760, 967.6469 (Figure 2). Note that m/z values of statistically significant triacylglycerols (TAGs) discussed here represent the average values taken from three MS spectra (repeated measurements).

The presence of fat residues in both vessels was further confirmed by targeted immunochemical tests. Results of specific ELISA tests on native β -Lactoglobulin (Table 2) confirmed the presence of milk protein residues in the bottom soil layer of vessel no. 5. A significantly positive reaction was observed (dual wave data, dwd : the difference at the two wavelengths of 450 and 650 nm was 0.044; the dwd of the negative control was 1.320). On the other hand, β -Lactoglobulin was not found in the soil from the bottom of vessel no. 4 (values approaching to negative control and dwd 1.812 were obtained). The presence of dairy products was also tested by casein ELISA kit. A positive reaction was observed in both studied vessels. Note that a weaker positive reaction was also observed in the reference soil sample from the surrounding area. Values of 0.13 and 0.17 (i.e., close to the value of

0.2 corresponding to 0.5 mg/kg of casein standard) were obtained that were significantly lower than the value determined for both vessels. These data confirmed the presence of dairy products in both ceramic vessels. The usage of dairy products in ancient diet has already been proved by many authors (analysis of organic residues of dairy products adherent to a surface of a ceramic vessel or soaked into ceramics) [15,16,21]. It can be emphasized that this is the first application of MALDI-MS to analyze ancient milk fat residues in the soil content of ceramic vessels.

Table 1. List of the most significant markers of the bottom soil layers taken from the two studied vessels.

	<i>m/z</i>	CN/DB	Theoretical Formula	dtm (mDa)
Ceramic vessel no. 4	673.4879	36:2	C ₃₉ H ₇₀ O ₆ K	−7.0
	687.5005	37:2	C ₄₀ H ₇₂ O ₆ K	−3.9
	701.5178	38:2	C ₄₁ H ₇₄ O ₆ K	−5.6
	715.5337	39:2	C ₄₂ H ₇₆ O ₆ K	−5.8
	731.5103	39:2	C ₄₂ H ₇₆ O ₇ K	12.5
Ceramic vessel no. 5	673.4808	36:2	C ₃₉ H ₇₀ O ₆ K	0.1
	687.4951	37:2	C ₄₀ H ₇₂ O ₆ K	1.5
	701.5114	38:2	C ₄₁ H ₇₄ O ₆ K	0.8
	715.5286	39:2	C ₄₂ H ₇₆ O ₆ K	−0.7
	731.5007	39:2	C ₄₂ H ₇₆ O ₇ K	22.1

CN: carbon number, equal to the total number of carbon atoms of the three fatty acid moieties; DB: number of double bonds; dtm: difference of measured mass from that calculated for a particular elemental composition.

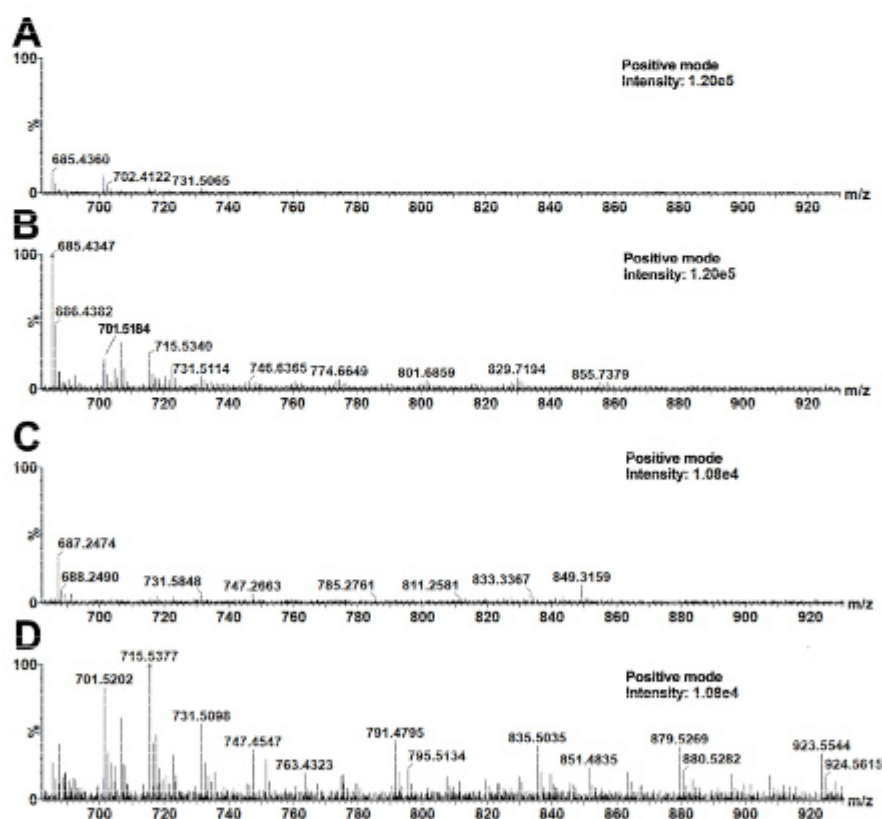


Figure 2. MALDI-MS spectra of acetone soil extracts from ceramic vessels no.4 (A,B) and no. 5 (C,D). The presented spectra represent one measurement of the 1st (A,C) and 5th (B,D) layers.

Although milk was part of ancient diet, it is questionable whether populations in Eneolith were already able to digest lactose (milk sugar). Recent findings from Hungary focused on the Iron Age show a possible milk consumption by nomads, based on the proven genetic proximity of the Hungarian population to eastern populations [39]. Nomads from the Late Bronze and Iron Age living in this

region usually belonged to the Indo-European historical Cimmerians [50]. However, it is still unknown when and where the European mutation arose. In this sense, the presence of bovine milk products from the end of the Eneolithic period in Moravia discussed and confirmed in this paper is extraordinarily important and evokes the need of a more proper genetic research of ancient remains.

Table 2. Results of the casein sandwich ELISA test and of the cattle β -lactoglobulin (β LG) competitive ELISA test used for the analysis of bottom soil layer samples taken from the studied vessels.

	Casein (ppm)	Evaluation	Cattle β LG (ppm)	Evaluation
Negative control	0.02	0	1.32	0
Positive control	0.2 *	+	0.021 **	+
Ceramic vessel no.4	0.36	+	1.81	0
Ceramic vessel no.5	0.52	+	0.044	+

+: positive, 0: negative, *: 0.5 mg/kg of casein standard, **: 10 mg/kg of β LG.

3. Materials and Methods

3.1. Archaeological Description of the Inspected Cremation Grave

The investigated cremation grave was discovered during a rescue excavation close to the village of Držovice (Prostějov, Central Moravia, Czech Republic, Figure 3) in the years 2014–2015. Five graves were found at the burial ground. The soil from two ceramic vessels coming from a grave denoted H4 was analyzed. The detailed archaeological description of the excavation close to the village of Držovice is presented in a paper by Fojtík [51]. The two ceramic vessels were described as a pair of Corded Ware beakers (ceramic vessel no.4 and no.5 with volumes of 0.8 and 0.6 L, respectively) with imprints of cord (circumferential grooves and a combination of inclined cuts on the neck). Beside the studied vessels, bone industries represented by a pair of massive chisels (radius or metapodium? *Bos taurus*, Supplement 1), a bone tip and awl (shinbone of medium-large mammal, presumably from sheep or goat, Supplement 2), and a worked tube bone (radius of sheep or goat, Supplement 2) were found in the grave. The presence of those bones illustrates the circumstances of the funeral, and they are described in more details.

The cord beakers with a sigmoid profile and the classic form of a jug of Dřevohostice type (CD1: variant Dřevohostice) belong to the earliest period of the Moravian Corded Ware culture (MCW; phase IIIa). The exact dating was performed by the radiocarbon method (Beta Analytic Radiocarbon Dating, Miami, USA) on a bone chisel found in the grave. The high-Probability Density Range Method, Intcal 13 was used, and the period of the bone material was determined to be in the ranges 2707–2571 B.C. (probability, prob = 62.3%), 2863–2807 (prob = 22%), 2759–2717 (prob = 9.9%), and 2513–2503 (prob = 1.1%). These data confirm that the bone chisel and consequently the grave belong to Eneolithic period. A particularly interesting item in the grave is a small bony tube (length: 94.75 mm; width 14.02 mm; outer diameter 14–15 mm, inner diameter 7.45–8.92 mm). This type of artefacts was found in Central Europe in the tombs of several groups of Corded Ware culture. Bony tubes could come from the earlier Eneolithic cultures in southern Ukraine and Pribajkali. The recent finding of a damaged and perhaps incomplete bone tube with a hint of engraved decoration in the late Jevišovice culture settlement at Kroměříž 3-Miňůvky could confirm the relationships of this tube to East (South-East) Europe.

The anthropological analysis followed the already published recommendations for the assessment of human cremated remains [52–54]. Most of the fragments ranged in color from light grey to white and were classified accordingly into the category of burning temperature 900 °C or higher [55]. Preserved parts of skulls indicated that the burial content represented remains of (at least) two human individuals, which was also supported by the weight of the bone fragments (2,146.6 g) [53,56]. One preserved third molar indicated that the age at death of one of the individuals was at least 18 years [57]. Skeletal

fragments (pieces larger than 2 mm) were measured by means of the original semiautomatic metric procedure developed by Polcerová [58,59]. The lateral angle values measured in the preserved pyramid of the temporal bone ranged from 54° to 62° , which is in the zone of variation occupied predominantly by females in the reference sample [60]. To sum up, the grave H4 represented remains which were well burned during regular cremation and contained skeletal and teeth fragments of two or more humans of whom at least one was an adult and at least one was a female (for more details see Supplement 3).

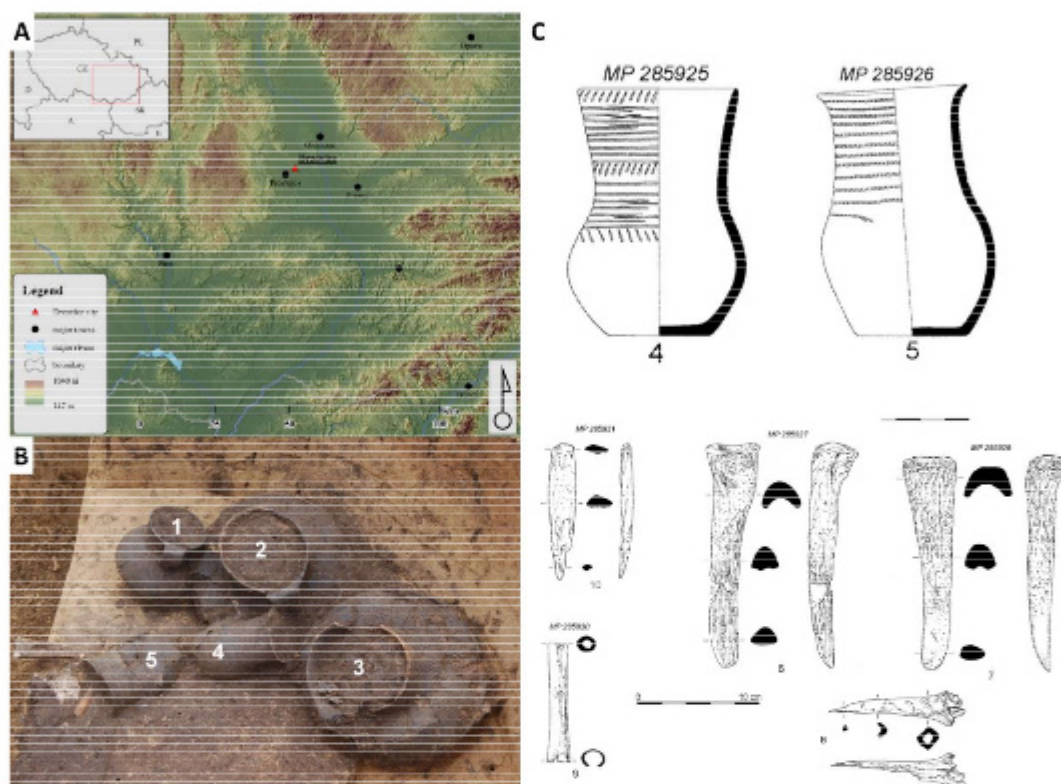


Figure 3. Place of rescue excavation (A), five ceramic vessels in the grave (B), and drawing of ceramic potteries and bone tools (C).

3.2. Sample Preparation

The ceramic vessels were compact but with visible cracks. The sherds were gently removed, and the internal part of the ceramic vessel (soil) that remained in a compact piece with the shape of the vessel was carefully reinforced by food plastic foil and transported to the laboratory. The soil material from the ceramic vessels was divided manually by a big knife in the vertical direction into five equal parts. Each part was consecutively extracted with four solvents with different polarity and acidity, i.e., water, 0.05% ammonium hydroxide in methanol, 1% formic acid in methanol, and acetone, providing the extraction of a wide number of chemical structures. All chemicals were purchased from Penta Ltd. (Prague, Czech Republic). The individual extracts were filtered through cellulose filter paper (black label, pore size 7–8 μm , Schleicher & Schuell A.G., Feldmeilen, Switzerland) and concentrated to a defined volume of 1 mL using a fine stream of nitrogen. The aqueous extracts were concentrated by lyophilization to the same volume. The concentrated extracts were subjected to analysis by MALDI–MS (experimental parameters are given below).

3.3. Matrix-Assisted Laser Desorption/Ionization–Mass Spectrometry and Multivariate Data Analysis

MALDI–mass spectrometry was used for a non-targeted analysis of the extracts of the soil content of both vessels. A Synapt G2-S high-resolution tandem mass spectrometer (Waters, Milford, MA, USA) with a vacuum MALDI source and a hybrid QqTOF type of mass analyzer with integrated two collision

cells and one ion mobility cell was used. Two microliters of sample extract were applied on MALDI target plate, and after solvent evaporation, the formed residue was covered by the matrix solution. As matrix, 2,4,6-trihydroxyacetophenone (THAP, Sigma-Aldrich, St. Louis, USA, dissolved in acetonitrile/water (1:1, *v/v*), at a concentration of 25 mg/mL) was used. This matrix is appropriate for lipid analysis by MALDI-MS technique [61]. The following parameters were chosen for of MALDI-MS: Mass range: 50–2000 Da, ionization mode: positive, MALDI extraction voltage: 10 V, hexapole bias: 10 V, laser: 1 kHz, Nd:YAG solid state, 355 nm wavelength with variable pulse energy, 50 μ J @ 1000 Hz, pulse width 2 ns, peak power 25 kW, laser energy: 450 (arb). MassLynx 4.1 (Waters) software was used for data collection.

The obtained MALDI-MS data were processed by MarkerLynx XS software, optional part of MassLynx, allowing extraction, normalization, and alignment of *m/z* values and intensities (formation of data matrix from raw MALDI-MS spectra). The method parameters were set as follows: Analysis type: Combined scan range, peak separation: 0.05 Da, marker intensity threshold: 1000 counts.

Logarithmic transformation was applied. The transformed data matrix was transferred to freeware environment for statistical computing R-project, version 3.5.0 [62] and studied by principal component analysis (PCA) and orthogonal projections to latent structures discriminant analysis (OPLS-DA) (package “muma” [63]). Pareto scaling was used. The outputs were evaluated in the form of appropriate biplots and S-plots. For hierarchical clustering analysis (HCA), the default package “stats” was used. The complete linkage algorithm was applied on the data [62].

3.4. Enzyme-Linked Immunosorbent Analysis

The soil samples from the studied Eneolithic ceramic vessels were tested for the presence of dairy products from cattle. Tests were made using BLOKITS BLG (β -Lactoglobulin, β LG) Assay kit (Neogen Corporation, MI, USA) and R4612 RIDASCREEN Fast Casein (R Biopharm AG, Germany). We used the competitive enzyme-linked immunosorbent assay (ELISA) test. In total, 2 mg of crushed and grinded sample was mixed with 150 ml of extraction buffer (Allergen extraction buffer without additive, concentration 1:10), mixed vigorously using a vortex, and put for 10 min into a water bath thermostated at 60 °C. After incubation, the sample was cooled down (ice water) and centrifuged for 5 s at low speed (1000 RPM). Then, 100 μ L of supernatant was used for the ELISA test. The procedure followed the protocol suggested by the kit producer [64]. β LG-biotin was added to the extract solution as the secondary antibody [38]. Measurements were done on a microtiter plate using ELISA competitive test. Negative reactions were revealed by a specific color (bright yellow). The labelled antigen competed for the primary antibody binding sites with the sample antigen (unlabeled). The samples were measured using an ELISA reader VERSAmax™ (Molecular Devices, San Jose, CA, USA) at 450 nm.

4. Conclusions

Matrix-assisted laser desorption/ionization–mass spectrometry combined with multivariate statistics revealed signals belonging to triacylglycerols in two ceramic Corded Ware beakers with volumes of 0.8 and 0.6 L. Those signals corresponded well with milk fat components formerly found in recent samples. This is the first application of matrix-assisted laser desorption/ionization–mass spectrometry for the analysis of milk fatty residues in ancient ceramic vessels. The enzyme-linked immunosorbent assay proved that the fats in both ceramic vessels originated from dairy products (i.e., positive reaction with casein). Moreover, the ELISA analysis of the soil sample from one Corded Ware beaker (0.6 L) provided a positive response in the β -Lactoglobulin assay. We can suppose that ceramic vessel no. 5 served for storage of bovine milk or dairy products. These results represent the first direct evidence of the utilization of milk products in the Eneolithic period in Moravian Corded Ware culture. Our data related to the utilization of milk in the Early Neolithic–Eneolithic period in Easter Central Europe (the Central Danube Region) significantly extend the former evidence of dairy products usage in Western Central Europe (Germany, Switzerland).

Supplementary Materials: The following are available online.

Author Contributions: Conceptualization, L.K., P.F. and P.B. (Petr Bednar); Methodology, L.K., L.P. V.K. J.P. (Jaroslav Pavelka), D.S.; Investigation, J.P. (Jaroslav Peska), P.F.; Resources, P.F.; Data Curation, P.B. (Petr Bartak), J.B., M.K., P.B. (Petr Bednar); Writing-Original Draft Preparation, L.K., M.K., P.B. (Petr Bednar); Visualization, L.K., J.P. (Jaroslav Peska), P.F., L.P.; Supervision, P.B. (Petr Bednar); Project Administration, J.P. (Jaroslav Peska), P.B. (Petr Bartak), P.B. (Petr Bednar); Funding Acquisition, L.K., J.P. (Jaroslav Peska), P.B. (Petr Bartak), P.B. (Petr Bednar).

Funding: The authors gratefully acknowledge the support of the Czech Science Foundation [17-17346S] and Palacký University Olomouc [IGA_PrF_2018_027] for financial support.

Acknowledgments: We thank Sandra Sázelová (Masaryk University, Brno, CZ) for assessment of the animal bones found within the burial content.

Conflicts of Interest: The authors declare no conflict of interest.

References

1. Stloukal, M. Problematika antropologického rozboru žárových pohřbů. (Výzkum pohřebiště v Moravičanech). *Archeol. Rozhledy* **1968**, *20*, 330–347.
2. Schmidt, C.W.; Symes, S.A. *The Analysis of Burned Human Remains First*; Academic Press: Cambridge, UK, 2008.
3. Parker Pearson, M. *The Archaeology of Death and Burial*; The History Press: Stroud, UK, 2010.
4. Gonçalves, D.; Cunha, E.; Thompson, T.J.U. Weight References for Burned Human Skeletal Remains from Portuguese Samples. *J. For. Sci.* **2013**, *5*, 1135–1140.
5. Gregg, M.W.; Slater, G.F. A New Method for Extraction, Isolation and Transesterification of Free Fatty Acids from Archaeological Pottery. *Archaeometry* **2010**, *52*, 833–854. [[CrossRef](#)]
6. Evershed, R.P.; Arnot, K.I.; Collister, J.; Eglinton, G.; Charters, S. Application of Isotope Ratio Monitoring Gas-Chromatography Mass-Spectrometry to the Analysis of Organic Residues of Archaeological Origin. *Analyst* **1994**, *119*, 909–914. [[CrossRef](#)]
7. Buckley, M.; Melton, N.D.; Montgomery, J. Proteomics analysis of ancient food vessel stitching reveals >4000-year-old milk protein. *Rapid Commun. Mass Spectrom.* **2013**, *27*, 531–538. [[CrossRef](#)]
8. Copley, M.S.; Berstan, R.; Dudd, S.N.; Docherty, G.; Mukherjee, A.J.; Straker, V.; Payne, S.; Evershed, R.P. Direct chemical evidence for widespread dairying in prehistoric Britain. *Proc. Natl. Acad. Sci. USA* **2003**, *100*, 1524–1529. [[CrossRef](#)] [[PubMed](#)]
9. Craig, O.E.; Mulville, J.; Pearson, M.P.; Sokol, R.; Gelsthorpe, K.; Stacey, R.; Collins, M. Archaeology: Detecting milk proteins in ancient pots. *Nature* **2000**, *408*, 312–312. [[CrossRef](#)]
10. Craig, O.E.; Allen, R.B.; Thompson, A.; Stevens, R.E.; Steele, V.J.; Heron, C. Distinguishing wild ruminant lipids by gas chromatography/combustion/isotope ratio mass spectrometry. *Rapid Commun. Mass Spectrom.* **2012**, *26*, 2359–2364. [[CrossRef](#)]
11. Evershed, R.P.; Payne, S.; Sherratt, A.G.; Copley, M.S.; Coolidge, J.; Urem-Kotsu, D.; Kotsakis, K.; Özdoğan, M.; Özdoğan, A.E.; Nieuwenhuys, O.; Akkermans, P.M. Earliest date for milk use in the Near East and southeastern Europe linked to cattle herding. *Nature* **2008**, *455*, 528–531. [[CrossRef](#)]
12. Sauter, F.; Puchinger, L.; Schoop, U.D. Studies in organic archaeometry VI—Fat analysis sheds light on everyday life in prehistoric Anatolia: Traces of lipids identified in chalcolithic potsherds excavated near Bogazkale, Central Turkey. *Arkivoc* **2003**, *15*, 15–21.
13. Oudemans, T.F.M.; Eijkel, G.B.; Boon, J.J. Identifying biomolecular origins of solid organic residues preserved in Iron Age Pottery using DTMS and MVA. *J. Archaeol. Sci.* **2007**, *34*, 173–193. [[CrossRef](#)]
14. Isaksson, S.; Hallgren, F. Lipid residue analyses of Early Neolithic funnel-beaker pottery from Skogsmossen, eastern Central Sweden, and the earliest evidence of dairying in Sweden. *J. Archaeol. Sci.* **2012**, *39*, 3600–3609. [[CrossRef](#)]
15. Salque, M.; Bogucki, P.I.; Pyzel, J.; Sobkowiak-Tabaka, I.; Grygiel, R.; Szmyt, M.; Evershed, R.P. Earliest evidence for cheese making in the sixth millennium BC in northern Europe. *Nature* **2013**, *493*, 522–525. [[CrossRef](#)]
16. Soberl, L.; Gasparic, A.Z.; Budja, M.; Evershed, R.P. Early herding practices revealed through organic residue analysis of pottery from the early Neolithic rock shelter of Mala Triglavca, Slovenia. *Doc. Praehist.* **2008**, *35*, 253–260. [[CrossRef](#)]

17. Mirabaud, S.; Rolando, C.; Regert, M. Molecular criteria for discriminating adipose fat and milk from different species by NanoESI MS and MS/MS of their triacylglycerols: Application to archaeological remains. *Anal. Chem.* **2007**, *79*, 6182–6192. [[CrossRef](#)] [[PubMed](#)]
18. Spangenberg, J.E.; Jacomet, S.; Schibler, J. Chemical analyses of organic residues in archaeological pottery from Arbon Bleiche 3, Switzerland—Evidence for dairying in the late Neolithic. *J. Archaeol. Sci.* **2006**, *33*, 1–13. [[CrossRef](#)]
19. Copley, M.S.; Berstan, R.; Dudd, S.N.; Aillaud, S.; Mukherjee, A.J.; Straker, V.; Payne, S.; Evershed, R.P. Processing of milk products in pottery vessels through British prehistory. *Antiquity* **2005**, *79*, 895–908. [[CrossRef](#)]
20. Copley, M.S.; Berstan, R.; Mukherjee, A.J.; Dudd, S.N.; Straker, V.; Payne, S.; Evershed, R.P. Dairying in antiquity. III. Evidence from absorbed lipid residues dating to the British Neolithic. *J. Archaeol. Sci.* **2005**, *32*, 523–546. [[CrossRef](#)]
21. Agozzino, P.; Avellone, G.; Donato, I.D.; Filizzola, F. Mass spectrometry for cultural heritage knowledge: Gas chromatographic mass spectrometric analysis of organic remains in Neolithic potsherds. *J. Mass Spectrom.* **2001**, *36*, 443–444. [[CrossRef](#)]
22. Salque, M.; Radi, G.; Tagliacozzo, A.; Uria, B.P.; Wolfram, S.; Hohle, I.; Stauble, H.; Whittle, A.; Hofmann, D.; Pechtl, J.; et al. New insights into the Early Neolithic economy and management of animals in Southern and Central Europe revealed using lipid residue analyses of pottery vessels. *Anthropozoologica* **2012**, *47*, 45–61. [[CrossRef](#)]
23. Dallongeville, S.; Garnier, N.; Rolando, C.; Tokarski, C. Proteins in Art, Archaeology, and Paleontology: From Detection to Identification. *Chem. Rev.* **2016**, *116*, 2–79. [[CrossRef](#)]
24. Calvano, CD; van der Werf, I.D.; Palmisano, F.; Sabbatini, L. Revealing the composition of organic materials in polychrome works of art: The role of mass spectrometry-based techniques. *Anal. Bioanal. Chem.* **2016**, *408*, 6957–6981. [[CrossRef](#)]
25. Hong, C.; Jiang, H.; Lü, E.; Wu, Y.; Guo, L.; Xie, Y.; Wang, C.; Yang, Y. Identification of Milk Component in Ancient Food Residue by Proteomics. *PLoS ONE* **2012**, *7*, 1–7. [[CrossRef](#)] [[PubMed](#)]
26. Fremout, W.; Kuckova, S.; Crhova, M.; Sanyova, J.; Saverwyns, S.; Hynek, R.; Kodicek, M.; Vandenabeele, P.; Moens, L. Classification of protein binders in artist's paints by matrix-assisted laser desorption/ionisation time-of-flight mass spectrometry: An evaluation of principal component analysis (PCA) and soft independent modelling of class analogy (SIMCA). *Rapid Commun. Mass Spectrom.* **2011**, *25*, 1631–1640. [[PubMed](#)]
27. Calvano, CD.; van der Werf, I.D.; Palmisano, F.; Sabbatini, L. Identification of lipid- and protein-based binders in paintings by direct on-plate wet chemistry and matrix-assisted laser desorption ionization mass spectrometry. *Anal. Bioanal. Chem.* **2015**, *407*, 1015–1022. [[CrossRef](#)] [[PubMed](#)]
28. Chambery, A.; Maro, A.D.; Sanges, C.; Severino, V.; Tarantino, M.; Lamberti, A.; Parente, A.; Arcari, P. Improved procedure for protein binder analysis in mural painting by LC-ESI/Q-q-TOF mass spectrometry: Detection of different milk species by casein proteotypic peptides. *Anal. Bioanal. Chem.* **2009**, *395*, 2281–2291. [[CrossRef](#)] [[PubMed](#)]
29. Kuckova, S.; Crhova, M.; Vankova, L.; Hnizda, A.; Hynek, R.; Kodicek, M. Towards proteomic analysis of milk proteins in historical building materials. *Int. J. Mass Spectrom.* **2009**, *284*, 42–46. [[CrossRef](#)]
30. Fremout, W.; Dhaenens, M.; Saverwyns, S.; Sanyova, J.; Vandenabeele, P.; Deforce, D.; Moens, L. Tryptic peptide analysis of protein binders in works of art by liquid chromatography–tandem mass spectrometry. *Anal. Chim. Acta* **2010**, *658*, 156–162. [[CrossRef](#)]
31. Child, A.M.; Pollard, A.M. A review of the applications of immunochemistry to archaeological bone. *J. Archaeol. Sci.* **1992**, *19*, 39–47. [[CrossRef](#)]
32. Collins, M.J.; Nielson-Marsh, C.M.; Hiller, J.; Smith, C.I.; Roberts, J.P.; Prigodich, R.V.; Weiss, T.J.; Csapó, J.; Millard, A.R.; Turner-Walker, G. The survival of organic matter in bone. *Archaeometry* **2002**, *44*, 383–394. [[CrossRef](#)]
33. Dongoske, E.K.; Martin, L.D.; Ferguson, J.T. Critique of the Claim of Cannibalism at Cowboy Wash. *Am. Antiquity* **2000**, *65*, 179–190. [[CrossRef](#)]
34. Brandt, E.; Wiechmann, I.; Grupe, G. How reliable are immunological tools for the detection of ancient proteins in fossil bones? *Int. J. Osteoarchaeol.* **2002**, *12*, 307–316. [[CrossRef](#)]
35. Pavelka, J.; Kovačiková, L.; Šmejda, L. The determination of domesticated animal species from a Neolithic sample using the ELISA test. *C. R. Palevol.* **2011**, *10*, 61–70. [[CrossRef](#)]

36. Björklund, E.; Pallaroni, L.; Von Holst, C.; Unglaub, W. Method of determination of appropriate heat treatment of animal meal by immunoassay developed for detection of cooked beef: Interlaboratory study. *J. AOAC Int.* **2001**, *84*, 1835–1839.
37. Pavelka, J.; Šmejda, L.; Hýnek, R.; Kučková, Š.H. Immunological detection of denatured proteins as a method for rapid identification of food residues on archaeological pottery. *J. Archaeol. Sci.* **2016**, *73*, 25–35. [[CrossRef](#)]
38. Burger, J.; Kirchner, M.; Bramanti, B.; Haak, W.; Thomas, M.G. Absence of the lactase-persistence-associated allele in early Neolithic Europeans. *Proc. Natl. Acad. Sci.* **2007**, *104*, 3736–3741. [[CrossRef](#)]
39. Gamba, C.; Jones, E.R.; Teasdale, M.D.; McLaughlin, R.L.; Gonzalez-Fortes, G.; Mattiangeli, V.; Domboróczki, L.; Kővári, I.; Pap, I.; Anders, A.; et al. Genome flux and stasis in a five millennium transect of European prehistory. *Nat. Commun.* **2014**, *5*, 1–9. [[CrossRef](#)]
40. Witas, H.W.; Płoszaj, T.; Jedrychowska-Dańska, K.; Witas, P.J.; Masłowska, A.; Jerszyńska, B.; Kozłowski, T.; Osipowicz, G. Hunting for the LCT-13910*T Allele between the Middle Neolithic and the Middle Ages Suggests Its Absence in Dairying LBK People Entering the Kuyavia Region in the 8th Millennium BP. *PLoS ONE* **2015**, *10*, e0122384. [[CrossRef](#)]
41. Itan, Y.; Powell, A.; Beaumont, M.A.; Burger, J.; Thomas, M.G. The Origins of Lactase Persistence in Europe. *PLoS Comput. Biol.* **2009**, *5*, e1000491. [[CrossRef](#)]
42. Malmström, H.; Linderholm, A.; Lidén, K.; Storå, J.; Molnar, P.; Holmlund, G.; Jakobsson, M.; Götherström, A. High frequency of lactose intolerance in a prehistoric hunter-gatherer population in northern Europe. *BMC Evol. Biol.* **2010**, *10*, 1–6. [[CrossRef](#)]
43. Haug, A.; Høstmark, A.T.; Harstad, O.M. Bovine milk in human nutrition—A review. *Lipids Health Dis.* **2007**, *6*, 25. [[CrossRef](#)]
44. Rozenberg, S.; Body, J.J.; Bruyere, O.; Bergmann, P.; Brandi, M.L.; Cooper, C.; Devogelaer, J.P.; Gielen, E.; Goemaere, S.; Kaufman, J.M.; et al. Effects of Dairy Products Consumption on Health: Benefits and Beliefs—A Commentary from the Belgian Bone Club and the European Society for Clinical and Economic Aspects of Osteoporosis, Osteoarthritis and Musculoskeletal Diseases. *Calcif. Tissue Int.* **2016**, *98*, 1–17. [[CrossRef](#)] [[PubMed](#)]
45. Holden, C.; Mace, R. Phylogenetic Analysis of the Evolution of Lactose Digestion in Adults. *Hum. Biol.* **1997**, *81*, 597–619. [[CrossRef](#)] [[PubMed](#)]
46. Mielke, J.H.; Konigsberg, L.W.; Relethford, J.H. *Human Biological Variation*, 2nd ed.; Oxford University Press: Oxford, UK, 2011.
47. Selhub, E.M.; Logan, A.C.; Bested, A.C. Fermented foods, microbiota, and mental health: Ancient practice meets nutritional psychiatry. *J. Physiol. Anthropol.* **2014**, *33*, 2. [[CrossRef](#)]
48. Kučera, L.; Kurka, O.; Barták, P.; Bednář, P. Liquid chromatography/high resolution tandem mass spectrometry—Tool for the study of polyphenol profile changes during micro-scale biogas digestion of grape marcs. *Chemosphere* **2017**, *166*, 463–472. [[CrossRef](#)]
49. Picariello, G.; Sacchi, R.; Addeo, F. One-step characterization of triacylglycerols from animal fat by MALDI-TOF MS. *Eur. J. Lipid Sci. Technol.* **2007**, *109*, 511–524. [[CrossRef](#)]
50. Chochorowski, J. *Ekspansja Kimmeryjska na Tereny Europy Środkowej*; Rozprawy Habilitacyjne Nr 260; Uniwersitet Jagielloński: Kraków, Poland, 1993.
51. Archeologický Ústav Akademie Věd České Republiky v Brně, Přehled Výzkumů. Available online: https://www.google.com.tw/url?sa=t&rct=j&q=&esrc=s&source=web&cd=1&ved=2ahUKEwiTgfv3tI3fAhVKE7wKHSTVCm0QFjAAegQIABAC&url=http%3A%2F%2Farub.avcr.cz%2Fmiranda2%2Fexport%2Fsitesavcr%2Farub%2Fprehled-vyzkumu%2Fprehled-vydanych-cisel%2Ffiles%2FPV-57-1_eneolit.pdf&usq=AOvVaw3s5mcRvYzCL62g0TySTvqf (accessed on 7 December 2018).
52. Chochol, J. Dosavadní výsledky anthropologického rozboru lužických žárových pohřbů z českých zemí. *Památky Archeol.* **1955**, *49*, 559–582.
53. Dokládál, M. *Morfologie Spálených Kostí: Význam pro Identifikaci Osob*; Masaryk University: Brno, Czech Republic, 1999.
54. Symes, S.A.; Rainwater, C.W.; Chapman, E.N.; Gipson, D.R.; Piper, A.L. Patterned thermal destruction of human remains in a forensic setting. In *The Analysis of Burned Human Remains*; Academic Press: San Diego, CA, USA, 2008; pp. 15–54.

55. Walker, P.L.; Miller, K.W.P.; Richman, R. Time, Temperature, and oxygen availability: An experimental study of the effects of environmental conditions on the color and organic content of cremated bone. In *The Analysis of Burned Human Remains*; Academic Press: San Diego, CA, USA, 2008; pp. 129–135.
56. Adams, B.J.; Byrd, J.E. *Recovery, Analysis, and Identification of Commingled Human Remains*; Humana Press: New York, NY, USA, 2008.
57. Lewis, M.J.; Senn, D.R. Dental age estimation. In *Manual of Forensic Odontology*, 5th ed.; CRC Press: Boca Raton, FL, USA, 2013; pp. 211–255.
58. Pars petrosa kosti spánkové v žárových hrobech. Available online: <https://is.muni.cz/th/mp8x9/?so=nx> (accessed on 7 December 2018).
59. Polcerová, L.; Králík, M.; Stabrava, P. Semi-Automatic Measurement of Cremated Human Remains Found on Archaeological Site of the Lusatian Culture near Town Příbor. *Pravěk NŘ* **2016**, *24*, 151–174.
60. Norén, A.; Lynnerup, N.; Czarnetzki, A.; Graw, M. Lateral Angle: A Method for Sexing Using the Petrous Bone. *Am. J. Phys. Anthropol.* **2005**, *128*, 318–323. [[CrossRef](#)]
61. Stubiger, G.; Belgacem, O. Analysis of lipids using 2,4,6-trihydroxyacetophenone as a matrix for MALDI mass spectrometry. *Anal. Chem.* **2007**, *79*, 3206–3213. [[CrossRef](#)]
62. R Core Team. *R: A Language and Environment for Statistical Computing*; R Foundation for Statistical Computing: Vienna, Austria, 2018.
63. Gaude, E.; Chignola, F.; Spiliotopoulos, D.; Mari, S.; Spitaleri, A.; Ghitti, M. muma: Metabolomics Univariate and Multivariate Analysis. Available online: <https://CRAN.R-project.org/package=muma> (accessed on 5 December 2018).
64. RIDASCREEN Fast Casein. *Enzyme Immunoassay for the Quantitative Determination of Casein*; R Biopharm AG: Darmstadt, Germany, 2016.

Sample Availability: Samples are not available from the authors.



© 2018 by the authors. Licensee MDPI, Basel, Switzerland. This article is an open access article distributed under the terms and conditions of the Creative Commons Attribution (CC BY) license (<http://creativecommons.org/licenses/by/4.0/>).



“Gold corrosion”: An alternative source of red stains on gold coins

Lukáš Kučera^a, Jan Rozsypal^a, Petr Bednář^a, Matěj Březina^b, Lukáš Kalina^b, Petr Bezdička^c, Miroslav Mašláň^a, Lukáš Richtera^{d,e,*}

^a Department of Analytical Chemistry, Faculty of Science, Palacký University, 17. listopadu 12, 779 00, Olomouc, Czech Republic

^b Materials Research Centre, Faculty of Chemistry, Brno University of Technology, Purkyňova 118, 612 00, Brno, Czech Republic

^c Institute of Inorganic Chemistry of the Czech Academy of Sciences, Husinec-Řež 1001, 250 68 Husinec-Řež, Czech Republic

^d Department of Chemistry and Biochemistry, Mendel University in Brno, Zemědělská 1, 613 00 Brno, Czech Republic

^e Central European Institute of Technology, Brno University of Technology, Technická 123, 612 00 Brno, Czech Republic

ARTICLE INFO

Keywords:

Corrosion
Gold
Defects
Red stains
Minting

ABSTRACT

Recently, the phenomena of red stains defects was found on historical and modern golden coins around the world. This “Gold corrosion” can be the reason for reduction of coin value, especially of modern high-premium coins. In such modern investment coins, the contamination of the surface by microscopic particles of metallic silver is reported to be a common cause of such stains. Corrosion of these particles (or even back reduction) is associated with a distinct change of colour. In the case of historical coins, this relatively simple explanation does not respond in some cases. The submitted study is dealing with analysis of red stains on of Austro-Hungarian gold ten crowns coins, which served as a common part of circulating currency. They were therefore minted in thousands/million pieces by standard procedures each year. It is therefore quite logical that these coins can have different mechanisms of red spots formation than modern high-premium coins. Red stains on Austro-Hungarian coins were analysed by the means of light (LM) and digital microscopy (DM), energy-dispersive X-ray spectroscopy (EDS), energy dispersive X-ray fluorescence spectroscopy (XRF), atomic force microscopy (AFM), X-ray photoelectron spectroscopy (XPS), Mössbauer spectroscopy, X-ray powder micro-diffraction (μ -XRPD) and Raman microscopy. The EDS, XRF and XPS analysis points to the presence of iron and oxygen in red stains, no silver or its corrosion products were detected. The exact determination of red stains was done by μ -XRPD and Raman microscopy where an iron(III) oxide-hydroxide (Goethite) was found as main product.

1. Introduction

In recent years, the phenomena “Gold corrosion” was studied in more details. All these studies provide direct evidence that the corrosive spots are mainly formed by silver sulphide (Ag_2S) and in some cases silver oxide, silver chloride, silver sulphate or copper sulphide [1–10]. This conclusion is in good agreement with the long term generally accepted hypothesis about the possible origin of these unwanted stains [1]. Note, that authors [9] detect next to silver and copper also traces of iron in red stain. Nevertheless, the iron was taken as a contamination rather than a main corrosion product [9]. All these published results are contrary to the fact, that the spots cannot be always eliminated by conventional treatment, i.e. solution of 20 % citric acid in water, 25 % ammonium solution or mixture of concentrated potash and sulphuric acid in ratio 1:2 (v/v) [1]. The fact that many modern gold coins of high fineness (Au 999.9) are after some time affected by red spots as well as the historical ones (hundreds of years old) shows that later formation of these spots is not necessarily connected with silver present in the alloy. The

most probable origin of red spots on the surface of gold coins is pushing of tiny silver particles into the gold matrix during the machining operations (milling, rolling or punching). Consequently, the silver is transformed to Ag_2S by sulphide compounds (H_2S and related compounds) or to Ag_2SO_4 [3,6,8]. Note, that besides oxidization of silver and formation of related corrosion products on the surface of gold coin also the reduction of those compounds due to the photochemical processes and formation of thin layer of pure silver can occur. Red colour of these spots is caused by interference phenomena. The red stains were already found on historical and modern golden coins around the world. Those defects can highly affect the value of modern gold coins, especially in the production of modern high-premium coins (high value collectible and investment coins), and additionally the coins are in some cases marked as copy due to the red stains on the surface. The crucial problem is that it takes long time (usually several years) to make these spots visible. Coins therefore leave the mint or distributor’s stores seemingly defect-free, and stains are latent. When the stains will occur on purchased gold coins in the hands of the customer, the usual argument of retail-

* Corresponding author at: Department of Chemistry and Biochemistry, Mendel University in Brno, Zemědělská 1, 613 00 Brno, Czech Republic.
E-mail address: richtera@mendelu.cz (L. Richtera).

<https://doi.org/10.1016/j.mta.2021.101025>

Received 16 October 2020; Accepted 31 January 2021

Available online 1 February 2021

2589-1529/© 2021 Acta Materialia Inc. Published by Elsevier B.V. All rights reserved.

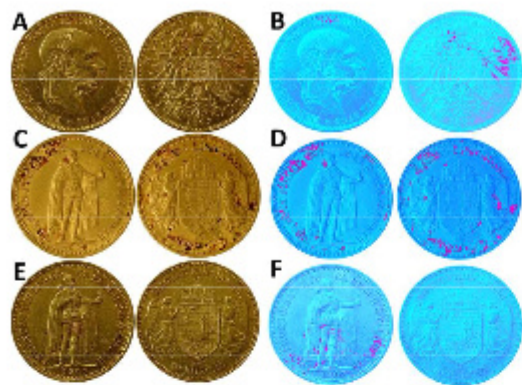


Fig. 1. Three Austro-Hungarian 10 Corona (Vienna mint) dated 1897 (A, B) and 10 Korona 1905 (C, D) and 1907 (E, F) (Kremnica mint). The false-coloured pictures B, D, F present highlighted places affected by corrosion (purple) (For interpretation of the references to color in this figure legend, the reader is referred to the web version of this article.).

ers and mints is that this was due to improper handling or improper storage. However, this is only an excuse, the presence of these impurities means a technological error in coins production, pure 0.999 gold coins could not show corrosion even after removal and improper storage or handling. Highlight that, red stains were also found on investment gold coins closed in the original etui (placed in directly in mint) that never were taken out. At present, the mints are aware of their misconduct by supporting various studies and are trying to implement control measures to varying degrees. Different studies identically recommend the same precaution - total separation of gold and silver coinage [3,8]. Other recommendations include enhanced air quality control and microscopic metal particle filtration [7]. In presented study, “corroded” gold coins were characterized by energy dispersive X-ray fluorescence spectroscopy (XRF), visible light (LM) and digital (DM) microscopy, scanning electron microscopy combined with energy-dispersive X-ray spectroscopy (SEM/EDS), X-ray photoelectron spectroscopy (XPS), Raman microscopy, X-ray powder micro-diffraction (μ -XRPD), atomic force microscopy (AFM) and Mössbauer spectroscopy to point out on the new origin of red stains.

2. Experimental

2.1. Coin under study

The studied material consist of three Austro-Hungarian gold ten crowns coins dated to 1897, 1905 and 1907 (Fig. 1), which served as a common part of circulating currency, that were minted in thousands/million pieces (specifically the mintage amount was for 10 C 1897: 1,803,000 pieces, 10 K 1905: 868,624 pieces and 10 K 1907: 752,217 pieces). Parameters of all coins were as follows: diameter 19 mm, thickness 0.9 mm, weight 3.39 g, purity Au 900/1000 (gold-copper alloy), Austrian 10 C was minted in Vienna mint (Fig. 1A-B) and Hungarian 10 K in Kremnica mint (Fig. 1C-F). For completeness it is worth noting that the parameters of gold circulation coins differed in different countries in 19th and 20th centuries, but the purity of 0.900 was usually the same for these coins intended for ordinary payments. Likewise, the technology used to produce and mint these coins was comparable in most mints at that time.

2.2. Scanning electron microscopy combined with Energy-dispersive X-ray spectroscopy (SEM/EDS)

Measurements were performed by ZEISS EVO LS 10 (Carl Zeiss Microscopy GmbH, Jena, Germany). The EDS analysis was performed using SEM-EDS with energy-dispersive analyser OXFORD X-Max 80 mm²

(Oxford Instruments, Abingdon, United Kingdom). The detection limit of major and minor elements is 0.1 %. Analysis parameters: Accelerating voltage 20 kV, working distance 12 mm, detector dead time approximately 50 %, effective acquisition time 100 s, average count rate 10,000 cps, beam current 7.5 nA. Quantitative calibration was performed on the silicon monocrystal. The measured data were analysed using Oxford AZtec software, the accuracy of measurement is 0.5 wt %, with the exception of carbon and oxygen. These elements can be detected qualitatively but with limited quantitative value. This is due to the built-up effect of carbon and oxygen compounds on the analysed sample in SEM. The typical margin of error for these elements is therefore approximately 3 wt %.

2.3. Light (LM) and digital microscopy (DM)

Surface analysis of golden coins was performed in terms of light optical microscopy (LM). ZEISS Stemi-2000C light optical microscope with additional light source was used for the coins observation. Surface observation was performed on ethanol cleaned coins using the additional light source for surface relief and colour differences revealing. The digital optical microscope (DM) VHX-5000 (Keyence, Japan) was used for image acquisition. A high-resolution zoom lens (VH-Z500R) was used to obtain images with the following parameter settings: 3D Image Stitching with a pitch of 0.2 μ m was used as the capture mode, magnification ranged from 1000–5000 \times , for the analysis of the images was used Keyence image acquisition software.

2.4. Atomic force microscopy (AFM)

AFM measurements of coin topography and surface potential were performed using Dimension Icon atomic force microscope (Bruker), equipped with Kelvin probe force microscopy (KPFM) module. Topography was obtained in Tapping Mode and surface potential was measured in Tapping Mode combined with LiftMode using amplitude modulated KPFM (KPFM-AM). Both operations were carried out with electrically conductive SCM-PIT-V2 antimony doped silicon probe, coated in platinum-iridium, with resonance frequency 50–100 kHz and spring constant 1.5–6.0 N m⁻¹. The data were processed using NanoScope Analysis software (all Bruker Corporation, Billerica, MA, USA).

2.5. X-ray photoelectron spectroscopy (XPS)

XPS analyses were carried out with Axis Ultra DLD spectrometer (Schimadzu, Japan) using a monochromatic Al K α ($h\nu = 1486.7$ eV) X-ray source operating at 150 W (10 mA, 15 kV). The spectra were obtained using an analysis area of approx. 300 \times 700 μ m. The high resolution spectra were measured with the step size 0.1 eV and 20 eV pass energy. Instrument base pressure during the measurements was consistently at 2 \cdot 10⁻⁸ Pa. Spectra were analyzed using CasaXPS software (version 2.3.15) and have been charge corrected to the main line of the carbon C 1s spectral component (C–C, C–H) set to 284.80 eV. A standard Shirley background was used for all sample spectra.

2.6. X-ray powder micro-diffraction (μ -XRPD)

Diffraction patterns were collected with a PANalytical X'PertPRO diffractometer equipped with a conventional X-ray tube (CoK α radiation, 1.7890 Å, 40 kV, 30 mA, point focus). A glass collimating monochromator with the length of 165 mm and the exit diameter of 0.1 mm was used in the primary beam. A multichannel position sensitive detector X'Celerator with an anti-scatter shield and the Fe beta filter was used in the diffracted beam. X-ray patterns were taken between 4 and 80 \cdot 2 θ with 0.0334 \cdot step and 2,200 s counting time per step that produces total counting time of about 11.25 h. Patterns were not pre-treated before interpretation, as no background correction was needed. Qualitative-phase analysis was performed using HighScorePlus software package

(Malvern PANalytical, the Netherlands, version 4.8.0) and the current PDF4+ database [11]. More details about the experimental procedure has been published by Švarcová et al. [12,13]. Estimation of weight fractions (quantitative phase analysis) was performed using the Rietveld method. The Profex / BGMN code was used for all calculations [14]. Structural models were taken from the PDF4+ database [11].

2.7. Raman microscopy

The selected areas on gold coins were analysed using DXR2 Raman microscope (Thermo Scientific, MA, USA) in imaging mode. The parameters of measurement were as follows: Laser 785 nm, laser energy 10 mW, aperture 50 μm Slit, collect exposure time 2 s, sample exposures 16, step in X-Y dimension 20 μm , objective with magnification 10 \times , thermoelectric-cooled CCGD detector. The data were measured and evaluated in Omnic 9 software for Dispersive Raman microscopy (Thermo Scientific, MA, USA).

2.8. Energy dispersive X-ray fluorescence spectrometer (ED-XRF)

An elemental analyser SPECTRO XEPOS energy dispersive X-ray fluorescence spectrometer (SPECTRO Analytical Instruments GmbH, Kleve, Germany) equipped with a 10 mm² Si-Drift Detector with Peltier cooling and a 75 μm Be side window was employed. The instrument uses a Pd-target end window tube at a maximum power of 50 W and a maximum voltage of 50 kV. Spectral resolution of the instrument (FWHM) is < 170 eV for Mn K α (measured under input count rate 10,000 pulses). SPECTRO XEPOS was operated and data were evaluated by means of the software Spectro X-Lab Pro, Version 2.5. For light elements excitation (Mg–V, tube voltage 24.82 kV, tube current 1.00 mA, measurement duration 200 s, impulse rate \leq 16,775 cps, relative dead time \leq 10.6 %, peak time 2 μs , gain 12.5 eV channel⁻¹, zero peak rate 5000 cps) HOPG (Highly Oriented Pyrolytic Graphite) crystal target was used. For heavier elements determination Mo secondary target (Cr–Y, Hf–U, tube voltage 44.70 kV, tube current 0.55 mA, measurement duration 200 s, impulse rate \leq 26,382 cps, relative dead time \leq 15.4 %, peak time 2 μs , gain 25.0 eV channel⁻¹, zero peak rate 5000 cps) and Al₂O₃ polarisation target (Zr–Ce, tube voltage 49.16 kV, tube current 0.50 mA, measurement duration 400 s, impulse rate \leq 667 cps, relative dead time \leq 0.9 %, peak time 2 μs , gain 50.0 eV channel⁻¹, zero peak rate 5000 cps) was used. Samples were measured in vacuum using the so-called Turboquant method (fundamental parameters method).

In the case of analysis of small areas, an aperture of pure molybdenum sheet (99.9% Mo, 3.6 \times 3.6 cm, 0.1 mm thickness, Koch-Light Laboratories Ltd., Colnbrook, Buckinghamshire, England) with an approximately square gap with area of 10.5 mm² was used to accurately demarcate analysed area. The aperture was placed directly on the coin surface and fixed with adhesive tape to prevent unwanted movement.

2.9. Mössbauer spectroscopy

Backscattering ⁵⁷Fe Mössbauer spectrum was measured by a system employing MS96 Mössbauer spectrometer [15] operating in a constant acceleration mode and equipped with a ⁵⁷Co(Rh) source at room temperature. The gas proportional counter, which registers 6.3 keV conversion x-ray, was used for accumulation of backscattering spectra. The acquired Mössbauer spectra were evaluated using the MossWinn software program [16]. The isomer shift values were referred to the centroid of the spectrum recorded from an α -Fe foil (thickness 30 μm) at room temperature.

3. Results and discussion

3.1. Chemical analysis of red stain

Gold coins affected by the red stains were investigated in the context of the present study by means of LM, DM, Raman microscopy, SEM/EDS,

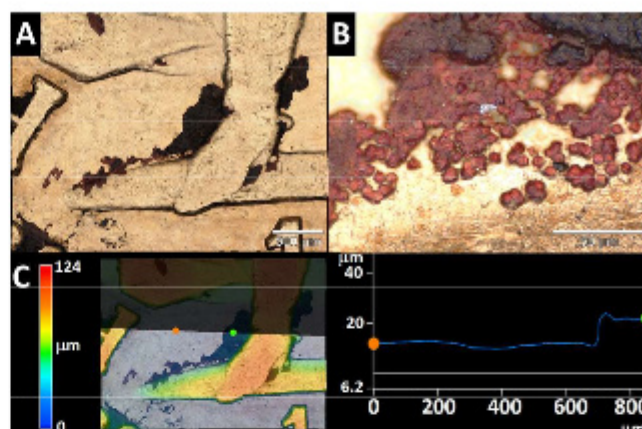


Fig. 2. (A) Optical image of red corrosion products on surface of gold Hungarian 10 K 1907, (B) cubic structure of crystals of red product, (C) height profile clear surface of coin – red stain (For interpretation of the references to color in this figure legend, the reader is referred to the web version of this article.).

XPS, XRF, AFM, μ -XRPD and Mössbauer microscopy. The coins in this study were covered by red stains in larger scale (i.e. Austrian Corona from 1897 and Hungarian Korona from 1905 and 1907, Fig. 2A). The area of spots on individual coins included in this study is summarized in Supplementary (Supplement 1). In higher magnification a cubic structure of crystals of a red product can be found (Fig. 2B). The height profile of red stain on gold coin (10 K 1907) is shown on Fig. 2C. The thickness of corrosion layer is about 14 μm in that case but it is not uniform, differs depending on the location, the degree of corrosion and also varies from coin to coin. Given the considered origin of corrosion, these differences are understandable and expected. These corrosive products cannot be removed mechanically without damaging the coin, they hold firmly on the surface of the material.

AFM technique was used for detailed determination of morphology and surface potential in affected areas by “corrosion”. The scanned area was selected using an optical microscope that is a part of instrument, in order to scan both corroded and clean surface in a single run (Fig. 3A, D, G). The recorded topographic images show the flat surface of the gold coin and then the markedly elevated corroded parts (Fig. 3B, E, H). The height difference is approximately 1.7, 2.2 and 4.6 μm for gold coins minted in 1897, 1905 and 1907, respectively. Note, that those values are roughly 12–33 times lower than determined height from digital microscopic analysis. This difference in the determination of the height profile may be due to the measurement of the relatively smaller area and edge of the spot using the AFM technique compared with DM. On the contrary the thickness measurement in DM can be highly affected by reflection (i.e. DM cannot focus exactly). Simultaneously obtained surface potential map (Fig. 3C, F, I) shows a striking difference between corroded part (red) and the rest of the scanned area (violet) which is, based on higher potential, made of more noble metals.

The determination of the chemical composition of red stains was in the first step performed by XRF with Mo aperture. The XRF instrument Spectro Xepos does not allow the exact localization of X-ray beam on sample and relatively large area is measured (see below). Even if the measurement in this way is possible and is able to confirm the presence of Fe on coins stained with red spots, the results are not very convincing. So for the precise definition of area of interest a Mo aperture was created (approx. hole size 3.1 \times 3.3 mm, exactly 10.5 mm²), which was placed directly on the surface of the coin. For maximizing of X-ray beam the Mo aperture was fixed in the measuring space of the instrument to ensure that the incident radiation was in maximum level. The measurement shows higher content of iron in all three gold coin samples (notice that in all cases silver was under the limit of quantification). For better comparison of areas with red stains and without them and for determina-

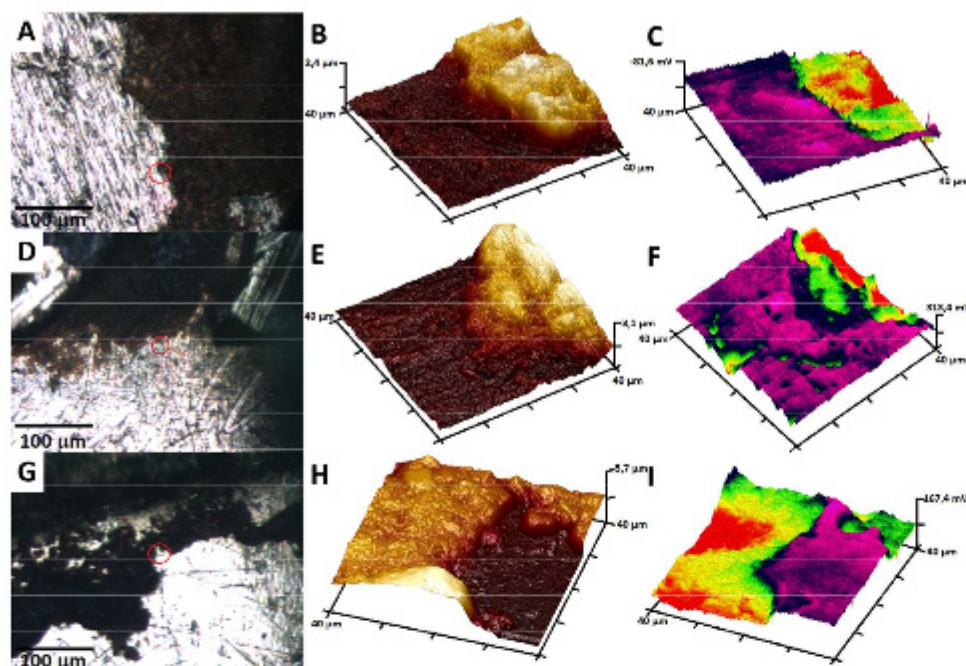


Fig. 3. Optical, 3D topography image obtained by Tapping Mode AFM and 3D potential map of a coin 1897 (A, B, C), 1905 (D, E, F) and 1907 (G, H, I), respectively (For interpretation of the references to color in this figure legend, the reader is referred to the web version of this article.).

Table 1

Au/Cu and Au/Fe ratios (ratio of each element intensity - counts) of red stains and pure golden surface of three-coin samples measured by XRF.

Sample (Coin)	Place	Au/Cu ratio	Au/Fe ratio
10 C 1897	red stain "letter X"	6.5	53
	pure golden surface	6.0	132
10 K 1905	red stain "letter EF"	8.4	9
	red stain "wing"	8.1	14
10 K 1907	pure golden surface	8.3	141
	red stain "boots"	8.7	27
	red stain "pants"	8.7	43
	pure golden surface	9.0	121

Table 2

Element content of red stains on gold coin samples measured by SEM/EDS (shown in mass %).

	10 C 1897		10 K 1905		10 K 1907	
Fe	33.44	± 0.15	43.46	± 0.20	46.45	± 0.19
O	32.93	± 0.16	34.26	± 0.17	32.72	± 0.15
Au	20.10	± 0.16	n.d.	± n.d.	n.d.	± n.d.
C	10.42	± 0.23	20.28	± 0.26	17.29	± 0.27
Cu	1.45	± 0.08	n.d.	± n.d.	n.d.	± n.d.
Ag	0.42	± 0.07	n.d.	± n.d.	n.d.	± n.d.

tion of origin of Fe a ratio of Au/Cu and Au/Fe counts was calculated. The Au/Cu ratio shows the roughly same value for intact surface and red stain (Table 1) and it excludes the formation of red stains by these Cu and Ag. On the other hand, the ratio Au/Fe in regions of red stains is roughly 2–15 times lower compared to intact region which clearly demonstrates the presence of iron in the stains (Table 1). The measured areas are shown in Fig 4.

SEM combined with EDS was used for red stains analysis. As in the previous case high content of iron (together with oxygen) was found, i.e. 33.4, 43.5 and 46.5 % of Fe, 32.9, 34.3 and 32.7 % of O for 10 C 1897, 10 K 1905 and 10 K 1907, respectively. Table 2 shows the mass percentage amount Fe, O, Au, C, Cu and Ag. The remaining percentages up to 100 are common minor elements (K, Na, Cl, Si, Al, Ca, N, Mg, P) occurring on objects of normal use (common surface contamination

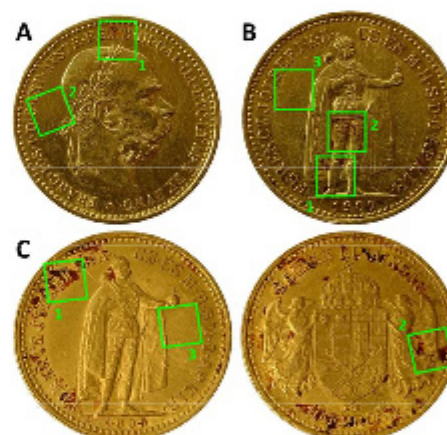


Fig. 4. Definition of measured areas by XRF on 10 Corona 1897 (A, 1 - red stain "letter X", 2 - pure golden surface), 10 Korona 1907 (C, 1 - red stain "boots", 2 - red stain "pants", 3 - pure golden surface) and 10 Korona 1905 (B, 1 - red stain "letter EF", 2 - red stain "wing", 3 - pure golden surface) (For interpretation of the references to color in this figure legend, the reader is referred to the web version of this article.).

with e.g. human sweat, dust and other impurities). Distribution of iron, oxygen, carbon, copper, silver and gold in analysed areas was determined on 10 C 1897, region "EX" by elemental mapping measurement (Fig. 5). The obtained results clearly show that iron and oxygen are situated only in red stains. Other elements originate from gold alloy used for minting are impurities from circulation and contact with other subjects (Fig. 5B,C). Note, that silver is in the analysed region of gold coin 1897 barely visible and for remaining two gold coins (1905 and 1907) is silver again under limit detection. This result completely refutes the theory that red spots on coins are caused only by Ag or Cu based corrosion products. In the case of circulating coins, it is important to note that any inconsistent remnants of silver on the surface of the coin may also be due to abrasion. During the validity of these gold coins, silver 1, 2 and 5 crown coins (in addition to small coins made of base metals) were also in circulation.

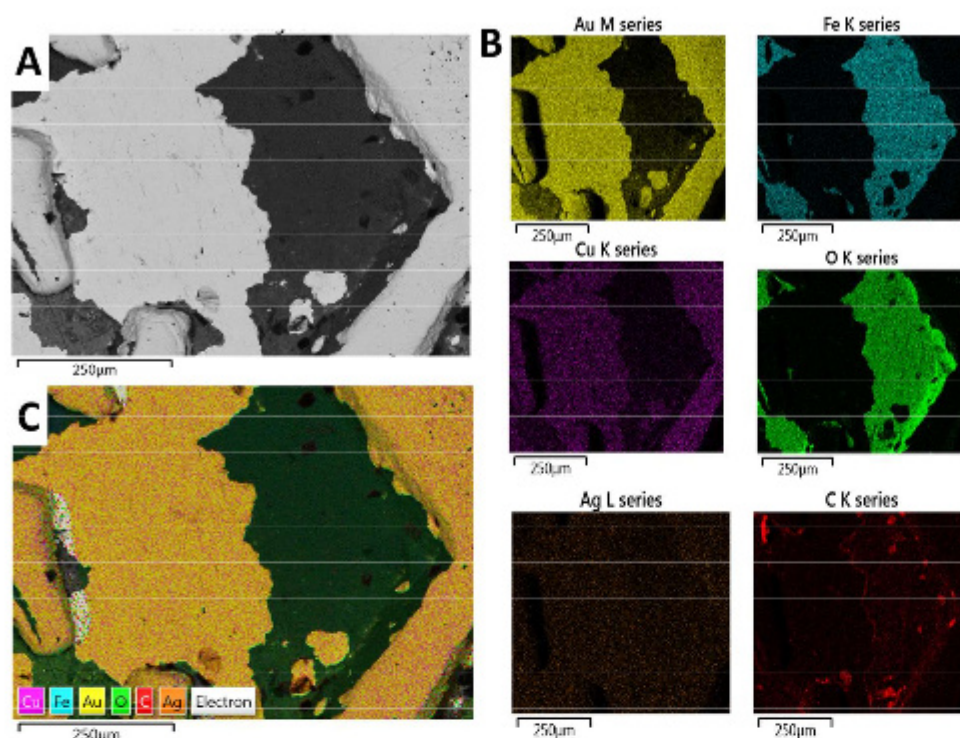


Fig. 5. EDS mapping: Distribution of iron, oxygen, carbon, copper, silver and gold in analysed area between E and X letter on 10 C 1897 (For interpretation of the references to color in this figure legend, the reader is referred to the web version of this article.).

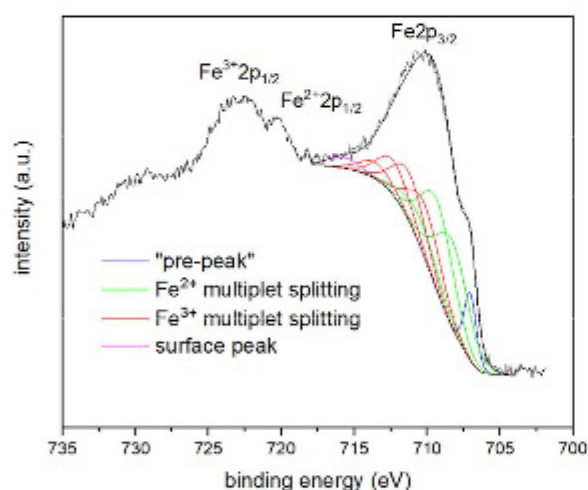


Fig. 6. XPS spectrum of red corrosion products on gold Hungarian 10 K 1907 (For interpretation of the references to color in this figure legend, the reader is referred to the web version of this article.).

Fig. 6 shows the high resolution XPS Fe2p spectra of measured samples. The oxidation states of iron are determined based on Gupta and Sen multiplet peak parameters [17]. The iron is presented mainly in the oxidation state Fe^{3+} . However, due to the usage of an argon ion beam for the cleaning of samples, the composition change occurred. In a multi-elemental material, elements may sputter at different rates, and hence change the stoichiometry of the analysed surface. In the case of transition metal oxides, such as iron oxides, oxygen atoms typically sputter at a higher rate than the metal atoms, leading to a reduction of the metal's oxidation state. That is the reason why the Fe^{2+} oxidation state is also detected. During the fitting process, a peak reporting to surface structures was added to fill the rest of the envelope. The single low intensity peak on the low binding energy ("pre peak") was also added to the account as well. This peak includes changes in surface structure caused

under the cover of inert gas. Those results confirm the assumption that red stains are formed by iron. Note, that Mössbauer spectroscopy was also applied on analysis of red spots. However, the detailed characterization of those products was problematic by this technique due to the small size of measured area (red stain size). Based on the isomer shift $0.34 \pm 0.02 \text{ mm s}^{-1}$ we can assume that red spot could be formed by iron compound (probably Fe_2O_3) and the particles (crystals) are smaller than 100 nm (quadrupole splitting $0.63 \pm 0.03 \text{ mm s}^{-1}$). Even, if the Mössbauer spectroscopy could not unequivocally identify chemical composition of red stains, it is another technique that points to the presence Fe corrosion products in red spots. It is consistent with results from other techniques used in this article (**Supplement 2**).

Raman microscopy was applied to analyse the red stains. Goethite can be easily identified in Raman spectrum by peak at 385 cm^{-1} [18]. Nevertheless, sometimes goethite peaks are overlapped by hematite peak at 412 cm^{-1} (Fe–O vibration). In our samples the most significant signal at 394 cm^{-1} was found. This signal belongs to Fe–O/OH. The same signal shift in goethite samples was already described by Sklute et al. [19]. The spectrum pattern from red stains region (i.e. signals of Fe–O at 238, 297, 394 and 549 cm^{-1}) was also found in reference goethite spectrum (RRUFF Raman Minerals signals [20]). Note, that increasing of laser energy from 10 to 20 mW cause the transformation of goethite to hematite, that can be observed by changing the ratio of signals $394/293 \text{ cm}^{-1}$ (**Fig. 7**). The results from Raman microscopy imaging show consistent distribution of goethite in red stains at signal 394 cm^{-1} (**Fig. 8A–C**). For an unambiguous confirmation of the phase composition of iron corrosion product, the $\mu\text{-XRPD}$ was used. **Fig. 9** shows the spectra of pure metal and two regions with red stains. Comparison of spectra with reference spectrum of goethite clearly confirm the presence of iron oxyhydroxide in red stains.

3.2. Origin of red stains on surface of gold ten-crowns

For an explanation of the presence of iron particles in a gold alloy can be used analogous information as mentioned Gusmano et al. in their work [6]. The iron particles may contaminate the gold alloy during the casting of gold in the iron mould. The solubility of iron in gold at the

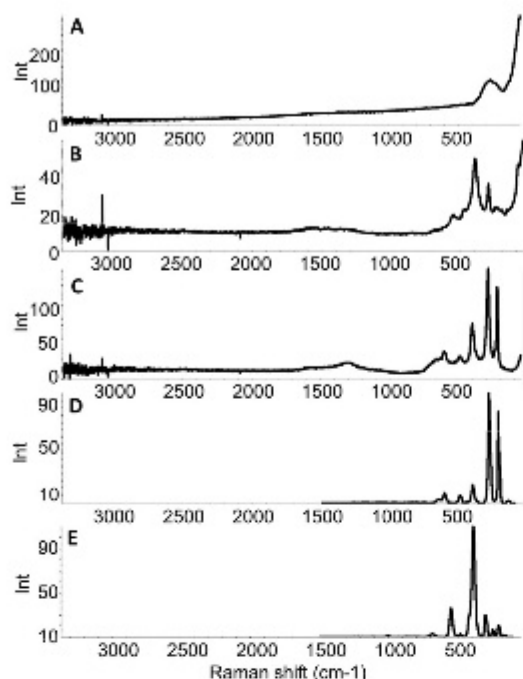


Fig. 7. Raman spectra of 10 Korona 1905 and reference materials. (A) area of pure gold, (B) analysis of red stain with laser energy 10 mW, (C) analysis of red stain with laser energy 20 mW, (D) spectrum of hematite standard, (E) spectrum of goethite standard.

melting temperature of gold is very high – several percent [21]. With decreasing temperature, the solubility of iron in gold decreases rapidly. During cooling, the iron particles in the melted gold start to segregate. After gold flans production iron particles that are present directly at the surface are cleaned by diluted nitric acid, but the particles that are deeper and covered by a thin gold layer are not etched with acid but can be uncovered during minting process (thereafter oxidize) or later due wiping coins in circulation. The fact that red spots sometimes appear on gold bars may speak in part in favor of this alternative. Unfortunately, we did not have the opportunity to analyse any such ingot with corrosion. However, given the technology of making gold bars, it is quite likely that at least some of the stains on these ingots could have their origin in iron based corrosion products. Another alternative how iron particles could be clogged into the gold strips is forcing-in of microscopic metal chips released from the steel machine parts serving for rolling golden strips or from steel punches. Due to fatigue of material, defects may occur resulting in the delamination of steel scales which are then moulded into coins. Precise determination of the origin of the Fe impurities may be possible by the XRPD (or μ -XRPD) measurement of the coins. If the Fe contaminated the gold during melting and casting, iron should be in solid solution with gold, on the other hand, if the contamination is caused by forging and coining, the Fe should be in the form of ferrite (or martensite). Iron in the solid solution and iron on the surface should be therefore clearly distinguishable by the XRPD analysis.

μ -XRPD analysis allowed to verify findings by Raman spectroscopy with unambiguous determination of goethite FeOOH (PDF4+ # 04-015-2900) in the red stain regions (Fig. 8, revers point #1, avers point #1). Additionally, μ -XRPD analysis helped, at least in the analysed avers point #2 on pure metal surface of the 10 K 1905 coin, to find out that

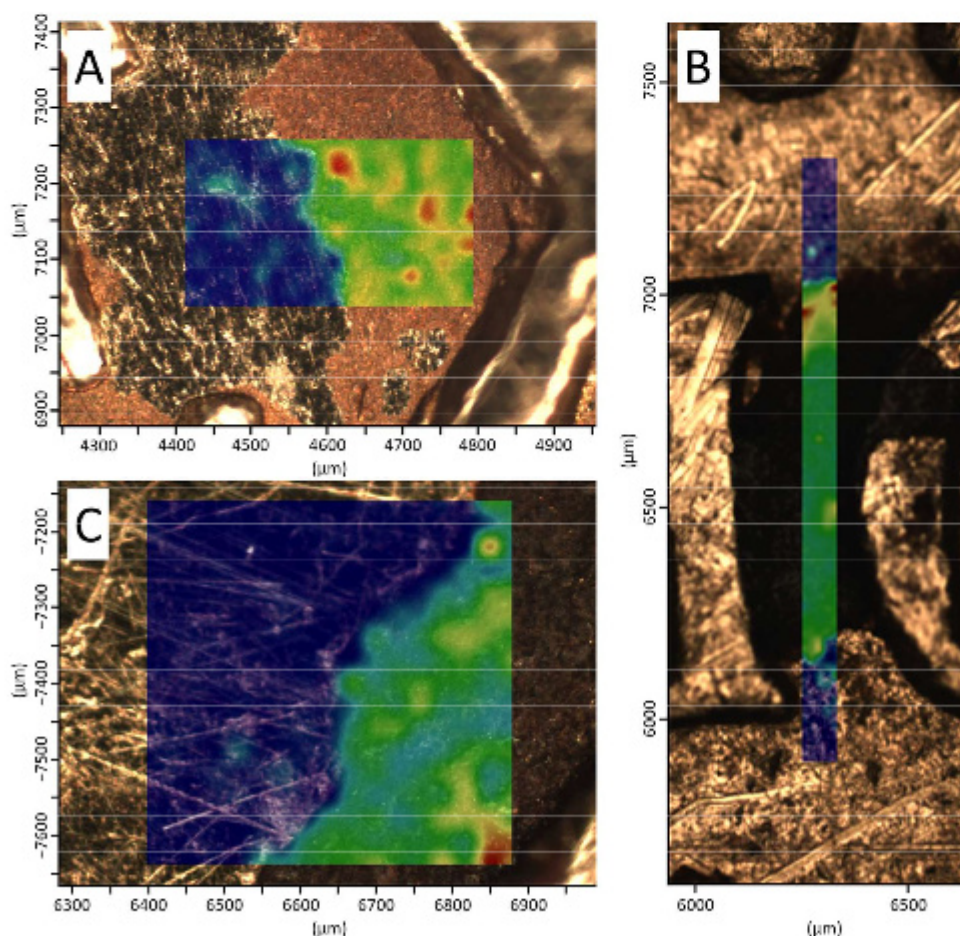


Fig. 8. Raman imaging of corrosion products on surface of Austro-Hungarian 10 Korona 1897 (A), 1905 (B) and 1907 (C) at the signal 394 cm^{-1} . The lowest intensity of Raman signal is shown by blue colour and the highest intensity by red colour (For interpretation of the references to color in this figure legend, the reader is referred to the web version of this article.).

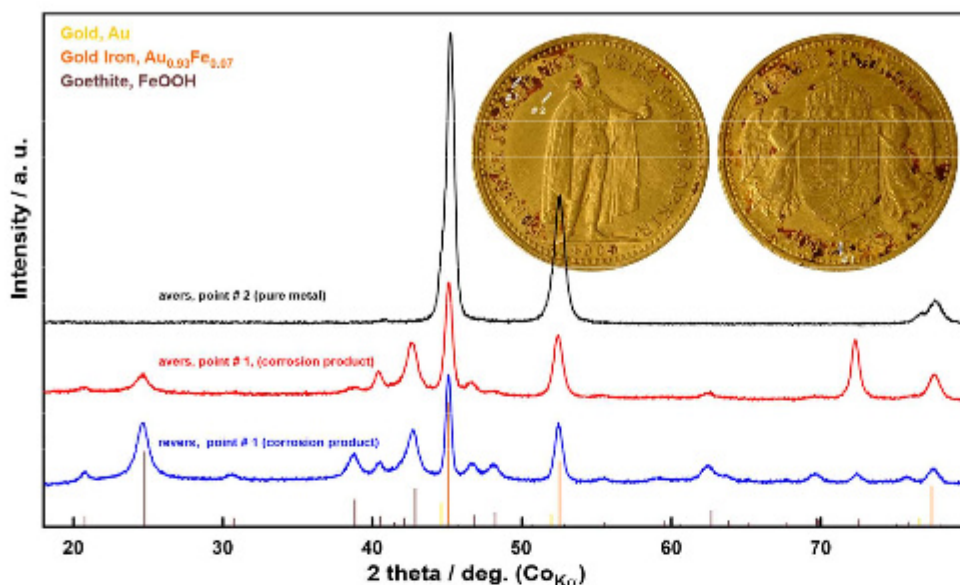


Fig. 9. μ -XRPD diffraction patterns of two analysed points of red stains on revers and avers surfaces compared to intact pure metal avers surface on 10 K 1905. Positions and intensities of reference database (PDF4+) records are sketched with colour bars: Au PDF4+ # 04-007-3092 (gold), $\text{Au}_{0.93}\text{Fe}_{0.07}$ PDF4+ # 04-018-6610 (orange) and FeOOH PDF4+ # 04-015-2900 (brown) (For interpretation of the references to color in this figure legend, the reader is referred to the web version of this article.).

the material of this coin was most probably contaminated by iron during the melting process. We have unambiguously revealed that at least two different phases co-exist in the analysed area. The first one (estimated about 16 wt %) is composed of pure gold and the second one (estimated about 84 wt %) could be attributed to $\text{Au}_{0.93}\text{Fe}_{0.07}$ (PDF4+ # 04-018-6610). See diffraction pattern of the pure gold surface (Fig. 8, avers point #2).

So, both sources of iron contamination were most probably found. The segregated grains of iron and/or mechanically introduced iron was converted by degradation processes to Fe oxide hydroxide (FeOOH , goethite). Iron that is comprised in the inter-metallic phase remained most probably intact.

Under certain circumstances, of course, the fact that the corrosion products of iron on the surface of gold coins adhered only secondarily cannot be ruled out. If such corrosion products were as firmly adhered to the surface as the products we had the opportunity to study, the fact that red spots on coins may have a different nature than that of silver- or copper-based corrosion products remains a key fact of our study. This fact is the key message for conservators and restorers who care for rare items, which are often a valuable cultural heritage. Knowledge of the chemical composition possibility of removal of these stains can better help them to choose a suitable method of their treatment and possibly removal. In this respect, the principle of the formation of iron-containing stains is a secondary problem, the fact that they exist is crucial.

4. Conclusions

Eight techniques (LM, DM, SEM/EDS, AFM, XPS, μ -XRPD, ED-XRF, Raman microscopy, Mössbauer spectroscopy) were used for the analysis of red stains on gold coins. Defects analysed in this study show a high content of iron and oxygen. Raman microscopy and μ -XRPD proved a goethite form of iron in red stains. Note, that this is the first direct evidence of contamination of gold coin by iron and consequent formation of "corrosion". The results show that silver and consequent formation of Ag_2S is not the only possibility for the formation of red stains. The coins that are minted in thousands/millions of pieces have higher risk to damage the parts of instruments in the mint and contaminate a golden alloy with iron particles. This study expands the knowledge of formation of "corrosion" products on gold coins surface and can be the primary impulse to control steel components during minting process. The results are also important for conservators working with gold coins in museum collections. More possibilities of chemical compositions of red stains logically entail the necessity of knowing their composition before cleaning

and preservation process to avoid expose coins or medals to aggressive procedures.

Declaration of Competing Interest

The authors declare that they have no known competing financial interests or personal relationships that could have appeared to influence the work reported in this paper.

Acknowledgment

The authors gratefully acknowledge the support of the Grant Agency of Czech Republic [17-17346S], Ministry of Education, Youth and Sports of the Czech Republic [LQ1601 and CZ.1.05/2.1.00/19.0377] and Palacky University Olomouc [IGA_PrF.2020_030]. In addition to the techniques described above, the XRPD was used to identify stains on the coin surface (Jiri Masilko and Pavla Roupčova). Unfortunately, the amount of red stains is in comparison to whole coin surface negligible (under the detection limit of conventional XRPD technique) and due to this fact, the composition of those spots cannot be characterized with XRPD. Detailed images of red stains were observed by SEM/EDS (Martin Zmrzly and Jaromir Wasserbauer) and digital microscopy (Viktor Jankovsky and Zuzana Koudelkova). Authors would like thank all colleagues mentioned above.

Supplementary materials

Supplementary material associated with this article can be found, in the online version, at [doi:10.1016/j.mta.2021.101025](https://doi.org/10.1016/j.mta.2021.101025).

References

- [1] M. Griesser, R. Denk, M. Griebel, R. Traum, H. Winter, The Past and the future - investigating brown spot corrosion on historic gold coins and metals to advance their preservation, *Numismatics & Technology: Question and Answers*, 2003.
- [2] L. Rupprecht, G. Gusmano, R. Montanari, Corrosion damage in modern gold coins, *Numismatics & Technology: question and answers*, 2003: Wien.
- [3] Y. Changjiang, L. Chenghao, W. Peng, Investigation of the tarnish on the surface of a panda gold coin, *Rare Met.* 26 (1) (2007) 68–73.
- [4] M.F. Guerra, I. Tissot, The role of nuclear microprobes in the study of technology, provenance and corrosion of cultural heritage: the case of gold and silver items, *Nucl. Instrum. Methods Phys. Res. B* 306 (2013) 227–231.
- [5] M. Griesser, R. Traum, K.E. Mayerhofer, K. Pipilits, R. Denk, H. Winter, Brown spot corrosion on historic gold coins and medals, *Surf. Eng.* 21 (5-6) (2013) 385–392.
- [6] G. Gusmano, R. Montanari, S. Kaciulis, G. Montesperelli, R. Denk, "Gold corrosion": red stains on a gold Austrian Ducat, *Appl. Phys. A* 79 (2) (2004) 205–211.

- [7] V. Corregidor, L.C. Alves, J. Cruz, Analysis of surface stains on modern gold coins, *Nucl. Instrum. Methods Phys. Res. B* 306 (2013) 232–235.
- [8] C.H. Liang, C.J. Yang, N.B. Huang, Investigating the tarnish and corrosion mechanisms of Chinese gold coins, *Surf. Interface Anal.* 43 (4) (2011) 763–769.
- [9] R. Traum, M. Griesser, *Naturwissenschaftliche Untersuchungen und Restauratorische Behandlung Korrosionsbefallener Goldmünzen und Medaillen*, in: Griesser, M., Huber, A., Oberthaler, E. Eds. *Korrosion an goldmünzen und medaillen*, Kunsthistorisches Museum, Wien 2006.
- [10] K.E. Mayerhofer, K. Piplits, R. Traum, M. Griesser, H. Hutter, Investigations of corrosion phenomena on gold coins with SIMS, *Appl. Surf. Sci.* 252 (1) (2005) 133–138.
- [11] ICDD (2019). *PDF-4+ International Centre for Diffraction Data*, Newtown Square, PA, USA 2020.
- [12] S. Švarcová, E. Kočí, P. Bezdička, D. Hradil, J. Hradilová, Evaluation of laboratory powder X-ray micro-diffraction for applications in the field of cultural heritage and forensic science, *Anal. Bioanal. Chem.* 398 (2010) 1061–1076.
- [13] D. Hradil, P. Bezdička, J. Hradilová, V. Vařutová, Microanalysis of clay-based pigments in paintings by XRD techniques, *Microchem. J.* 125 (2016) 10–20.
- [14] N. Döbelin, R. Kleeberg, Profex: a graphical user interface for the Rietveld refinement program BGMN, *J. Appl. Crystallogr.* 48 (2015) 1573–1580.
- [15] J. Pechousek, M. Mashlan, Mössbauer spectrometer as a virtual instrument in the PXI/Compact PCI modular system, *Czech. J. Phys.* 55 (2005) 853–864.
- [16] Z. Klencsár, E. Kuzmann, A. Vértes, User-friendly software for Mössbauer spectrum analysis, *J. Radioanal. Nucl. Chem.* 210 (1996) 105–118.
- [17] R.P. Gupta, S.K. Sen, Calculation of multiplet structure of core p-vacancy levels. II, *Phys. Rev.* 12 (15) (1975) 71–77.
- [18] M. Hanesch, Raman spectroscopy of iron oxides and (oxy) hydroxides at low laser power and possible applications in environmental magnetic studies, *Geophys. J. Int.* 177 (2009) 941–948.
- [19] E.C. Sklute, S. Kashyap, M.D. Dyar, J.F. Holden, T. Tague, P. Wang, S.J. Jaret, Spectral and morphological characteristics of synthetic nanophase iron (oxyhydr)oxides, *Phys. Chem. Miner.* 45 (1) (2018) 1–26.
- [20] B. Lafuente, R.T. Downs, H. Yang, N. Stone, The power of databases: the RRUFF project, in: T. Armbruster, R. M. Danisi (Eds.), *Highlights in Mineralogical Crystallography*, W. De Gruyter, Berlin, 2015.
- [21] H. Okamoto, T.B. Massalski, L.J. Swartzendruber, P.A. Back, The Au–Fe (Gold–Iron) system, *Bull. Alloy Ph. Diagr.* 5 (6) (1984) 592–601.

Schönwälderová, Nikol; Šlězár, Pavel; Kučera, Lukáš

Analýza zbytků barev z fragmentu kresby na březové kůře z Litovle

Studia archaeologica Brunensia. 2022, vol. 27, iss. 1, pp. 143-152

ISSN 1805-918X (print); ISSN 2336-4505 (online)

Stable URL (DOI): <https://doi.org/10.5817/SAB2022-1-6>

Stable URL (handle): <https://hdl.handle.net/11222.digilib/145219>

License: [CC BY-SA 4.0 International](#)

Access Date: 17. 02. 2024

Version: 20220831

Terms of use: Digital Library of the Faculty of Arts, Masaryk University provides access to digitized documents strictly for personal use, unless otherwise specified.

Analýza zbytků barev z fragmentu kresby na březové kůře z Litovle

Analysis of pigment residue on fragment of paint on medieval birch bark from Litovel

Nikol Schönwälderová / Pavel Šlézar / Lukáš Kučera

Abstrakt

V rámci archeologického výzkumu v kostele sv. Marka v Litovli byla v uloženinách z 16.–18. století nalezena březová kůra s inkoustovou kresbou květinového motivu. Cílem výzkumu bylo zjistit, jaké barvy či pigmenty byly použity na vytvoření rostlinného motivu na kůře. Pomocí rentgeno-fluorescenční spektrometrie byly zachyceny tři významné prvky – železo, olovo a měď. Na základě výsledků z Ramanovy mikroskopie se nám podařilo identifikovat zelený pigment jako malachit a červený jako hematit, tedy součást červené hlíny. Vyšší obsah železa v tmavých linkách pravděpodobně pochází ze železitoduběnkového inkoustu.

Klíčová slova

pigment, archeometrie, Ramanova spektrometrie, rentgeno-fluorescenční spektrometrie

Abstract

During archaeological research in Litovel, a birch bark from the 16th–18th century with floral motif. The aim of the work was to find out what colors or pigments were used to create a plant motif on the bark. Three important elements – iron, lead and copper – were captured by X-ray fluorescence spectrometry. Based on the results from Raman microscopy, we were able to identify the green pigment as malachite and the red pigment as hematite, ie part of the red clay. The higher iron content in the dark lines probably comes from iron-tube ink.

Key words

pigment, archaeometry, Raman spectroscopy, X-ray fluorescence spectrometry

1. Úvod

Během rozsáhlého archeologického výzkumu v kostele sv. Marka v Litovli v roce 1999 byl učiněn objev inkoustem kresleného rostlinného ornamentu na útržku březové kůry. Výzkum v interiéru kostela byl vyvolán narušenou statikou objektu po povodních v roce 1997. V současnosti se jedná o trojlodní kostel s kaplí při jižní boční lodi, polygonálním chórem a sakristií na severu a s hranolovou věží v jihozápadním nároží stavby. V jádru gotická stavba, jmenovitě připomínaná roku 1382, byla upravována ve 2. polovině 15. století a zejména v období renesance, ze které pochází sakristie nesoucí leptopočty z roku 1529 a 1532. Nynější podobu stavba získala během barokní přestavby v letech 1675–1680 (Faltýnek–Šlězár 2006, 309–315; Šlězár 2008, 28–67).

Archeologickým výzkumem se podařilo odkrýt část presbytáře prvotního kostela z poslední čtvrtiny 13. století a takřka celý půdorys nově vystavěného kostela ze 14. století. Kromě tradičních sondážních odkryvů pod podlahou kostela, ze kterých pochází řada prozkoumaných zdív, hrobů, artefaktů, stavebních prvků a sutí, byla pozornost věnována také suchým zásypům kleneb jihozápadní kruchty. Při prosévání zásypů byly získány hojné devocionálie i předměty denní potřeby litovelských měšťanů, jako jsou zlomky keramických nádob, stovky růžencových korálek z různých materiálů, kovové, kostěné, dřevěné a nitěné knoflíky, četné kovové předměty jako medailonky, špendlíky a soubor čtrnácti mincí. Dále se zde našly útržky látek a několik papírových svatých obrázků (sv. Salvator, sv. František z Assisi, oplakávání Krista aj.). Nechyběly ani kožené a dřevěné artefakty, např. písálky, a potřeby na psaní (hrudky bílé křídly). Kromě artefaktů samotných napomá-

hají dataci celého souboru nálezů do rozmezí 16. až 18. století nalezené mince, přičemž většina ražeb patří do průběhu 17. století, což odpovídá i závěrům stavebně-historických průzkumů. Datace však odpovídá pouze době zánikové transformace artefaktu, tedy době ukončení existence předmětu v lidském světě (Faltýnek–Šlězár 2006, 309–315; Faltýnek–Šlězár 2007, 73–84; Šlězár 2008, 28–67; Šlězár 2018, 87–97, 101–102). Jedním z nálezů ze zásypů kleneb jihozápadní kruchty byl fragment březové kůry (cca 4,0 × 2,2 cm) s inkoustem provedenou barevnou kresbou rostlinného motivu (inv. č. 672/3, Obr. 1). Na kůře jsou nakresleny stonky a zelený list s červeně zbarveným poupětem, zvýrazněným tmavou linkou. Patrně jde o růži šípkovou (*Rosa canina*, určil Mgr. Petr Kočár, Ph.D.), i když tvar listu pro růži typický není. Pravděpodobně byl list silně stylizován (např. kresba bez předlohy). Mohlo by jít také o růži alpskou (*Rosa alpina*), která je v horní části takřka bez trnů a vzhled listů je dokonce bližší ztvárnění listu na kresbě. Na základě počtu vybíhajících větvíček se lze vyjádřit i k původnímu vzhledu kresby. Vedle větvičky s poupětem byly na kresbě ještě další dvě větvičky a jeden list. Větvička sousedící bezprostředně s poupětem nesla pravděpodobně rovněž poupě. Třetí větvička nesla rozkvetlý květ růže. Zbytky korunního lísku jsou dobře patrné, naznačeny jsou třemi obloučky. Stejně tak je na torzu kresby dobře patrné, kde se nacházel i druhý list růže, kresba jeho konce se na svitku rovněž dochovala. Zda mohl být fragment součástí dobového „herbáře“, nelze rozhodnout. Stejně tak i zda mohla kresba nést nějaké symbolické sdělení, vzhledem k bohaté symbolice růže (např. symbol lásky, smrti, mlčenlivosti, čistoty, růže bez trnů = bez hříchu, mariánský motiv aj., srov. Lurker 2005, 438–439).



Obr. 1. Litovel, okr. Olomouc, kostel sv. Marka, vzorek březové kůry s rostlinným motivem

Fig. 1. Litovel, Olomouc district, St. Mark's Church, sample of birch bark with plant motif

2. Metodika měření

2.1. Ramanova spektroskopie

Vzorek březové kůry byl měřen pomocí Ramanova mikroskopu DXR2 (Thermo scientific, MA, USA), umožňujícího 1D („liniový profil“) nebo 2D zobrazení povrchu. Parametry měření byly: laser 785 a 532 nm, energie laseru 0,5 mW, počet expozičních 16, doba jedné expozice 2 sekundy, šířka clony 50 μm , zvětšení mikroskopu 10 \times .

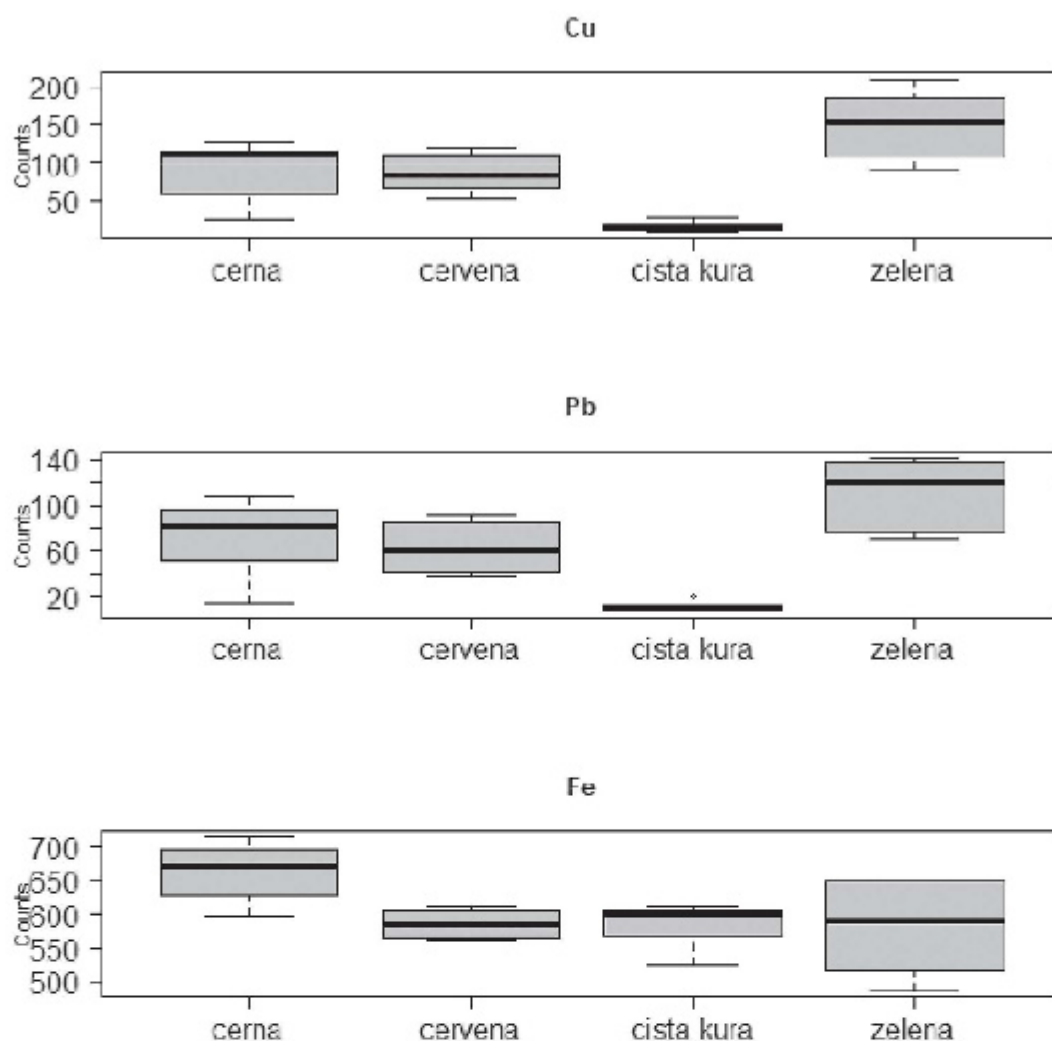
2.2. Rentgenová-fluorescenční spektrometrie

K elementární analýze byl použit energiově disperzní rentgenově-fluorescenční spektrometr Vanta (Olympus, MA, USA). Parametry měření: geochemický mód, rozsah excitační energie

8–40 keV, doba měření 120 s, křemíkový drifto-
vý detektor. Pro měření vzorků pomocí mřížky
(pro následné vyhodnocení obrazu) byl celkový
čas měření 30 s. Získaná data byla vyhodno-
cována pomocí programu R software (*R Core
Team 2022*).

3. Výsledky a diskuze

Pro měření tohoto významného vzorku byly po-
užity pouze nedestruktivní a neinvazivní meto-
dy. V prvním kroku byly jednotlivé barevné ob-
lasti (zelená, červená, černá) a oblast čisté kůry
měřeny pomocí ručního XRF. Na základě srovnání
těchto oblastí pomocí krabicových grafů
(boxplotů, Obr. 2) je patrné, že vysoký význam
pro odlišení čisté kůry a barevných oblastí mají
prvky Fe, Cu a Pb. Zajímavý je zvýšený obsah že-
leza v černé oblasti, což může poukazovat na po-
užití železitoduběnkového inkoustu. Měď může



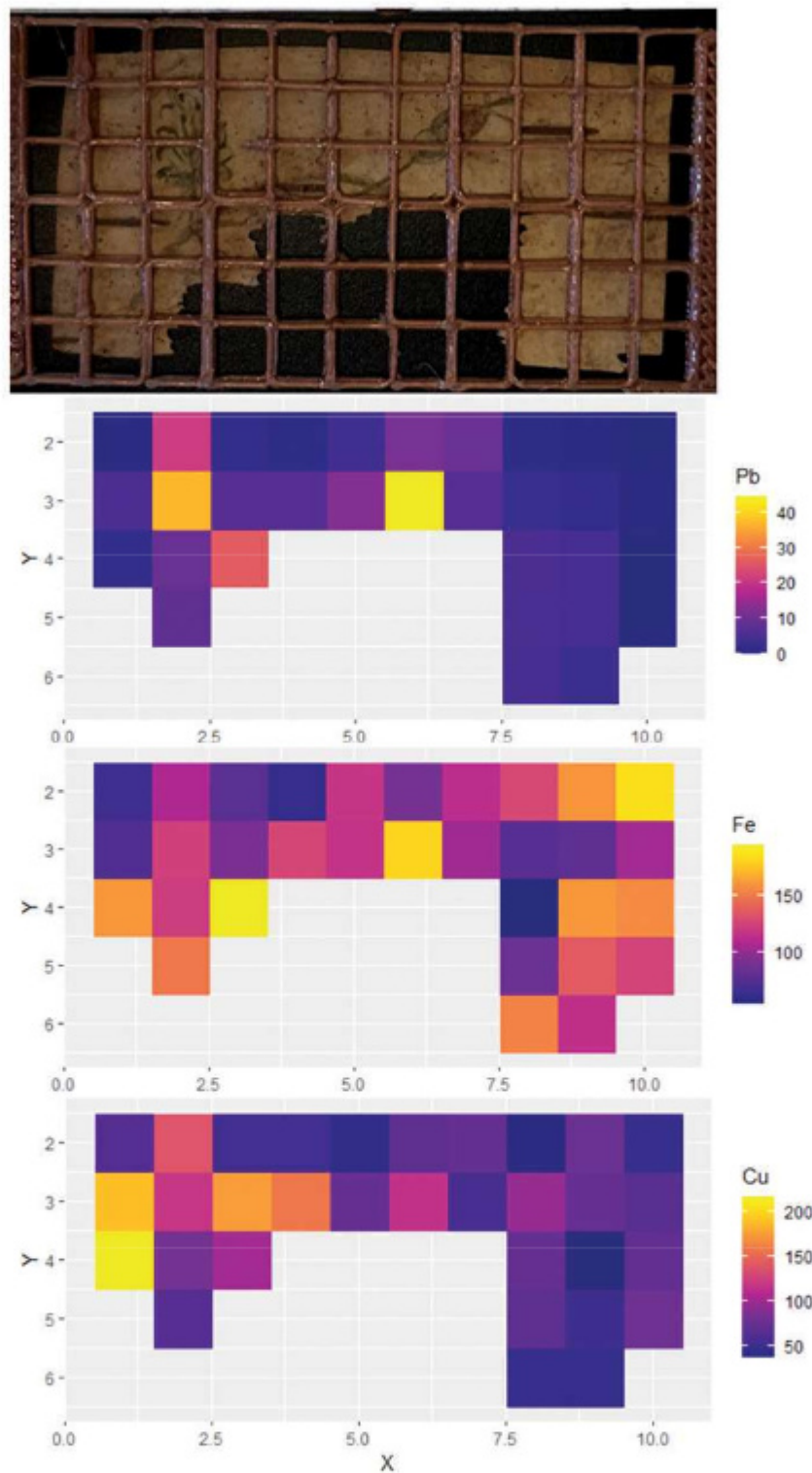
Obr. 2. Krabicový graf intenzity vybraných prvků (Cu, Pb a Fe) na vzorku březové kůry

Fig. 2. Box-plot of intensity of selected elements (Cu, Pb and Fe) on birch bark sample

poukazovat na přítomnost malachitu a olova na olovnatou bělobou. Pro zjištění distribuce jednotlivých prvků v rámci celého vzorku byla kůra měřena pomocí mřížky (Obr. 3). Vyšší obsah mědi se vyskytuje v oblasti lístků a zelené části květu. Můžeme tedy předpokládat, že ke kresbě byl použit měďnatý pigment. Vyšší obsah olova se vyskytuje také v oblasti listu a spodní části květu. Jednou z možností je smíchání zeleného měďnatého pigmentu s olovnatou bělobou pro získání světlejších tónů. Distribuce železa je bohužel velmi heterogenní a na základě zobra-

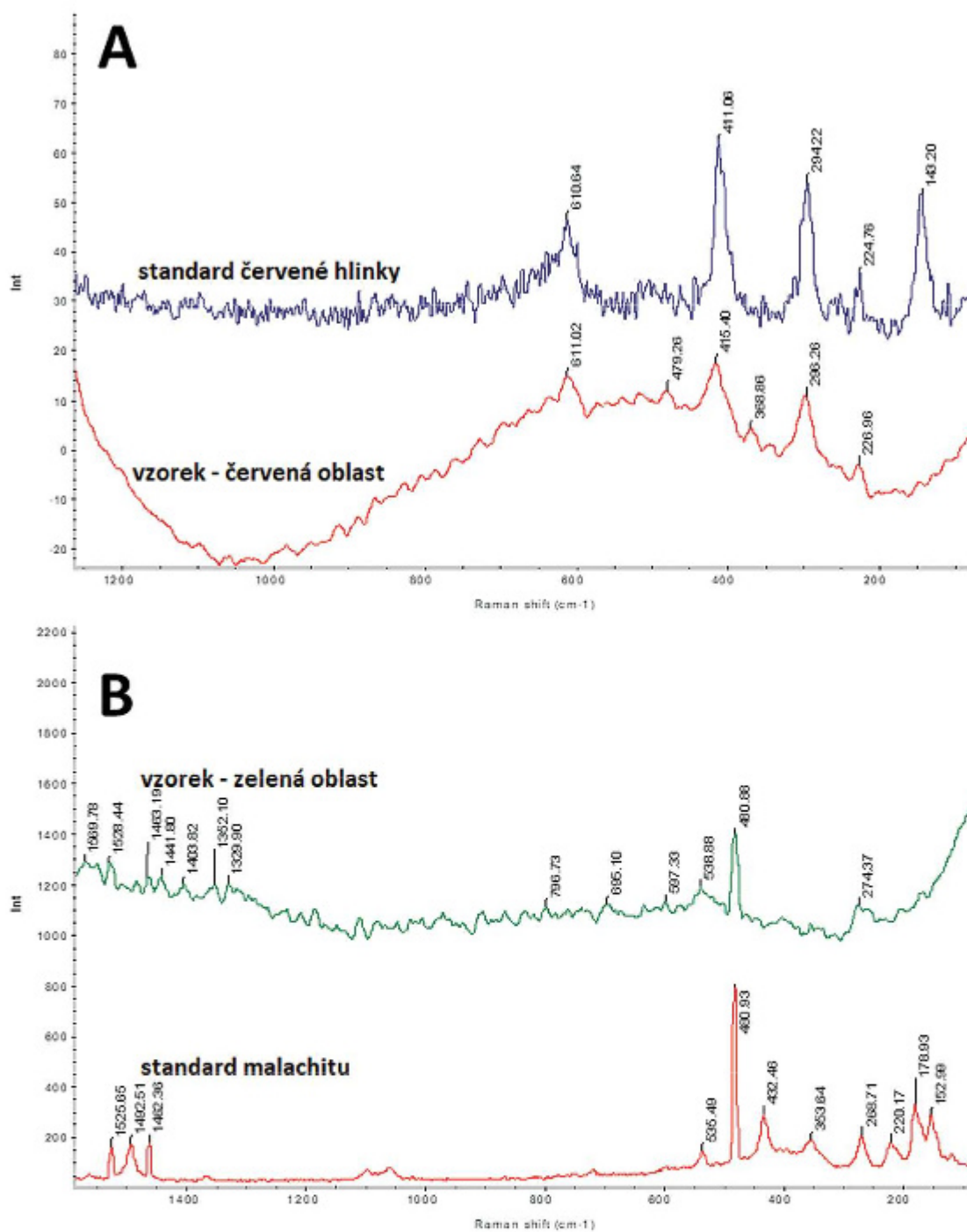
zovací metody není možné jednoznačně určit vyšší obsah železa v jednotlivých částech kresby.

Následně pro přesnější určení minerálů byla použita Ramanova spektroskopie (Obr. 4). Spektra získaná měřením jednotlivých barevných oblastí byla srovnána s autentickými standardy. Na základě srovnání těchto spekter můžeme konstatovat, že červený pigment obsahuje hematit (pravděpodobně pigment červená hlínka) a zelený zase signály náležející malachitu. Ramanova spektrometrie tedy potvrdila náš předpoklad z XRF měření.



Obr. 3. XRF zobrazování distribuce prvků na vzorku březové kůry

Fig. 3. XRF imaging of element distribution on sample of birch bark



Obr. 4. Ramanova spektra červené (A) a zelené (B) oblasti a jejich srovnání s autentickými standardy

Fig. 4. Raman spectra of red (A) and green (B) area and their comparison with authentic standards

4. Závěr

Malba, kresba či psaný text se už řadu tisíciletí používá na zachycení pocitu nebo příběhu. Kromě ústního sdělení, písní, legend a částečně samotných artefaktů se jednalo o způsob, jak předávat informace a sdělení dál, například dalším generacím v rámci rodiny. Pro zhotovení pomůcek na kresbu a malbu se využívaly anorganické pigmenty pouze z přírodních zdrojů (okrajově také synteticky připravené) a také organická barviva. Fragment březové kůry s inkoustovou kresbou, který byl nalezen v Litovli, je rozhodně jeden z příkladů uvedení typu artefaktů se sdělením. Na zlomku kůry se nachází nakreslený zelený list s červeně zabarveným poupětem a se stonky, na některých částech kresby jsou patrné rostlinné vzory olemované tmavou linkou. Cílem tohoto výzkumu byla analýza barev za účelem určení jejich původu. Jako první bylo využito měření ručního XRF, přičemž na základě výsledků je jasné, že prvky Fe, Cu a Pb mají odlišení od čisté kůry k barevným oblastem. Zajímavý je zvýšený obsah železa v černé oblasti kresby, což by mohlo poukazovat na využití železitoduběnkového inkoustu. Distribuce železa je bohužel velmi heterogenní a na základě měření pomocí mřížky není možné sledovat distribuci železa v jednotlivých částech kresby. Jako další nedestruktivní metoda byla využita Ramanova mikroskopie. Spektra získaná z barevných oblastí byla srovnána s autentickými standardy. Na základě srovnání spekter můžeme konstatovat, že červený pigment obsahuje hematit a zelený zase signály malachitu.

Nález inkoustové kresby na březové kůře dává podnět k úvahám, zda by březová kůra mohla být na našem území, podobně jako v zahraničí (například v Novgorodu), levným

a vhodným materiálem pro příležitostné zaznamenávání písemných údajů. Ostatně obliba tohoto materiálu pro psaní je známa již od antiky (Janin 2007; Šlězár 2018, 101). Používání březových kůr k psaní na našem území výslovně uvádí Václav Hájek z Libočan ve své Kronice české z roku 1541: „*I rozkázal to všecko pořád na korách březových poznamenati a pro budoucí paměť a další správu schovati.*“, „*...slovanskými literami a slovy na korách březových k tomu připravených popsat...*“ (Hájek 1541, III/37, VIII/45). Z kontextu sdělení vyplývá, že Hájek tento způsob zaznamenání údajů považuje za starobylý. Nicméně, Hájekova Kronika česká je faktograficky kontroverzním dílem a Hájek sám často přebíral celé pasáže od jiných autorů. Hodnověrnost tohoto sdělení tudíž není jistá, i když z něj zřejmě vyplývá nějaká znalost používání březové kůry k záznamu textů.

Vysoká hladina spodní vody v Litovli dokázala uchovat středověké artefakty a ekofakty z organických materiálů ve velmi dobrém stavu i v běžných uličních vrstvách. V Litovli bylo objeveno několik svitků březových kůr, na žádném z nich však prozatím nebyly makroskopicky pozorovány vyryté znaky či písmena. Na základě nálezů fragmentu březové kůry s inkoustovou kresbou z kostela sv. Marka však existuje možnost, že k záznamům na březové kůry mohl být v minulosti inkoust používán. Inkoust se lépe dochovává nikoliv ve vlhkém prostředí, ale v suchých podmínkách (jako jsou právě zásypy klenb), což však vzhledem k obecně nízké četnosti nalezených artefaktů z organických materiálů ztěžuje možnost ověření této hypotézy. O gramotnosti litovelských měšťanů již ve středověku svědčí nálezy psacích pomůcek – železných písátek (stilů) – rydel, kterými se psalo do voskových tabulek (Šlězár 2018, 101).

Tato práce vznikla za podpory projektu OA ITI – ARTECA: Pokročilé fyzikálně-chemické metody ve výzkumu a ochraně kulturního a uměleckého dědictví Reg. č.: CZ.02.1.01/0.0/0.0/17_048/0007378 financovaného z EFRR/ESF.

Bibliografie

- Faltýnek, K. – Šlězár, P. 2006:* Archeologické výzkumy sakrálních staveb v Litovli, *Archaeologia historica* 31, 303–322.
- Faltýnek, K. – Šlězár, P. 2007:* Litovel, náměstí Svobody. Kostel sv. Marka. Nálezová zpráva, sv. 1. Olomouc.
- Hájek z Libočan, V. 1541:* Kronika česká. Praha.
- Janin, V. L. 2007:* Středověký Novgorod v nápisech na březové kůře. Praha.
- Lurker, M. 2005:* Slovník symbolů. Praha.
- R Core Team 2022:* R: A language and environment for statistical computing. R Foundation for Statistical Computing, Vienna, Austria.
- Šlězár, P. 2008:* Kostely a sakrální stavby v Litovli. Archeologické památky střední Moravy, sv. 17. Olomouc.
- Šlězár, P. 2018:* Archeologie středověkého města. In: K. Konečný (ed.): Litovel. Velké dějiny města, svazek 1. Od nejstarších dob do roku 1918. Olomouc, 68–103.

Analysis of pigment residue on fragment of paint on medieval birch bark from Litovel

During archaeological research in Litovel, a birch bark from the 16th–18th century with floral motive, probably rose. Three important elements – iron, lead and copper – were captured by X-ray fluorescence spectrometry. Based on the results from Raman microscopy, we were able to identify the green pigment as malachite and the red pigment as hematite, ie part of the red clay. The higher iron content in the dark lines probably comes from iron-tube ink. After all, the popularity of this material for writing has been known since antiquity. The use of birch bark for

writing in our territory is explicitly stated by Václav Hájek of Libočany in his Chronicle of Bohemia from 1541. Additionally, several scrolls of birch bark have been discovered in Litovel, but no engraved characters or letters have been recorded macroscopically on any of them so far. Perhaps only ink was used for birch bark recordings (Russian sources mention ink inscriptions), which is well preserved only in dry conditions. Identification of text or painting remains will be a matter of further research.

Nikol Schönwälderová

- Gymnázium Ladislava Jaroše Holešov
Palackého 524/37, Holešov 769 01

PhDr. Pavel Šlězár, Ph.D.

- Národní památkový ústav
Územní odborné pracoviště v Olomouci
Horní nám. 25, Olomouc 779 00
slezar.pavel@npu.cz

RNDr. Lukáš Kučera, Ph.D.

- Katedra analytické chemie
Přírodovědecká fakulta
Univerzita Palackého v Olomouci
17. listopadu 12, Olomouc 779 00
-



Toto dílo lze užít v souladu s licenčními podmínkami Creative Commons BY-SA 4.0 International (<https://creativecommons.org/licenses/by-sa/4.0/legalcode>). Uvedené se nevztahuje na díla či prvky (např. obrazovou či fotografickou dokumentaci), které jsou v díle užity na základě smluvní licence nebo výjimky či omezení příslušných práv.



Human “barcode”: Link between phosphate intensity changes in human enamel and light microscopy record of accentuated lines

Soňa Vacková^{a,b}, Miroslav Králík^a, Klára Marečková^c, Lucie Ráčková^{d,a}, Leslie Quade^a, Lenka Sedláčková^f, Pavel Fojtík^g, Lukáš Kučera^{e,*}

^a Department of Anthropology, Faculty of Science, Masaryk University, Kotlářská 2, CZ – 611 37, Brno, Czech Republic

^b Centre for Paleolithic and Paleoanthropology Dolní Vestonice, Institute of Archeology, Czech Academy of Sciences, Cechyňská 363/19, CZ - 602 00, Brno, Czech Republic

^c Brain and Mind Research, Central European Institute of Technology, Masaryk University (CEITEC MU), Kamenice 753/5, 625 00, Brno, Czech Republic

^d Research Centre for Toxic Compounds in the Environment (RECETOX), Masaryk University, Kamenice 5, 625 00, Brno, Czech Republic

^e Department of Analytical Chemistry, Faculty of Science, Palacký University, 17. Listopadu 12, 779 00 Olomouc, Czech Republic

^f Archela Brno z. ú., Bezručova 15/78, 602 00 Brno, Czech Republic

^g Institute of Archaeological Heritage Brno, Kaloušova 1321/30, 614 00 Brno, Czech Republic

ARTICLE INFO

Keywords:

Raman microscopy
Transmitted light microscopy
Thin section
Dental enamel
Phosphate
Accentuated stress lines

ABSTRACT

Disruption of metabolic processes during human enamel mineralization may result in the appearance of accentuated lines in enamel. These accentuated lines in the enamel relate to stress events that were experienced and overcome in early ontogenetic phases. Accentuated lines are visible in transmitted light microscopy as dark areas. However, their appearance is variable even within single tooth. The objective of this study is to analyze the distribution of phosphate in human enamel with a focus on accentuated stress lines by Raman microscopy. Transmitted light microscopy and Raman microscopy records of 15 human teeth (11 samples from archaeological excavations, 4 from recent population) were compared, using visual evaluation and statistical methods (correlation of pixel light intensities in the microscopic images). The data obtained by Raman microscopy suggests a relationship between low phosphate content (signal at 960 cm^{-1}) and accentuated stress lines in human enamel.

1. Introduction

Dental enamel mineralization in human teeth takes place in periodically recurring intervals, resulting in formation of characteristic growth marks observable in mature enamel microstructure (incremental lines) [1–3]. These incremental growth marks can be divided into short-period marks forming in 24-h intervals and long-period marks (periodicity of several days) called Retzius striae/lines (RL) (shown as perikymata at the enamel surface) [4]. Dental enamel matrix secreting cells (ameloblasts) are sensitive to fluctuations in metabolic processes during enamel development, which can affect the rate of secretion [5], or can cause a change in the structure of the matrix produced [6]. Once secreted, the enamel matrix is mineralized. Enamel mineralization only occurs during early stages of ontogenetic development and unlike other bone tissues, it does not remodel afterwards. This means that potential metabolic disturbances (e.g., infectious pathogens, malnutrition) occurring in early life remain “written” in enamel as developmental

defects. These defects have alternatively been referred to as “accentuated stress lines (ALs)” [7,8], “Wilson bands” [9,10] or “accentuated striae of Retzius” [11,12]. These disruptions to normal enamel growth, as well as the sensitivity of ameloblasts to metabolic stressors and the retention of these markers within enamel after mineralization, make it possible to study the chronology of dental development. This includes establishing the timing of stress events experienced in the early stages of ontogenesis, creating a “time-lapse record” in dental enamel (as well as in dentine). This principle of dental “time-lapse records” is increasingly used for analytical purposes in paleoanthropology [5,13–16] and bioarchaeology [8,17–21] to reconstruct individual life histories from archaeological human skeletal remains. This human “barcode” pattern is unique to each person, preserving a record of individual life experience. However, several events occurring during the life history of all individuals can lead to the formation of specific accentuated lines, including lines related to birth, the neonatal line [7,22] or accentuated lines related to weaning [19,23,24]. Accentuated lines related to events

* Corresponding author.

E-mail address: lukas.kucera@upol.cz (L. Kučera).

<https://doi.org/10.1016/j.microc.2021.106370>

Received 18 March 2021; Received in revised form 4 May 2021; Accepted 5 May 2021

Available online 8 May 2021

0026-265X/© 2021 Elsevier B.V. All rights reserved.

that most or all individuals experience manifest in the dental enamel record of the majority of population.

Microstructural studies of hard dental tissues and stress lines are subjective and depend, to a large extent, on the observer's experience. Furthermore, the quality of thin-sections and the chosen evaluation method substantially impact the analysis of hard dental tissues [25,26]. Additionally, the appearance, length, breadth and visibility of ALs are variable [10,27] and it is necessary to define what is considered as AL [27]. The current challenge is to refine detection and objective quantification (width and frequency measurements) of accentuated lines, as well as their more detailed specifications and internal breakdown (e.g., the degree and nature of stress that affects the body [26]). Similar methodological efforts applied to images of tooth thin-sections generated from a light microscope are limited by the difficult standardization of light (differences in the thickness of the cuts, which cannot be precisely standardized) and numerous taphonomic changes in dental tissues.

Tooth enamel is highly mineralized and contains 95% carbonated hydroxyapatite crystals (HAP). The rest of tooth enamel is composed of proteins and water [28,29]. Inductively-coupled plasma combined with mass spectrometry is the most commonly used technique for analysis of tooth enamel [30–34]. However, this method requires partial destruction of the sample through laser ablation. In contrast, Raman spectroscopy is a non-invasive analytical method used to study dentin demineralization. This method was already used for the early detection of dental caries [35], for analyzing the influence of tooth bleaching solutions on phosphate concentrations in dental enamel [36,37], chemical enamel composition effect on tooth color [38], changes in mineral matrix of dental enamel after external ionizing radiation [39] and the estimation of post-mortem interval in forensic sciences [40]. Therefore, Raman microscopy (RM) is a potentially promising method, which would improve the detection of non-standard, or irregularly-shaped areas of tooth enamel (ALs). However, the method must first be verified, by comparing Raman microscopy concentration records of enamel components against line sequences (which can be observed optically) in transmitted light microscopy (LM). To the best of our knowledge, there is only one publication exploring analysis of stress signature markers in dental enamel using Raman microscopy. However, this study was focused on non-human primates and analysis was performed on sections of embedded tooth blocks [41]. Because we wanted to compare the exact same accentuated lines visible LM with RM record, we used thin sections for evaluation. Comparing embedded tooth block RM record and thin section LM record could cause even more error or shifts in the data. We are not aware of any published studies that have specifically combined accentuated stress lines analysis in human tooth enamel via Raman microscopy and transmitted light microscopy on the histological thin sections. The aim of the current study is to compare the sequence of changes (a time-lapse record of mineralization in the enamel of a human tooth) by Raman microscopy (phosphate intensity) and transmitted light microscopy in human dental enamel. Subsequently, the determination of ALs using RM and LM is statistically compared.

2. Materials and methods

2.1. Sample preparation

The studied material consisted of 15 human teeth, including both permanent and deciduous teeth. The study included the teeth of individuals from archaeological sites that had good preservation, no crown abrasion, and no macroscopically observed taphonomic changes that could affect quality of histological section. At the same time, teeth were selected from individuals, for whom it was possible to age at death using anthropological methods (or from a questionnaire survey in the case of recent samples). Children's teeth were selected based on the presence of a neonatal line that separates the prenatal enamel from the postnatal. Eleven of the 15 teeth originated from two archaeological

sites dated to 1000 – 1300 CE. These comprised Brno-Vídeňská street (BV), excavated by Archaia o.p.s. [26] and Dětkovice – Za zahradama (D), excavated by Institute for Archaeological Heritage [42–45]. Four recent teeth were sourced from the European Longitudinal Study of Pregnancy and Childhood (ELSPAC) [46] (Table 1). Thin-sections of teeth samples were prepared according to published protocols [47–49]. Briefly, teeth were embedded in epoxy resin (Araldite 2020) to harden the sample before sectioning. Subsequent histological analysis was performed through odontochemistry [12,18], which allows enamel growth increments to be monitored as a space–time record. For this reason, a consistent section plane of the sample was necessary. Canines were cut in labio-palatal/labio-lingual direction in the mesiodistal plane and molars were sectioned in bucco-lingual/bucco-palatal direction through mesial or distal cusps using low-speed circular saw (Struers, Accutom 100). Sections were ground to a final thickness of approximately 100 µm and were mounted on a slide with epoxy resin (Araldite 2020). Cover slips were not used to allow subsequent Raman spectroscopy analysis.

2.2. Transmitted light microscopy (LM)

Thin-sections were studied using a Leica DM2500 LED optical microscope combined with Leica DMC 6200 microscope camera. Because images of enamel from the whole tooth are necessary for subsequent ALs identification, photomontages of microphotographs were put together in Photoshop CS4 and final records were analyzed in ImageJ software.

First, ALs were identified in enamel at the objective magnification 50× following recommendations by Fitzgerald and Saunders [27]. Because analysis on Raman spectroscopy in imaging mode is a time-consuming process, we selected several smaller areas of enamel where a) ALs or at least clear series of RLs were clearly visible and b) area included the enamel-dentin junction (EDJ). Enamel was divided in inner, middle and outer area [50] and number of ALs in these areas was recorded (Fig. 1).

2.3. Raman microscopy (RM)

Selected areas were recorded at the magnification 10× by digital microscope and then analyzed by DXR2 Raman microscope (Thermo Scientific, MA, USA) in imaging mode. The parameters of measurement were as follows: laser 785 nm, laser energy 5 mW, aperture 50 µm Slit, collect exposure time 2 s, sample exposures 16, step in X–Y dimension 5 µm, thermoelectric-cooled CCD detector. The data were measured and evaluated in Omnic 9 software for Dispersive Raman microscopy

Table 1

List of analyzed samples. Sex and age in samples 1 – 11 was determined by standard anthropological methods [53–56], Sex in samples 12–15 during ELSPAC questionnaire survey from participants, dental age using anthropological method [56] BV = Brno-Vídeňská street site, D = Dětkovice site, ELSPAC = recent teeth from ELSPAC study, F = Female, M = Male.

Sample ID	Origin	ID of an individual	FDI	Sex	Age (years)
1	BV	H812	33	F	20–25
2	BV	H815	33	M	20–25
3	BV	H841	33	M	20–25
4	BV	H849	85	NA	6.5–7.5
5	BV	H3812	46	NA	8.5–9.5
6	BV	H3824	46	NA	8.5–9.5
7	BV	H3824	85	NA	8.5–9.5
8	D	H1	26	NA	14.5–15.5
9	D	H30	26	NA	8.5–9.5
10	D	H70	16	NA	7.5–8.5
11	D	H70	36	NA	8.5–9.5
12	ELSPAC	Z_006	64	F	9.5–10.5
13	ELSPAC	Z_006	74	F	9.5–10.5
14	ELSPAC	Z_003	65	M	7.5–8.5
15	ELSPAC	Z_004	65	M	7.5–8.5

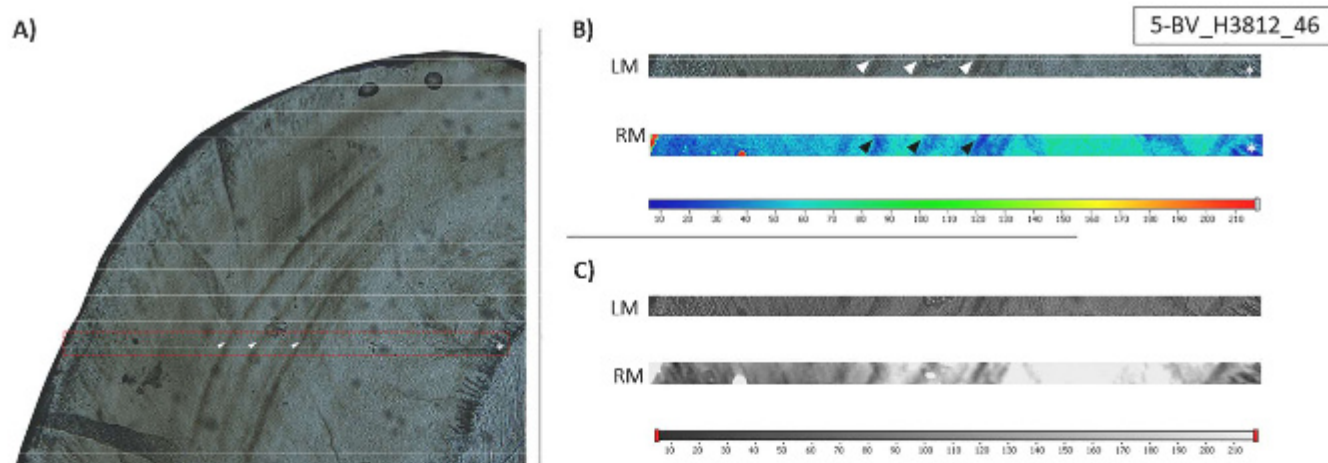


Fig. 1. A – Microphotography of permanent mandibular right 1st molar (FDI 46), sample 5-BV_H3812_46, magnification 50 \times . Red dotted rectangle defines the area of Raman spectroscopy analysis. Arrows point to ALs in enamel, asterisk points to EDJ. B – Detail on section from part A, arrows and asterisk point to same structures as in part A, magnification 100 \times . Red areas on RM record corresponds with artefacts from thin section production (air bubbles). C – Sections from part B converted into grey scale, used in further analysis. (LM = Transmitted light microscope record, RM = Raman microscope record, AL = Accentuated stress lines, EDJ = enamel-dentin junction).

(Thermo Scientific, MA, USA). The results from Raman microscopy imaging show distribution of phosphate group in selected areas at signal 960 cm^{-1} [51].

2.4. Adjustment of LM and RM records for further statistical evaluation

Data from light microscopy and Raman microscopy were visually compared (Supplement 1, Figs. A.1–A.14). Both records were converted from RGB spectrum to grayscale to simplify data for better evaluation of changes in both records. Light microscopy records were converted in Photoshop CS4 and Raman microscopy records were converted directly in software Omnic 9. Finally, every pair of records were formatted to have the same dimensions in pixels, the same resolution and color spectrum. Black areas in Raman microscopy records correspond with the lower concentration of phosphate (dark blue color in RGB imaging record) and white corresponds with high phosphate concentration (red color in RGB imaging record).

Every pair of records was then separately analyzed in ImageJ software in order to obtain numeric values of pixel light intensities. Using ROI manager in Image J software, light microscopy record was transected with three horizontally directed, parallel line segments. The three lines were placed as close to each other as possible. Line segment lengths were identical with the width of record and their positions had to intersect accentuated lines (ALs). We used Multi Plot tool from ROI manager of ImageJ in order to get pixel intensity of these three segmented lines. Final data containing the position of each pixel and corresponding value of light intensity pixels, and values of pixel intensity for every segmented line were recorded. Data from Raman microscopy was processed analogously. At the end of the process, every pair of 2D records had a data set for light microscopy and a dataset for Raman microscopy in values of light intensity of grayscale images. Final records are in a standardized position with unified orientation of the teeth structures, where the direction towards tooth cusp is at the top, dentin is on the left and outer enamel is on the right of the image.

2.5. Statistical analysis

Univariate records of pixel light intensities were compared in pairs (light microscopy vs. Raman microscopy) by means of statistical methods using R-software [52]. This procedure has been taken as a comparison of two time-series with equal distances and numbers of measurements. Values of the three separate measurements (of the three-

line segments) were averaged for each device leading to one, more robust record for each device and sample. Each of the two averaged univariate records was numerically standardized separately for each sample (mean = 0, sd = 1). The standardized data were modelled with fine smoothing spline (with $df = 30$) by the R-function *smooth.spline*. Predictions of the spline models for the original pixel position were correlated between the two records (light microscopy vs. Raman microscopy) by means of Spearman rank order correlation coefficient. Other function was cross-correlations (function *ccf*) with default setting of maximum lag of $10 \cdot \log_{10}(N/m)$ where N is the number of pixels measured in a given sample in one line and m the number of series. Light microscopy and Raman microscopy represent two independent records of the same sample, which is connected with two different light/optic distortions. Each of the records were manually cropped in image software separately. These procedures might slightly shift or otherwise distort the record when directly compared. This could be a source of respective shifts in correlated curves. Therefore, we used cross-correlation (with an appropriate lag) to find the highest possible matching of the two curves.

Side by side, we compared both records by careful qualitative visual inspection through manual comparison of the images placed Morphoscopic description were recorded and a comparison of matching and non-matching items was performed. We evaluated the number of ALs in LM and RM records and signal intensity of phosphate group in RM records.

This assessment was recorded in Table 2, and, finally, compared with the results of the quantitative statistical methods described above.

3. Results and discussion

The visual assessment shows that decrease/increase of signal intensity at 960 cm^{-1} (vibration of phosphate group) in RM records was in partial congruence with LM records in the majority of samples (Table 2, Figs. A1-A11, A14-A15, Fig. 1). At least one AL in LM record was also observed in RM record. Signal intensity decreased in EDJ positions except for sample 12, where a signal increase was observed (Fig. A12). In all samples (except for sample 1), accentuated stress lines detected by LM contain a lower content of phosphate, as evidenced by RM (Fig. A1). In sample 1, the intensity of phosphate increased in AL position in the inner enamel area. However, the signal increase in this area could be a consequence of localized sample surface irregularities. Signal intensity of phosphate group resulted in generally lower values throughout the

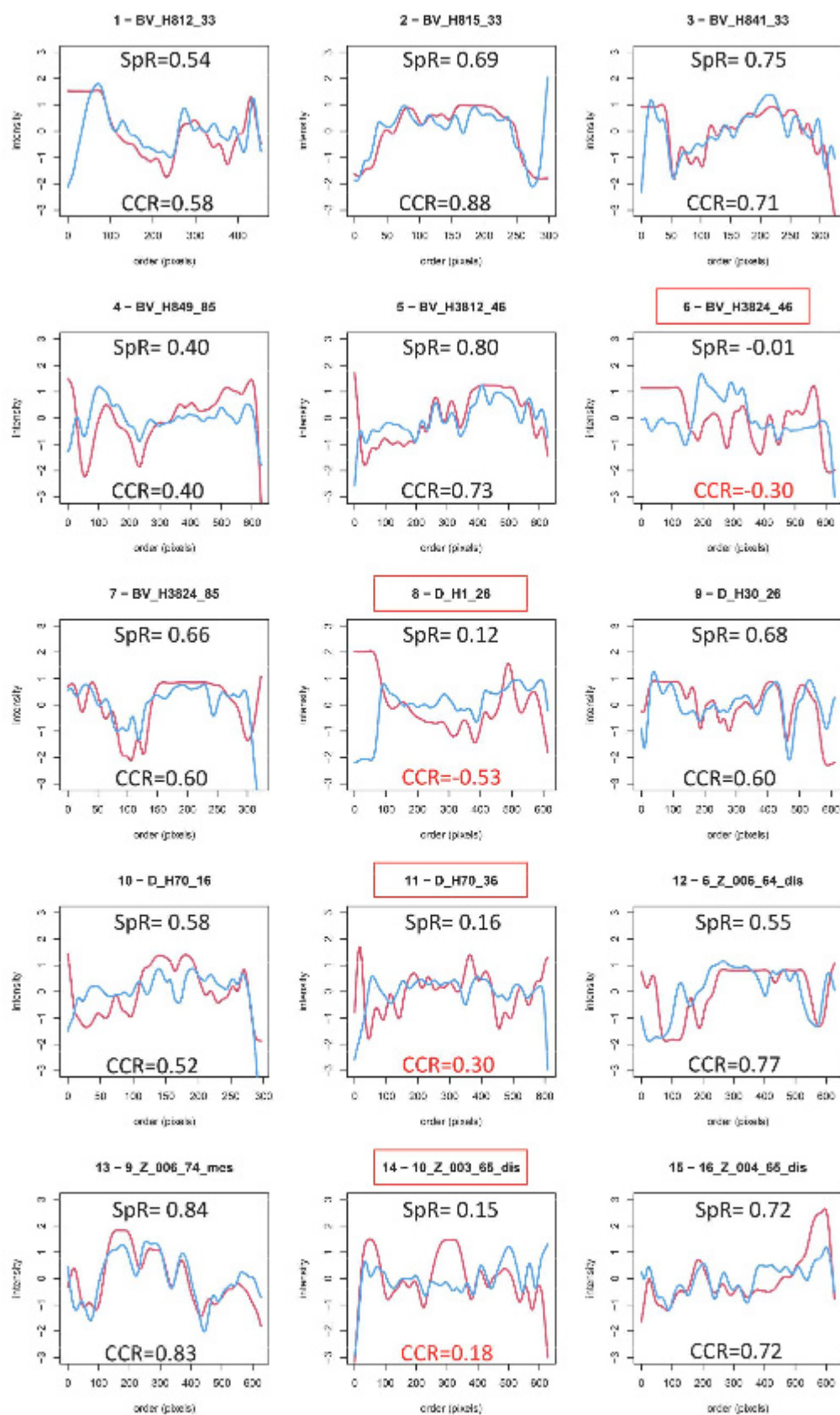


Fig. 2. Comparison of standardized values: blue – light microscopy, red – Raman microscopy fitted by smoothing spline, $df = 30$. SpR = Spearman correlation coefficient, CCR = Cross-correlation coefficient. Samples 6, 8, 11 and 14 (in red rectangle) showed lower correlations.

Table 2

Qualitative evaluation of RM and LM records. $n AL(i)$ = number of accentuated stress lines in inner part of enamel, $n AL(m)$ = number of accentuated stress lines in middle part of enamel, $n AL(o)$ = number of accentuated stress lines in outer part of enamel, $n AL(sum)$ = total number of accentuated stress, EDJ = enamel-dentin junction, AL = accentuated stress line, RL = Retzius lines.

Sample ID	Analyzed segment location	Description light microscopy	Description Raman microscopy	Conclusion
1	Cuspal enamel	<ul style="list-style-type: none"> $n AL(i) = 2$ $n AL(m) = 2$ $n AL(o) = 0$ $n AL(sum) = 4$ EDJ = clearly visible 	<ul style="list-style-type: none"> Signal intensity decrease in positions of AL (i) = 1 Signal intensity increase in positions of AL (i) = 1 Signal intensity decrease in positions of AL (m) = 1 Signal intensity decrease/increase in outer enamel = 0 Signal intensity decrease in EDJ = yes 	Lower signal intensity values through the enamel with several increases/decreases in ALs positions and decrease in EDJ positions. Congruence in inner enamel ALs positions and partially in middle enamel ALs positions.
2	Lateral enamel	<ul style="list-style-type: none"> $n AL = 0$ RL = clearly visible with more intensity in outer enamel direction EDJ = clearly visible 	<ul style="list-style-type: none"> Signal intensity decrease/increase in RL positions = no Signal intensity decrease in EDJ = yes 	Lower signal intensity values through the enamel with single decrease in EDJ position. RLs are not visible in RM record.
3	Cuspal enamel	<ul style="list-style-type: none"> $n AL(i) = 0$ $n AL(m) = 2$ $n AL(o) = 2$ $n AL(sum) = 4$ EDJ = clearly visible 	<ul style="list-style-type: none"> Signal intensity decrease/increase in inner enamel = 0 Signal intensity decrease in positions of AL (m) = 1 Signal intensity decrease in positions of AL (o) = 1 Signal intensity decrease/increase in outer enamel = 0 Signal intensity decrease in EDJ = yes 	Lower signal intensity values through the enamel with single decrease in EDJ position. Higher signal intensity values in outer enamel direction are visible. Partial congruence in middle and outer enamel ALs positions in form of signal intensity decrease.
4	Cuspal enamel	<ul style="list-style-type: none"> $n AL(i) = 0$ $n AL(m) = 1$ $n AL(o) = 0$ $n AL(sum) = 1$ EDJ = clearly visible 	<ul style="list-style-type: none"> Signal intensity decrease/increase in inner enamel = 0 Signal intensity decrease in positions of AL (m) = 1 Signal intensity decrease/increase in outer enamel = 0 	Lower signal intensity values through the enamel with decrease in EDJ position and one AL position. Higher signal intensity values in inner enamel direction are visible. Partial congruence in middle enamel ALs positions in

Table 2 (continued)

Sample ID	Analyzed segment location	Description light microscopy	Description Raman microscopy	Conclusion
5	Cuspal enamel	<ul style="list-style-type: none"> $n AL(i) = 0$ $n AL(m) = 3$ $n AL(o) = 0$ $n AL(sum) = 3$ EDJ = clearly visible 	<ul style="list-style-type: none"> Signal intensity decrease in EDJ = yes Signal intensity decrease/increase in inner enamel = 0 Signal intensity decrease in positions of AL (m) = 3 Signal intensity decrease/increase in outer enamel = 0 Signal intensity decrease in EDJ = yes 	form of signal intensity decrease. Lower signal intensity values through the enamel with decreases in EDJ position and all three ALs positions. Higher signal intensity values in inner enamel direction are visible.
6	Cuspal enamel	<ul style="list-style-type: none"> AL(i) = 1 $n AL(m) = 0$ $n AL(o) = 0$ $n AL(sum) = 1$ EDJ = clearly visible 	<ul style="list-style-type: none"> Signal intensity decrease in positions of AL (i) = 1 Signal intensity decrease/increase in middle enamel = 0 Signal intensity decrease/increase in outer enamel = 0 Signal intensity decrease in EDJ = yes 	Lower signal intensity values through the enamel with decrease in EDJ position and AL positions. Higher signal intensity values in outer enamel direction are visible.
7	Cuspal enamel	<ul style="list-style-type: none"> $n AL(i) = 0$ $n AL(m) = 1$ $n AL(o) = 0$ $n AL(sum) = 1$ EDJ = clearly visible 	<ul style="list-style-type: none"> Signal intensity decrease/increase in inner enamel = 0 Signal intensity decrease in positions of AL (m) = 1 Signal intensity decrease/increase in outer enamel = 0 Signal intensity decrease in EDJ = yes 	Higher signal intensity values through the enamel with decrease in EDJ position and AL positions.
8	Cuspal enamel	<ul style="list-style-type: none"> $n AL(i) = 0$ $n AL(m) = 1$ $n AL(o) = 0$ $n AL(sum) = 1$ EDJ = clearly visible 	<ul style="list-style-type: none"> Signal intensity is uniform with increasing tendency from EDJ to outer enamel direction. No signal intensity decrease/increase visible in single AL position. 	Higher signal intensity values through the enamel with increasing tendency from EDT to outer enamel.
9	Cuspal enamel	<ul style="list-style-type: none"> $n AL(i) = 1$ $n AL(m) = 1$ $n AL(o) = 1$ $n AL(sum) = 3$ EDJ = clearly visible 	<ul style="list-style-type: none"> Signal intensity decrease in positions of AL (i) = 1 Signal intensity decrease in positions of AL (m) = 1 	Middle signal intensity values through the enamel with decreases in EDJ position and all three AL positions.

(continued on next page)

Table 2 (continued)

Sample ID	Analyzed segment location	Description light microscopy	Description Raman microscopy	Conclusion
10	Cuspal enamel	<ul style="list-style-type: none"> n AL(i) = 1 n AL(m) = 1 n AL(o) = 0 n AL (sum) = 2 EDJ = clearly visible 	<ul style="list-style-type: none"> Signal intensity decrease in positions of AL (o) = 1 Signal intensity decrease in EDJ = yes Signal intensity decrease in positions of AL (i) = 1 Signal intensity decrease in positions of AL (m) = 1 Signal intensity decrease/increase in outer enamel = 0 Signal intensity decrease in EDJ = yes 	Higher signal intensity values through the enamel with decreases in EDJ position and AL positions.
11	Cuspal enamel	<ul style="list-style-type: none"> n AL(i) = 1 n AL(m) = 1 n AL(o) = 1 n AL (sum) = 3 EDJ = clearly visible 	<ul style="list-style-type: none"> Signal intensity is uniform with decreasing tendency from EDJ to outer enamel direction. No signal intensity decrease/increase in ALs positions. 	Higher signal intensity values through the enamel with no decreases in EDJ position and AL positions.
12	Cuspal enamel	<ul style="list-style-type: none"> n AL(i) = 0 n AL(m) = 1 n AL(o) = 0 n AL (sum) = 1 EDJ = clearly visible 	<ul style="list-style-type: none"> Signal intensity decrease/increase in inner enamel = 0 Signal intensity decrease in positions of AL (m) = 1 Signal intensity decrease/increase in outer enamel = 0 Signal intensity decrease in EDJ = no 	Higher signal intensity values through the enamel with decreases in AL positions. No signal intensity decreases visible in EDJ position.
13	Cuspal enamel	<ul style="list-style-type: none"> n AL(i) = 0 n AL(m) = 1 n AL(o) = 0 n AL (sum) = 1 EDJ = clearly visible 	<ul style="list-style-type: none"> Signal intensity decrease/increase in inner enamel = 0 Signal intensity decrease in positions of AL (m) = 1 Signal intensity decrease/increase in outer enamel = 0 Signal intensity decrease in EDJ = no 	Middle-higher signal intensity values through the enamel with decreases in AL positions. No signal intensity decrease visible in EDJ position.
14	Cuspal enamel	<ul style="list-style-type: none"> n AL(i) = 1 n AL(m) = 0 n AL(o) = 0 n AL (sum) = 1 	<ul style="list-style-type: none"> Signal intensity is uniform through all area with not clear decrease 	Middle-higher signal intensity values through the enamel with decrease in EDJ position and no

Table 2 (continued)

Sample ID	Analyzed segment location	Description light microscopy	Description Raman microscopy	Conclusion
15	Cuspal enamel	<ul style="list-style-type: none"> n AL(i) = 1 n AL(m) = 0 n AL(o) = 0 n AL (sum) = 1 EDJ = clearly visible 	<ul style="list-style-type: none"> EDJ = clearly visible in single AL(i) position. Signal intensity decrease in EDJ = yes Signal intensity is uniform through the area with increasing tendency from EDJ to outer enamel direction. Signal intensity decrease in EDJ = no 	decrease in AL position. High signal intensity values through the enamel. No signal increases/decreases visible in EDJ or AL position.

enamel in samples 1–6 and 9 (Fig. 1, Figs. A1–A5, A8) and middle/higher values in samples 7, 8, 10–15 (Figs. A6, A7, A9–A14).

Retzius lines observed in LM record of sample 2 were not visually detected in RM data record in RGB imaging (Fig. A2B). This fact may signalize that RLs contains similar phosphate values as surrounding enamel. However, RM grayscale record shows slightly visible lines in places of RLs. In addition, statistical analysis indicated moderate to strong correlation between those records (Fig. 2 -sample 2). These results suggest that RLs visually detected in LM record contain slightly lower phosphate values than surrounding enamel. Phosphate signal decrease is not as visible as in ALs positions, but is still present, based on the results of correlation analysis.

The statistical assessment shows that, in most of the samples, distribution of the light intensity values was mostly skewed toward the lower values with many more outliers in the lower tail (dark pixels) than in the opposite side of the distribution. Correlation between pixel intensities from the Raman image record and the record from light microscopy within the whole sample ($N = 7935$, i.e., merging all standardized values into one correlation) was low and positive (Spearman $R = 0.33$, $S = 5.5535e + 10$, $p\text{-value} < 2.2e-16$). Separate correlations for each sample (Fig. 2), were mostly moderate to highly positive in its value (ranging from Spearman $R = 0.40$ to 0.84) and highly statistically significant, with four exceptions (sample 6, 8, 11, and 14) that will be discussed more closely later in this text. Cross-correlation method confirmed these results. In many samples, an appropriate shift (in some samples to one, and in others to the opposite direction, Table A2) within the defined lags evidently improved (increased) the correlation between records from Raman microscopy and light microscopy. Based on the correlation analysis, records from transmitted light microscopy correspond with Raman microscopy records.

In the four analyzed samples (6, 8, 11, and 14) previously highlighted, correlations between pixel intensities from RM and LM records were much lower than in the remaining samples (Fig. 2). Sample 6's RM record in RGB imaging (Fig. A5B) is in congruence with LM record (signal decrease in single AL position and in EDJ position) visually, but the RM record in grayscale differs from the LM grayscale. One possible explanation is that grayscale imaging mode introduced more 'noise' that could have affected statistical results. In LM record of sample 8 (Fig. A7), there is a visibly darker part of enamel in the outer enamel direction and signal intensity in RM record is high in value. However, the higher intensity of signal at 960 cm^{-1} in the outer part of enamel in Raman imaging record could be related to inequality of thickness in prepared tooth thin section, or dental caries based on LM record. The quality of transmitted light microscopy record strongly depends on thin section quality which is also dependent upon thin section thickness. If the thin section is

comparatively thick (as a result of inconsistency in thin section preparation process), the final record from transmitted light microscopy can be shifted/blurred, and therefore may not match well with the Raman microscopy record. On the other hand, Raman microscopy records the sample on the surface, so when disagreement between LM and RM record occurs, Raman microscopy shows that the problem may be sample thickness or irregularities of sample surface. Exact sample thickness can be determined using a digital microscope or a more sensitive method (atomic force microscope). After removing first 100 pixels from both records (dark area in LM), CCR = 0.713, which provides strong positive correlation between LM and RM records (Fig. A15). Sample 11's RM and LM records in grayscale visually correspond more than RGB imaging records (Fig. A10C), but correlation between them is low (Fig. 2, sample 11). The reason may be 'noise' introduced from sample preparation (e. g., bubbles in resin), which could affect quality of both LM and RM records. The result of such 'noise' may be lower visibility of microstructures in the LM record and sample thickness irregularities may cause uneven signal decreases/increases in the RM record. There is no visual congruence between sample 14's LM and RM records, which is in accordance with correlation analysis results (Fig. A13, Fig. 2 – sample 14). RM analysis did not detect signal intensity decrease or increase in single AL position visible at LM record.

As previously described, results can be seriously affected by several factors. Taphonomic factors can influence enamel microstructure (bacterial degradation and decomposition of the enamel) and methodological inconsistencies (e.g., bubbles in resin) can introduce 'noise' that can seriously increase the complexity of the results and make interpretation challenging.

4. Conclusions

Raman microscopy was used for analysis of accentuated stress lines in human enamel. The changes in intensity of phosphate in tooth samples generally agrees with changes in accentuated lines measured by transmitted light microscopy of dental enamel longitudinal thin sections. These accentuated lines, which form a "barcode" appearance in dental enamel, are mostly areas with reduced phosphate concentrations, i.e., hypomineralized lines. Based on obtained results, we suppose that Raman microscopy of ALs could offer new and alternative perspectives on the enamel structures. In most cases, we found that the optical change in the light microscope corresponds to the change in phosphate concentration in Raman microscope. However, RM may not detect everything that is recognized by LM. This suggests that that something changes optically without altering the phosphate content, or that RM may distinguish differences that we do not see in an LM. As this is a pilot study combining the two described methodological approaches, it is necessary to develop this methodology further. We should focus on between LM and RM records to discover exactly what they mean. This may provide more information about sample variability and/or applicability of used method. In the future, together with a more detailed assessment of the concentration of phosphates in individual AL, these deviations could help to classify stress lines into subtypes, corresponding to different progress or intensities of stress in the body occurring in early ontogenetic stages.

CRedit authorship contribution statement

Soňa Vacková: Writing - original draft, Methodology, Data curation, Investigation. **Miroslav Králík:** Writing - review & editing, Conceptualization, Supervision. **Klára Marečková:** Data curation, Investigation. **Lucie Ráčková:** Data curation, Investigation. **Leslie Quade:** Writing - review & editing. **Lenka Sedláčková:** Resources, Writing - review & editing. **Pavel Fojtík:** Resources, Writing - review & editing. **Lukáš Kučera:** Writing - original draft, Data curation, Supervision, Investigation.

Declaration of Competing Interest

The authors declare that they have no known competing financial interests or personal relationships that could have appeared to influence the work reported in this paper.

Acknowledgments

The authors gratefully acknowledge the support of the Grant Agency of Czech Republic [17-17346S], support of Masaryk University Development Fund [MUNI/A/1609/2020] and [MUNI/FR/1515/2018].

Institutional review board statement

The study *Ontogenic record in tooth microstructure* was conducted according to the guidelines of the Declaration of Helsinki, and approved by the ELSPAC ethics committee at Masaryk University on 14th December 2018.

Informed consent statement

Informed consent was obtained from all subjects involved in the study *Ontogenic record in tooth microstructure*.

Appendix A. Supplementary data

Supplementary data to this article can be found online at <https://doi.org/10.1016/j.microc.2021.106370>.

References

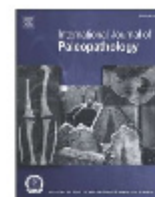
- [1] T.M. Smith, Experimental determination of the periodicity of incremental features in enamel, *J. Anat.* 208 (1) (2006) 99–113, <https://doi.org/10.1111/j.1469-7580.2006.00499.x>.
- [2] D.J. Reid, M.C. Dean, Variation in modern human enamel formation times, *J. Hum. Evol.* 50 (3) (2006) 329–346, <https://doi.org/10.1016/j.jhevol.2005.09.003>.
- [3] D.J. Reid, R.J. Ferrell, The relationship between number of striae of Retzius and their periodicity in imbricational enamel formation, *J. Hum. Evol.* 50 (2) (2006) 195–202, <https://doi.org/10.1016/j.jhevol.2005.09.002>.
- [4] M.C. Dean, Growth layers and incremental markings in hard tissues; a review of the literature and some preliminary observations about enamel structure in *Paranthropus boisei*, *J. Hum. Evol.* 16 (2) (1987) 157–172, [https://doi.org/10.1016/0047-2484\(87\)90074-1](https://doi.org/10.1016/0047-2484(87)90074-1).
- [5] D. Guatelli-Steinberg, What can developmental defects of enamel reveal about physiological stress in nonhuman primates? *Evol. Anthropol. Issues News Rev.* 10 (4) (2001) 138–151, <https://doi.org/10.1002/evan.1027>.
- [6] A.H. Goodman, J.C. Rose, Assessment of systemic physiological perturbations from dental enamel hypoplasias and associated histological structures, *Am. J. Phys. Anthropol.* 33 (S11) (1990) 59–110, [https://doi.org/10.1002/\(ISSN\)1096-8641.1002/ajpa.v33.i11+10.1002/ajpa.1330330506](https://doi.org/10.1002/(ISSN)1096-8641.1002/ajpa.v33.i11+10.1002/ajpa.1330330506).
- [7] W. Dirks, L.T. Humphrey, M.C. Dean, T.E. Jeffries, The relationship of accentuated lines in enamel to weaning stress in juvenile baboons (*Papio hamadryas anubis*), *Folia Primatol. (Basel)* 81 (4) (2010) 207–223, <https://doi.org/10.1159/000321707>.
- [8] K.O. Lorentz, S.A.M. Lemmers, C. Chrysostomou, W. Dirks, M.R. Zaruri, F. Foruzanfar, S.M.S. Sajjadi, Use of dental microstructure to investigate the role of prenatal and early life physiological stress in age at death, *J. Archaeol. Sci.* 104 (2019) 85–96, <https://doi.org/10.1016/j.jas.2019.01.007>.
- [9] T.M. Smith, Incremental dental development: Methods and applications in hominoid evolutionary studies, *J. Hum. Evol.* 54 (2008) 205–224, <https://doi.org/10.1016/j.jhevol.2007.09.020>.
- [10] C.M. Fitzgerald, J.C. Rose, Reading Between the Lines: Dental Development and Subadult Age Assessment Using the Microstructural Growth Markers of Teeth, in: *Biol. Anthropol. Hum. Skelet.*, John Wiley & Sons, Ltd, 2007: pp. 237–263. <https://doi.org/10.1002/9780470245842.ch8>.
- [11] J.A. Gamble, J.L. Boldsen, R.D. Hopps, Stressing out in medieval Denmark: an investigation of dental enamel defects and age at death in two medieval Danish cemeteries, *Int. J. Paleopathol.* 17 (2017) 52–66, <https://doi.org/10.1016/j.ijpp.2017.01.001>.
- [12] S. Hillson, *Tooth Development in Human Evolution and Bioarchaeology*, Cambridge University Press, New York, 2014.
- [13] G. Macho, D. Reid, M. Leakey, N. Jablonski, A. Beynon, Climatic effects on dental development of *Theropithecus oswaldi* from Koobi Fora and Ologesailie, *J. Hum. Evol.* 30 (1) (1996) 57–70, <https://doi.org/10.1006/jhevol.1996.0004>.
- [14] T.M. Smith, C. Austin, D.R. Green, R. Joannes-Boyau, S. Bailey, D. Dumitriu, S. Fallon, R. Grün, H.F. James, M.-H. Moncel, L.S. Williams, R. Wood, M. Arora,

- Wintertime stress, nursing, and lead exposure in Neanderthal children, *Sci. Adv.* 4 (2018) eaau9483, <https://doi.org/10.1126/sciadv.aau9483>.
- [15] M.C. Dean, Retrieving chronological age from dental remains of early fossil hominins to reconstruct human growth in the past, *Philos. Trans. R. Soc. B Biol. Sci.* 365 (1556) (2010) 3397–3410, <https://doi.org/10.1098/rstb.2010.0052>.
- [16] K. McGrath, L.S. Limmer, A.-L. Lockey, D. Guatelli-Steinberg, D.J. Reid, C. Witzel, E. Bocaage, S.C. McFarlin, S. El Zaatari, 3D enamel profilometry reveals faster growth but similar stress severity in Neanderthal versus *Homo sapiens* teeth, *Sci. Rep.* 11 (2021) 522, <https://doi.org/10.1038/s41598-020-80148-w>.
- [17] A. Hupková, W. Dirks, M. Králík, M. Račanská, Retrieval of a developmental record from dental remains: Stress chronology and age at death assessment of a juvenile skeleton from a medieval site in Moravia, Czech Republic, in: S. Sázalová, M. Novák, A. Mizerová (Eds.), *Forgot. Times Spaces New Perspect. Paleontological Paleontological Archeol. Stud.*, Masaryk university, Brno, 2015; pp. 520–531. 10.5817/CZ.MUNI.M210-7781-2015-39.
- [18] A. Hupková, S. Šaliová, M. Králík, R. Malček, Nejsou čary jako čary: inkrementální linie v mikrostruktuře zubů a jejich využití při analýze kosterních nálezů, 21 (2016) 113–138. 10.5817/SAB2016-2-7.
- [19] W. Birch, M.C. Dean, A method of calculating human deciduous crown formation times and of estimating the chronological ages of stressful events occurring during deciduous enamel formation, *J. Forensic Leg. Med.* 22 (2014) 127–144, <https://doi.org/10.1016/j.jflm.2013.12.002>.
- [20] T.J. Shepherd, W. Dirks, C. Mannee, S. Hodgson, D.A. Banks, P. Averley, T. Pless-Mulloli, Reconstructing the life-time lead exposure in children using dentine in deciduous teeth, *Sci. Total Environ.* 425 (2012) 214–222, <https://doi.org/10.1016/j.scitotenv.2012.03.022>.
- [21] E. Žadzińska, W. Lorkiewicz, M. Kurek, B. Borowska-Strugińska, Accentuated lines in the enamel of primary incisors from skeletal remains: a contribution to the explanation of early childhood mortality in a medieval population from Poland, *Am. J. Phys. Anthropol.* 157 (2015) 402–410, <https://doi.org/10.1002/ajpa.22731>.
- [22] G.A. Macho, Primate molar crown formation times and life history evolution revisited, *Am. J. Primatol.* 55 (4) (2001) 189–201, [https://doi.org/10.1002/\(ISSN\)1098-234510.1002/ajp.v55.410.1002/ajp.1054](https://doi.org/10.1002/(ISSN)1098-234510.1002/ajp.v55.410.1002/ajp.1054).
- [23] I. Schour, The neonatal line in the enamel and dentin of the human deciduous teeth and first permanent molar, *J. Am. Dent. Assoc.* 23 (1936) 1946–1955.
- [24] W. Dirks, D.J. Reid, C.J. Jolly, J.E. Phillips-Conroy, F.L. Brett, Out of the mouths of baboons: Stress, life history, and dental development in the Awash National Park hybrid zone, Ethiopia, *Am. J. Phys. Anthropol.* 118 (2002) 239–252, <https://doi.org/10.1002/ajpa.10089>.
- [25] T.M. Smith, D.J. Reid, J.E. Sirianni, The accuracy of histological assessments of dental development and age at death, *J. Anat.* 208 (1) (2006) 125–138, <https://doi.org/10.1111/joa.2006.208.issue-110.1111/j.1469-7580.2006.00500.x>.
- [26] S.S. Andra, C. Austin, M. Arora, The tooth exposure in children's health research, *Curr. Opin. Pediatr.* 28 (2016) 221–227, <https://doi.org/10.1097/MOP.0000000000000327>.
- [27] C.M. FitzGerald, S.R. Saunders, Test of histological methods of determining chronology of accentuated striae in deciduous teeth, *Am. J. Phys. Anthropol.* 127 (3) (2005) 277–290, <https://doi.org/10.1002/ajpa.v127:310.1002/ajpa.10442>.
- [28] A.G. Fincham, J. Moradian-Oldak, J.P. Simmer, The Structural Biology of the Developing Dental Enamel Matrix, *J. Struct. Biol.* 126 (3) (1999) 270–299, <https://doi.org/10.1006/jsbi.1999.4130>.
- [29] J.D. Pasteris, B. Wopenka, E. Valsami-Jones, Bone and tooth mineralization: why apatite? *Elements* 4 (2) (2008) 97–104, <https://doi.org/10.2113/GSELEMENTS.4.2.97>.
- [30] M. He, H. Lu, C. Luo, T. Ren, Determining trace metal elements in the tooth enamel from Hui and Han Ethnic groups in China using microwave digestion and inductively coupled plasma mass spectrometry (ICP-MS), *Microchem. J.* 127 (2016) 142–144, <https://doi.org/10.1016/j.microc.2016.02.009>.
- [31] I. Guede, M.C. Zuluaga, L.A. Ortega, A. Alonso-Olazar, X. Murelaga, M. Pina, F. J. Gutierrez, Analyses of human dentine and tooth enamel by laser ablation-inductively coupled plasma-mass spectrometry (LA-ICP-MS) to study the diet of medieval Muslim individuals from Tauste (Spain), *Microchem. J.* 130 (2017) 287–294, <https://doi.org/10.1016/j.microc.2016.10.005>.
- [32] A. Hanč, A. Olszewska, D. Barankiewicz, Quantitative analysis of elements migration in human teeth with and without filling using LA-ICP-MS, *Microchem. J.* 110 (2013) 61–69, <https://doi.org/10.1016/j.microc.2013.02.006>.
- [33] J. Farell, D. Amarasiriwardena, A.H. Goodman, B. Arriaza, Bioimaging of trace metals in ancient Chilean mummies and contemporary Egyptian teeth by laser ablation-inductively coupled plasma-mass spectrometry (LA-ICP-MS), *Microchem. J.* 106 (2013) 340–346, <https://doi.org/10.1016/j.microc.2012.09.005>.
- [34] E. Webb, D. Amarasiriwardena, S. Tauch, E.F. Green, J. Jones, A.H. Goodman, Inductively coupled plasma-mass (ICP-MS) and atomic emission spectrometry (ICP-AES): versatile analytical techniques to identify the archived elemental information in human teeth, *Microchem. J.* 81 (2005) 201–208, <https://doi.org/10.1016/j.microc.2005.04.002>.
- [35] E. Marín, N. Hiraiishi, T. Honma, F. Boschetto, M. Zanocco, W. Zhu, T. Adachi, N. Kanamura, T. Yamamoto, G. Pezzotti, Raman spectroscopy for early detection and monitoring of dentin demineralization, *Dent. Mater.* 36 (12) (2020) 1635–1644, <https://doi.org/10.1016/j.dental.2020.10.005>.
- [36] J. Silveira, S. Coutinho, D. Marques, J. Castro, A. Mata, M.L. Carvalho, S. Pessanha, Raman spectroscopy analysis of dental enamel treated with whitening product – Influence of saliva in the remineralization, *Spectrochim. Acta. A. Mol. Biomol. Spectrosc.* 198 (2018) 145–149, <https://doi.org/10.1016/j.saa.2018.03.007>.
- [37] T. Vargas-Koudriavtsev, R. Durán-Sedó, P. Sáenz-Bonilla, V. Bonilla-Mora, M. Guevara-Bertsch, R.A. Jiménez-Corales, O.A. Herrera-Sancho, Effect of tooth-bleaching agents on phosphate concentration in dental enamel by means of Raman spectroscopy, *Rev. Odontológica Mex.* 19 (2015) e228–e235, <https://doi.org/10.1016/j.rodMex.2015.10.013>.
- [38] J.-Y. Lee, H.-J. Kim, E.-S. Lee, E. de Josselin, H.-J. de Jong, B.-I. Jung, Quantitative light-induced fluorescence as a potential tool for detection of enamel chemical composition, *Photodiagnosis Photodyn. Ther.* 32 (2020), 102054, <https://doi.org/10.1016/j.pdpdt.2020.102054>.
- [39] L.A. Darchuk, L.V. Zaverbna, A. Worobiec, R. Van Grieken, Structural features of human tooth tissues affected by high dose of external ionizing radiation after nuclear catastrophe of Chernobyl plant, *Microchem. J.* 97 (2) (2011) 282–285, <https://doi.org/10.1016/j.microc.2010.09.016>.
- [40] A. Baide, C. Farber, M. Krimmer, D. Wescott, K. Kurouski, Non-invasive post-mortem interval diagnostics using a hand-held Raman spectrometer, *Forensic Chem.* 20 (2020), 100270, <https://doi.org/10.1016/j.forc.2020.100270>.
- [41] C. Austin, T.M. Smith, R.M.Z. Farahani, K. Hinde, E.A. Carter, J. Lee, P.A. Lay, B. J. Kennedy, B. Sarrafpour, R.J. Wright, R.O. Wright, M. Arora, Uncovering system-specific stress signatures in primate teeth with multimodal imaging, *Sci. Rep.* 6 (2016) 18802, <https://doi.org/10.1038/srep18802>.
- [42] L. Sedláčková, Předběžné hlášení o provedení záchranného archeologického výzkumu "Bytový dům Vědecká, II. Etapa, Brno", 2013.
- [43] P. Fojtík, NZ Dětkovice 2009, Za zahrádama, "terénní úpravy zářezu sílnice III. třídy č. 37762, k. ú. Dětkovice, okr. Prostějov", č. akce 148/09., Ústav archeologické památkové péče Brno, Brno, 2009.
- [44] P. Fojtík, NZ Dětkovice 2010, Za zahrádama, "předstihový výzkum na ploše určené k výstavbě RD, parc. č. 1106, k. ú. Dětkovice, okr. Prostějov", č. akce 212/10., Ústav archeologické památkové péče Brno, Brno, 2010.
- [45] P. Fojtík, NZ Dětkovice 2010, Za zahrádama, "přelozka optického kabelu na parc. č. 1106, k. ú. Dětkovice, okr. Prostějov", č. akce 59/10., Ústav archeologické památkové péče Brno, Brno, 2010.
- [46] P. Piler, V. Kandrnl, L. Kukla, L. Andryšková, J. Švancara, J. Jarkovský, L. Dusek, H. Pihlhart, M. Bobák, J. Klánová, Cohort Profile: The European Longitudinal Study of Pregnancy and Childhood (ELSPAC) in the Czech Republic, *Int. J. Epidemiol.* 46 (2017) 1379–1379f. 10.1093/ije/dyw091.
- [47] H.H. de Boer, M.J. Aarents, G.J.R. Maat, Manual for the preparation and staining of embedded natural dry bone tissue sections for microscopy, *Int. J. Osteoarchaeol.* 23 (1) (2013) 83–93, <https://doi.org/10.1002/oa.1242>.
- [48] S. Sázalová, S. Borjová, S. Šaliová, The upper paleolithic hard animal tissue under the microscope: selected examples from Moravian sites, *Quat. Int.* (2020), <https://doi.org/10.1016/j.quaint.2020.10.027>.
- [49] P.F. Rossi, L. Bondioli, G. Geusa, R. Marchiarielli, Osteodental biology of the people of *Portus Romae* (Necropolis of Isola Sacra, 2nd–3rd Cent. AD). I. Enamel microstructure and developmental defects of the primary dentition, *Digit. Arch. Hum. Paleobiology.* 1 (1999).
- [50] A.D. Beynon, M.C. Dean, D.J. Reid, On thick and thin enamel in hominoids, *Am. J. Phys. Anthropol.* 86 (2) (1991) 295–309, [https://doi.org/10.1002/\(ISSN\)1096-864410.1002/ajpa.v86:210.1002/ajpa.1330860216](https://doi.org/10.1002/(ISSN)1096-864410.1002/ajpa.v86:210.1002/ajpa.1330860216).
- [51] J.A. Stammerer, B. Purgstaller, D. Hippler, V. Mavromatis, M. Dietzel, In-situ Raman spectroscopy of amorphous calcium phosphate to crystalline hydroxyapatite transformation, *MethodsX* 5 (2018) 1241–1250.
- [52] R Core Team, R: A Language and Environment for Statistical Computing, R Foundation for Statistical Computing, Vienna, Austria, 2020. <https://www.R-project.org/>.
- [53] P. Murali, J. Bruzek, F. Houët, E. Cunha, DSP: A tool for probabilistic sex diagnosis using worldwide variability in hip-bone measurements, *Bull. Mém. Société D'Anthropologie Paris.* (2005) 167–176.
- [54] S. Brooks, J.M. Suchey, Skeletal age determination based on the os pubis: A comparison of the Acsádi-Nemeskéri and Suchey-Brooks methods, *Hum. Evol.* 5 (1990) 227–238. 10.1007/bf02437238.
- [55] C.O. Lovejoy, R.S. Meindl, T.R. Prybeck, R.P. Mensforth, Chronological metamorphosis of the auricular surface of the ilium: a new method for the determination of adult skeletal age at death, *Am. J. Phys. Anthropol.* 68 (1985) 15–28.
- [56] S.J. AlQahtani, M.P. Hector, H.M. Liversidge, Brief communication: the London atlas of human tooth development and eruption, *Am. J. Phys. Anthropol.* 142 (2010) 481–490, <https://doi.org/10.1002/ajpa.21258>.



Contents lists available at ScienceDirect

International Journal of Paleopathology

journal homepage: www.elsevier.com/locate/ijpp

Brief communication

A pathological lesion or a postmortem artefact? An interdisciplinary approach to deal with an interesting early medieval case

Martina Fojtová^{a,*}, Jan Křístek^{b,c}, Lukáš Kučera^d^a Anthropos Institute, Moravian Museum, Brno, Czech Republic^b Department of Radiology, Masaryk Memorial Cancer Institute, Brno, Czech Republic^c Department of Medical Imaging, Faculty of Medicine, Masaryk University, Brno, Czech Republic^d Department of Analytical Chemistry, Faculty of Science, Palacký University, Olomouc, Czech Republic

ARTICLE INFO

Keywords:

Pseudopathology

Radiography

Soil inclusion

X-ray fluorescence spectrometry (XRF)

Computer tomography (CT)

Taphonomy

ABSTRACT

Objective: This study evaluates a case of pseudopathology and the effects that postmortem taphonomic changes and environmental influences can have on bone.**Material:** A skeleton of a young male from the early medieval site Staré Město, dated to the 9th–10th century CE.**Methods:** The skeletal remains were subjected to detailed macroscopic and X-ray examination, and then a CT scan and XRF analysis were performed.**Results:** X-ray examination of the mandible revealed unusually dense structures, whose appearance was not consistent with any known pathology. Based on the results of CT scanning, it was hypothesized that these were cavities filled with alluvial sediment. X-ray fluorescence spectrometry (XRF), focusing on the determination of the silica content, revealed a high intensity of silica in the samples of the affected area of the bone.**Conclusion:** The hypothesis that the inclusions were composed of waterborne sediment was supported.**Significance:** Although it is well known that soil can infiltrate bones buried in the ground, its appearance on plain radiographs is not that commonly known. The case illustrates the usefulness of differentiating true pathologies from postmortem alterations to avoid inappropriate interpretations.**Limitations:** No similar cases have been described.**Suggestion for further research:** In palaeopathological evaluation, the use of multiple imaging and evaluative techniques should be implemented to differentiate pathological lesions from pseudopathology.

1. Introduction

Distinguishing pathological lesions from conditions that only resemble them is one of the most challenging problems in palaeopathology. Examples of pseudo-lesions, including the presence of non-metric traits and postmortem alterations caused by biological, physical or chemical factors influencing buried bones, must be taken into account during palaeopathological examination. Taphonomy has received much attention in recent years (Haglund and Sorg, 2002; Duday and Guillon, 2006; Duday et al., 2009; Fernández-Jalvo and Andrews., 2016; Stodder., 2018; Knüsel and Schotsmans., 2022; etc.). As early as 1967, Wells warned against hasty diagnoses in the evaluation of prehistoric skeletal findings and introduced the term "pseudopathology". Although this topic has been addressed in research (e.g., Fulcheri et al., 1986; Corron et al., 2017; Carotenuto et al., 2019), there are instances when macroscopic

differentiation between antemortem and postmortem effects is impossible. At times, X-ray examination is sufficient to make the determination (see Wells, 1967), and many issues can be resolved through the use of light microscopy (Schultz, 1996; Ortner, 2003). However, in some cases, advanced imaging techniques such as computer tomography (CT) and x-ray fluorescence (XRF), can be more beneficial.

In this paper, we introduce a case from the site "Na Valách" in Staré Město in the Czech Republic. We aim to show how the bone structure has been altered due to taphonomic processes, mimicking a pathological condition, and to increase the recognition of pseudopathology.

2. Material

In 2018, during a rescue archaeological research carried out in a part of the burial ground "Na Valách" in Staré Město, Zlín Region, Czech

* Correspondence to: Anthropos Institute, Moravian Museum, Zelný trh 6, 65937 Brno, Czech Republic.

E-mail address: mfojtova@mzm.cz (M. Fojtová).

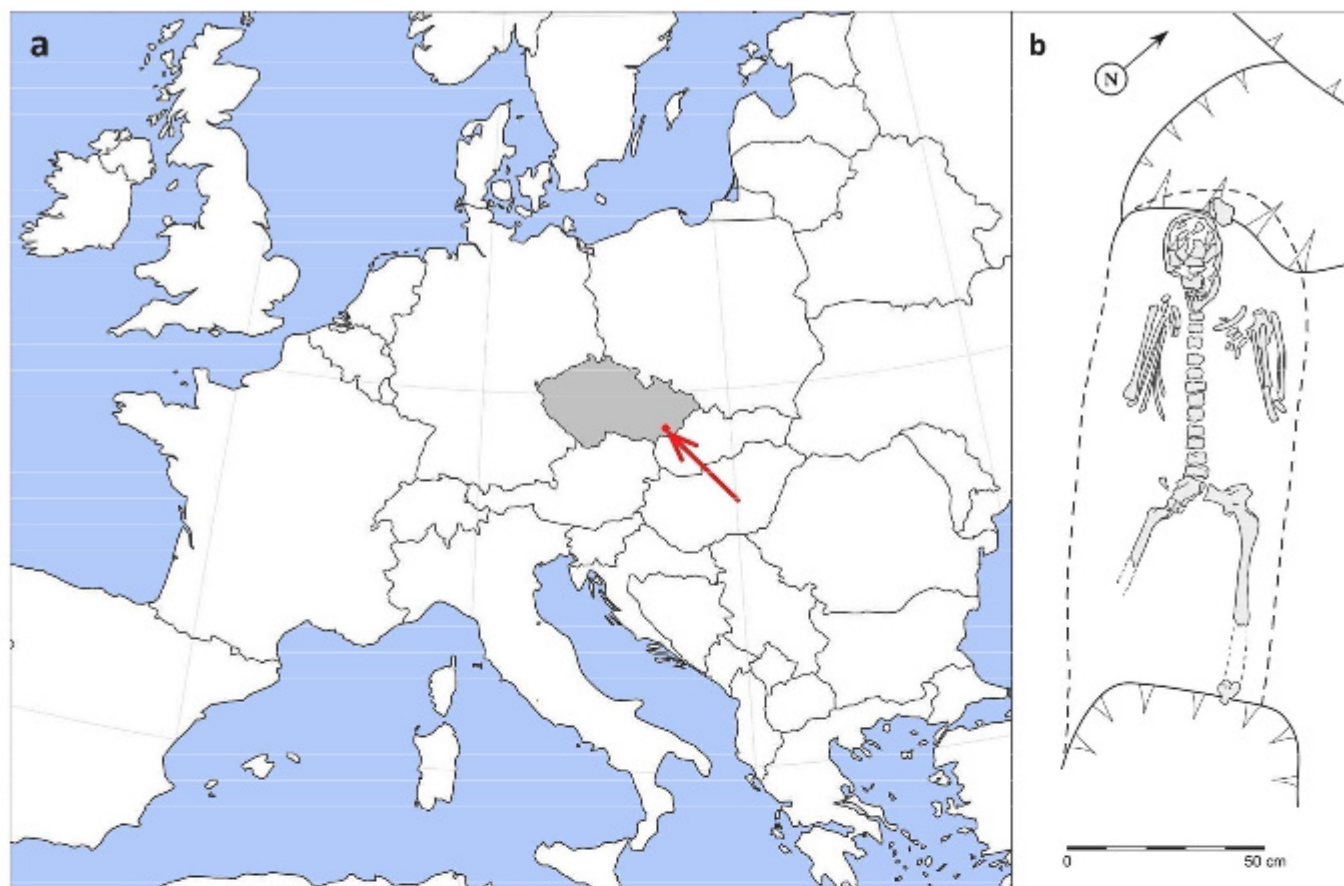


Fig. 1. a) Location of the site on a map of Europe; b) Grave 7/2018.

Republic (see Fig. 1a), human skeletal remains of 26 individuals from a total of 23 graves were excavated (Fojtová and Galuška, 2022). The large early medieval site has been dated to the late 8th to the mid-10th century CE, and in the past 100 years, more than 2000 graves have been excavated there (see Hrubý, 1955; Hochmanová-Vávřová, 1962; Galuška, 2002). Based on the grave finds, the part of the burial site

excavated in 2018 was used from the second half of the 9th to the first half of the 10th century. Grave 7/2018 contained a male of 18–29 years of age, buried on their back with the upper limbs tightly flexed at the elbows and with hands almost touching the shoulders (Fig. 1b). A part of the grave had been damaged by a recent pit. The grave pit was very shallow – only about 40 cm below the present-day surface. Originally,

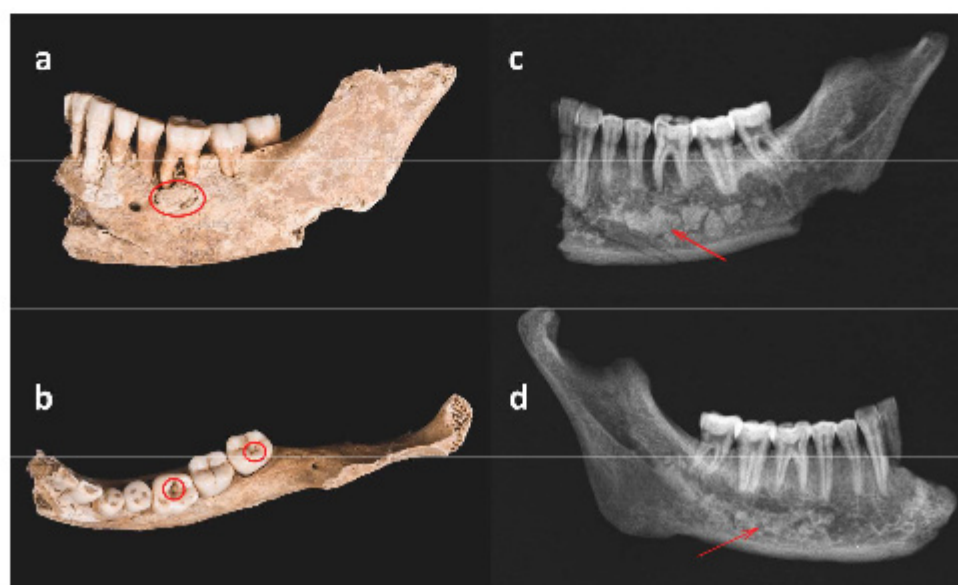


Fig. 2. Left mandible in lateral (a) and superior (b) view with two fistulas draining a periapical lesion of the first molar and carious defects on the first and third molars (circles); Radiographs of the left (c) and right mandible (d) with dense shadows visible (arrows).



Fig. 3. CT images of the mandible recovered from grave 7/2018.

the grave was deeper, but as a result of later agricultural use of the site and landscaping related to construction, the topsoil was gradually reduced. There are two other similarly shallow graves in this part of the burial site (Fojtová and Galuška, 2022). What drew our attention to this case was the extensive destruction of the dentition – there were numerous carious lesions on the teeth of both jaws.

3. Methods

To determine the sex of the individual, skull morphology was assessed (Ferembach et al., 1980). Due to the poor preservation of the skeleton, the tooth wear method (Lovejoy, 1985) was used and, since the molars of both jaws show almost no signs of attrition, we evaluated the skeletal maturation phase (spheno-occipital synchondrosis and femoral head fusion – Schaefer et al., 2009). For macroscopic and X-ray evaluation of the bones, criteria based on Aufderheide and Rodríguez-Martín (1998), Vyhnaněk (1999), and Ortner (2003) were used.

Radiographs were obtained using a stationary X-ray machine Samsung GC 80 A. The images were processed with TomoCon Lite software. CT scanning used a Canon Aquilion 64 CT scanner – a standard diagnostic multidetector CT scanner with 64 rows of detectors, with post-processing 3D analysis performed in a Siemens Syngo Via software environment.

For X-ray fluorescence spectroscopy analysis (XRF), two samples were taken from the affected area under tooth roots and a reference sample was taken from the mandibular ramus where no shadows were observed. All samples came from the same jaw, the sampling sites' selection was based on the radiograph (Fig. 5a, b). A total of 100 mg of sample was taken from the bone using a 0.75 mm carbide drill and Proxxon Micromot 60/EF drill (Proxxon GmbH, Föhren, Germany). Elemental analysis of the samples was performed using an Olympus Vanta X-ray fluorescence spectrometer. The measurement parameters were as follows: analytical mode, excitation energy range: 8–40 kV, acquisition time: 310 s.

4. Results and discussion

4.1. Macroscopical and X-ray examination of the mandible

The macroscopically visible pathological changes in the mandible (several carious lesions, one of which developed a periapical lesion drained by fistulas) (see Fig. 2a, b) prompted the idea to radiograph the jaw to assess intraosseous changes. As expected, post-inflammatory bone changes with periapical and peridental osteolysis corresponding to a periapical cyst or abscess are seen around the lower left first molar, with fistula formation that perforated the outer surface of the alveolar bone. The findings correspond to a chronic inflammatory state, in clinical practice usually presented by variously long periods of relatively mild discomfort interspersed with painful exacerbations (Alt et al., 1998). A relatively extensive carious lesion is also evident on the lower left third molar, with reactive changes in the surrounding bone. However, the image also showed unexpected artifacts. In the bone marrow, multiple, largely confluent shading of dense mass are evident, with granular and fibrillar structures present in places. More or less the whole mandibular body is affected, without lateral predilection (Fig. 2c, d).

4.1.1. Differential diagnosis

A group of specialists consisting of several pathologists and paleopathologists, three dentists, an anatomist, and a radiologist was consulted. The group independently suggested the following possible differential diagnoses:

1. Foreign material
2. Odontome and its variants (ossifying fibroma, calcifying odontogenic cyst, Pindborg tumour, adenomatoid ameloblastoma, ameloblastic fibroma or fibro-odontoma, odontoameloblastoma, odontogenic fibroma)
3. Osteopetrosis
4. Extensive osteopoikilosis
5. Melorheostosis
6. Paget's disease
7. Osteoplastic metastases, e.g., prostate cancer
8. Deposition of heavy metals (lead, mercury)
9. Diffuse inflammatory foci with recalcification

4.2. CT scanning

Since the group of specialists did not reach a consensus, we decided to include a CT scan of the jaw to provide further information (Fig. 3). The CT scan showed the fine granular character of the densities, without the cystic components or expansive manifestations and mass effect that would be expected in an expansive bone formation process. Thus, odontomas was excluded from the differential diagnosis with a high degree of certainty (Shimizu et al., 2014).

The relatively extensive involvement of the mandible suggests that the changes might be associated with a condition that affected the rest of the skeleton (Mallya and Lam, 2018). However, no changes corresponding to whole-body involvement were found in the other preserved skeletal components. Therefore, osteopetrosis, osteopoikilosis, melorheostosis, Paget's disease, osteoplastic metastases, and heavy metal poisoning could also be excluded from the differential diagnosis with a high degree of probability (Ortner, 2003).

The density of the material is significantly higher than the surrounding cortical bone (approximately 800–1000 HU for the cortex, 1500–1900). If we were to consider abnormally extensive calcification in a diffuse inflammatory process, which is highly unlikely in the absence of osteolytic involvement, this newly formed sclerotic bone should not exceed the density of the surrounding bone. However, the results of the density measurements show nearly double the density values. Thus, the hypothesis of recalcified post-inflammatory foci can be excluded.

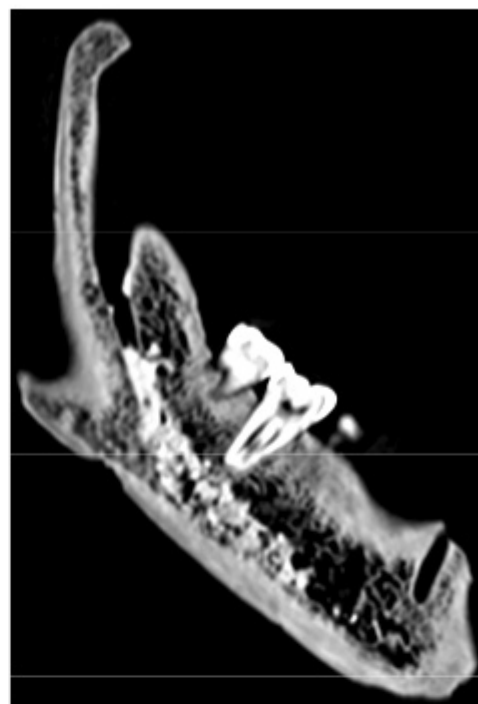


Fig. 4. Magnified image of the mandible showing collections of dense material primarily within the mandibular canal and adjacent alveoli.

Table 1
Relative content of silicon in the samples.

	Si [%]	Ca/Si
REF	0.87 ± 0.08	0.013 ± 0.001
SMP1	3.65 ± 0.71	0.072 ± 0.014
SMP2	1.36 ± 0.06	0.023 ± 0.001

It can be seen that maximum density appears in the mandibular canal and among the cancellous bone nearby. The entrance to the canal at the mandibular foramen is unobstructed (Fig. 4). If we consider the possibility of long-term deposition of fine sediments in a moist environment, then the mandibular canal and its secondary branches would form a logical trajectory of micro-sediments to the mandibular structures. Therefore, we concluded that the areas of density are deposits of fine sediment with a siliceous component. Hence, these are postmortem changes.

4.3. X-ray fluorescence spectrometry

Based on the results of CT scanning, it was hypothesized that the areas of density were caused by alluvial sediment. To prove this, the samples from the mandible were assessed by X-ray fluorescence spectrometry (XRF), focusing on evaluating the content of silicon, calcium, and phosphorus. Since silicon is found in rocks and soil mainly in the form of silicon dioxide, the increased amount of silicon could have entered the bone tissue mechanically, i.e., water and sand could have penetrated the internal structures of the bone. Although soil deposits could have been visible with an endoscope, the instrument was unavailable. Similarly, small particles of the soil in the bone can be detected microscopically (Schultz, 1986; Ortner, 2003) but sampling is destructive, and cannot be commonly applied.

Table 1 shows the higher intensity of silica in the affected area (SMP1 and SMP2) on the mandible compared to the reference sample (REF). Additionally, the calcium/silica ratio was calculated to make the samples independent of the measuring properties of the instrument and thus

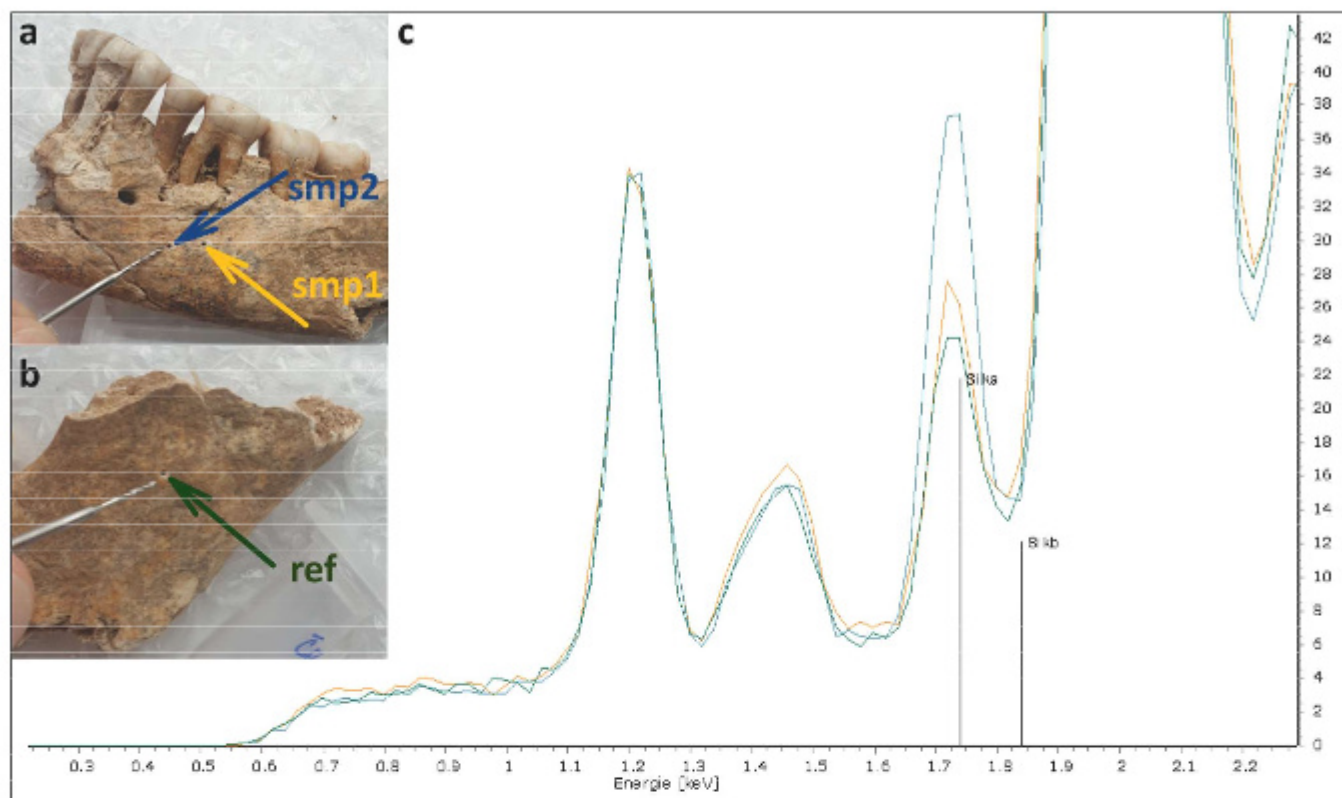


Fig. 5. XRF sampling points (a, b); Comparison of Si intensities in samples (c).

make them more robust. Nevertheless, the samples show the same pattern as when the raw data were used. This result confirms the increased content of silicon in the samples. Fig. 5c shows the higher counts in samples 1 and 2 compared to the reference sample (K α line of silicon in XRF spectra).

4.4. Discussion of possible environmental influences

The hypothesis of alluvial sediment filling is supported by the fact that the burial site “Na Valách” is located in the Morava River floodplain, on a slightly elevated promontory made up of hard fluvial sandy gravels, which slightly (about 2 m) exceeded its surroundings. At the base of this promontory, archaeological evidence has been found of terrain depressions, probably filled with water either permanently or during flood periods (Havlíček et al., 2005). While floods were not very frequent in the 9th century CE and limited to a narrow strip around the river, from the 10th century onwards, due to deforestation and a reduction in the retention capacity of the landscape, radical changes in the runoff ratios of precipitation in the entire Morava River basin occurred. As floods became more frequent and destructive during the High Middle Ages, settlements moved away from the river floodplain towards its edges (Havlíček, 1999).

As a result of the rise in the water table, the mandibular canal and adjacent bone cavities of Grave 7/2018 could have been filled with fine sediment. The later creation of a garden, certainly watered regularly, on the site of the grave, may also have influenced the process.

5. Conclusions

Postmortem taphonomic changes often lead to the formation of structures that can easily be misinterpreted as pathological lesions. In this study, we used CT imaging and XRF analysis to exclude pathological conditions in an early medieval Slavic male mandible and to assess the origin of the unusual formations. Although the presence of soil

inclusions, for example, in the medullary cavities of long bones is common in archaeological bone, its appearance on plain radiographs is less commonly observed and evaluated. It is necessary to realise that fine soil particles can also infiltrate unexpected anatomical areas. Our case illustrates the usefulness of interdisciplinary collaboration during palaeopathological evaluation and the importance of differentiating true pathologies from postmortem alterations to avoid inappropriate interpretations.

Funding

The article appears through the institutional support of long-term conceptual development of research institutions provided by the Ministry of Culture (ref. MK000094862).

CRediT authorship contribution statement

Fojtová Martina: Conceptualization, Investigation, Supervision, Writing – original draft, Writing – review & editing. **Křístek Jan:** Investigation, Methodology, Software, Writing – original draft. **Kučera Lukáš:** Methodology, Software, Validation, Writing – original draft.

Declaration of Competing Interest

None.

Acknowledgements

We would like to thank all our colleagues who were trying to help us diagnose this case. Thanks also to the radiographers Eva Antonínová and Michal Fronc of the Masaryk Memorial Cancer Institute in appreciation for their commitment and enthusiasm when scanning something different in the late evening hours following a busy day.

References

- Alt, K.W., Türp, J.C., Wächter, R., 1998. Periapical lesions – clinical and anthropological aspects. In: Alt, K.W., Rösing, F.W., Teschler-Nicola, M. (Eds.), *Dental Anthropology. Fundamentals, Limits, and Prospects*. Springer, Wien, pp. 247–276.
- Aufderheide, A.C., Rodríguez-Martín, C., 1998. *The Cambridge Encyclopedia of Human Paleopathology*. Cambridge University Press, Cambridge.
- Carotenuto, G., Schmidt, C.W., Viciano, J., D'Anastasio, R., 2019. Pseudopathological vertebral changes in a young individual from Herculaneum (79C.E.). *Andr. Anz.* 76 (1), 79–89. <https://doi.org/10.1127/anthranz/2019/0944>.
- Corron, L., Huchet, J.-B., Santos, F., Dutour, O., 2017. Using classifications to identify pathological and taphonomic modifications on ancient bones: Do “taphognomic” criteria exist? *Bull. Mem. Soc. Anthropol. Paris* 29 (1–2), 1–18. <https://doi.org/10.1007/s13219-016-0176-3>.
- Duday, H., Cipriani, A.M., Pearce, J., 2009. *The Archaeology of the Dead: Lectures in Archaeoanatomy*. Oxbow Books, Oxford.
- Duday, H., Guillon, M., 2006. Understanding the circumstances of decomposition when the body is skeletonized. In: Schmitt, A., Cunha, E., Pinheiro, J. (Eds.), *Forensic Anthropology and Medicine*. Humana Press, Totowa, pp. 117–157. https://doi.org/10.1007/978-1-59745-099-7_6.
- Ferembach, D., Schwidetzky, I., Stloukal, M., 1980. Recommendations for age and sex diagnoses of skeletons. *J. Hum. Evol.* 9, 517–549. [https://doi.org/10.1016/0047-2484\(80\)90061-5](https://doi.org/10.1016/0047-2484(80)90061-5).
- Fernández-Jalvo, Y., Andrews, P., 2016. *Atlas of Taphonomic Identifications. 1001+ Images of Fossil and Recent Mammal Bone Modification*. Springer, Dordrecht.
- Fojtová, M., Galuska, L., 2022. Zvláštní rané středověké hroby objevené ve Starém Měste – „Na Valách“ a problém jejich interpretace. *Prehl. Vyzk.* 63 (2), 9–60. <https://doi.org/10.47382/pv0632-02>.
- Fulcheri, E., Massa, E.R., Garetto, T.D., 1986. Differential diagnosis between palaeopathological and non-pathological post-mortem environmental factors in ancient human remains. *J. Hum. Evol.* 15 (1), 71–75. [https://doi.org/10.1016/s0047-2484\(86\)80067-7](https://doi.org/10.1016/s0047-2484(86)80067-7).
- Galuska, L., 2002. Deset let archeologických výzkumů Moravského zemského muzea v oblasti Starého Města (1992–2001). *Prehl. Vyzk.* 43, 51–69.
- Haglund, W.D., Sorg, M.H. (Eds.), 2002. *Advances in Forensic Taphonomy. Method, Theory and Archaeological Perspectives*. CRC Press, Boca Raton.
- Havlíček, P., 1999. Die geologischen Verhältnisse in der Umgebung der Siedlungsagglomeration der grossmährischen Machtzentren Mikulčice und Staré Město. In: Poláček, L., Dvorská, J. (Eds.), *Probleme der mitteleuropäischen Dendrochronologie und naturwissenschaftliche Beiträge zur Talaua der March*. Institute of Archaeology of the Czech Academy of Sciences, Brno, pp. 181–197.
- Havlíček, P., Galuska, L., Poláček, L., 2005. Die geologische situation im Bereich des grossmährischen Zentrums von Staré Město – Uberské Hradiště. In: Poláček, L. (Ed.), *Studien zum Burgwall von Mikulčice VI*. Institute of Archaeology of the Czech Academy of Sciences, Brno, pp. 93–108.
- Hochmanová-Vávrová, V., 1962. Velkomoravské pohřebiště ve Starém Měste „Na Valách“. Výzkum v letech 1957–1959. *Acta Mus. Moraviae. Sci. Soc.* 47, 201–270.
- Hrubý, V., 1955. Staré Město. Velkomoravské pohřebiště „Na valách“. Czechoslovak Academy of Sciences, Praha.
- Kniisel, C.J., Schotsmans, E.M.J., 2022. *The Routledge Handbook of Archaeoanatomy. Bioarchaeology of Mortuary Behaviour*. Taylor & Francis, New York.
- Lovejoy, C.O., 1985. Dental Wear in the Libben Population: Its Pattern and Role in the Determination of Adult Skeletal Age at Death. *Am. J. Phys. Anthropol.* 68 (1), 47–56. <https://doi.org/10.1002/ajpa.1330680105>.
- Mallya, S., Lam, E., 2018. *White and Phorah's Oral Radiology, Principles and Interpretation*, 8th ed., Mosby/Elsevier, St. Louis.
- Ortner, D.J., 2003. *Identification of Pathological Conditions in Human Skeletal Remains*. Academic Press, San Diego.
- Schaefer, M., Black, S., Scheuer, L., 2009. *Juvenile Osteology. A Laboratory and Field Manual*. Elsevier, Burlington – London – San Diego.
- Schultz, M., 1986. Die mikroskopische Untersuchung prähistorischer Skelettfunde. Anwendung und Aussagemöglichkeiten der differentialdiagnostischen Untersuchung in der Paläopathologie. Basel-Landschaft Amt für Museen und Archäologie, Basel.
- Schultz, M., 1996. Microscopic investigation of excavated skeletal remains: a contribution to paleopathology and forensic medicine. In: Haglund, W.D., Sorg, M.H. (Eds.), *Forensic Taphonomy*. CRC Press, Boca Raton, pp. 201–222. <https://doi.org/10.1201/9781439821923.ch14>.
- Shimizu, M., Ogawa, D., Okamura, K., Kawazu, T., Chikui, T., Yoshiura, K., 2014. Dentigerous cysts with calcification mimicking odontogenic tumors: differential diagnosis by CT. *Oral. Radiol.* 31 (1), 14–22. <https://doi.org/10.1007/s11282-014-0173-5>.
- Stodder, A.L.W., 2018. Taphonomy and the nature of archaeological assemblages. In: Katzenberg, M.A., Grauer, A.L. (Eds.), *Biological Anthropology of the Human Skeleton*, third ed. Wiley-Blackwell, New York, pp. 73–115. <https://doi.org/10.1002/9781119151647.ch3>.
- Vyhnaněk, L., 1999. Nárys kosterní paleopatologie se zaměřením na radiodiagnostiku. In: Stloukal, M. (Ed.), *Antropologie – příručka pro studium kostry*. National Museum, Praha, pp. 386–432.
- Wells, C., 1967. Pseudopathology. In: Brothwell, D., Sandison, A.T. (Eds.), *Diseases in Antiquity*. C.C. Thomas, Springfield, pp. 5–19.

Abhandlung

Markéta Lundová, Lukáš Šín, Hana Dehnerová, Radka Pechancová, Ondřej Kurka, Petr Bednář, Lukáš Kučera*

Evaluation of chemical composition of *cribra orbitalia* from post-medieval children graves (Olomouc, Czech Republic)

<https://doi.org/10.1515/pz-2022-2045>

Zusammenfassung: Bei einer archäologischen Rettungsgrabung im Zentrum der Stadt Olomouc (Region Mähren, Tschechischen Republik) wurden mehrere Gräber gefunden. Diese waren Teil eines nicht mehr existierenden Friedhofs in der Umgebung der Kirche St. Peter und Paul. Die Forschung konzentrierte sich auf die Analyse von 13 Schädelproben von Kindern, die von einer chronischen Pathologie namens "*Cribra orbitalia*" (CO) betroffen waren. Röntgenfluoreszenzspektrometrie (XRF) und induktiv gekoppelte Plasma-Massenspektrometrie (ICP-MS) wurden verwendet, um Unterschiede in den Proben in Bezug auf das Alter einer Person, den Porositätsgrad (der den Fortschritt von CO darstellt) und andere beobachtete Pathologien zu untersuchen. Beide Techniken bewiesen, dass das Verhältnis von Calcium zu Eisen mit dem Alter des Kindes ohne Rücksicht auf den Grad der CO-Schädigung allmählich zunimmt. Darüber hinaus wurden die

ICP-MS-Daten mittels Hauptkomponentenanalyse ausgewertet, die darauf hinwies, dass die höchsten Pb-Gehalte in Proben von an Rachitis erkrankten Menschen gefunden wurden. Die vorläufigen Ergebnisse zeigen, dass mehr Forschung zu dieser Pathologie durchgeführt werden sollte – nicht nur für nachmittelalterliche, sondern auch für prähistorische.

Schlüsselworte: *cribra orbitalia*, Grab, Blei, Anämie, Eisen

Abstract: During an archaeological rescue excavation in center of city Olomouc (Moravia region, Czech Republic) several graves were found. Those graves were a part of a defunct cemetery situated in the area surrounding a church of St. Peter and Paul. The research was focused on analysis of 13 children's skull samples affected by a chronic pathology known as "*cribra orbitalia*" (CO). X-ray fluorescence spectrometry (XRF) and inductively coupled plasma-mass spectrometry (ICP-MS) were used to examine differences in the samples with respect to an individual's age, degree of porosity (representing the progress of CO) and other observed pathologies. Both techniques proved that the ratio of calcium to iron gradually increases with the age of the child without regard to the degree of CO damage. Moreover, the ICP-MS data were evaluated using principal component analysis, which pointed out that the highest contents of Pb were found in samples from individuals suffering from rickets. The preliminary results reveal that more research on this pathology should be performed – not only for post-medieval individuals but also in prehistorical ones.

Keywords: *cribra orbitalia*, grave, lead, anemia, iron

*Corresponding author: Lukáš Kučera, Ph.D., Department of Analytical Chemistry, Faculty of Science, Palacký University, 17. listopadu 12, 779 00, Olomouc, Czech Republic. E-Mail: lukas.kucera@upol.cz

Markéta Lundová, Department of Analytical Chemistry, Faculty of Science, Palacký University, 17. listopadu 12, 779 00, Olomouc, Czech Republic. E-Mail: l.maki@seznam.cz

Lukáš Šín, Ph.D., Archaeological Centre Olomouc, U Hradiska 42/6, 779 00, Olomouc, Czech Republic. E-Mail: sin@ac-olomouc.cz

Hana Dehnerová, M.Sc., National heritage institute, Regional office in Olomouc, Department of archaeology, Horní náměstí 25, 779 00, Olomouc, Czech Republic. E-Mail: dehnerova.hana@npu.cz

Radka Pechancová, Ph.D., Department of Analytical Chemistry, Faculty of Science, Palacký University, 17. listopadu 12, 779 00, Olomouc, Czech Republic. E-Mail: radka.pechancova@seznam.cz

Ondřej Kurka, Ph.D., Department of Analytical Chemistry, Faculty of Science, Palacký University, 17. listopadu 12, 779 00, Olomouc, Czech Republic. E-Mail: Ondrej.Kurka@upol.cz

Petr Bednář, Ph.D., Assoc. Prof., Department of Analytical Chemistry, Faculty of Science, Palacký University, 17. listopadu 12, 779 00, Olomouc, Czech Republic. E-Mail: petr.bednar@upol.cz

1 Introduction

Cribra orbitalis (CO) is one of the most frequently found pathological phenomena in human remains. CO is porotic or sieve-like lesion in the bony orbital roof¹. It occurs to a greater extent on children's and adolescent's skeletal remains² and was firstly described in the 19th century by H. Welcker. CO often appears on the skeletal remains of medieval population that lived in unfavorable conditions, such as high population density, insufficient hygienic conditions, and limited access to food resources³. Fornaciari *et al.* in 1982 studied the relationship between CO and the level of iron in the bone tissue from the skeletal remains of children under age 18 in the Carthage (Tunisia). The authors confirmed significantly lower levels of iron in bone in individuals with CO compared to healthy individuals (atomic absorption spectrometry was used). The results point out to link between anemia (low amount of iron) and CO that could be caused also by malnutrition⁴. The hypothesis of iron deficiency and anemia is contrary to the haematological research of Walker *et al.* in 2009. This research shows that iron deficiency cannot sustain massive production of red blood cells, which causes expansion of bone marrow and is responsible for these disorders. However, some evidence suggest that the accelerated loss and compensatory red blood cell overproduction observed in haemolytic and megaloblastic anemias are the most likely a cause of porotic hyperostosis⁵.

Grupe (1995) also investigated this pathology on ten skeletal remains from Bavaria (5th – 7th century) including collagen extraction, amino acid analysis and trace element analysis (calcium, phosphorus and iron). The examined group showed higher values of proline, lysine, hydroxylysine and the ratio of iron to calcium, which refutes the hypothesis of iron deficiency and leans towards hypothesis of vitamin C deficiency. A significant amino acid deficiency in the examined individuals was demonstrated only for hydroxyproline⁶. Other investigations of Nubian population from Missiminia, northern Sudan showed that histologic bone structure does not support the diagnosis of anemia. The histologic thin-sections were analyzed in polarized light to clarify the possible sources of CO. In 56.5% of *cribra orbitalis* cases, there were no histologic features indicating changes due to anemia. Authors hy-

pothesize that it is signs of other pathological conditions, e. g. inflammation, osteoporosis and/or pseudopathological cases⁷.

Sguazza *et al.* (2016) analyzed an adult female skull with partially preserved hair from the crypt of St. Maria Annunciata in Milan dating to the 15th–17th century using inductively coupled plasma-mass spectrometry (ICP-MS). High content of Pb was found in an individual with CO, i. e. 8.6 $\mu\text{g.g}^{-1}$ and 7.9 $\mu\text{g.g}^{-1}$ for skull and hair, respectively, compared with reference samples from the crypt (0.15 and 0.10 $\mu\text{g.g}^{-1}$, respectively). The presence of higher content of lead in this sample can be explained e. g. by use of lead for domestic, medical and cosmetic purposes in the 17th and the 18th century⁸. Zarina *et al.* (2016) performed the analysis of 72 skeletal remains from southeastern Latvia from the 17th to the 18th century by ICP-MS and isotope ratio mass spectrometry analysis ($\delta^{13}\text{C}$, $\delta^{15}\text{N}$, $\delta^{18}\text{O}$). A significant relationship between low levels of rubidium and iron, and lower levels of the isotope $\delta^{15}\text{N}$ have been reported. The authors connect these results with nutritional deficiency or a parasitic disease⁹. Thus, two most common explanations for the formation of *cribra orbitalis* are currently described. First and prevailing opinion is that malnutrition and/or physiological life cycle changes lead to anemia (subsequently leading to CO). Second explanation is parasitic diseases occurring due to lower hygienic levels may also lead to CO. Note, that both processes could have happened simultaneously.

The aim of this work was to analyze 14 skull samples of post-medieval children found in the center of city Olomouc (Czech Republic), close to a church of St. Peter and Paul using X-ray fluorescence spectrometry and inductively coupled plasma-mass spectrometry to find differences in samples with respect to the age of studied individuals, degree of porosity of orbit (representing the progress of CO), and other observed pathologies.

2 Materials and methods

2.1 Archaeological context and anthropological evaluation

During an archaeological rescue excavation performed in the centre of Olomouc city at Křížkovského 512 street (dis-

1 Wapler *et al.* 2003

2 Walker *et al.* 2009.

3 Welcker 1888.

4 Fornaciari *et al.* 1982.

5 Walker *et al.* 2009.

6 Grupe 1995.

7 Wapler *et al.* 2003

8 Sguazza *et al.* 2016.

9 Zarina *et al.* 2016.

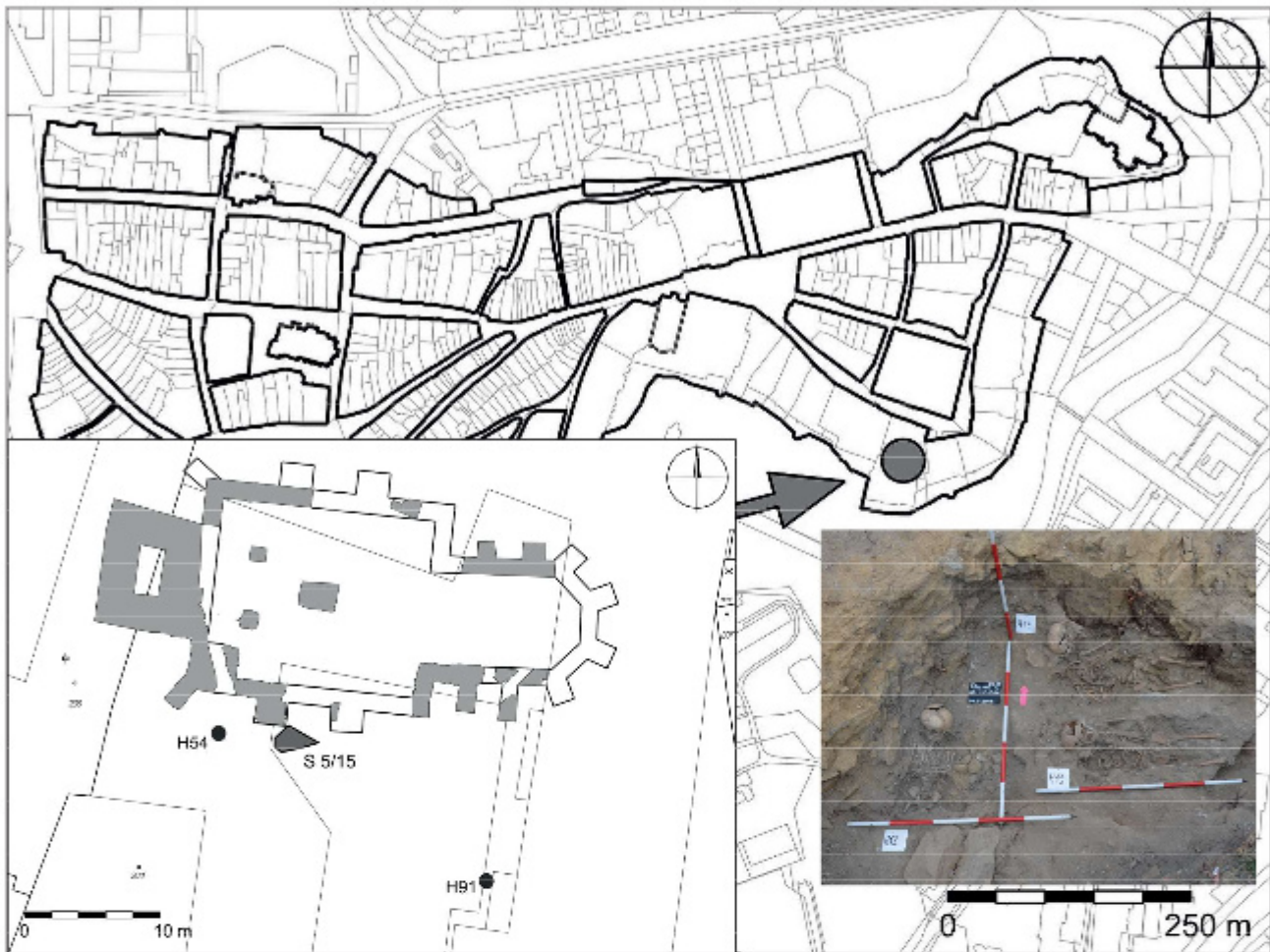


Fig. 1: Map of city center Olomouc and inset of examined area Křížkovského 512 with S5/15 probe and graves H54 and RH91, inset show S5/15 probe with graves H12, H13 and H14 (J. Grégr a H. Dehnerová).

trict Předhradí) in years 2015–2017, 542 graves were found (Fig. 1). In this work, all skull samples of medieval children (13 pieces) affected by CO and one healthy individual (reference sample) (Fig. 2; age determination for each individual was based on methodology of Uberlaker¹⁰ and Florkowski/Kozłowski¹¹) were analyzed. All of orbits from 13 children skulls exhibiting CO were classified using the Stuart-Macadam grading system¹². This system contains a set of ascending grades which correspond to: capillary impressions on the bone – grade 1 (5 individuals), scattered fine foramina – grade 2 (2 individuals), large and small isolated foramina – grade 3 (5 individuals), and trabecular bone linkage – grade 4 (1 individual). This grading system also includes a grade 5, which shows outgrowth of

trabeculae. However, this is not representative of CO and has only been reported to occur in vitamin C deficiency (scurvy). This grade was not detected in our samples¹³ (Tab. 1). Note, that 2 adult individuals (1 male, 1 female) were also affected by CO, but due to the higher bone remodeling processes were omitted for this study. The survey also provided evidence of settlement in the area in the prehistory and early Middle Ages. The graves were part of a defunct cemetery (used since 1391 and abolished in 1784, data from the first written sources) situated in the area surrounding the church of St. Peter and Paul (stone foundations of the church were found). The church existed in this area from the 14th century until 1792. Moreover, an Augustinian monastery including the church of St. Jacob was found in the south part of this area (documented

¹⁰ Uberlaker 1978.

¹¹ Florkowski/Kozłowski 1994.

¹² Stuart-Macadam 1991.

¹³ Naveed et al. 2012.



Fig. 2: Example of skull with *cribra orbitalia* (H18).

Tab. 1: List of studied individuals with *cribra orbitalia*.

Grave #	Age	Location of CO	CO grading	Observed disease
RH91	2 years (\pm 8 months)	-	0	-
H12	2 years (\pm 8 months)	left orbit	3	anemia, rickets
H15	2 years (\pm 8 months)	right orbit	1	-
H10	2–4 years	left orbit	1	-
H21	2–4 years	both orbits	4	rickets
H8	2–4 years	right orbit	2	-
H18	4 years (\pm 12 months)	both orbits	2	-
H54	4–6 years	left orbit	3	rickets
H19	6 years (\pm 24 months)	right orbit	1	-
H13	6–9 years	both orbits	1	anemia
H14	9–12 years	right orbit	3	-
H11	10 years (\pm 30 months)	right orbit	3	anemia
H36	10 years (\pm 30 months)	right orbit	3	anemia
H32	12–15 years	right orbit	1	-

since the 13th century)¹⁴. Composition of the parishioners was diverse and included also craftsmen and fishermen from the suburbs, nobles and burghers, in addition to the people belonging to the church society (e. g. ministers of the church – singers, bell towers, officials, servants from canon residences, etc.)¹⁵.

The examined area contains 542 individual graves in total, where 486 graves are located in the north part of the area and the remaining 56 graves in southern part. Burial in the southern area of the church was complicated by the relatively high-rise bedrock made up of the Kulm crumb. The area was used for funeral purpose only for a limited time frame – the graves were not disturbed and the distance among them was wide. This part of cemetery is dated to the span of the 14th–16th century. Burials belonging to the early Middle Ages were not found and in contrast to the northern area, also no baroque burials were found. However, they could be removed by modern building modifications¹⁶. The deceased were placed there in a stable position on their backs, with their head situated to the west and their feet to the east, with the exception of the S5/15 trench, in which four children were buried with their head situated to the north (graves H8, H12, H15, H18). The S5/15 trench is situated in a natural fissure in the rock massive, near the western supporting pillar of the southern perimeter wall of the nave of the church (Fig. 1). The natural fissure reached a depth of 2.1–2.4 m below the surface of the surrounding bedrock. During the second half of the 16th century, a total of 27 individuals were placed in the natural fissure in at least eight levels (16 individuals of them were children, i. e. H8 – H15, H17–H19, H21, H22, H32, H36 and a newborn, H4)¹⁷. Majority of those individuals were situated directly in the space of the S5/15 trench. The relative position of the graves in this probe from bottom to top was as follows: graves H35 and H36 (the lowest level), followed by the graves H32, H33, H27 (in the intermediate level), and subsequently the graves H20, H21 and H22. All associated individuals were situated with their head to the west. The first child grave (H18, the western wall of the fissure) with head situated to the north was located on the top of these graves, followed by the graves H17, H16, H19, H15, H13, H14, H12, H9, H10, H11, H8, H4, H5, H6, H1, H2 and H3.

The next studied grave H54 was located 5 m to the west of S5/15 trench. The grave RH91, used as a reference sample, was located 21 m to the southeast of S5/15 trench

(situated in monastery cemetery) (Fig. 1). The most frequently represented finds from the graves include a pair of fasteners – an eye with a hook made of copper or some other non-ferrous metal¹⁸.

Fastening, a universal part of clothes, was used from the second half of the 15th century to the present. It has been found in the individuals H8, H12 (eye), H13, H14, H15 (on three parts of the body – on the collarbone, on the ribs and under the ribs) and H54 (tinned, also in three places – on the neck, in the area of the right shoulder joint and on the rib). In the individual H8, fragments of a bronze wire were found in the oral cavity. The inventory of the individual H54 contained the most items: in addition to the above-mentioned fasteners, a pair of brass buckles was found in the chest area, while brass belt fittings and small glass beads (a total of 312 pieces) were found in the occipital area and probably came from the cap (Fig. 3, probably “crown of death”). This grave could be dated to the second half of the 15th century – first half of the 16th century¹⁹.

2.2 Chemicals and reagents

All chemicals used to prepare the stock standard solutions were at least of analytical grade. Single element aqueous calibration solutions ASTASOL[®] at the concentration $1\,000 \pm 2\text{ mg L}^{-1}$ (Ca, Fe, Pb), a multi-element calibration solution ASTASOL[®] at the concentration $10 \pm 0.1\text{ mg L}^{-1}$ containing Sc, Y, In, Tb and Bi for internal standard solution preparation, HNO₃ (69 %, Analpure[®]), H₂O₂ ($\geq 30\%$, analytical grade+) and HCl (36 %, Analpure[®]) were obtained from Analytika Ltd. (Prague, Czech Republic). Two certified reference materials (CRMs) of lake water (TM 25.6 and TMDA 64.3) were purchased from EC, Canada. Ultrapure water with the resistivity 18.2 M Ω -cm obtained from the Milli-Q water system (Millipore Corporation, Molsheim, France) was used to prepare all sample and calibration solutions. All kinds of glassware and plastic labware used for ICP-MS determinations were pre-treated by overnight leaching in 10 % nitric acid solution, rinsed multiple times with ultrapure water, and dried in an oven to avoid contamination with elemental impurities.

14 Dehnerová/Šlězár 2020, 15–16.

15 Kouřil 1979; 1980.

16 Dehnerová/Šlězár 2020, 23–24.

17 Šín 2017; Šín/Dehnerová 2019.

18 Šlancarová 2018a, 99–100.

19 Ibid. 200–201; 207.

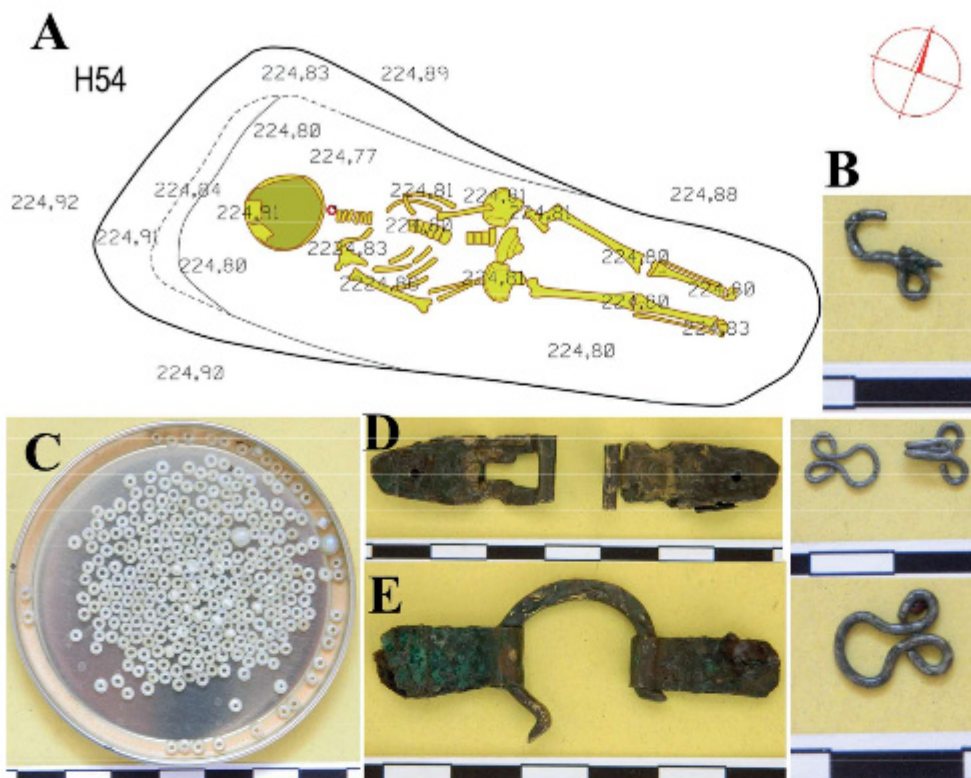


Fig. 3: Layout of grave H54 (A) with three fasteners (B), small glass beads (C), brass buckles in the chest area (D) and brass belt fittings (E) as part of inventory (Dehnerová 2015).

2.3 X-ray fluorescence spectrometry (XRF)

The bone samples were manually milled and homogenized in a mortar. Elemental analysis of the bone samples was performed using an X-ray fluorescence spectrometer (Olympus, MA, USA). The measurement parameters were as follows: Geochem mode, excitation energy range 8–40 kV, time of acquisition 90s. Each sample was measured in six replicates.

2.4 Inductively coupled plasma-mass spectrometry (ICP-MS)

A microwave digestion unit UltraWAVE (Milestone, Italy) was employed for sample mineralization. Prior to the mineralization step, the bone samples were manually milled and homogenized in a mortar. Subsequently, 20 mg of homogenized bone tissues were digested with mixture of concentrated HNO_3 (4 mL), H_2O_2 (1 mL) and HCl (0.25 mL) in quartz vials with Teflon caps using the following two-step digestion program: 110 bar and 220 °C, first cycle time 15 min, second cycle time 10 min. After the digestion and cooling, digests were diluted with

ultrapure water to 25 mL and stored at 4 °C until ICP-MS analysis. Blank samples were prepared by digestion of mixture of acids but without the sample matrix. Nevertheless, for Ca determination, all samples were diluted 100x with deionized water due to high Ca contents in bone tissue samples. All measurements were carried out using an inductively coupled plasma mass spectrometer 7700x ICP-MS (Agilent Technologies Ltd., Japan), fitted with an ASX-520 autosampler, a MicroMist concentric nebulizer, a cooled Scott-type double pass spray chamber and an octopole reaction cell operating in helium mode to overcome spectral interferences. The instrumental conditions for determination of total Ca, Fe, and Pb contents by ICP-MS operating at a spectrum mode were as follows: RF power of 1550 W, plasma gas Ar flow rate of 15.0 $\text{L}\cdot\text{min}^{-1}$, auxiliary gas Ar flow rate of 1.07 $\text{L}\cdot\text{min}^{-1}$, nebulizer gas Ar flow rate of 0.9 $\text{L}\cdot\text{min}^{-1}$, collision gas He flow rate of 4.3 $\text{mL}\cdot\text{min}^{-1}$, a dwell time of 100 ms for analyzed isotopes ^{44}Ca , ^{56}Fe , ^{209}Pb , ^{45}Sc and ^{209}Bi (^{45}Sc and ^{209}Bi served as an internal standards). It was prepared by a hundredfold dilution of a multi-element calibration solution containing Sc, Y, In, Tb, and Bi ($c = 10 \pm 0.1 \text{ mg}\cdot\text{L}^{-1}$) with ultrapure water. Semi-quantitative analysis of selected isotopes (up to 70 elements) was measured

Tab. 2: Pb content in studied samples, measured by ICP-MS.

Sample	Mean ($\mu\text{g}\cdot\text{g}^{-1}$)	SD ($\mu\text{g}\cdot\text{g}^{-1}$)
RH91	3.3	0.1
H12	43.1	1.7
H15	38.8	2.7
H10	14.2	0.5
H21	59.7	4.9
H8	21.8	1.5
H18	27.8	1.3
H54	68.0	4.3
H19	25.4	0.9
H13	30.7	3.0
H14	4.5	0.2
H11	28.8	1.7
H36	4.6	0.4
H32	4.1	0.3

with the same parameters. All ICP-MS analyses were performed in six replicates. For total Ca, Fe and Pb determination, stock standard solutions were diluted with deionized water with the addition of same mixture of acids as for sample mineralization.

The used ICP-MS method was validated in terms of linearity, trueness and precision. Linearities of calibration curves were evaluated within a range from 62.5 to 12500 $\mu\text{g}\cdot\text{g}^{-1}$ for Ca, from 0.6 to 12,500 $\mu\text{g}\cdot\text{g}^{-1}$ for Fe and from 1.25 to 625 $\mu\text{g}\cdot\text{g}^{-1}$ for Pb. The calibration models for all studied isotopes were linear, with the resulting correlation coefficients not lower than 0.9999. The trueness of the method was determined by analyzing two CRMs (TM 25.5 and TMDA 64.3). It was expressed by recovery and ranged between 107 and 113 % for Fe and Pb. Recovery of Ca was not determined because neither CRMs did not contain certified concentration of Ca. Precision (expressed as relative standard deviation (RSD) in %) was not higher than 5 % for both Fe and Pb. For quality control and estimation of stability of ICP-MS measurements, QC sample (at the level of 125 $\mu\text{g}\cdot\text{g}^{-1}$ for Ca, Fe and 62.5 $\mu\text{g}\cdot\text{g}^{-1}$ for Pb) was repeatedly analyzed at the beginning, during and at the end of ICP-MS measurement. Calculated recoveries for Ca, Fe, Pb were 103 %, 106 %, 95 %, and precisions expressed as RSD were 3 %, 3 % and 4 %, respectively. Additionally, the internal standard solution was simultaneously introduced to the ICP-MS spectrometer to reduce non-spectral interferences. Signals of Ca and Fe isotopes were corrected to ^{45}Sc isotope, whereas Pb isotope was corrected to ^{209}Bi isotope.

2.5 Statistical evaluation

The obtained ICP-MS raw data were studied by unsupervised Principal component analysis (PCA) and comparison of boxplot of Pb content. Logarithmic transformation and Pareto scaling was applied. The transformed data matrix was transferred to freeware environment for statistical computing R-project, version 3.5.0²⁰. Outputs were evaluated in the form of appropriate score and loadings plots. For PCA and visualization the default package “stats” and “ggplot2” were used, respectively²¹.

3 Results and discussion

The 13 samples taken from the skulls affected by CO and from one healthy individual (reference sample) were homogenized and measured by XRF, and by ICP-MS as a confirmatory method. In the first step, we focused on determination of content of iron in bone samples, due to the commonly accepted theory of anemic disease and low amount of iron causing CO. Fig. 4AB shows high intensity of iron in the reference sample and very low intensity in samples with CO. Therefore, we believe that in these individuals with CO, reduced iron levels in the bones could lead to anemia. However, if we focus on the ratio Ca/Fe (Fig. 4CD), we can see the dependence of iron content on age. This ratio gradually increases with the age of the child, but it does not correlate with the degree of orbital damage (Tab. 1).

Fig. 5A shows the score-plot from PCA of dataset containing the amounts of measured elements. Each sample was measured in five chemical replications represented by five points of a particular color. With the exemption of pairs H10–H12 and H21–H54, respectively, the datapoints related to each individual (replications) is separated from the other ones. A distinct segregation of reference sample (RH91) from samples affected by CO was observed. First two components explain 59.5 % of the variability in data. Note, that the cumulative proportion of variance explains 68.8 % and 77.6 % when third component and third plus fourth components are included, respectively. Loadings plot (Fig. 5B) shows that Pb strongly influences both principal components 1 (PC1) and 2 (PC2). The lowest content of Pb (Fig. 5C, Table 2) was observed in the reference sample RH91 (3.3 $\mu\text{g}\cdot\text{g}^{-1}$), followed by samples H32, H14 and H36 with content of 4.1, 4.5 and 4.6 $\mu\text{g}\cdot\text{g}^{-1}$, respectively.

²⁰ R Core Team 2020.

²¹ Wickham 2016.

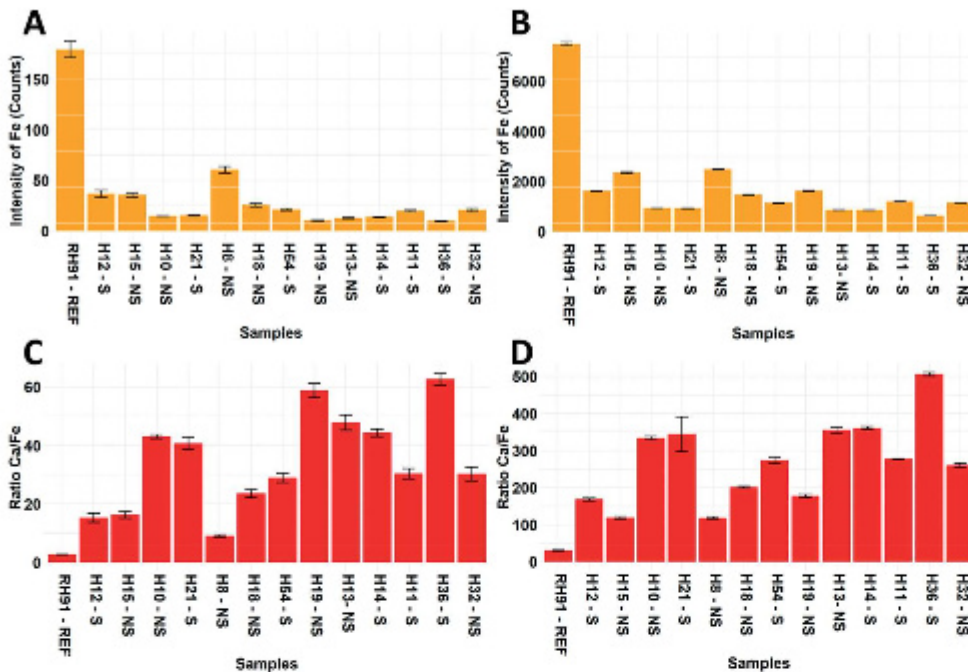


Fig. 4: Intensities of Fe in studied samples measured by XRF (A) and ICP-MS (B), and ratio of signal of Ca to Fe analyzed using XRF (C) and ICP-MS (D) (REF – reference sample, S – significant porosity of CO, NS – no significant porosity of CO).

The highest content of Pb were found in samples H54 ($68.0 \mu\text{g}\cdot\text{g}^{-1}$), H21 ($59.7 \mu\text{g}\cdot\text{g}^{-1}$) and H12 ($43.1 \mu\text{g}\cdot\text{g}^{-1}$). Note that those individuals were also affected by rickets (Tab. 1). Sguazza *et al* (2016) describe the link between content of Pb and CO. The authors supposed that chronic lead intoxication could (in addition) cause other diseases, especially anemia²². The Pb levels in human skeletal remains will therefore reflect their *in vivo* exposures in the past. Besides that, we cannot neglect the postmortem contamination, as it can contribute to significant measured values of Pb (100-fold greater than the background level)²³. Burials H12 and H21 (trench S5/15) were inhumed along the southern wall of the church. Thus, the Pb contamination (relevant to postmortem changes) can be caused by the rainwater flowing down from the roof with assumed leaden structural elements²⁴. Nevertheless, the connection between the Pb contamination and the rickets (H12, H21, H54) points to the context with *in vivo* exposure. Lead poisoning can also inhibit vitamin D synthesis due to its effect on the metabolism of calcium and phosphorus (by inhibition of

one of the required enzymes). This condition results in hypocalcemia, hypophosphatemia and hyperphosphaturia due to the decrease in intestinal absorption of both these minerals and Pb poisoning in children could result in bone demineralization and rickets²⁵.

4 Conclusion

The XRF and ICP-MS were used to evaluate elemental composition of 14 child skulls affected by CO. The research was focused on determination of iron content which should be the main indicator of anemia. The ratio of calcium to iron gradually increases with the age of the child without regard to the degree of CO damage. We presume that reduced iron levels could be a secondary sign, not the primary cause of CO. Moreover, principal component analysis reveals a significant influence of lead on PC1 and PC2. The highest content of lead was found in samples affected by rickets, which agrees with lead intoxication resulting in hypocalcemia, hypophosphatemia and hyperphosphaturia. Note that eating dis-

²² Sguazza *et al.* 2016.

²³ Grandjean 1988.

²⁴ Bond *et al.* 2013; Drasch 1982; Unger 2006.

²⁵ Loghman-Adham 1997; Rodríguez/Mónica Mandalunis 2018.

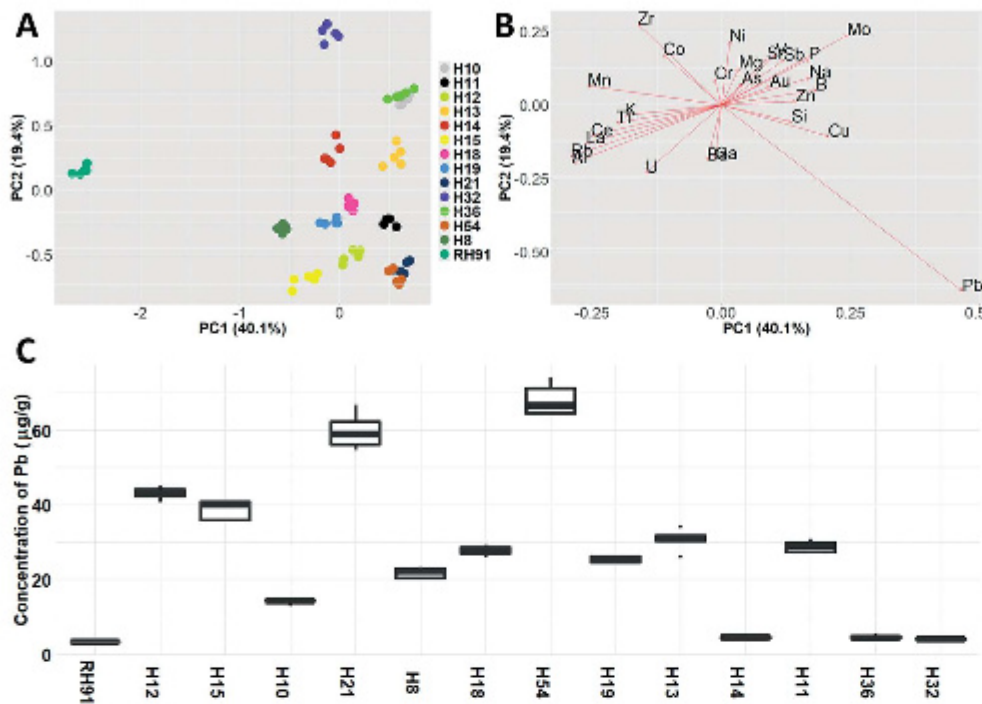


Fig. 5: Principal component analysis of ICP-MS results: raw data (A), loadings plot (B) and box plot of Pb content in studied samples (C).

orders, parasitic diseases, and other diseases that we are not able to clearly identify might also play an important role here. The authors realize that this research was made on the small set of samples. However, the preliminary results point out that more research on this pathology should be performed not only for post-medieval individuals, but also in prehistorical ones.

Acknowledgments: The authors gratefully acknowledge to ERDF/ESF “Arteca: Advanced physical-chemical methods of research and protection of cultural and artistic heritage” [No. CZ.02.1.01/0.0/0.0/17_048/0007378] and the Grant Agency of Czech Republic [17-17346S] for financial support.

References

- Bond et al 2013: J. W. Bond/S. V. Hainsworth/T. L. Lau, Lead Theft – A Study of the “Uniqueness” of Lead from Church Roofs. *Journal of Forensic Sciences* 58/4, 2013, 1003–1007.
- Dehnerová/Šlězár 2020: H. Dehnerová/P. Šlězár, Kostel sv. Petra v Olomouci ve středověku z pohledu archeologických pramenů. *Historica Olomucensia* 59. Sborník prací historických 2020, 13–51.
- Drasch 1982: G. A. Drasch, Lead burden in prehistorical, historical and modern human bones. *Science of the Total Environment* 24/3, 1982, 199–231.
- Florkowski/Kozłowski 1994: A. Florkowski/T. Kozłowski, Ocena wieku szkieletowego dzieci na podstawie wielkości kości. *Przegląd Antropologiczny* 57/1–2, 1994, 71–86.
- Fornaciari et al 1982: G. Fornaciari/F. Mallegni/D. Bertini/V. Nuti, *Cribrā Orbitalia* and Elemental Bone Iron in the Punic of Carthage, *OSSA* 8, 1982, 63–77.
- Grandjean 1988: P. Grandjean, Ancient skeletons as silent witnesses of lead exposures in the past. *Critical Reviews in Toxicology* 19/1, 1988, 11–21.
- Grupe 1995: G. Grupe, Etiology of the *cribra orbitalia*: effect of amino acid profile in bone collagen and the iron content of bone minerals. *Zeitschrift für Morphologie und Anthropologie* 81/1, 1995, 125–137.
- Kohout 2009: Š. Kohout, Územní vývoj a výstavba opevnění. In: J. Schulz (Ed.), *Dějiny Olomouce 1* (Olomouc 2009) 138–140.
- Kouřil 1979: M. Kouřil, Příspěvky k místopisu olomouckého Předhradí. *Historická Olomouc a její současné problémy I*, 1979, 109–114.
- 1980: –, K místopisu olomouckého Předhradí od poloviny 15. století do počátku 16. století. *Historická Olomouc a její současné problémy III*, 1980, 108–112.
- Loghman-Adham 1997: M. Loghman-Adham, Renal Effects of Environmental and Occupational Lead Exposure. *Environmental health perspectives* 105/9, 1997, 928–938.
- Naveed et al. 2012: H. Naveed/S. F. Abed/I. Davagnanam/J. M. Uddin/P. J. Adds, Lessons from the past: *cribra orbitalia*, an orbital roof pathology. *Orbit* 31/6, 2012, 394–399.
- R Core Team 2020: R Core Team, R: A language and environment for statistical computing. R Foundation for Statistical Computing (Vienna 2020). URL <https://www.R-project.org/>.

- Rodríguez/Mandalunis 2018: J. Rodríguez/P. M. Mandalunis, A Review of Metal Exposure and its Effects on Bone Health. *Journal of Toxicology* 2018/4, 2018, 1–11.
- Sguazza *et al.* 2016: E. Sguazza/D. Gibelli/M. Caligara/D. Candia/P. M. Galimberti/C. Cattaneo, The Role of Toxicological Analyses in Anthropology: A Case Report on Lead Intoxication. *Archaeometry* 58/1, 2016, 152–158.
- Stuart-Macadam 1991: P. L. Stuart-Macadam, Anaemia in Roman Britain: Poundbury camp. In: H. Bush/M. Zvelebil (Eds.), *Health in Past Societies: Biocultural Interpretations of Human Skeletal Remains in Archaeological Contexts* (Oxford: British Archaeological Research International Series 1991) 101–113.
- Štín 2017: L. Štín, *Antropologická zpráva. Olomouc – Křižkovského 10 (okr. Olomouc). Rok výzkumu 2015*, Archeologické centrum Olomouc, p. o. (Olomouc 2017), unpublished.
- /Dehnerová 2019: –/H. Dehnerová, *Novověký pohřeb ženy s dítětem – tafonomická analýza. Ročenka 2018*. Archeologické centrum Olomouc, p. o. (Olomouc 2019) 226–234.
- Šlancarová 2018a: V. Šlancarová, *Středověký šperk. Archeologické nálezy z jižní Moravy. Spisy Filozofické fakulty Masarykovy univerzity v Brně 481* (Brno 2018).
- 2018b: –, *Středověký šperk. Archeologické nálezy z jižní Moravy. Spisy Filozofické fakulty Masarykovy univerzity v Brně 481: Katalog nálezů* (Brno 2018). <https://digilib.phil.muni.cz/handle/11222.digilib/138548> [cit. 10.4.2021].
- Ubelaker 1978: D. H. Ubelaker, *Human Skeletal Remains: Excavation, Analysis, Interpretation* (Chicago 1978).
- Unger 2006: J. Unger, *Pohřební ritus 1. až 20. století v Evropě z antropologicko-archeologické perspektivy*, Nadace Universitas Masarykiana (Brno 2006).
- Walker *et al.* 2009: P. L. Walker/R. R. Bathurst/R. Richman/T. Gjerdrum/V. A. Andrushko, The causes of porotic hyperostosis and *cribra orbitalia*: A reappraisal of the iron-deficiency-anemia hypothesis. *American Journal of physical Anthropology* 139/2, 2009, 109–125.
- Wapler *et al.* 2003: U. Wapler/E. Crubézy/M. Schultz, Is *cribra orbitalia* synonymous with anemia? Analysis and interpretation of cranial pathology in Sudan. *American Journal of Biological Anthropology* 123/4, 2003, 333–339.
- Welcker 1888: H. Welcker, *Cribrā Orbitalia*, ein etiologisch-diagnostisches Merkmal am Schädel mehrerer Menschenrassen. *Archiv für Anthropologie* 17, 1888, 1–18.
- Wickham 2016: H. Wickham, *ggplot2: Elegant Graphics for Data Analysis* (New York 2016).
- Wright/Chew 1998: L. E. Wright/F. Chew, Porotic Hyperostosis and Paleoepidemiology: A Forensic Perspective on Anemia among the Ancient Maya. *American Anthropology* 4, 1998, 924.
- Zarina *et al.* 2016: G. Zarina/S. B. Sholts/A. Tichinin/V. Rudovica/A. Viksna/A. Engizere/V. Muznieks/E. J. Bartelink/S. K. T. S. Warmlannder, *Cribrā orbitalia* as a potential indicator of childhood stress: Evidence from paleopathology, stable C, N, and O isotopes, and trace element concentrations in children from a 17th–18th century cemetery in Jekabpils, Latvia. *Journal of trace elements in medicine and biology* 38, 2016, 131–137.